

Adsorption and Micellization of Surfactants

comparison of theory and experiment



40951

Promotor: dr. J. Lyklema
Hoogleraar in de fysische chemie, met bijzondere
aandacht voor de grensvlak- en kolloïdchemie

Co-promotor: dr. ir. L. K. Koopal
Universitair hoofddocent bij de vakgroep Fysische
en Kolloïdchemie

NN05201, 1991

Marcel Böhmer

Adsorption and Micellization of Surfactants

comparison of theory and experiment

Proefschrift

ter verkrijging van de graad van
doctor in de landbouw- en milieuwetenschappen
op gezag van de rector magnificus,
dr. H. C. van der Plas,
in het openbaar te verdedigen
op dinsdag 17 december 1991
des namiddags te vier uur in de aula
van de Landbouwwuniversiteit te Wageningen

Wm 001051

**BIBLIOTHEEK
LANDBOUWUNIVERSITEIT
WAGENINGEN**

Chapter 2: published in *Langmuir* **1990**, 6, 1478
Chapter 3: submitted for publication in *Langmuir*
Chapter 4: *Journal of Physical Chemistry* in press
Chapter 5: submitted for publication in *Langmuir*

Stellingen

I

Micellen van ionogene oppervlakte actieve stoffen gedragen zich als deeltjes met een constante wandlading.

Dit proefschrift H4

II

Als oppervlakte actieve stoffen aggregeren in oplossing zullen ze dit ook doen aan vast/vloeistof grensvlakken.

Dit proefschrift

III

Bij de adsorptie van oppervlakte actieve molekulen kan de verdeling van stof over de oppervlakte- en de oplossingskant van de gevormde bilaag geschat worden aan de hand van de wandlading.

Dit proefschrift H6

IV

Twee-staps adsorptie-isothermen van ionogene surfactanten treden alleen op als de lading van het adsorbens zich niet kan aanpassen.

Dit proefschrift H5, 6

V

Het volumefractieprofiel van een stof, die zich ophoopt bij een met alkylketens gemodificeerd oppervlak, heeft altijd een maximum in het grensvlak tussen verankerde ketens en vloeistof.

M. R. Böhmer, L. K. Koopal, R. Tjissen J., Phys. Chem. 1991, 95, 6285

VI

Dat retentie in "reversed phase liquid chromatography" een maximum kent als functie van de bezettingsgraad van het oppervlak, wil niet zeggen dat het geen zin heeft kolommateriaal met een hoge bezettingsgraad te synthetiseren.

VII

Het minimum in het berekende volumefractieprofiel van polyelektrolieten bij een oppervlak met tegengestelde lading geeft een mogelijke verklaring voor de zeer langzame evenwichtsinstelling in deze systemen.

H. A. van der Schee, J. Lyklema, J. Phys. Chem. 1984, 88, 6661

VIII

Om de stressbestendigheid te testen zouden aankomende topmanagers als onderdeel van de sollicitatie-procedure een tenniswedstrijd moeten spelen.

IX

In de tertiaire oliewinning is het sop de kool nog niet waard.

X

Liever "with love" dan met lof.

Proefschrift *Marcel Böhmer*

Adsorption and Micellization of Surfactants, Comparison of theory and experiment

Wageningen 17 december 1991

CHAPTER 1

Introduction	1
---------------------	----------

Surfactants	1
Outline of this study	5
References	6

CHAPTER 2

Micellization and Adsorption of Nonionic Surfactants

Analysis based on a self-consistent field lattice model	9
----------------------------------------------------------------	----------

Abstract	9
Introduction	9
SCFA theory	11
Choice of parameters	13
Results	15
Micelles and membranes	15
Adsorption on hydrophilic surfaces	18
Adsorption on hydrophobic surfaces	26
Conclusions	29
References	30

CHAPTER 3

Adsorption of Nonionic Surfactants on Hydrophilic Surfaces

An experimental and theoretical study on association in the adsorbed layer	33
-----------------------------------------------------------------------------------	-----------

Abstract	33
Introduction	33
Materials	36
Ludox AS40	36
Silicon Wafers	36
Surfactants and other chemicals	36
Methods	37

Determination of adsorption isotherms	37
Determination of layer thicknesses	38
Determination of solvent relaxation	39
Neutron reflection	40
Results	41
Adsorption isotherms	41
Layer thickness measurements	45
Mobility in the adsorbed layer	48
Segment density profiles	52
Theoretical method and results	61
Outline	61
Choice of parameters	64
Theoretical results	65
Discussion	70
Conclusions	71
References	72

CHAPTER 4

Micellization of Ionic Surfactants

<u>analysis based on a self-consistent field lattice model</u>	<u>75</u>
----------------------------------------------------------------	-----------

Abstract	75
Introduction	75
SCFA theory	78
General outline	78
Chain statistics	80
Electrostatic interactions	82
Excess and aggregation numbers	85
Thermodynamics of small systems	86
Numerical procedure	87
Choice of parameters	88
Results	90
Aggregate shape	90
Volume fraction profiles	91
Charge distribution and potential profile	96

Free energy of micelle formation	102
Micelle size and total surfactant concentration	104
Effect of salt concentration on the cmc	107
Branching	109
Aggregate shape and salt concentration	110
Conclusions	113
References	114

CHAPTER 5

Adsorption of Ionic Surfactants on Constant Charge Surfaces

Analysis based on a self-consistent field lattice model 117

Abstract	117
Introduction	117
SCFA theory	119
Lattice model and electrostatics	119
Volume filling	122
Contact interactions	123
Self consistency	123
Chain statistics	124
Choice of parameters	126
Results	127
Critical micelle concentrations	127
Adsorption isotherms	128
Structure of the adsorbed layer	131
Charge and potential profiles	133
Effect of the surface charge	136
Effect of chain length	139
Effect of adsorption energy	140
Discussion	141
Comparison: experimental results by Bijsterbosch	141
Aggregation in the adsorbed layer	144
Conclusions	146
References	147

CHAPTER 6

Adsorption of Ionic Surfactant on Variable Charge Surfaces I

Charge effects and structure of the adsorbed layer 149

Abstract	149
Introduction	149
Experimental	154
Chemicals	154
Adsorption Isotherms	154
Electrophoretic Mobilities	155
Surface charge determination	155
Experimental results	155
Adsorption as a function of salt concentration	155
Adsorption as a function of pH	158
Surface charge and surfactant adsorption	159
Counterion effect	164
Structure of the adsorbed layer	166
Adsorption of SNBS from Na ₂ SO ₄ solutions	167
SCFA theory	169
Introduction	169
Choice of parameters	170
Theoretical results	171
Adsorption isotherms at different salt concentrations	171
Volume fraction profiles	173
Quality of the predictions	175
Adsorption as a function of the surface potential	177
Surface charge and surfactant adsorption	178
Surface charge and head-on adsorption	181
Discussion	181
Constant charge and constant potential	181
Hemi-micelles or admicelles?	183
Conclusions	183
References	184

CHAPTER 7

Adsorption of Ionic Surfactants on Variable Charge Surfaces II

Molecular architecture and structure of the adsorbed layer 187

Abstract	187
Introduction	187
Experimental	190
Chemicals	190
Methods	190
Experimental results	191
Chain length	191
Branching	193
Aggregation in region II	194
SCFA theory	197
system and parameters	197
Theoretical results	198
Critical micelle concentrations	198
Chain length	198
Branching	200
Volume fraction profiles	202
Discussion	204
Conclusions	206
References	206
 SUMMARY	 209
SAMENVATTING	215
CURRICULUM VITAE	224
DANKWOORD	225

CHAPTER 1

Introduction

Surfactants

Surfactants tend to enrich strongly at interfaces. An important group of surfactants are the amphiphilic molecules, consisting of a hydrocarbon or hydrophobic part and a hydrophilic part. The hydrophobic part, the *tail*, prefers an apolar ("oil-like") environment over an aqueous one, the hydrophilic part, the *head*, prefers to be in contact with an aqueous solution rather than with an apolar medium. It is this property of surfactant molecules that makes them surface active; they will accumulate strongly at boundaries between an aqueous and an apolar phase. At the interface they will try to arrange themselves such that the hydrophilic part is towards the aqueous phase and the hydrophobic part towards the apolar phase.

The structure of surfactant molecules makes them useful chemicals in many processes such as cleaning, flotation, and tertiary oil recovery.⁽¹⁾ One mechanism of cleaning is that addition of an aqueous surfactant solution can lead to the solubilization of substances that would normally not dissolve in an aqueous solution. At sufficiently high concentration, surfactant molecules form micelles⁽¹⁻³⁾; aggregates of surfactant molecules with a hydrocarbon core consisting of tails and surrounded by head groups, see Figure (1) for a schematic representation. Due to the presence of the hydrophobic core, hydrophobic molecules can dissolve in the micelles, and, subsequently, be removed. In this way the use of organic solvents may be avoided. In many other systems surfactant aggregates serve as carriers for hydrophobic molecules. For instance, in micellar chromatography surfactants are used to separate molecules which have different solubility in micelles.^(4,5) In (bio)chemical reactions surfactant aggregates are often used for catalysis.^(1,6)

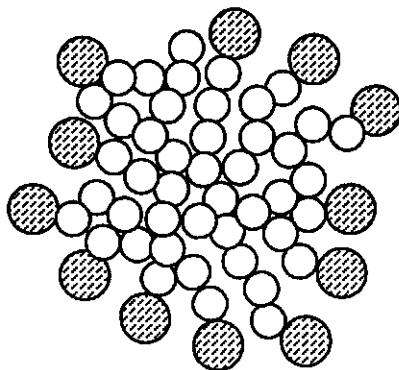


Figure 1: Schematic cross section of a micelle. The surfactant head groups, indicated as hatched circles, are mostly in the outer shell of the micelle where they have contacts with water, whereas the tails, indicated as a chain of white circles, are predominantly located in the micelle interior, forming the hydrophobic core.

Another separation technique, based on the adsorption of surfactants at the solid/liquid interface, is flotation. It is used to separate mixtures of fine particles, dispersed in an aqueous solution. Air bubbles are led through the mixture and they will stick to the more hydrophobic particles. Consequently, these particles will be transported to the liquid/air interface and can be separated from the others. In this way fractionation can be achieved on the basis of differences in hydrophobicity. The hydrophobicity of the particles can be affected by surfactant adsorption. For flotation the structure of the adsorbed layer is of crucial importance. If surfactants adsorb with their head groups on the surface and their tails towards the solution side, see Figure (2a), they provide for a nice hydrophobic outer surface for attachment of an air bubble. However, if more surfactant is added, a second layer may form as indicated in Figure (2b). Now the head groups on the solution side of the surfactant layer screen the hydrophobic part and bubble attachment will be hampered. As a

consequence the flotation recovery of a hydrophilic mineral may pass through a maximum as a function of the adsorbed amount.⁽⁷⁾

The last example is the use of surfactants in tertiary oil recovery. In principle, a high recovery can be obtained by flooding an oil reservoir with a surfactant solution. The function of the surfactant is to wash the oil out of the reservoir. One of the problems in the application of this technique is the loss of surfactant by adsorption on the reservoir rock surface. In order to prevent adsorption on the reservoir rock surface the surfactant molecules should be made selective, they should accumulate at the oil/water interface but not at the aqueous/solid interface.

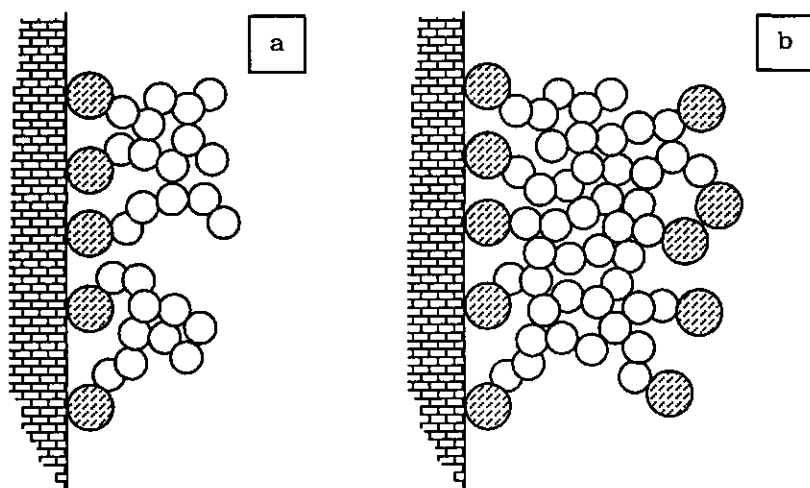


Figure 2: Schematic cross section of adsorbed layers of surfactants. In Figure (2a) the head groups (hatched) are on the surface and the tails (white) are located at the solution side. In Figure (2b) a bilayer has been formed, with a head group region both at the surface and the solution side, separated by a hydrophobic core.

Insight in the physical behavior of surfactants both in solution and near interfaces is a requirement for optimization of the use of surfactants. For solubilization purposes it is necessary to know at

what concentration micelle formation starts, what the structure of the micelle is, and how micelle formation is affected by varying the architecture of the surfactant molecules.^(3,8-12) In surfactant adsorption the adsorbed amount and structure of the adsorbed layer depend on molecular properties, concentration, and the interactions with the surface.^(13,14) The study of surfactant aggregates and surfactant adsorption is also interesting from a scientific point of view. To illustrate this it is noted that the head groups of the micelle in Figure (1) are not located exactly on the surface of a sphere but they have a fairly broad distribution. A similar head group distribution exists at the solution side of the bilayer, see Figure (2b). The structure of micelles and adsorbed layers remain to be investigated in more detail. Also the reasons for changes in the adsorbed layer, see Figures (2a) and (2b) have only been partially elucidated.

In dilute aqueous solutions surfactants will form micelles by association of their tails. These micelles are usually small because the head groups repel each other. For nonionic (uncharged) surfactants with long head groups this repulsion is caused by spatial restrictions, which is termed steric repulsion. For ionic surfactants the head groups are charged and they repel each other through electrostatic repulsion. The tendency of the tails to associate and the repulsion between head groups are also of major importance in surfactant adsorption. Therefore, there are advantages in combining the studies of surfactant adsorption and micellization. However, for adsorption on a solid surface also surface properties, such as the electrostatic charge and hydrophilicity, must be considered. For instance, on a hydrophobic surface the surfactant tails will attach to the surface, whereas on a hydrophilic surface the head groups will be in contact with the surface.

To study micellization and adsorption theoretically a model is needed in which the properties listed above are considered. We will use a model, which is essentially a version of the lattice models of Scheutjens et al.⁽¹⁵⁻¹⁹⁾ and Leermakers et al.⁽²⁰⁻²²⁾ for polymer adsorption and membrane formation, respectively. The model takes

many relevant properties of surfactants into account: (1) the distinction between head group and tail, (2) the fact that the chains are flexible, and (3) the interactions between the molecules, which can either be non-electrostatic, electrostatic, or steric.

The main result of the calculations are the volume fraction profiles, in an adsorbed layer or across a micelle. The volume fraction profiles of all components: surfactant head and tails, solvent, and, if present, salt ions, result from the minimization of the free energy. In this way information on the equilibrium structure of for instance the adsorbed layer is derived from first principles rather than that an a priori assumption is made as is done in many other models.^[23-26] From the volume fraction profiles the aggregation number of a micelle or the amount adsorbed on a surface at a certain equilibrium concentration can be calculated and they provide detailed information on the structure of the micelle or the adsorbed layer. In this thesis experiment and theory will be combined to obtain insight into the physics underlying the structural aspects of micelles and adsorbed layers of surfactants.

Outline of this study

To deal with different aspects of surfactants the thesis contains six other chapters. In chapter 2 the effect of the head group size on the micellization and adsorption of nonionic surfactants on hydrophilic and hydrophobic surfaces will be studied. In chapter 3 attention will be paid to a special case: the adsorption of nonionics with a long head group onto a hydrophilic surface. From experimental results obtained by various techniques, it will be shown that the basic theory is not suitable to describe this system. A modification will be used to obtain better agreement with experiment. The next four chapters deal with ionic surfactants. In chapter 4 the extension of the theory to describe ionic interactions will be presented and results will be given for micellization. In chapter 5 adsorption on a surface with a constant charge will be analyzed. Detailed comparisons will be made

with the adsorption data of ionic surfactants on silica.⁽²⁷⁾ In chapters 5 and 6 adsorption on surfaces with variable charge will be treated. Experimental results obtained for alkylbenzene sulfonates adsorbed on rutile will be compared with theoretical calculations with special reference to the electrostatic effects in chapter 6 and to those of the structure of the hydrophobic tails in chapter 7.

References

- 1 Rosen, M. J. "Surfactants and Interfacial Phenomena", 2nd ed. Wiley Interscience, NY, 1989
- 2 Tanford, C. "The Hydrophobic Effect", Wiley Interscience NY, 1980
- 3 Israelachvili, J. N.; Mitchell, D. J.; Ninham, B. W. *J. Chem. Soc. Faraday Trans. 2* **1976**, 72, 1525,
- 4 Hinze, W. L.; Armstrong, D. W. (ed) "Ordered Media in Chemical Separation", Am. Chem. Soc. Washinton D. C. 1987
- 5 Van der Horst, F. A. L. *Ph. D. Thesis*, University of Utrecht, The Netherlands, 1989
- 6 Dekker, M.; Hilhorst, R.; Laane, C. *Analyt. Biochem.* **1989**, 178, 217
- 7 Mishra, S. K., Surfactant Science Series **1988**, 27, 195
- 8 Evans, H. C. *J. Chem. Soc.* **1956**, 117, 579
- 9 Engberts, J. B. F. N.; Nusselder, J. J. H. *Pure and Appl. Chem.* **1990**, 62, 47
- 10 Binana-Limbélé, W.; Van Os, N. M.; Rupert, L. A. M.; Zana, R. *J. Colloid Interface Sci.* **1991**, 141, 157
- 11 Gruen, D. W. R. *J. Phys. Chem.* **1985**, 89, 146
- 12 Szleifer, I.; Ben Shaul, A.; Gelbart, W. M. *J. Chem. Phys.* **1986**, 85, 5345
- 13 Hough, D. B.; Rendall, H. M. in "Adsorption from Solution at the Solid/Liquid Interface", Parfitt, G. D.; Rochester, C. H. eds. Academic Press, London 1983 p. 247
- 14 Chander, S.; Fuerstenau, D. W.; Stigter, D. in "Adsorption from Solution", Ottewill, R. H.; Rochester, C. H.; Smith, A. L. Eds. Academic Press London 1983 p197
- 15 Scheutjens, J. M. H. M. *Ph. D. Thesis*, Wageningen Agricultural University, The Netherlands, 1985
- 16 Scheutjens, J. M. H. M.; Fleer, G. J. *J. Phys. Chem.* **1979**, 83, 1619
- 17 Scheutjens, J. M. H. M.; Fleer, G. J. *J. Phys. Chem.* **1980**, 84, 178
- 18 Evers, O. A.; Scheutjens, J. M. H. M.; Fleer, G. J. *Macromolecules* **1990**, 23, 5221
- 19 Böhmer, M. R.; Evers, O. A.; Scheutjens, J. M. H. M. *Macromolecules* **1990**, 23, 2288
- 20 Leermakers, F. A. M. *Ph. D. Thesis*, Wageningen Agricultural University, The

Netherlands, 1988

- 21 Leermakers, F. A. M.; Scheutjens, J. M. H. M. *J. Chem. Phys.* **1988**, *89*, 3264
- 22 Leermakers, F. A. M.; Scheutjens, J. M. H. M. *J. Colloid Interface Sci.* **1990**, *136*, 231
- 23 Gu, T.; Rupprecht, H. *Colloid Polym. Sci.* **1990**, *268*, 1148
- 24 Scamehorn, J.; Schechter, R. S.; Wade, W. H. *J. Colloid Interface Sci.* **1982**, *85*, 463
- 25 Harwell, J. H.; Hoskins, J. C.; Schechter, R. S.; Wade, W. H. *Langmuir* **1985**, *1*, 251
- 26 Cases, J. M. *Bull. Minéral.* **1979**, *102*, 684
- 27 Bijsterbosch, B. H. *J. Colloid Interface Sci.* **1974**, *47*, 186

CHAPTER 2

Micellization and Adsorption of Nonionic Surfactants

Analysis based on a self-consistent field lattice model

Abstract

An extension of the self-consistent field theory for chain molecules of Scheutjens and Fleer is used to study the micellization of non-ionic surfactants and their adsorption from aqueous solution on hydrophilic and hydrophobic surfaces. The theory predicts that the critical micelle concentration increases and the aggregation number decreases if the hydrophilic block becomes longer. This is in agreement with experimental findings. On hydrophilic surfaces, where the chains adhere with their hydrophilic segments to the surface, the affinity increases with the hydrophilic chain length. The adsorption isotherm reaches a plateau value at the cmc. At constant hydrophobic block length, the plateau adsorption decreases with increasing length of the hydrophilic block. If the ratio between the number of hydrophobic and hydrophilic segments is around one, strong cooperative adsorption and the formation of a "surfactant bilayer" are predicted. On a hydrophobic surface the hydrophobic segments adhere to the surface and for all chain lengths studied a monolayer of surfactant is predicted. Also in this case the plateau adsorption decreases with increasing length of the hydrophilic chain. The results agree well with experimental results for both types of surfaces.

Introduction

The adsorption from solution of flexible, low molecular weight amphiphilic molecules, such as surfactants, has been frequently investigated because of its importance in many fields of science. Several models have been developed to describe surfactant adsorption on homogeneous and heterogeneous surfaces, see e.g. refs (1-8). In the models for ionic surfactants⁽¹⁻⁶⁾, the head groups are assumed to form the boundary of the adsorbed layer on either the adsorbent or solution side (surfactant monolayer model) or on both

sides of the adsorbed layer (surfactant bilayer model). With modeling of nonionic surfactants a homogeneous adsorbed layer^(4,7) or a three stage adsorption process⁽⁸⁾ is assumed. The main disadvantage of all these models is that assumptions are made on the segment density distributions in the adsorbed layer. Such assumptions are not required in modern statistical thermodynamic treatments, like the self-consistent field theory by Scheutjens and Fler, originally developed to study the adsorption of homopolymers from solution.^(9,10)

Recently the theory by Scheutjens and Fler has been modified to study the behavior of amphiphilic chain molecules near interfaces^(11,12) and an extension has been presented which describes the association of amphiphilic molecules in solution, such as micellization and membrane formation.^(11,13) We will denote the modern version of the theory with the letters SCFA, self-consistent field theory for adsorption or association. In the case of association in solution the SCFA theory, which describes the formation of one micelle or membrane, has been combined with the thermodynamics of small systems.⁽¹⁴⁾ In the SCFA theory all molecules are allowed to distribute themselves throughout the system, consisting of a bulk solution in contact with an interface or a specific type of aggregated structure. The equilibrium density profile for each type of segment is found as the result of the minimization of the free energy of the system.

In this paper we will use the SCFA theory to study the behavior of nonionic surfactants in solution and adsorbed on a hydrophilic or a hydrophobic interface. The series of surfactants studied has a fixed number of hydrophobic segments and a varying number of hydrophilic segments. We will compare the calculations with experimental results for the micellization of alkyl(phenol) poly(oxyethylenes)^(15,16) and their adsorption on hydrophilic silica⁽¹⁶⁻¹⁸⁾ or hydrophobic latices.^(19,20) For a description of the SCFA theory for amphiphilic molecules we refer to literature.^(4,9,11) Here we will only summarize the main principles.

SCFA theory

In the SCFA theory each molecule is seen as a sequence of segments all equal in size. The molecules are placed in a lattice, which facilitates the counting of conformations of the molecules. The lattice consists of M lattice layers numbered $z = 1, \dots, M$. To study the association of amphiphilic chain molecules in solution and the adsorption of these molecules from solution, we use two lattice geometries: flat and spherical. In a lattice of flat geometry, the number of lattice sites in each lattice layer is the same. A flat lattice can be used to study flat aggregates such as membranes^(11,13) and adsorption on flat surfaces.^(9,10,11) In the case of adsorption layer 1 is adjacent to the solid surface (layer 0). In a lattice with spherical geometry the number of lattice sites per layer increases with increasing layer number, starting from layer 1 in the centre of the lattice. Using a spherical lattice we can study globular associated structures to which we will refer as micelles.⁽¹¹⁾

Every lattice site in the system is filled by a solvent molecule or a segment of an amphiphilic molecule; consequently, the sum of the volume fractions is unity in every lattice layer. Each layer is assumed to be homogeneous, i.e., a mean field approximation is used within a layer. However, in direction z , perpendicular to the lattice layers, a concentration gradient may exist for each type of segment. The solvent is modeled as a monomer of segment type W (water). Its volume fraction in layer z is denoted by $\phi_W(z)$. The amphiphilic molecules are flexible chains consisting of a series of segments of type A and a series of segments of type B . The total chain length is r . The volume fractions of A and B in layer z are given by $\phi_A(z)$ and $\phi_B(z)$, respectively. The total volume fraction of the amphiphilic segments i in layer z equals $\phi_i(z) = \phi_A(z) + \phi_B(z)$. The equilibrium volume fraction of a molecule i in the bulk solution is given by ϕ_i^b , for the surfactant: $\phi_i^b = \phi_A^b + \phi_B^b$.

The various segments are allowed to interact with each other and with the solvent. The magnitude of the contact interaction between

segment types x and y is expressed by Flory-Huggins interaction parameter χ_{xy} . The expression for the Gibbs energy of a free segment x in layer z , relative to that in the bulk solution, shortly the potential $u_x(z)$, reads⁽¹¹⁾

$$u_x(z) = u'(z) + kT \sum_y \chi_{xy} (\langle \phi_y(z) \rangle - \phi_y^b) \quad (1)$$

The contact fraction $\langle \phi_x(z) \rangle$ is a weighted volume fraction to account for the fact that segment x in layer z has also contacts in layers $z-1$ and $z+1$. For flat symmetry we used a hexagonal lattice where the fraction of contacts in each of the adjacent layers, λ_1 , is 0.25 and the fraction of contacts in the same layer, λ_0 , is 0.5. For spherical lattices the contact fractions are equal to those of a hexagonal lattice when z approaches infinity. The equations for the λ values in a curved lattice have been given elsewhere.⁽¹¹⁾ The potential $u'(z)$ is independent of the segment type and accounts for the fact that the sum of the volume fractions in layer z has to equal unity. For a monomeric solvent (water, W, in our case) $u'(z)$ reduces to $\ln(\phi_W^b / \phi_W(z))$, which is directly related to the entropy of mixing in each layer.

The conformational statistics of the amphiphilic molecules in the lattice are evaluated using a step weighted walk procedure, which is given elsewhere.^(9,11) Each step depends on the position of the previous segment and is weighted with a segment weighting factor $G_x(z)$ defined as

$$G_x(z) = \exp(-u_x(z) / kT) \quad (2)$$

The expression for $u_x(z)$ is given by eq (1). The most probable set of conformations corresponds with the situation where the system is at its minimum free energy. As the volume fractions are calculated from the potentials but also determine the potentials, see eq (1), numerical methods must be applied to find the self-consistent

potential field and the corresponding equilibrium volume fraction profile.

The segment density profiles are used to calculate the excess amount, θ_i^{exc} , in either an associated structure or in the adsorbed layer. In the case of adsorption, the excess amount of segments i is conveniently expressed per surface site:

$$\theta_i^{exc} = \sum_z (\phi_i(z) - \phi_i^b) \quad (3)$$

For practical systems the amount adsorbed is often expressed as the number of molecules per unit surface area. This quantity is closely related to n_i^{exc} or θ_i^{exc} divided by the chain length r_i of molecule i :

$$n_i^{exc} = \theta_i^{exc} / r_i \quad (4)$$

For spherical aggregates in solution, θ_i^{exc} , is usually given as the excess amount of segments of molecule i in the system:

$$\theta_i^{exc} = \sum_z L(z)(\phi_i(z) - \phi_i^b) \quad (5)$$

where the number of lattice sites in layer z is given by $L(z)$.

With respect to the formation of association structures it should be noted that if the total volume fraction, $\bar{\phi}_i$, of amphiphile is larger than the critical micelle or critical membrane volume fraction, micelles or membranes will be present. The adsorption of amphiphile is now determined by the equilibrium bulk volume fraction of free surfactant, which remains nearly constant upon increasing the total volume fraction.

Choice of parameters

With the interaction parameters chosen, the properties of nonionic surfactants in water, such as their capability of forming micelles, should be reproduced. The Flory-Huggins parameter χ_{AW} for the

interaction between a segment of type A and the solvent W should reflect the poor solubility of segments A in the solvent W. To achieve this, we have chosen $\chi_{AW} = 2$. The A segments are hydrophobic and the interaction between A and W can be compared with the interaction between CH_2 groups and water. With $\chi_{AW} = 2$, the dependence of the critical micelle concentration, cmc, of A_nB_m as a function of the hydrophobic block length n corresponds with the experimentally observed dependence of the cmc on alkyl chain length.

The interaction parameter χ_{BW} between segments of type B and the solvent W has been given the value 0.4, indicating that the solvent is a moderately good solvent for B. This value agrees with the interaction parameter between poly(oxyethylene) and water derived by Van den Boomgaard⁽²¹⁾ and by Amu.⁽²²⁾ The value of χ_{BW} has some effect on the cmc of an A_nB_m surfactant: lower values of χ_{BW} lead to higher cmc's. The increase in cmc with the length of the B block, however, hardly depends on the precise value of χ_{BW} , as long as χ_{BW} is between 0 and 0.5.

The interaction between the hydrophilic segments B and the hydrophobic segments A should be repulsive. To mimic moderately strong repulsion between segments A and segments B, we have chosen $\chi_{AB} = 2$. Such a high value has to be chosen to ensure spatial separation of head group segments and tail segments, which is necessary for the formation of micelles. At low χ_{AB} values, below 1.5, no stable micelles can be formed.

The interactions with the surface will be specified later.

Above, the segments of type B are used as a model for EO units, whereas the segments of type A should mimic CH_2 groups. It is obvious that an EO unit is much bigger than a CH_2 group; nevertheless we use one segment of type A for a CH_2 group and one segment of type B for an EO unit. If we would take three segments for an EO unit, the chain flexibility would be overestimated and if we group 3 CH_2 groups in one segment, very large positive values of χ_{AW}

have to be taken, which, unfortunately, lead to enormous lattice artifacts. In principle the problem of limited chain flexibility can be tackled by application of a rotational isomeric state scheme.^[23] Such a more rigorous treatment will not affect the trends in adsorption and micellization of amphiphilic chain molecules very strongly. For the moment we have used the more simple first order Markov statistics.

Results

Micelles and Membranes

To study the association behavior, calculations were performed for a series of $A_{10}B_n$ molecules in lattices with spherical and flat geometry. The critical micelle volume fraction and the critical membrane volume fraction are obtained as described in ref (11). The critical micelle volume fraction and critical membrane volume fraction divided by the total chain length of the amphiphilic molecule are measures for the critical concentrations, at which these aggregates are formed. The concentration where phase separation occurs can be calculated using the extended Flory-Huggins formulas for the chemical potential of amphiphilic molecules, also given in ref (11).

Results with respect to the association behavior for the series $A_{10}B_n$ as a function of n are shown in Figure (1). If the number of B segments is smaller than three no membrane or micelle formation occurs but phase separation takes place. If the number of B segments is more than three, micelles are preferred over membranes and the formation of two phases: the equilibrium solution concentration ϕ/r , and hence the chemical potential, at which micelles are formed is lower than the concentration required for membrane formation or phase separation.

The cmc increases approximately linearly with the number of segments of type B. This agrees with experimental results for octylphenol poly(oxyethylenes)^(16,17) and decyl-poly(oxyethylenes).⁽¹⁵⁾ With the interaction parameters chosen the increase in the cmc with increasing length of the head group B_n is well predicted for octylphenol poly(oxyethylenes): the cmc doubles if the number of head group segments increases from 12 to 30. For small B blocks the calculated slope is somewhat smaller than found experimentally for monodisperse decyl-poly(oxyethylenes). We stress that for long EO blocks no monodisperse samples are available; therefore, we had to compare our calculated results with surfactants that have polydisperse head groups.

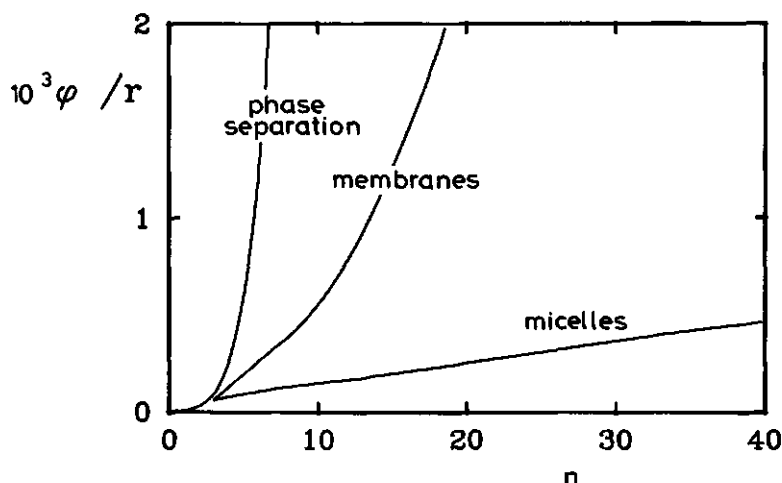


Figure 1: Equilibrium volume fractions of $A_{10}B_n$ molecules, for phase separation, membrane formation and micelle formation as a function of the B block length. $\chi_{AW} = \chi_{AB} = 2$, $\chi_{AB} = 0.4$.

With increasing length of the head group the molecules become more hydrophilic and, in associated structures, the steric hindrance between the head groups increases. The latter effect is especially evident from the growing difference between the critical membrane

concentration and the critical micelle concentration if the length of the B block becomes longer. In flat aggregates there is more steric hindrance between the head groups than in globular aggregates. The number of lattice sites per layer increases with z in a spherical lattice. This gives the head groups, which are located in the outer region of the spherical structure considerably more space.

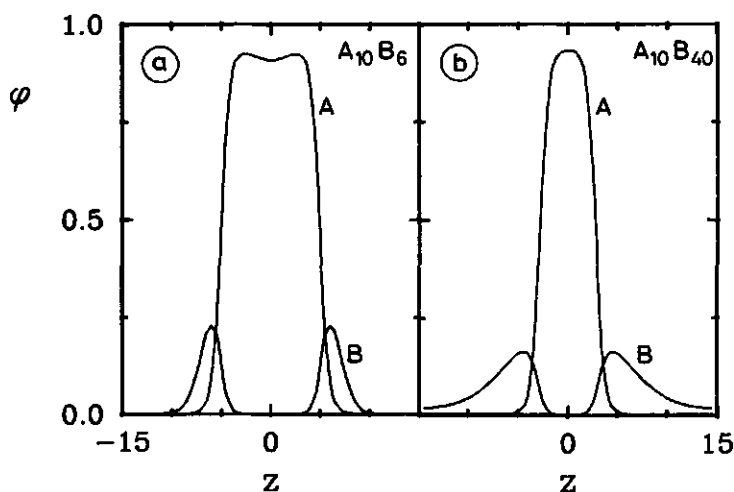


Figure 2: Volume fraction profiles for $A_{10}B_6$ (a) and $A_{10}B_{40}$ (b) micelles. The volume fractions for segments of type A and type B are indicated. The overall concentration $\bar{\phi}/r$ is 5×10^{-4} . See Figure (1) for the interaction parameters.

In Figure (2) the segment density profiles of the A and B segments in $A_{10}B_6$ and $A_{10}B_{40}$ micelles are shown at the same overall concentration ($\bar{\phi}_t/r = 0.5 \times 10^{-3}$). The segments of type A are in the center of the micelle while the B segments are on the outside. Some solvent is still present in the interior of the micelle (not shown in the figure), which is an artifact due to the poor model used for water: a monomer without a preferential orientation. The aggregation number of $A_{10}B_6$ molecules is much bigger than that of $A_{10}B_{40}$ although the number of B segments in both micelles are not too different. Steric hindrance between the hydrophilic B blocks prevents the formation of large micelles of $A_{10}B_{40}$.

The number of molecules per micelle at a constant overall concentration ($\bar{\phi}_l/r = 0.5 \times 10^{-3}$) decreases with increasing length of the B block, especially for relatively small B blocks. This is shown Figure (3). This trend compares well with the experimental trend in the aggregation numbers measured for octylphenol poly(oxy-ethylenes)^(16,17) using pyrene solubilization.

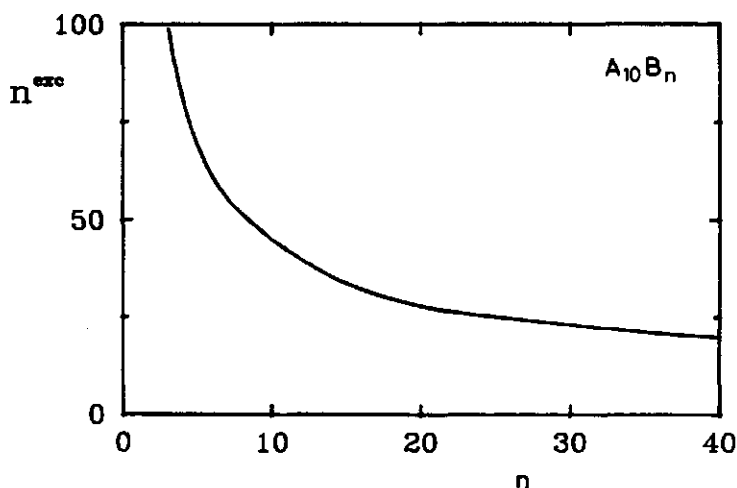


Figure 3: The aggregation number of $A_{10}B_n$ micelles at a constant overall concentration of 5×10^{-4} as a function of the number of B segments in the molecule. See Figure (1) for interaction parameters.

Adsorption on Hydrophilic Surfaces

Adsorption isotherms were calculated for the same homologous series of amphiphilic molecules $A_{10}B_n$. Upon adsorption of a segment only a fraction λ_1 of its contacts with the solution are replaced by contacts with the surface. The segment free energy of displacement, $\chi_{d(x)}$ of a water molecule on the surface by a segment of type x can be defined as

$$\chi_{d(x)} = \lambda_1 (\chi_{xs} - \chi_{xw} - \chi_{ws} + \chi_{ww}) \quad (6)$$

By definition $\chi_{ww} = 0$, furthermore χ_{ws} is chosen to be 0 since only the differences between the χ_{xy} values determine the free energy of displacement. In general the hydrophilic segments will have a relatively strong interaction with the surface and the hydrophobic segments a weak interaction. Let us assume that $\chi_{BS} = -6$ and $\chi_{AS} = 0$, then $\chi_{d(B)} = -1.6$ and $\chi_{d(A)} = -0.5$. The sensitivity for the adsorption for the value of $\chi_{d(x)}$ will be discussed below.

Results are presented in Figure (4a) for 6 different values of n . On the horizontal axis the *overall* concentration is given as $\bar{\phi}/r$. The cmc values are indicated with an asterisk. Above the cmc the volume fraction of free chains hardly increases; consequently, a (pseudo) plateau in the adsorption isotherm is reached if the B block is not too long. For a B block considerably longer than the A block (i.e. $A_{10}B_{30}$ and $A_{10}B_{40}$) the adsorption reaches a near saturation value before the cmc is reached and the shape of the isotherms is similar to that of a homopolymer of type B. The $A_{10}B_{16}$ takes an intermediate position. The small irregularities in the adsorption isotherms are caused by lattice artifacts, which become more prominent if high χ -values are chosen.

At very low volume fractions, the affinity increases with increasing length of the B block, see Figure (4b). At very low adsorbed amounts the B block adsorbs in a predominantly flat conformation, and interaction between adsorbed chains does not occur (isolated chain). Since chains with more B segments have a higher adsorption (free) energy, these chains show more adsorption in the limit of isolated chains. On the other hand, the cooperativity in the adsorption with increasing volume fraction is stronger if the B block is smaller. This increase in adsorption must be due to unfavorable interaction between A segments and solvent: the A segments associate to reduce the number of contacts with the solvent. The association is more pronounced if the A/B ratio increases, a similar trend was found from the influence of the A/B ratio on the cmc.

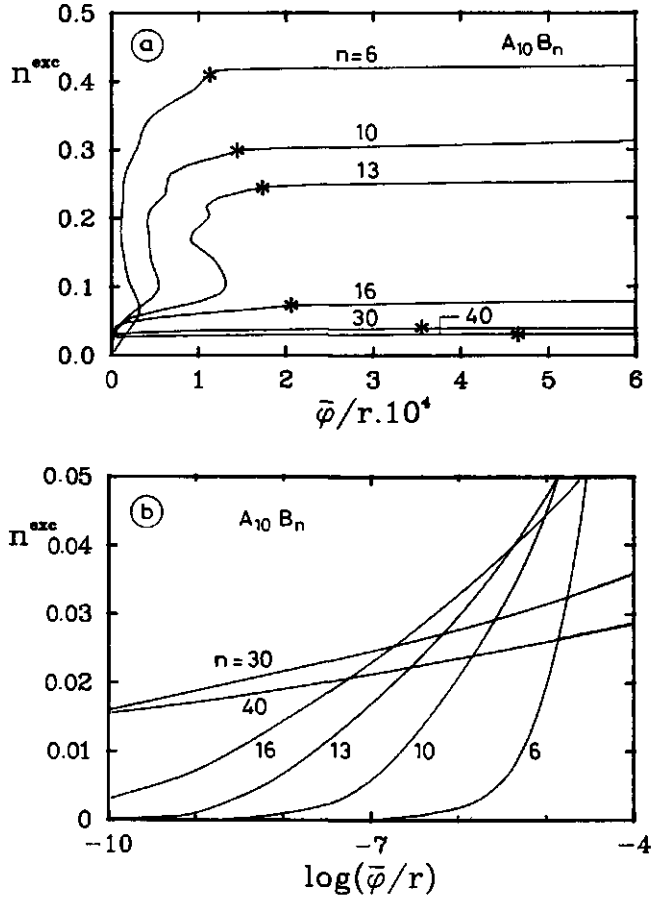


Figure 4: Adsorption isotherms for amphiphilic chain molecules on a hydrophilic surface (4a) An asterisk indicates the cmc. The initial part of the adsorption isotherms is shown in (4b). The interaction parameters are $\chi_{BS} = -6$, $\chi_{AS} = \chi_{WS} = 0$, $\chi_{AW} = \chi_{AB} = 2$, $\chi_{BW} = 0.4$.

The A/B ratio also affects the maximum attainable adsorption, see Figure (4a): the higher the A/B ratio, the higher the adsorption at the cmc. For $A_{10}B_6$, $A_{10}B_{10}$, and $A_{10}B_{13}$, the shape of the isotherm indicates that phase separation or "surface condensation" occurs in the adsorbed layer, due to association of the A segments. As a consequence the adsorption will increase stepwise and a surfactant

bilayer is formed. If the B block is long, steric hindrance prevents such bilayer formation. This compares well with the fact that the difference between the critical micelle concentration and the critical membrane concentration increases if the B block becomes longer. $A_{10}B_{16}$ reaches its cmc just before the bilayer can form, but the effect of the presence of the segments of type A is still prominent.

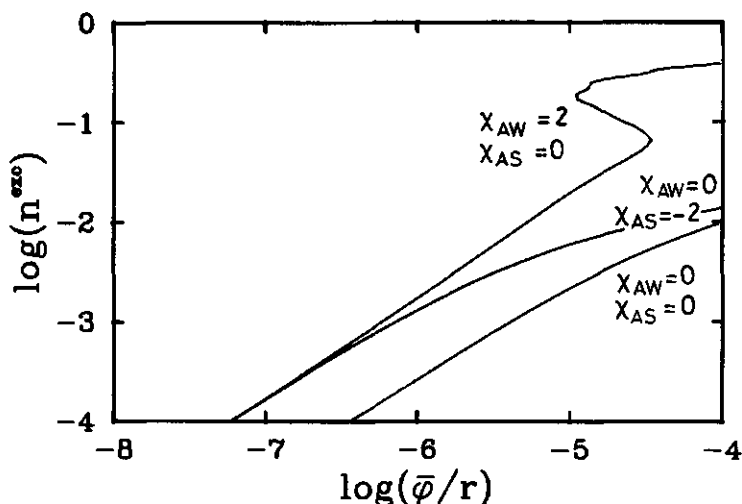


Figure 5: Adsorption isotherms of $A_{10}B_6$ for different values of χ_{AW} and χ_{AS} (indicated). Values for the other interaction parameters are the same as in Figure (4).

To study the effect of the interaction between water and a segment of type A on the adsorption of $A_{10}B_6$ in more detail, calculations were performed with $\chi_{AW} = 0$ and all other interaction parameters the same as in the previous calculations. The results are given in Figure (5), where the isotherm of $A_{10}B_6$ with $\chi_{AW} = 2$ is also shown. The adsorbed amount for $A_{10}B_6$ with $\chi_{AW} = 0$ is lower than the adsorption for $A_{10}B_6$ with $\chi_{AW} = 2$ for all concentrations. The lateral interactions between segments of type A have disappeared if $\chi_{AW} = 0$, but also the free energy of displacement has become less negative, see eq (6).

Replacement of AW contacts by AS contacts is no longer favorable, which is the reason that the isotherms do not coincide at low coverages. If χ_{AS} is changed to -2 while $\chi_{AW} = 0$, the free energy of displacement is the same as for the combination $\chi_{AW} = 2$ and $\chi_{AS} = 0$, in that case the calculated isotherm does coincide with the isotherm of $A_{10}B_6$ with $\chi_{AW} = 2$ at very low coverages, see Figure (5). An increase in the concentration leads at low adsorption values to a deviation. Due to the association of A segments the $\chi_{AW} = 2$ isotherm increases more strongly.

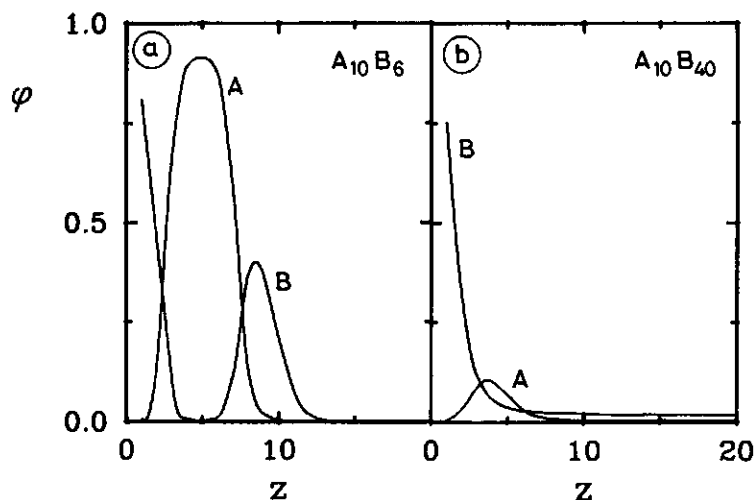


Figure 6: Volume fraction profiles of $A_{10}B_6$ (a) and $A_{10}B_{40}$ (b) in the adsorbed layer at the plateau of the isotherm on a hydrophilic surface. The volume fractions of segments of type A and of type B are indicated. See Figure (4) for interaction parameters.

Clearly a small net displacement energy of A on the surface has a pronounced effect on the initial part of the isotherm, see Figure (5). The plateau of the adsorption isotherm, however, is almost independent of χ_{AS} as long as (the absolute value of) χ_{AS} is small compared to χ_{BS} , because at higher surface coverages the A segments are displaced by B segments.

The volume fraction profiles, $\phi_x(z)$, in the plateau of the isotherm are given in Figure (6) for segments of type A and type B for $A_{10}B_6$ and $A_{10}B_{40}$. For $A_{10}B_6$ a thick asymmetrical surfactant bilayer is formed, B segments are present both at the surface and at the solution side, spatially separated from each other by a layer of segments of type A. For $A_{10}B_{40}$ no maximum in the volume fraction of B segments at the solution side is found, no bilayer is formed. Adsorbed and free surfactant bilayers become more and more unfavorable as the number of B segments rises. Note that the adsorbed layer thickness is considerably smaller than twice (e.g. $A_{10}B_6$) or once (e.g. $A_{10}B_{40}$) the extended chain length.

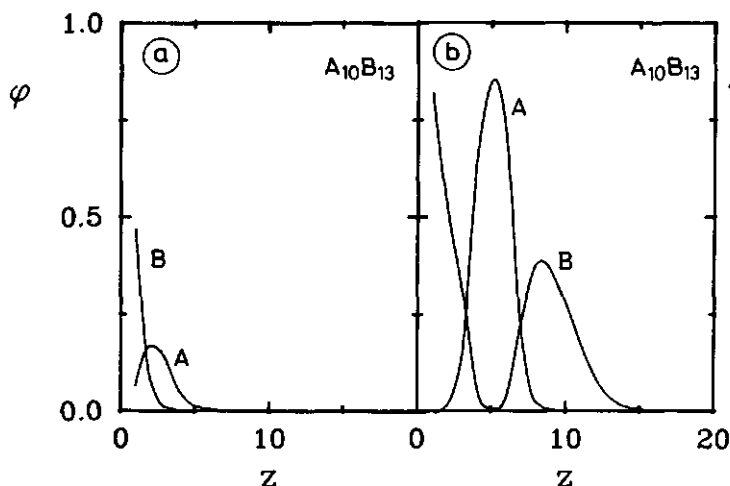


Figure 7: Volume fraction profiles of $A_{10}B_{13}$ just before (a) and after (b) the phase separation in the adsorbed layer. See Figure (4) for interaction parameters.

In Figure (7) the segment density distributions for $A_{10}B_{13}$ are shown at a bulk volume fraction just before the phase transition at the surface occurs (Figure 7a) and at a bulk volume fraction corresponding with the plateau of the isotherm (Figure 7b). At low bulk volume fraction the segment density distributions resemble

those of $A_{10}B_{40}$. Beyond the phase transition, the segment density profiles are comparable to those of $A_{10}B_6$. However, the hydrophobic core of the surfactant bilayer formed by $A_{10}B_{13}$ is much thinner than that of $A_{10}B_6$, due to steric hindrance between the B blocks for $A_{10}B_{13}$.

The calculated isotherms can be compared with experimental results by Levitz and Van Damme^(16,17) who measured the adsorption of a series of alkylphenol poly(oxyethylenes) on Spherosil, a hydrophilic silica. Their adsorption isotherms are replotted in Figure (8). Very similar isotherms were measured by Partyka et al.⁽¹⁸⁾ for the same system. Also for other nonionic surfactants, like decyl methyl sulfoxide, adsorbed onto silica, similar isotherms were found.⁽²⁴⁾ The experimental trend is well reproduced by our calculations. A step in the isotherm has been found experimentally for octylphenol $(EO)_6$, which has a monodisperse EO block. The isotherms of the polydisperse octylphenol $(EO)_{9.5}$ and octylphenol $(EO)_{12.5}$ increase more gradually than predicted by the SCFA theory. This might be due to polydispersity, which is probably also the reason for the increase in adsorption above the cmc.

Calorimetric data of Denoyel et al.⁽²⁵⁾ with the same systems show two domains: at low adsorbed amounts the heat effect is exothermal, and the contacts between surface and surfactant segments are enthalpically favorable. At higher adsorption values an endothermal effect is observed, with a molar enthalpy which is of the same order of magnitude as the molar enthalpy of micellization, indicating the role of hydrophobic lateral interaction. With an increase in EO length, the heat effect at low coverage is enlarged whereas at higher coverages the endothermic effect is diminished. These trends are in agreement with the present calculations, where we also find two domains in the adsorption isotherm. The first part is dominated by the adsorption of B segments on the surface, the second part stems from the accumulation of A segments.

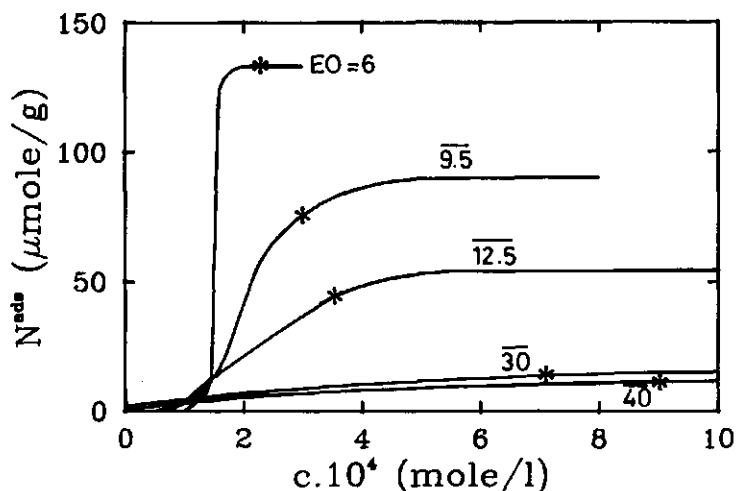


Figure 8: Adsorption isotherms of octylphenol poly(oxyethylenes) on Spherosil.⁽¹⁷⁾ The cmc's are indicated with an asterisk. The average value of the number of EO-units is given.

Using pyrene as a fluorescent probe, Levitz et al.^(16,17) studied the structure of the adsorbed layer of octylphenol poly(oxyethylenes). Pyrene solubilization was found to occur for all chain lengths studied, indicating that a non-polar domains exist in the adsorbed layer. For surfactants with small head groups a homogeneous adsorbed layer was formed in the plateau of the isotherm. For surfactants with longer head groups, however, aggregates were formed on the surface with sizes comparable to the sizes of micelles. In our calculations we find bilayer formation if the B block is shorter than 16 segments, in agreement with the measurements by Levitz et al. With the SCFA theory we cannot calculate aggregation numbers in the adsorbed layer, as we used a simple planar geometry in combination with the mean field approximation within each lattice layer. Nevertheless, we also find, already at very low volume fractions, a large effect of the lateral attraction on the adsorption, see Figures (4) and (5).

Adsorption on Hydrophobic Surfaces

To study the adsorption of $A_{10}B_n$ molecules on hydrophobic surfaces, the Flory-Huggins interaction parameter between the segments of type A and the surface S is set to -4 and both for B segments and water $\chi_{Sx} = 0$. Hence in this case the free energy of displacement of a water molecule on the surface by an A segment is given by -1.5 and that of a B segment by -0.1 , see eq (6).

The calculated isotherms are given in Figure (9). The adsorption isotherms as presented in Figure (9a) seem of the Langmuir type. The increase in adsorption with concentration levels off considerably before the cmc is reached for all isotherms. A pseudo-saturation adsorption is reached at the cmc for $A_{10}B_6$, $A_{10}B_{10}$ and $A_{10}B_{13}$. For the $A_{10}B_{30}$ and $A_{10}B_{40}$ surfactants the plateau value is reached before the cmc. Chains with small B blocks show a higher adsorption in the plateau region and are more high affinity than chains with larger B blocks. The decrease in adsorption on hydrophobic surfaces with increasing length of the B block and the shape of the adsorption isotherms agree with experimental isotherms of a series of nonylphenol poly(oxyethylenes) on polystyrene and poly(methyl methacrylate) as measured by Kronberg et al.^(19,20)

The initial part of the isotherms is enlarged in Figure (9b). Because the number of A segments per molecule is the same for all chain lengths the adsorption isotherms coincide at low surface coverages. Figure (9b) also reveals that the isotherms are not really of the L-type, as soon as some material is present at the surface a strong increase in the adsorption occurs for chains with relatively small B blocks, due to the association of the hydrophobic chains. If the head group is long, steric hindrance between the B segments prevents strong association of the A blocks. For $n = 6$ a weak surface condensation occurs.

The effect of the solubility of A segments in water on the adsorption was studied by comparing the isotherms for $\chi_{AW} = 2$ and $\chi_{AW} = 0$.

Calculated results for $A_{10}B_6$ are presented in Figure (10). If $\chi_{AW} = 0$ and all other interaction parameters are unchanged, the adsorption is smaller than the adsorption for $A_{10}B_6$ with $\chi_{AW} = 2$ for all concentrations. For $\chi_{AW} = 0$ no association of A segments occurs and the free energy of displacement has changed because AS contacts are no longer favored over AW contacts. If the free energy of

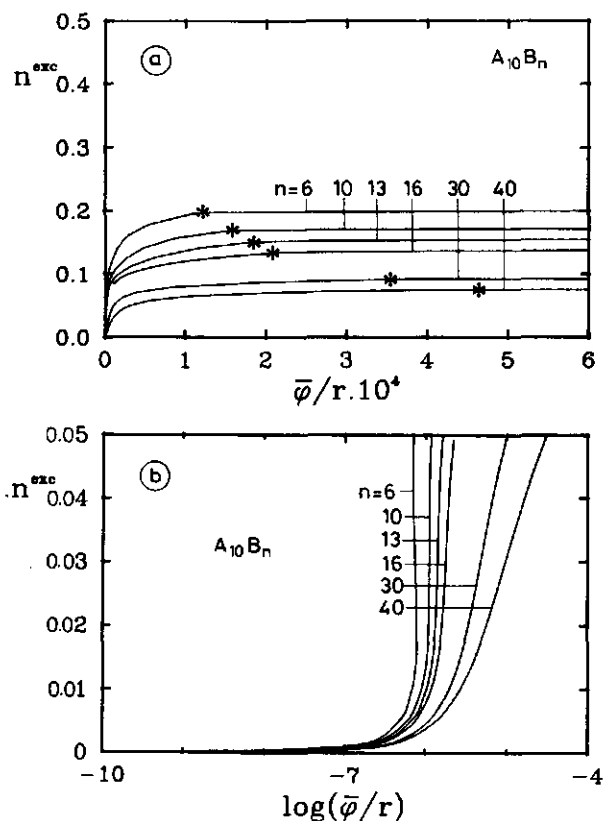


Figure 9: Calculated adsorption isotherms for a series of amphiphilic chain molecules with a varying number of hydrophilic (B) segments on a hydrophobic surface (9a). The initial part of the isotherms is shown in Figure (9b). The cmc's are indicated with an asterisk. The interaction parameters are $\chi_{AS} = -4$, $\chi_{BS} = 0$, $\chi_{AW} = \chi_{AB} = 2$ and $\chi_{BW} = 0.4$.

displacement is kept the same, which is achieved by taking $\chi_{AS} = -6$. the isotherms coincide at very low surface coverage but deviate at higher coverage because of the lateral attraction between A segments. The surface condensation already noted for $A_{10}B_6$ in Figure (9b) shows up more clearly in the top isotherm.

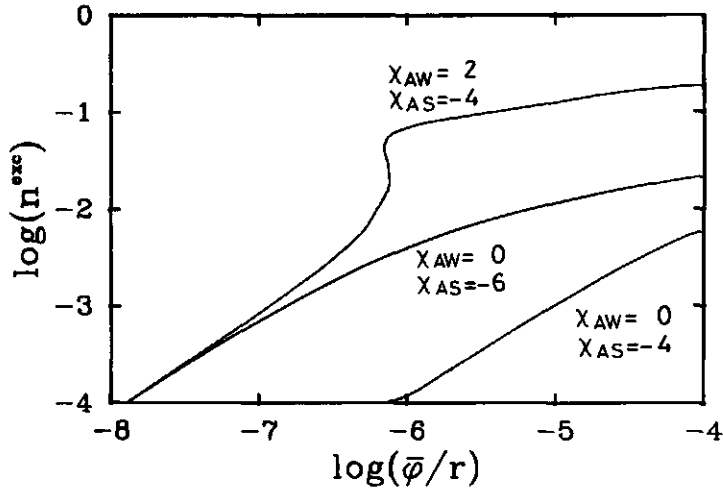


Figure 10: Calculated adsorption isotherms of $A_{10}B_6$ for different values of χ_{AW} and χ_{AS} (indicated). Values for the other interaction parameters are the same as in Figure (9).

Volume fraction profiles of the various segment types in the adsorbed layer at the plateau of the adsorption isotherm are given in Figure (11) for $A_{10}B_6$, $A_{10}B_{13}$ and $A_{10}B_{40}$. The A segments are located at the surface side, the B segments are at the solution side. The height and the position of the maximum in the volume fraction profile of segments B hardly changes if the length of the B block changes. The B segments are accommodated by making the distribution wider and more skewed. This shows that steric hindrance due to the B blocks is the limiting factor for the adsorption of $A_{10}B_n$ molecules with a long B block on hydrophobic surfaces. In a similar fashion as for the hydrophilic surface the

adsorbed layer thickness at the adsorption plateau is in all cases much smaller than the extended chain length.

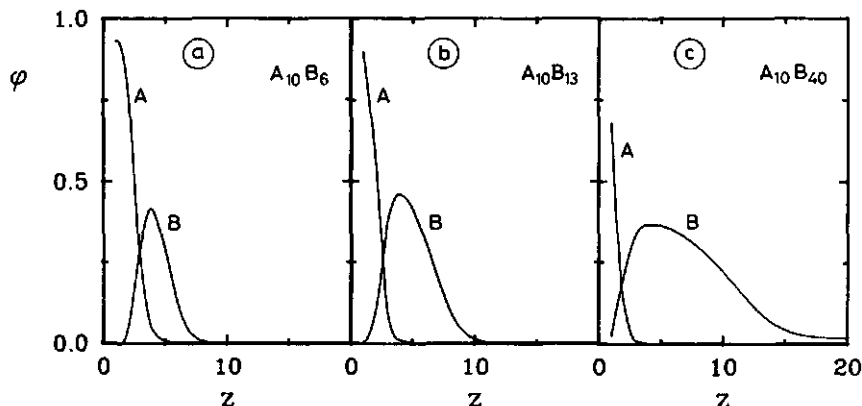


Figure 11: Volume fraction profiles for $A_{10}B_6$ (a), $A_{10}B_{13}$ (b) and $A_{10}B_{40}$ (c) in the adsorbed layer at the plateau of the isotherm on a hydrophobic surface. The volume fractions of segments of type A and of type B are indicated. See Figure (9) for interaction parameters.

Conclusions

With the SCFA theory the behavior of nonionic surfactants, with respect to micellization and adsorption on hydrophilic and hydrophobic surfaces, can be described successfully with a minimum number of relevant parameters.

In agreement with experimental findings, the cmc increases and the aggregation number of the micelles decreases as the hydrophilic block becomes longer.

On both hydrophilic and hydrophobic surfaces the plateau adsorption decreases with increasing length of the hydrophilic block.

On hydrophilic surfaces strong cooperativity in the adsorption occurs and a bilayer is formed if the hydrophilic block is small. At the cmc the adsorption reaches a pseudo-plateau value. Long hydrophilic blocks prevent strong cooperativity in the isotherm and surfactant bilayer formation by steric hindrance, moreover the plateau adsorption is reached before the cmc.

On hydrophobic surfaces strong cooperativity in the adsorption occurs for nonionic surfactants with a relatively short hydrophilic chain. For all chain lengths studied, surfactant monolayers are formed. The increase in adsorption with concentration levels off considerably before the cmc is reached. Beyond the cmc a pseudo-saturation value is attained.

The predicted trends in adsorption on both types of surfaces correspond very well with experimental results.

References

- 1 Koopal, L. K.; Ralston, J. J. *Colloid Interface Sci.* **1985**, *112*, 362
- 2 Harwell, J. H.; Hoskins, J. C.; Schechter, R. S.; Wade W. H. *Langmuir* **1985**, *1*, 251
- 3 Yeskie, M. A.; Harwell, J. H. *J. Phys. Chem.* **1988**, *92*, 2346
- 4 Koopal, L. K.; Wilkinson, G. T.; Ralston, J. J. *Colloid Interface Sci.* **1988**, *126*, 493
- 5 Cases, J. M. *Bull. Minéral.* **1979**, *102*, 684
- 6 Scamehorn, J. F.; Schechter, R. S.; Wade, W. H. *J. Colloid Interface Sci.* **1982**, *85*, 463
- 7 Kronberg, B. J. *Colloid Interface Sci.* **1983**, *96*, 55
- 8 Klimenko, N. A.; Polyakov, V. Y.; Permilovskaya, A. A. *Kolloidn. Zh.* **1979**, *36*, 861
- 9 Scheutjens, J. M. H. M.; Fleer, G. J. *J. Phys. Chem.* **1979**, *83*, 1619
- 10 Scheutjens, J. M. H. M.; Fleer, G. J. *J. Phys. Chem.* **1980**, *84*, 178
- 11 Van Lent, B.; Scheutjens J. M. H. M. *Macromolecules* **1989**, *22*, 1931
- 12 Koopal, L. K.; Böhmer, M. R. in "Fundamentals of Adsorption", Vol. III, Mersmann, A., ed., Engineering Foundation, American Institute of Chemical Engineers, New York 1990.
- 13 Leermakers, F. A. M.; Scheutjens, J. M. H. M.; Lyklema J. *Biophys. Chem.* **1983**, *18* 353

- 14 Hall, D. G.; Pethica, B. A. in *Nontonic Surfactants*, Schick, M.J. Ed., Marcel Dekker, New York, 1976; Ch. 16
- 15 Mukerjee, P.; Mysels, K. J. *Critical Micelle Concentrations of Aqueous Surfactant Systems* (NSRDS-NBS 36), U.S. Government Printing Office, Washington D. C., 1971
- 16 Levitz, P.; Van Damme, H.; Keravis, D. *J. Phys. Chem.* **1984**, *88*, 2228
- 17 Levitz, P.; Van Damme, H., *J. Phys. Chem.* **1986**, *90*, 1302
- 18 Partyka, S.; Zaini, S.; Lindheimer, M.; Brun, B. *Colloids Surf.* **1984**, *12*, 255
- 19 Kronberg, B.; Stenius, P.; Thorssell, Y. *Colloids Surf.* **1984**, *12*, 113
- 20 Kronberg, B.; Stenius, P.; Igeborn, G. *J. Colloid Interface Sci.* **1984**, *102*, 418
- 21 Van den Boomgaard, A. *PhD. Thesis*, Wageningen Agricultural University, Wageningen, The Netherlands 1985
- 22 Amu T. C. *Polymer*, **1982**, *23*, 1775
- 23 Leermakers, F. A. M.; Scheutjens, J. M. H. M. *J. Chem. Phys.* **1988**, *89*, 3264
- 24 Zhu B. Y.; Zhao, X., *J. Colloid Interface Sci.* **1988**, *125*, 727
- 25 Denoyel, R.; Rouquerol, F.; Rouquerol, J. in *Fundamentals of Adsorption Vol. II*, Liapis A. J. ed., Engineering Foundation, American Institute of Chemical Engineers, New York 1987

CHAPTER 3

Adsorption of Nonionic Surfactants on Hydrophilic Surfaces

*An experimental and theoretical study on association
in the adsorbed layer*

Abstract

The adsorption of the nonionic dodecyl poly(oxyethylenes) $C_{12}(EO)_6$ and $C_{12}(EO)_{25}$ from aqueous solutions on hydrophilic surfaces was studied. The adsorption and the layer thickness of $C_{12}(EO)_6$ exhibit a sudden increase at a concentration close to the cmc. Neutron reflection shows that in the plateau of the adsorption isotherm a bilayer has been formed. The adsorption of $C_{12}(EO)_{25}$ increases gradually with solution concentration. The adsorbed amount and layer thickness are much higher than those for EO oligomers. The hydrophobic chain parts in the $C_{12}(EO)_{25}$ layer could not be localized exactly by neutron reflection, but association between the aliphatic chain parts must occur to obtain the measured adsorbed amounts and layer thicknesses. NMR measurements indicate that the EO segments in the adsorbed layers of $C_{12}(EO)_6$ and $C_{12}(EO)_{25}$ have more conformational restrictions than those in PEO layers because of the association of the aliphatic tails.

For $C_{12}(EO)_6$ the self-consistent field lattice theory for adsorption and/or association (SCFA) predicts stepwise adsorption and bilayer formation. For $C_{12}(EO)_{25}$ the adsorption and layer thickness are grossly underestimated. With an extended SCFA theory which allows for inhomogeneities perpendicular and parallel to the surface, the formation of small aggregates on the surface can be predicted. For $C_{12}(EO)_{25}$ the 2D-SCFA gives much better agreement between theory and experiment.

Introduction

The adsorption of nonionic surfactants of the alkylpoly(oxyethylene) or alkylphenol(oxyethylene) type at the solid/aqueous interface has been the subject of much experimental and theoretical research, see refs (1-14) for some recent work. In general the adsorption of

nonionic surfactants leads to an increase in colloidal stability of the particles. This is one of the reasons for the wide-spread use of these surfactants. Contrary to ionic surfactants, nonionics cannot easily make hydrophilic particles hydrophobic, therefore they cannot be used to increase flotation recovery.

Besides the industrial relevance of the adsorption of nonionics, the structure of the adsorbed layer of nonionic surfactants is also of purely scientific interest. Experimental evidence, of which the fluorescence spectroscopy measurements by Levitz et al.⁽¹⁻⁴⁾ are most appealing, shows that the adsorbed nonionic surfactants aggregate strongly on hydrophilic surfaces such as silica. In the case of surfactants having short head groups relative to the length of the aliphatic chain part bilayers are formed on the surface. If the head group is long, however, the adsorbed layer consists of small aggregates. Further evidence for the existence of hydrophobic domains in adsorbed layers of nonionics has been derived from dye solubilization measurements.⁽⁷⁾ In addition, neutron reflection experiments by Lee et al.⁽⁵⁾ showed that $C_{12}(EO)_6$ forms a bilayer on quartz with head groups at the surface and at the solution side separated by a hydrophobic core.

Information regarding the adsorbed layer of surfactants has also been obtained with the self-consistent field lattice theory for adsorption and/or association, SCFA⁽¹⁴⁾, originally developed to study polymer adsorption.⁽¹⁵⁻¹⁷⁾ With this theory, adsorption isotherms and the structure of the adsorbed layer, which appears as the volume fraction profile perpendicular to the surface, have been obtained.⁽¹⁴⁾ In this previous chapter we presented results for the adsorption of nonionics on hydrophilic and hydrophobic surfaces as a function of the polar chain length. The agreement between theory and experiment was reasonable: for surfactants with rather short head groups on hydrophilic surfaces bilayers were predicted and the experimentally observed decrease in plateau adsorption as a function of the length of the polar chain part could also be calculated. However, for the adsorption of surfactants with long polar head

groups no strong accumulation of hydrophobic segments was found. This did not agree with the experiments by Levitz et al.⁽¹⁻⁴⁾

One of the basic assumptions in the SCFA theory is that each lattice layer parallel to the surface is homogeneous and a mean field approximation is used in each layer. If a bilayer is present the separation between hydrophilic and hydrophobic chain parts will mainly be perpendicular to the surface and this assumption seems justified. For surfactants that cannot form a homogeneous bilayer, for example because the head group is much longer than the hydrocarbon part, a segregation of chain parts may also take place parallel to the surface: in this case the mean field approximation in each layer parallel to the surface is not correct. To investigate the structure of the adsorbed layers of nonionics on hydrophilic surfaces in more detail, especially those with long polar head groups, we use an extended (2D) SCFA theory which allows for inhomogeneities both parallel and perpendicular to the surface.⁽¹⁸⁾ The results will be compared with calculations using the 1-dimensional SCFA theory. An additional check of the aggregation in the layer can be made by comparing adsorption results for a surfactant with a long polar head group with those for a molecule consisting of this head group only.

In order to compare experimental and theoretical results monodisperse surfactants are required and experimental techniques are needed that do not only give the adsorbed amount but also give information on the structure of the layer. We will measure isotherms of monodisperse $C_{12}(EO)_6$ and nearly monodisperse $C_{12}(EO)_{25}$ and $(EO)_{22}$ adsorbed on SiO_2 surfaces by depletion measurements and reflectometry.⁽¹⁹⁾ Dynamic light scattering and streaming potential measurements^(20,21) are used to obtain the hydrodynamic layer thicknesses. The distribution of surfactant perpendicular to the surface is studied with neutron reflection.^(5,22) To study the region close to the surface 1H -NMR of the solvent is a promising technique.⁽²³⁾ For PEO and PVP adsorbed from aqueous solutions water relaxation appears to be a measure of the fraction of the

adsorbed PEO and PVP molecules present in the form of trains. We will test if this applies to surfactants as well.

Materials

Ludox AS40

Ludox AS40 is a colloidal silica, obtained from Dupont, and dialyzed against Super Q deionized water for two weeks to remove excess salt. The specific surface area is $140 \text{ m}^2/\text{g}$, the average particle diameter of these spherical particles is 22 nm.

Silicon wafers

Silicon wafers were purchased from Wacker Chemitronic GmbH (F.R.G). Wafers were oxidized in an oven at 1000°C during one hour. This process gave an oxide layer of about 100 nm. 1.5 cm wide strips were used for the reflectometry experiments. After rinsing with Super Q deionized water and red glowing in a gas flame, the wafers could be re-used.

Surfactants and other chemicals used

Monodisperse $\text{C}_{12}(\text{EO})_6$ (Nikkol) was a gift from Koninklijke Shell Research Laboratories Amsterdam (KSLA), The Netherlands. $\text{C}_{12}(\text{EO})_{25}$, which is slightly polydisperse in the EO part, was purchased from Nikkol directly. The cmc's were determined from γ -lnc plots using the Wilhelmy plate technique and found to be $7.5 \cdot 10^{-5}$ and $3.1 \cdot 10^{-4} \text{ M}$ respectively. Poly-(ethylene oxide) with a molecular weight of 960 and $M_n/M_w = 1.04$ was a GPC calibration sample from Polymer Laboratories and will be denoted as $(\text{EO})_{22}$. Deionized Super Q water was used throughout this study.

Methods

Determination of adsorption isotherms

Depletion measurements: Adsorption isotherms on Ludox AS40 are determined using the depletion method with 0.3% (v/v) Ludox at 20°C. After centrifugation for one hour at 20.000 rpm in a Beckmann J2-21M centrifuge, the equilibrium concentrations in the supernatant are determined by surface tension measurements at low concentrations or by the molybdophosphoric acid assay⁽²⁴⁾ at high concentrations. The surface tension measurements are performed using the Wilhelmy plate technique, the γ -ln*c* curve is used as a calibration curve. For the molybdophosphoric acid assay a straight calibration line was obtained for both surfactants and for (EO)₂₂.

Reflectometry: The reflectometer described by Dijt et al.⁽¹⁹⁾ is employed. A strip of an oxidized silicon wafer is used as the adsorbing surface. The surfactant solution is delivered at the silicon wafer using a stagnation point flow, described by Dijt et al. The temperature is set to 20°C. In the set-up a polarized He/Ne laser beam hits the wafer at the Brewster angle which is 70° for the silicon water-interface. The reflected beam is split into its parallel and perpendicular components which are detected by photo-diodes. The signals are then combined to give the output signal *S*, which is given by:

$$S = \frac{I_s - I_p}{I_s + I_p} \quad (1)$$

where the intensities are denoted by *I* and the subscripts *s* and *p* refer to the perpendicular (senkrecht) and parallel components respectively. Using the optical matrix method^(25,26) Dijt et al. showed that *S* is proportional to the adsorbed amount, *Γ*, and independent of the structure of the adsorbed layer. In addition to the thickness of the oxide layer on the wafer, obtained by ellipsometry, the refractive index increment is needed to convert *S* to *Γ*. From data given by Chiu and Chen⁽²⁷⁾ for a number of nonionic surfactants with ethylene-

oxide head groups, we deduced that we can use $dn/dc = 0.136 \text{ cm}^3/\text{g}$ for surfactants of the $C_n(\text{EO})_m$ type, just as Dijt et al. used for PEO.

Determination of layer thicknesses

Dynamic light scattering (DLS): DLS is used to determine the hydrodynamic radius of the Ludox particles in the absence and presence of surfactant. A He/Ne laser beam passes through the cuvette, the detection angle is set to 90° and the temperature is 20°C , particle concentrations of 0.25% (v/v) are used. The scattering from the sample, which is immersed in a toluene bath, is processed with an ALV5000-Multiple Tau Digital correlator linked to a photomultiplier. A cumulant fit is used to fit the auto-correlation function from which the diffusion coefficient is obtained. From the diffusion coefficient the hydrodynamic radius is calculated using the Stokes-Einstein relation. The method and its application to Ludox AS40 is described in more detail by van der Beek et al.⁽²⁸⁾

Streaming potential: The reduction of the streaming potential in a narrow capillary due to surfactant adsorption can also be used to obtain the hydrodynamic layer thickness. A streaming potential set-up, built by Dijt et al.⁽²⁹⁾ is used. The flow of a surfactant solution in 10^{-3} mol/dm^3 NaCl through an acid-cleaned glass capillary is controlled by an N_2 pressure of 0.3 bar. The capillary is 21 cm long and has an inner diameter of 0.4 mm. The potential difference between the ends of the capillary is measured using platinum electrodes immersed in two containers containing electrolyte solution and a Fluke 8022 multimeter. The whole set-up is placed in a Faraday's cage. In between experiments the capillary is cleaned by rinsing with 10^{-3} mol/dm^3 NaCl solution. The measured streaming potential difference is converted to the hydrodynamic layer thickness, δ_h using the following equation, given by Koopal et al.⁽²⁰⁾ and by Cohen Stuart and Tamai⁽²¹⁾:

$$\delta_h = \kappa^{-1} \ln \frac{V_{s,0}}{V_{s,s}} \quad (2)$$

The double layer thickness, κ^{-1} , is 10 nm at the salt concentration applied, $V_{s,o}$ is the streaming potential in the absence of an adsorbed layer, $V_{s,s}$ is the streaming potential in the presence of the adsorbed layer. Equation (2) applies to the situation that (1) the adsorbed layer is thinner than κ^{-1} , (10 nm), (2) the surface charge of the capillary is not affected by adsorption and (3) the electrical double layer remains undisturbed by the adsorbed surfactant.⁽²⁰⁾ Under these conditions the difference between $V_{s,o}$ and $V_{s,s}$ is caused only by the change in position of the plane of shear.

Determination of solvent relaxation

Information regarding the mobilities in the adsorbed surfactant layer can be obtained by proton spin-spin relaxation measurements of the water, just as for polymers.⁽²³⁾ Measurements are made on a 20 MHz mini-spec NMR apparatus using the Carr-Purcell pulse sequence, i.e. $90-\tau-(180-2\tau)_x$, at a Ludox AS40 concentration of 5.5% (v/v). The delay time, τ , is set to 0.5 ms for the samples containing 5.5% Ludox and 1 ms for aqueous solutions without silica. Some test runs were performed with low τ values, 0.16 ms, to check for the presence of a fast component. The average of two measurements is fitted using a single exponential and a double exponential fit. The double exponential fit gives an additional, usually faster, component with a contribution of less than 2% to the amplitude of the total signal. Both the relaxation time, T_2 and the amplitude of this minor component were neither constant nor systematically varying and are therefore assumed to be due to experimental error. Only the T_2 value obtained for the main component, which might as well be obtained with the single exponential fit, contains information on the system.

In the system different types of protons are present: water protons, both bound to the surface and the surfactant (hydration) and free in solution, protons of the silanol groups on the surface and the protons belonging to the surfactant molecules. Following ref (23) we can assume that the only protons detected are those of bound and free water molecules. Surfactant protons do not give a significant

contribution since for a concentrated surfactant solution the echo train can be fitted with a single exponential, i.e. only one dynamically averaged signal is obtained. Van der Beek et al.⁽²³⁾ showed that in Ludox suspensions the spin-lattice relaxation time does not change between pH 4 and pH 10, although the number of silanol groups varies considerably in this region, especially between 7 and 10.⁽³⁰⁻³²⁾ Based on these observations it is concluded that only the free and bound water molecules have to be considered. Therefore the measured relaxation time, T_2 is interpreted as:

$$1/T_2 = (1 - P_b)/T_{2f} + P_b/T_{2b} \quad (3)$$

The indices f and b indicate free and bound, respectively, P_b is the fraction of time spent in the "bound" environment. The results will be expressed in terms of the specific relaxation rate, R_{2sp}

$$R_{2sp} = T_2^0/T_2 - 1 \quad (4)$$

where T_2^0 is the relaxation time of pure water.

Neutron reflection

Neutron reflection experiments are carried out to study the segment density distribution using the D₁₇ small angle scattering machine at the Institute Laue-Langevin, Grenoble. A Suprasil quartz block of 100x50x10 mm is mounted vertically in a cell as described elsewhere.⁽⁵⁾ The cell is oriented with respect to the neutron beam such that the neutrons arrive at the solid/liquid interface through the quartz block. The observed reflectivity is normalized with respect to that of a beam passing straight through the block. Two neutron wavelengths are used, 1.2 and 3.0 nm and the reflection angle, θ , is varied between 1° and 12° to obtain values of momentum transfer (scattering vector $Q = 4\pi\sin\theta/\lambda$) in the range 0.05-0.8 nm⁻¹. The beam is 20 mm high and 0.35 mm wide. The adsorbed layer of C₁₂(EO)₆ is measured at 0.2 mmol/dm³, which is about 3 times higher than the cmc. The adsorbed layer of C₁₂(EO)₂₅ is measured at

two concentrations, 0.13 and 0.4 mmol/dm³, the latter concentration is slightly higher than the cmc. All adsorbed layers are measured at different solvent contrasts, where use was made of the difference in scattering length of H and D. As solvents pure D₂O and an H₂O/D₂O mixture with the same scattering length density as the quartz, denoted as CMQ: contrast matched to quartz, were used. In addition, for C₁₂(EO)₂₅ measurements a H₂O/D₂O mixture with a scattering length density, ρ_s , of $2 \cdot 10^{-4}$ nm⁻² denoted as HD2, was used. For the analysis the assumption has to be made that the adsorbed layer is the same in D₂O and H₂O.

The observed reflectivity curves are fitted using the optical matrix method⁽²⁶⁾, as adapted to the reflection of neutrons by Penfold.⁽³³⁾ In this method the variation in composition normal to the interface is modeled by a series of parallel layers or blocks of uniform composition. The thickness chosen for these blocks depends on the spatial resolution of the experiment in real space which in turn depends on the maximum value of momentum transfer and the number of isotopic combinations measured. Different models for the structure of the adsorbed layer are tried, which will be commented upon in the results section. The average ρ_s , per layer parallel to the surface has been calculated from the number and type of nuclei present in the layer using tabulated scattering lengths.⁽³⁴⁾ From the scattering length density profile the reflectivity curves are calculated using a program from MIRA[®] software. The simplest model of the adsorbed layer which fits the reflectivity curves for all the contrasts used, is adopted as the structure of the adsorbed layer.

Results

Adsorption isotherms

Batch adsorption: The results for the adsorption isotherms on Ludox AS40 of C₁₂(EO)₆, C₁₂(EO)₂₅ and (EO)₂₂ are given in Figure (1). For C₁₂(EO)₆, Figure (1a), the adsorption stays relatively low until close

to the cmc and then increases sharply until almost $4 \mu\text{mol}/\text{m}^2$ or $2 \text{ mg}/\text{m}^2$. Beyond the cmc there is still some increase in the adsorption. In connection with this observation we note that the surface tension also shows some decrease after the cmc has been passed and that the aggregation numbers of micelles usually increase with surfactant concentration. For $\text{C}_{12}(\text{EO})_{25}$, (Figure 1b) note the ordinate axis scale difference with Figure (1a), the maximum adsorbed amount is lower, about $0.8 \mu\text{mol}/\text{m}^2$, but in terms of mg/m^2 the adsorption is still fairly high, about $1 \text{ mg}/\text{m}^2$. The adsorption of $\text{C}_{12}(\text{EO})_{25}$ is significantly higher than that of EO_{22} which is less than $0.2 \mu\text{mol}/\text{m}^2$, Figure (1b). The adsorption isotherm of $\text{C}_{12}(\text{EO})_{25}$ does not show such a strong cooperative behavior as that of $\text{C}_{12}(\text{EO})_6$, but the isotherm is probably slightly sigmoidal. Some self-enhancing effect might be present. The experimental errors in the concentrations determined by measurement of the surface tension are relatively large, especially for $\text{C}_{12}(\text{EO})_{25}$ where the $\gamma\text{-}\ln c$ curve has a rather small slope. If we assume an error of $1 \text{ mN}/\text{m}$ in the surface tension measurements this leads to an uncertainty of 30% in the equilibrium concentration. Therefore the sigmoidal nature of the $\text{C}_{12}(\text{EO})_{25}$ isotherm is not firmly established.

Reflectometry: The adsorption isotherms of $\text{C}_{12}(\text{EO})_6$ and $\text{C}_{12}(\text{EO})_{25}$ on oxidized silicon wafers are shown in Figure (2). The isotherms are very similar to those on Ludox: In this case a clear sigmoidal isotherm shape is obtained for both surfactants. For both surfactants the maximum adsorbed amount as well as the initial adsorption is lower than on Ludox. For $\text{C}_{12}(\text{EO})_6$ no significant adsorption could be measured at concentrations lower than about $0.075 \text{ mmol}/\text{dm}^3$. Above this concentration the adsorbed amount increases stepwise to $\Gamma = 2.5 \mu\text{mol}/\text{m}^2$, indicating that true surface condensation takes place. For $\text{C}_{12}(\text{EO})_{25}$, even at very low concentrations some adsorption is detected, see Figure (2b). In the case of $(\text{EO})_{22}$, for which the "saturation" level was measured by Dijt et al.⁽¹⁹⁾, is again much lower than that of $\text{C}_{12}(\text{EO})_{25}$, about $0.15 \mu\text{mol}/\text{m}^2$. The isotherm shapes and adsorbed amounts, especially if compared with

(EO)₂₂ show that substantial attraction between the aliphatic tails takes place for both surfactants.

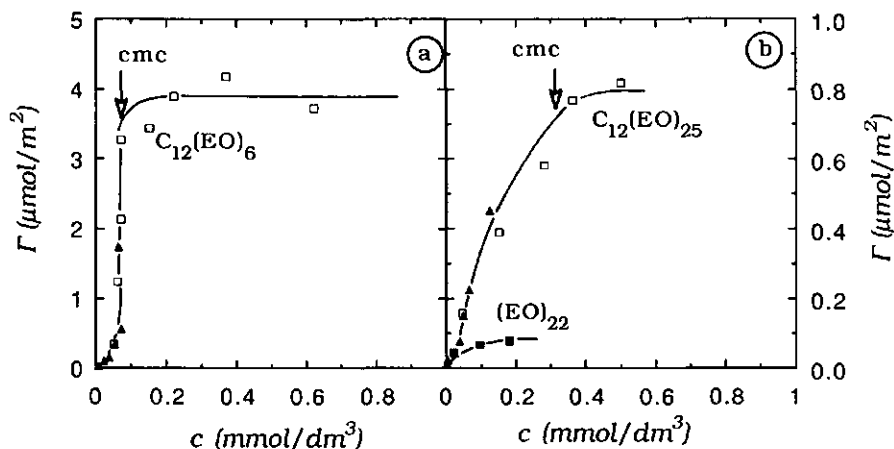


Figure 1: Adsorption isotherms of $C_{12}(EO)_6$ (Figure a), and $C_{12}(EO)_{25}$ and $(EO)_{22}$ (Figure b) on Ludox AS40. The cmc values are indicated. To obtain the equilibrium concentrations either surface tension measurements (triangles) or the molybdo-phosphoric acid assay was used (squares).

Discussion: The shape and the maximum of the $C_{12}(EO)_6$ adsorption isotherms agree very well with other measurements of adsorption isotherms of nonionic surfactants with rather short polar head groups.^(1,5-12) For a surfactant with a longer polar head group, e.g. $C_{12}(EO)_{25}$, the adsorbed amount decreases and the condensation step disappears. The shape of the isotherm, however, indicates that lateral attraction is still present. This is also in agreement with literature data.^(2,3,10) Also the pronounced increase in adsorption due to linking an aliphatic part to an EO chain has been documented before.⁽¹⁰⁾

Information regarding the orientation of the adsorbed molecules can be deduced from comparing adsorption isotherms. The adsorption isotherms of $C_{12}(EO)_6$ and $C_{12}(EO)_{25}$ on the wafers show a cross-over

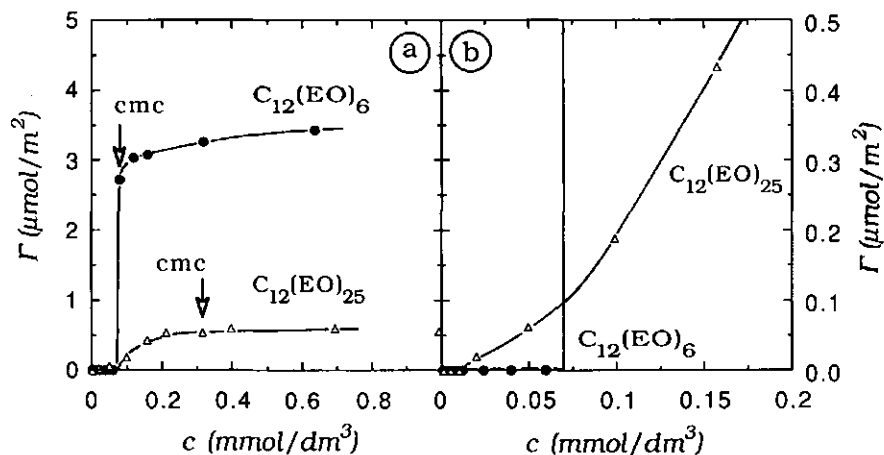


Figure 2: Adsorption isotherms of $C_{12}(EO)_6$ and $C_{12}(EO)_{25}$ on oxidized silicon wafers as measured by reflectometry (a). The initial part of the isotherm is enlarged in Figure (b).

point. In the previous chapter⁽¹⁴⁾ we demonstrated, using SCFA theory that cross-overs for these systems occur if the head groups adsorb on the surface. The adsorption energy per head group must be low since for $C_{12}(EO)_6$ no adsorption could be detected at low concentrations. If the aliphatic tail were to adsorb on the surface it would be easy for the aliphatic segments to contact each other. Theoretical calculations have shown that in this case the adsorption becomes strongly cooperative at very low concentrations, which is not the case in the experimental isotherms. On Ludox the tails may have some affinity for the surface as well. The initial part of the isotherm of $C_{12}(EO)_6$ is higher on Ludox than on the wafers, while that of $C_{12}(EO)_{25}$ is about the same as in the reflectometry experiment. Consequently, we could not find a cross over point for the Ludox system. At high adsorbed amounts the head groups will have displaced the aliphatic tails. The conclusion that EO groups adsorb on silica surfaces is supported by the fact that PEO adsorbs on silica from aqueous solutions.^(23,28) Moreover, the adsorption energy

for PEO from CCl_4 on silica is strongly negative, indicating that the interaction between EO and the surface is much stronger than that between an apolar molecule and the surface.⁽³⁵⁾

Layer thickness measurements

Dynamic light scattering: For the bare AS40 particles we obtained a hydrodynamic radius of 16.5 nm, which is in good agreement with the data given by van der Beek et al.⁽²⁸⁾ However it is substantially larger than the radius given by the manufacturer, 11 nm, which may be caused by a different way of averaging over the particles.⁽²⁸⁾ Surfactant adsorption causes an increase in the hydrodynamic radius which is given in Figure (3a) for $\text{C}_{12}(\text{EO})_6$ and for $\text{C}_{12}(\text{EO})_{25}$. In Figure (3a) the hydrodynamic radius of Ludox with $(\text{EO})_{22}$ is also given. The curves roughly follow the adsorption isotherms. For $\text{C}_{12}(\text{EO})_6$ no initial increase in the radius occurs, then suddenly at a concentration about 0.07 mmol/dm^3 a sharp increase of about 3 nm takes place and a plateau value is reached. For $\text{C}_{12}(\text{EO})_{25}$ a more gradual increase is observed, and a limiting layer thickness of 3.5 nm is found. No increase of the hydrodynamic radius is found for $(\text{EO})_{22}$.

Streaming potential: The layer thicknesses measured via the streaming potential method are given in Figure (3b). For $\text{C}_{12}(\text{EO})_6$, the hydrodynamic layer thickness as a function of concentration follows the adsorption isotherm. First no significant decrease of the streaming potential is observed then it increases sharply to a value of about 3 nm. After the cmc the thickness still increases slightly until about 4 nm.

For $\text{C}_{12}(\text{EO})_{25}$ quick measurements were possible only at concentrations above the cmc, where the plateau value is about 4.7 nm which is slightly higher than that for $\text{C}_{12}(\text{EO})_6$. At lower concentrations a rapid decrease of the streaming potential was followed by a slow decrease. The decrease did not lead to a constant value but kept on decreasing even below the potential measured in the plateau at high concentrations. As the original potential could not

be reproduced after rinsing with water, which is also in contrast with the other experiments, we concluded that it must be due to an impurity and we took only the fast part of the curve to measure the streaming potential. Consequently the errors are larger than those for $C_{12}(EO)_6$. In any case the increase of the layer thickness with solution concentration is more gradual for $C_{12}(EO)_{25}$ than for $C_{12}(EO)_6$, just as with the adsorption isotherms. For $(EO)_{22}$ no decrease of the streaming potential could be detected.

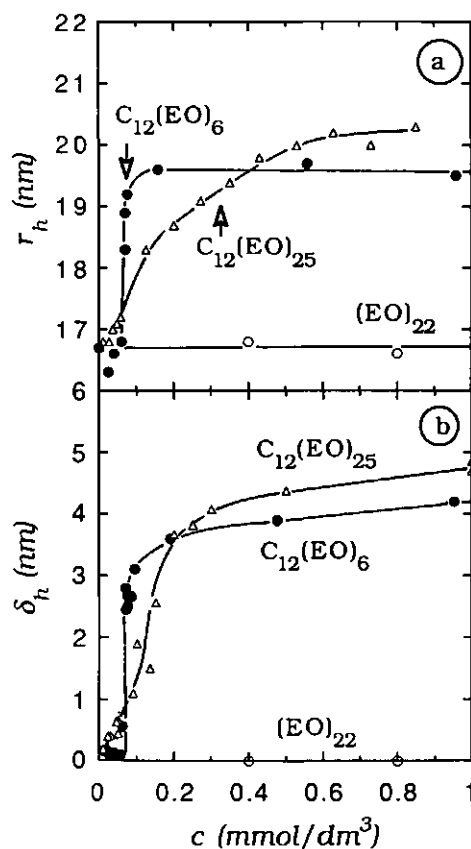


Figure 3: Layer thicknesses of $C_{12}(EO)_6$, $C_{12}(EO)_{25}$, and $(EO)_{22}$.

Figure (3a): Dynamic light scattering: hydrodynamic radius of Ludox AS40 as a function of surfactant concentration.

Figure (3b): Hydrodynamic layer thickness obtained from streaming potential measurements on a glass capillary covered with surfactant.

Discussion: With dynamic light scattering the measured layer thicknesses do not offer a totally independent confirmation of the shape of the adsorption isotherms, since the equilibrium surfactant concentrations had to be calculated from the measured adsorption isotherms. The streaming potential measurements, however, are independent and show that also on the glass capillary $C_{12}(EO)_6$ does not adsorb until it is close to the cmc and then a condensation occurs.

The layer thickness of $C_{12}(EO)_6$ above the cmc measured with DLS is lower by about 1 nm than that measured with the streaming potential. For the calculation of the hydrodynamic layer thickness from the change in streaming potential we made the assumption that the electric double layer remains undisturbed, which might not be realistic. Using small angle neutron scattering a thickness of 4 nm was found⁽⁶⁾ and in neutron reflection measurements, see below and Lee et al.⁽⁵⁾, a thickness of about 5 nm was obtained. Gellan and Rochester⁽⁹⁾ report a value of 4.4 nm for $C_{12}(EO)_5$ layers on silica slides measured by X-ray diffraction. Therefore, the DLS thickness seems to be somewhat low. This is probably due to the polydispersity of the Ludox: the dispersity changes if all particles are covered with a layer of the same thickness. With the way of averaging over the particles this leads to an underestimation of the hydrodynamic radius. The measured layer thickness of 4 nm for $C_{12}(EO)_6$ suggests that a bilayer is formed, since the stretched length of a $C_{12}(EO)_6$ molecule, which it is highly unlikely occur in practice, is slightly less than 4 nm.

From both measurements, DLS and streaming potential, we find that the $C_{12}(EO)_{25}$ layer is 0.5 nm thicker than the $C_{12}(EO)_6$ layer, even though the adsorbed amount (in mg/m^2) is twice as small. The difference in thickness is small, and although we find it with both methods, it might still be in the range of experimental error. Therefore we may conclude that the $C_{12}(EO)_{25}$ layer is at least as thick as the $C_{12}(EO)_6$ layer. The surfactant layers are very thick compared to PEO layers, a PEO of a molecular weight of 23.000

(\approx (EO)₅₀₀) is needed for a layer with the same thickness and the (EO)₂₂ does not show any effect on the hydrodynamic radius.

With streaming potential measurements it is also possible to investigate the kinetics of adsorption. At high concentrations the adsorption and desorption of C₁₂(EO)₆ was very fast. Surprisingly, we found very slow kinetics for C₁₂(EO)₆ near the cmc. At lower pressures, the process was faster, and the layer thicknesses reached, were slightly higher. This could be an interesting effect for further study. We speculate that at high pressures the layer of surfactant is subject to such a high shear that it partly flushes out. This effect is apparently stronger close to the cmc, where the mass transport from the solution to the surface takes place by monomers whereas well above the cmc most of the transport takes place in the form of micelles.

Mobility in the adsorbed layer

T₂ measurements: The specific relaxation rate of Ludox suspensions is given in Figure (4). The relaxation increases linearly with the volume fraction of Ludox AS40 just as Van der Beek et al.⁽²³⁾ found for Ludox HS-40. We did not find a change in *T₂* as a function of the surfactant concentration (concentrations up 0.1 mol/dm³ were tested) in the absence of Ludox, which also agrees with the findings by van der Beek et al. for PEO and PVP. In the presence of Ludox, however, the surfactant did cause an effect on *T₂*. The specific relaxation rate, *R_{sp}*, normalized with respect to the specific relaxation rate for 5.5% Ludox in pure H₂O, *R_{sp}⁰*, is plotted as a function of the equilibrium concentration in Figure (5). The curves roughly follow the adsorption isotherms, but we must note that the equilibrium concentrations are derived from the adsorption isotherms in Figure (1), so that the results are not entirely independent. For (EO)₂₂ we obtained about the same enhancement of the relaxation rate as found by van der Beek et al. Again the difference between (EO)₂₂ and C₁₂(EO)₂₅ is striking; for the surfactant a much more pronounced enhancement is found.

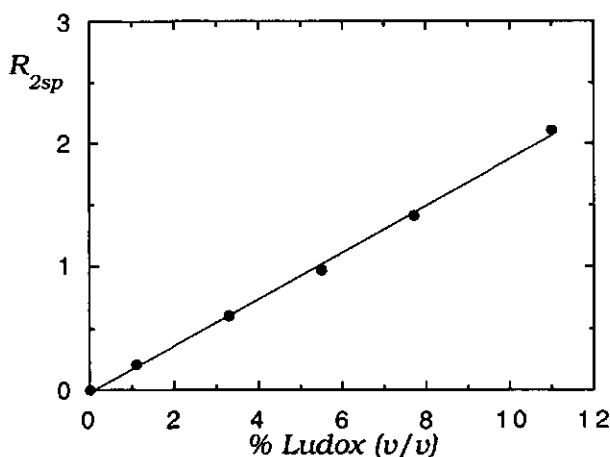


Figure 4: The specific relaxation rate as a function of the volume fraction Ludox AS40.

Our results indicate that the conclusion of van der Beek et al. that for polymers ^1H NMR detects the train segments does not apply to these surfactants. The measured signal shows the reduction of the mobility of water. Apparently in an adsorbed surfactant layer much more reduction of water mobility takes place than in an adsorbed PEO layer, where only the hydration water of EO segments close to the surface is partly immobilized. The high reduction in mobility for both surfactants is additional evidence that the structure of not only the $\text{C}_{12}(\text{EO})_6$ layer but also that of the $\text{C}_{12}(\text{EO})_{25}$ layer is very different from a PEO layer. The large reduction of mobility is caused by the high adsorbed amount compared to that for PEO in a rather thin layer. The surfactant EO groups will be forced in specific conformations which leave little room for free movements, contrary to the situation with adsorbed PEO which has a lot of loops and tails. This difference will be enhanced because the part of the head group attached to the aliphatic chain part is restricted in its movement by the association of tails.

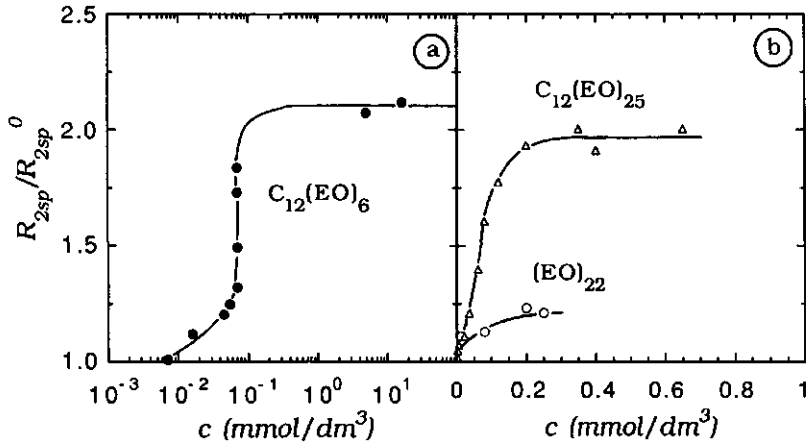


Figure 5: The specific relaxation rate of surfactant/water/silica systems at 5.5% (v/v) Ludox, normalized with respect to the relaxation rate in 5.5% Ludox in the absence of surfactant, as a function of the equilibrium surfactant concentration.

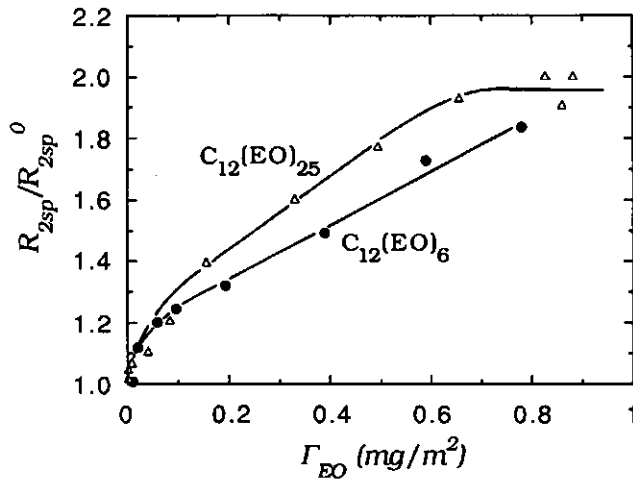


Figure 6: Normalized relaxation rates of surfactant/water/silica systems as a function of the number of $\mu\text{mol/m}^2$ EO adsorbed.

In Figure (6) we give the specific relaxation rate as a function of the adsorbed amount of EO, expressed in mg/m^2 . For $\text{C}_{12}(\text{EO})_6$ a sharp initial increase is followed by a constant slope. The point where the constant slope starts, corresponds to the point where the adsorption isotherm starts to increase vertically, see Figure (1). Most likely the first molecules are adsorbed in a flat conformation, reducing the mobility of a lot of hydration water, possibly also from the aliphatic tail. At higher coverage bilayer formation may occur. The mobility of the hydration water of the head groups at the surface side is greatly reduced but the head groups at the solution side may retain considerable freedom. Since the slope is constant it seems likely that the layer will have a bilayer structure from the beginning of the sharp increase in the adsorption isotherm.

For $\text{C}_{12}(\text{EO})_{25}$ a more gradually changing slope is obtained, indicating a more gradual change of the layer structure with adsorbed amount. The initial part is again steep, flat adsorption is likely to occur. Next a curve with a gradually decreasing slope is observed. Molecules adsorbing at coverages larger than $0.5 \mu\text{mol}/\text{m}^2$, hardly cause any additional immobilization of water. Apparently, some of the EO segments at the solution side are rather free to move. In the intermediate part of the curve the relaxation enhancement by $\text{C}_{12}(\text{EO})_{25}$ is higher than for $\text{C}_{12}(\text{EO})_6$ if plotted per EO adsorbed. The reason for this is not entirely clear, $\text{C}_{12}(\text{EO})_{25}$ molecules may encounter more conformational restrictions than $\text{C}_{12}(\text{EO})_6$ in assembling their hydrophobic parts. However, it is also possible that more EO groups of $\text{C}_{12}(\text{EO})_{25}$ are in contact with the surface at the same coverage than those of $\text{C}_{12}(\text{EO})_6$. For $\text{C}_{12}(\text{EO})_6$ adsorbed as a bilayer about half of the EO head groups are at the surface side, whereas for $\text{C}_{12}(\text{EO})_{25}$ more than half of the EO may be close to the surface.

Some other experimental indications exist that the adsorbed layer of surfactants may be rather rigid.^(36,37) Using fluorescence spectroscopy and ESR Somasundaran and co-workers have shown that the hydrophobic core in the adsorbed layer has a higher

microviscosity than micelles of these surfactants.^(36,37) Therefore it is not correct to see the adsorbed layer as adsorbed micelles. Due to the interactions with the surface a significant reduction of the conformational entropy of the surfactant molecules occurs.

Segment density profiles

From neutron reflectivity curves measured in the absence of surfactant the mean square roughness of the quartz block was determined to be 1.2 nm. Reflectivity curves measured in the presence of surfactant are shown in Figures (7) to (9). Figure (7) shows the results for $C_{12}(EO)_6$ in CMQ (7a and 7c) and D_2O (7b and 7d). The experimental points in Figures (7a) and (7c) are the same. The curves refer to different models of the adsorbed layer used in the calculation of the reflectivity profiles. Similarly the points in Figures (7b) and (7d) are the same. Figure (8) shows the results for $C_{12}(EO)_{25}$ in three different solvents at a concentration of 0.4 mmol/dm³: CMQ (8a and 8d), D_2O (8b and 8e) and with a scattering length density, $\rho_s = 2 \cdot 10^{-4} \text{ nm}^{-2}$ (8c and 8f). Figure (9) shows the results for a $C_{12}(EO)_{25}$ concentration of 0.13 mmol/dm³ in these three different solvents.

Calculations: In order to interpret the measured reflectivity, theoretical calculations of the reflectivity are made using the optical matrix method⁽³³⁾, based on different models for the adsorbed layer. For the calculations the adsorbed layer was either taken to be a single block profile of homogeneous average composition or of three blocks with an EO-CH₂-EO composition, where the EO block close to the surface was assumed to be identical with that at the solution side. The space that was not occupied by surfactant was assumed to be filled with water molecules, see Figure (10).

The characteristic parameters for the calculation of the reflectivity curve are the thickness and the scattering length density ρ_s of the block (or blocks) The latter are calculated from the scattering length l , and the volume, V , of the molecules present. For instance, the

scattering length density of a homogeneous block containing solvent and surfactant can be calculated using:

$$\rho_s = \frac{n l_{\text{solvent}} + l_{\text{surfactant}}}{n V_{\text{solvent}} + V_{\text{surfactant}}} \quad (5)$$

where n is the number of solvent molecules per surfactant.

In the three block bilayer model the volume of a C_{12} chain in the hydrophobic region was fixed at 0.327 nm^3 . We assume that in the CH_2 rich block each aliphatic chain is surrounded by other aliphatic chains. Consequently, the area per adsorbed molecule and the thickness of the hydrocarbon region could not be varied independently. Water molecules and EO groups determine the volume and hence the thickness of the EO blocks, because the area per molecule is taken to be the same as that of the C_{12} chains, see Figure (10). The final parameter used in the calculation is the fractional coverage of the surface with this bilayer structure. The resulting model is similar to that in ref (5). Note that in this model a bilayer or, because the surface coverage is not necessarily 100%, a "broken bilayer" structure is assumed. Boundary effects between parts of the surface covered with surfactant and parts where only solvent is present are neglected, which is justified if the aggregates are large. The data required for the calculations are listed in Table I:

Table I: Volumes and scattering lengths of relevant species, volume, V , in nm^3 , scattering length, l , in nm.

	$C_{12}\text{EO}_6$	C_{12}	EO_6	$C_{12}\text{EO}_{25}$	EO_{25}	H_2O	D_2O
V	0.708	0.327	0.381	1.915	1.588	0.030	0.030
l	$1.12\text{E-}5$	$-1.37\text{E-}5$	$2.48\text{E-}5$	$8.98\text{E-}05$	$1.04\text{E-}04$	$-1.68\text{E-}6$	$1.91\text{E-}5$

$C_{12}(\text{EO})_6$:

The best fit of the experimental data to a single homogeneous block in contrast matched water is shown in Figure (7a). This fit is obtained for a scattering length density of $2.5 \cdot 10^{-4} \text{ nm}^{-2}$ and a block thickness of 5.0 nm , which corresponds to an adsorbed amount of

$3.3 \mu\text{mol}/\text{m}^2$. In D_2O no good fits could be obtained for a layer of this composition; it is too low at high Q as shown in Figure (7b).

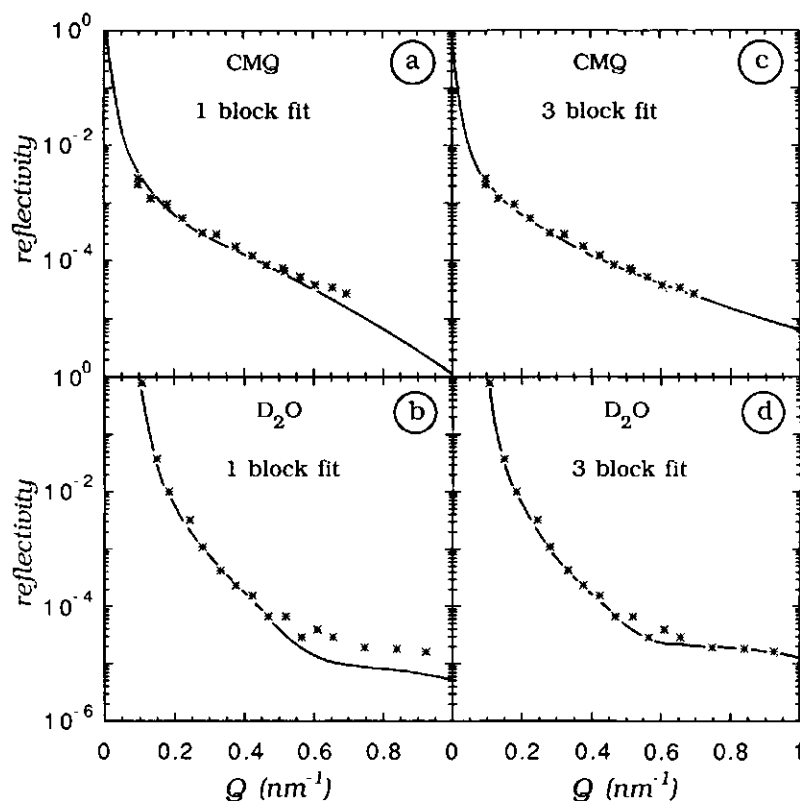


Figure 7: Reflectivity curves for $\text{C}_{12}(\text{EO})_6$ in contrast matched water (CMQ) (7a, 7c) and in D_2O (7b, 7d). The curves are results of single block fits at a layer thickness of 5.0 nm and an adsorbed amount of $3.3 \mu\text{mol}/\text{m}^2$ (7a, 7b) or three-block fits at a layer thickness of $1.81+1.6+1.81 \text{ nm}$ and an adsorbed amount of $3.3 \mu\text{mol}/\text{m}^2$, (7b, 7d).

To obtain a better fit the EO-CH₂-EO three block model was used. Initially the thickness of the hydrocarbon region was investigated. Two extreme possibilities were tried, firstly a bilayer in which the

hydrocarbon chains were arranged end to end giving an aliphatic region twice the thickness of a single aliphatic extended C_{12} chain, which is 1.67 nm.⁽³⁸⁾ This model was found to be incompatible with the experimental data whatever the water content and therefore thickness of the EO block was chosen, because the resulting layer thickness was too great. Secondly complete interdigitation of the hydrophobic chains was investigated. In this case a hydrocarbon layer thickness of 1.6 nm was used giving rise to an area per surfactant molecule of 0.41 nm². An excellent fit to the experimental data was obtained providing two water molecules per EO segment were included in both EO layers. This gave an EO {EO(H₂O)} block thickness of 1.81 nm. In order to fit this model a fractional surface coverage of the bilayer structure of 41% was required, giving an adsorbed amount of 3.3 $\mu\text{mol}/\text{m}^2$.

Just as in ref (5) we find that the surface is not fully covered with a surfactant bilayer, however the coverage we obtained here is lower than that obtained by Lee et al.⁽⁵⁾ The somewhat low adsorbed amount compared to these previous results may be due to defects in the quartz surface. In the experiments described in ref (5) a less rough quartz block was used and recent experiments seem to indicate that the coverage increases with decreasing surface roughness.⁽³⁹⁾ In spite of the different adsorbed amount the structure, perpendicular to the surface, is almost identical with the previous results. Lee et al. also performed experiments at high pH, for which they found a reduced adsorbed amount but no change in the structure of the layer. Following their conclusion that for adsorption of $C_{12}(\text{EO})_6$ at high pH an "island like" or a "broken" bilayer is also present on the surface, we conclude that such a bilayer structure is consistent with the present experiments. An overview of the fitting parameters used is given in tables II and III.

The adopted broken bilayer structure may be too simple. Only if the aggregates on the surface are large, can boundary effects between aggregate and solvent be neglected and is the calculation of the thicknesses of the different regions from the molecular volumes

warranted. If the aggregates are small head groups may be located at the same distance from the surface as tail groups and significant mixing of head groups in the block where the tails are located may take place. This will affect the parameters used in the fit. At present we have no reason to believe that the aggregates are so small that this effect is significant. In fact, by using fluorescence spectroscopy⁽²⁾ it has been shown that any aggregates of nonionic surfactants with a small head group, adsorbed on silica are too big to be detected as such. Moreover, these surfactants form very big micelles in solution. Therefore the most likely conclusion is that they associate into large double pancake-like aggregates on a hydrophilic surface.

The fitted thickness of the EO blocks indicates that neither is the EO part of the molecule completely stretched nor is the EO part close to the surface adsorbed in a flat conformation. The total thickness of the aliphatic part is about one stretched chain length. The adsorbed amount agrees very well with the adsorbed amounts measured on Ludox and wafers. The layer is a little thicker (5.2 nm) than the hydrodynamic layer thickness but this may be due to the roughness of the quartz block (which is included in the thickness).

C₁₂(EO)₂₅:

For a C₁₂(EO)₂₅ concentration of 0.4 mmol/dm³ the experimental data for all three contrasts used, could be fitted to a single homogeneous block with a thickness of 5.2 nm and an adsorbed amount of 0.85 μmol/m². The results are given in Figure (8a-c) and it appears that the observed reflectivity can be fitted reasonably well using the single block model at all three contrasts used. The fitted thickness is almost the same as that of the C₁₂(EO)₆ layer, which is in agreement with the other layer thickness measurements.

The three block model, with a thin aliphatic layer of 0.5 nm, leads for the given the architecture of the molecule to an EO layer thickness of 2.4 nm, if once again we allow 2 water molecules per EO group. This results in a bilayer with a total thickness of 5.3 nm. This three block model gives a similar fit to the reflectivity curve as the

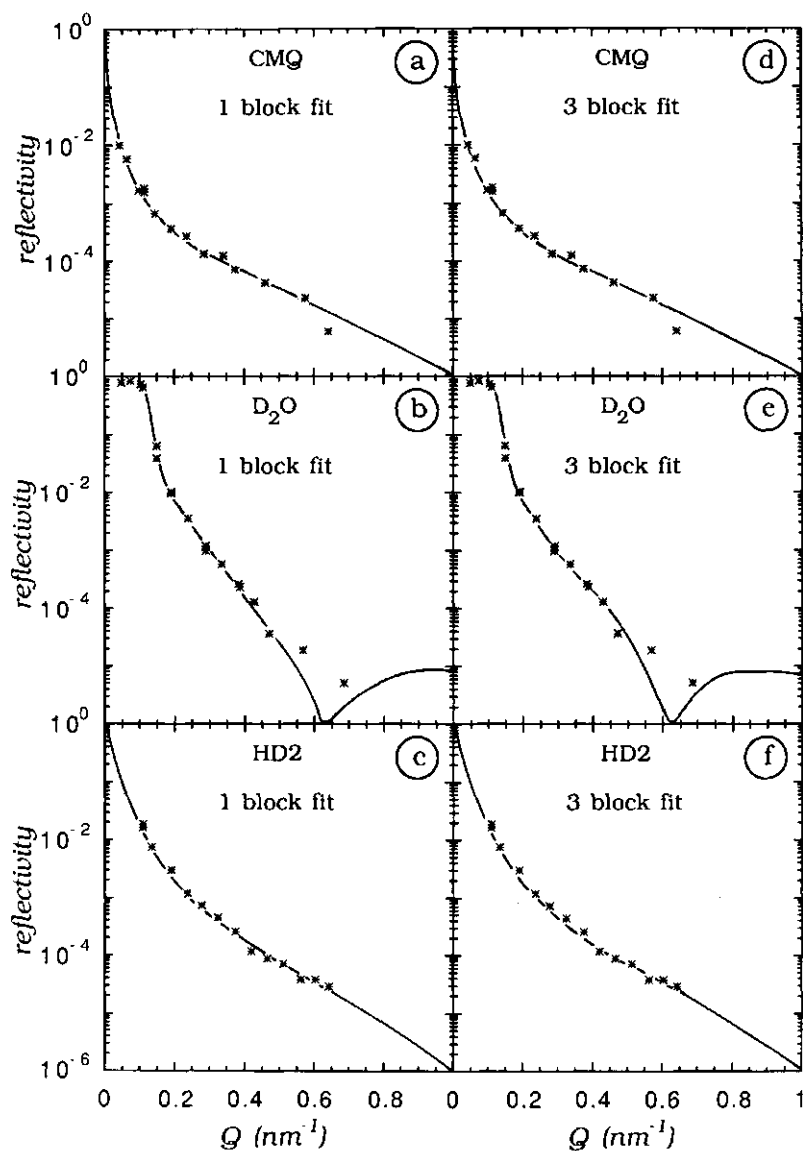


Figure 8 Reflectivity curves for $C_{12}(EO)_{25}$ in contrast matched water and single block fits for (CMQ), D_2O and in HD2 at a layer thickness of 5.3 nm and an adsorbed amount of $0.85 \mu\text{mol}/\text{m}^2$ at a solution concentration of $4E-04M$, (a, b, c). Three block fits are given in Figures (8d-f) for CMQ, D_2O and HD2 respectively, adsorbed amount $0.63 \mu\text{mol}/\text{m}^2$, thickness $2.4+0.5+2.4$ nm.

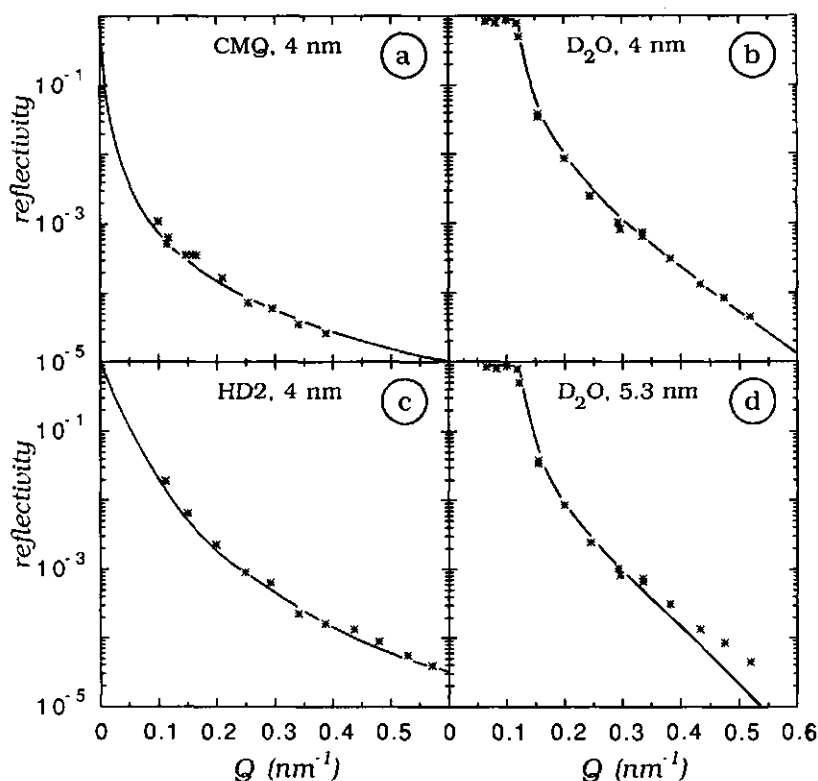


Figure 9: Reflectivity curves and the single block fits for $C_{12}(EO)_{25}$ in contrasted match water (CMQ) (a) and in D_2O (b) and HD2, (c) at a layer thickness of 4.0 nm and a coverage of $0.50 \mu\text{mol}/\text{m}^2$ at a solution concentration of $0.13 \text{ mmol}/\text{dm}^3$. A the best fit obtained with a layer thickness of 5.3 nm in D_2O is given in Figure (d).

one block model but the adsorbed amount goes down to $0.63 \mu\text{mol}/\text{m}^2$, see Figures (8d-f). At this adsorbed amount and structure the bilayer layer cannot be homogeneous and just as in the case of $C_{12}(EO)_6$ it will, most likely, consist of aggregates. Contrary to the $C_{12}(EO)_6$ layer, these aggregates may be rather small as indicated by

fluorescence spectroscopy.⁽³⁾ We have to conclude that in the case of C₁₂(EO)₂₅ the contribution of the aliphatic part of the molecule is too small to localize its position unambiguously. Nevertheless, because the neutron reflection results are only compatible with a large adsorbed amount and a rather thick layer these measurements also indicate that strong association of the aliphatic chain parts takes place.

Table II: Adsorbed layer characteristics obtained with neutron reflection. Results of best fits of the reflectivity curves, the thickness, τ , is in nm, the concentration, c , is given in mmol/dm³ and the adsorption Γ in $\mu\text{mol}/\text{m}^2$, see text for explanation

surfactant	c	model	total τ	$\tau(\text{EO})$	$\tau(\text{C})$	Γ
C ₁₂ (EO) ₆	0.2	3 blocks	5.2	1.81	1.6	3.3
C ₁₂ (EO) ₂₅	0.4	1 block	5.2	--	--	0.85
C ₁₂ (EO) ₂₅	0.4	3 blocks	5.3	2.4	0.5	0.63
C ₁₂ (EO) ₂₅	0.13	1 block	4.0	--	--	0.55

Table III: Scattering length densities, ρ_s , in 10^4 nm^{-2} used for the calculations.

surfactant	c (mM)	solvent	1 block	3 blocks	
			ρ_s	$\rho_s(\text{EO})$	$\rho_s(\text{C})$
C ₁₂ (EO) ₆	0.2	D ₂ O	4.54	5.16	3.58
C ₁₂ (EO) ₆	0.2	CMG	2.50	2.84	1.84
C ₁₂ (EO) ₂₅	0.4	D ₂ O	5.24	5.45	4.33
C ₁₂ (EO) ₂₅	0.4	CMG	2.93	2.98	2.26
C ₁₂ (EO) ₂₅	0.4	HD2	1.71	1.79	1.28
C ₁₂ (EO) ₂₅	0.13	D ₂ O	5.42	-----	-----
C ₁₂ (EO) ₂₅	0.13	CMG	2.94	-----	-----
C ₁₂ (EO) ₂₅	0.13	HD2	1.76	-----	-----

For a concentration of 0.13 mmol/dm³ the single block model fits rather well using a thickness of 4.0 nm and an adsorbed amount of 0.55 $\mu\text{mol}/\text{m}^2$, see Figure (9). The difference in thickness of about 1.5 nm and the decrease in adsorbed amount between the two concentrations is in agreement with other layer thickness

measurements. As the errors in these fits are quite large (which is most likely a result of the steepness of the adsorption isotherm which makes the adsorbed amount very sensitive to the surfactant concentration) we refrained from trying more complex models for the structure of the adsorbed layer.

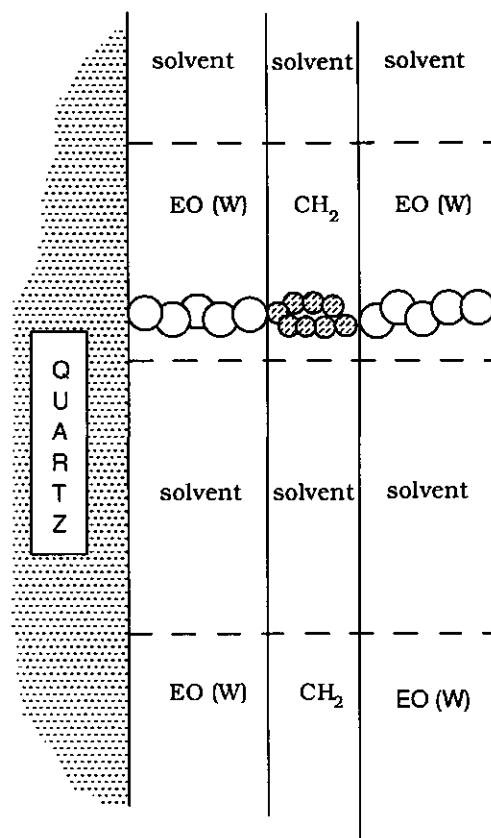


Figure 10: Overview of the 3-block model. The space next to the surface consists of three blocks, an EO rich block, a CH_2 rich block and again an EO rich block. Neutron reflection only gives the average profile perpendicular to the surface.⁽⁵⁾ The indicated regions of surfactant bilayer and solvent are assumed in the model calculations, see text.

Theoretical method and results

Outline

The Self-Consistent Field lattice theory for Adsorption and Association (SCFA) has been used before to model adsorption and micellization of nonionic surfactants.⁽¹⁴⁾ For a description of the model we refer to refs (15-17), here we only summarize the main principles and assumptions. The SCFA theory is an extension of the theory of polymer solutions by Flory⁽⁴⁰⁾ to systems which have inhomogeneities in one direction, for example perpendicular to a surface. The theory involves a lattice which is completely filled with molecules, and each molecule consist of a number (≥ 1) of segments. The layers are numbered $z = 1$ for the layer closest to the surface until $z = M$. A mean field approximation is used in every lattice layer parallel to the surface, so only inhomogeneities perpendicular to the lattice layers can be considered. Every segment type, x , has a volume fraction $\phi_x(z)$ in layer z . The segments of a chain molecule are connected to each other and the relative occurrence of each chain conformation must be calculated to obtain the equilibrium volume fraction profile. To this end the conformation of a chain is treated as a step weighted walk on the lattice, in each step of this walk the contact interactions, quantified by χ -parameters, and the entropy of mixing appear. Together with the condition that the sum of the volume fractions must be unity in every layer the volume fractions of every segment type x in every layer z can be obtained numerically.⁽¹⁷⁾

To study systems which have inhomogeneities in two directions Leermakers et al. extended the SCFA theory.⁽¹⁸⁾ They considered a number of equidistant concentric rings in each lattice layer as shown in Figure (11). The rings in a layer z are numbered starting from $R = 1$ in the central ring. At the outer boundary of the last ring a reflecting mirror is placed. The number of lattice sites in a ring, $L(R)$, varies as a function of R .⁽¹⁸⁾ Within every ring the mean field approximation is applied and the volume fraction of segment x now is a function of both z and R : $\phi_x(z, R)$. The sum of the volume fractions

of the segments in each ring (z, R) is again unity. Using this lattice, inhomogeneities in two directions, perpendicular as well as parallel to the surface, can be studied. Just as in the case of the 1D SCFA theory the Gibbs energy per segment, $u_x(z, R)$, which is now also a function of R , has to be calculated:

$$u_x(z, R) = u'(z, R) + kT \sum_y \chi_{xy} (\langle \phi_y(z, R) \rangle - \phi_y^b) \quad (6)$$

In this equation $u'(z, R)$ is independent of the segment type and it ensures the complete filling of ring (z, R) as commented on elsewhere.⁽¹⁷⁾ The carets indicate a weighted average of the volume fraction which has contributions from the volume fractions in neighboring rings: ($z-1, R-1$), ($z-1, R$) and ($z-1, R+1$) from the previous layer, ($z, R-1$), (z, R) and ($z, R+1$) from layer z and ($z+1, R-1$), ($z+1, R$) and ($z+1, R+1$) from the next layer.⁽¹⁸⁾ As the number of lattice sites varies with R , the weight of the contributions from the neighboring rings also varies with R . The $u_x(z, R)$ functionality is calculated with respect to the bulk solution where the equilibrium volume fraction of x is denoted by ϕ_x^b .

The weight of each conformation is calculated using a step weighted walk procedure described elsewhere.⁽¹⁸⁾ Each step depends on the position of the previous segment and is weighted with the segment weighting factor, $G_x(z, R)$:

$$G_x(z, R) = \exp[-u_x(z, R) / kT] \quad (7)$$

For monomers the volume fractions can be calculated from the segment weighting factors setting simply $\phi_x(z, R) = \phi_x^b G_x(z, R)$. For chain molecules the volume fractions can only be calculated after combination of two step weighted walk procedures, one starting at one chain end and one starting at the other chain end. As the volume fractions are not only calculated from $u_x(z, R)$ but are also part of eq (1), the solution of the set of equations can only be found numerically.

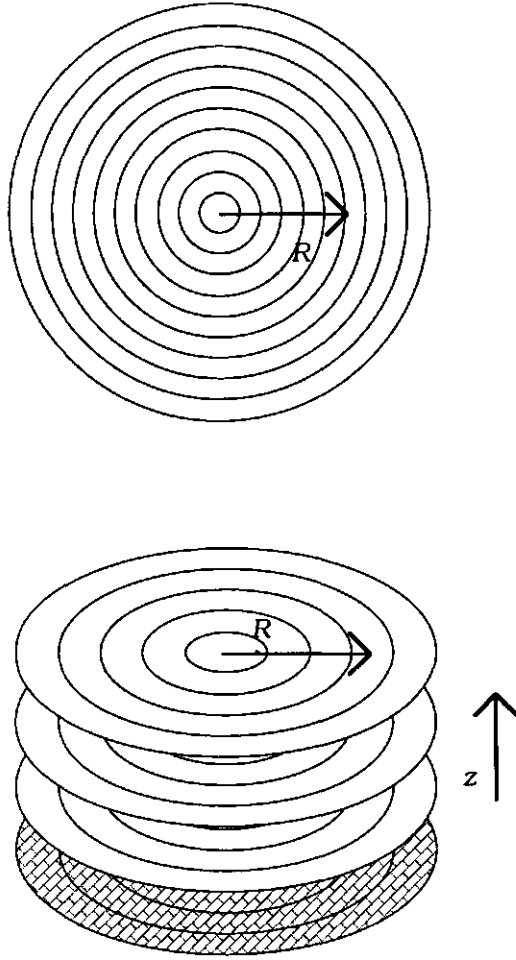


Figure 11: Representation of the 2D, cylindrical symmetrical lattice. The layers contain concentric rings. The hatched plane represents the surface.

From the equilibrium volume fraction profile the excess adsorbed amount, n_i^{exc} , of molecule i with chain length r_i can be calculated using:

$$n_i^{exc} = \sum_z \sum_R L(R) (\phi_i(z, R) - \phi_i^b) / r_i \quad (8)$$

In bulk, surfactant molecules associate in micelles. For concentrations higher than the cmc, ϕ_x^b in the above equations represents the bulk volume fraction of free molecules. It is therefore necessary to know the cmc, which were calculated using the 1D SCFA theory for a spherical lattice.^(14,41) After the cmc is reached the chemical potential hardly changes, although the total surfactant concentration may change markedly. Using the combination of SCFA theory and small system thermodynamics the equilibrium surfactant concentrations can be calculated for a given total surfactant concentration which then serve as a starting point for the adsorption calculation, see ref (42).

Choice of parameters

The solvent, W, consists of one segment. The surfactants, $C_{12}(EO)_6$ and $C_{12}(EO)_{25}$ are modeled as flexible chain molecules, A_4B_6 and A_4B_{25} , i.e. they are composed of 4 hydrophobic segments, A, and 6 or 25 hydrophilic segments, B. The EO oligomer is modeled as a chain of 25 B segments. Contrary to the previous chapter⁽¹⁴⁾, where one CH_2 unit was modeled as one statistical segment, we here group 3 CH_2 units in one A segment to obtain a more realistic size ratio between the head group (EO) and tail group and to decrease the flexibility of the tail. The interaction parameters used must reflect the typical surfactant properties of these molecules. The head group segments are soluble in water, we use $\chi_{BW} = 0.4$, a measured value.^(43,44) In micelles the head groups should be spatially separated from the tails, a positive χ_{AB} value is needed to achieve this, we choose $\chi_{AB} = 2$. For the interaction parameter between the solvent and the aliphatic segments we need a rather high positive value for χ_{AW} , to reproduce the poor solubility of aliphatic segments in water. We choose $\chi_{AW} = 4.3$. With this value the change in critical micelle concentration as a function of aliphatic chain length can be reproduced with the theory, using a lattice of spherical geometry. The B segments are assumed to adsorb on the surface, S, which can be expressed through a negative χ -value, we will use $\chi_{BS} = -3$. This value is smaller than that in ref (14), where we used -6, the latter

choice gave rise to high-affinity isotherms for surfactants with long head groups which is not in agreement with experimental findings. For the interaction between W and S we use $\chi_{WS} = 0$. The A segments do not adsorb, we therefore choose $\chi_{AS} = 4.3$ which is the same value as for χ_{AW} . This choice ensures that no preferential adsorption of A on the surface occurs as the interaction of A with the surface is just as unfavorable as the interaction of A with W. The segment free energy of displacement of W for A on the surface, as defined in ref (14), is zero.

For the 2D calculations we used a lattice with 16 layers and 10 rings. This is rather small with respect to the chain length of the surfactant. The maximum size of the system is dictated by the maximum number of equations that can be handled. As there is one equation for every segment type (A, B, W) in every ring and in every layer this leads to $30 \cdot 16 = 480$ equations in the present case. The small size of the system was an additional reason for the reduction of the aliphatic chain length compared to the previous chapter.

Theoretical results

The adsorption isotherms of A_4B_6 , A_4B_{25} and B_{25} calculated with the 1D SCFA theory are given in Figure (12). An arrow indicates the cmc, beyond which no further increase in adsorption occurs. For A_4B_6 , (Figure 12a) the initial adsorption is very low and just before the cmc a phase separation takes place in the adsorbed layer leading to a large condensation step. The oscillations in the adsorption isotherm are due to lattice artefacts which are especially evident if high χ -values are chosen. For A_4B_{25} , Figure (12b) a more gradual increase is found and a much lower plateau value is reached than for A_4B_6 . Note the scale difference with Figure (12a). The differences between A_4B_{25} and B_{25} are much smaller than observed experimentally for $C_{12}(EO)_{25}$ and the (EO) oligomer. The volume fraction profiles of A and B at the cmc are shown in Figure (13). A_4B_6 clearly forms a bilayer, head groups are located at the surface and at the solution side, in between an aliphatic core is present formed by the tails. For

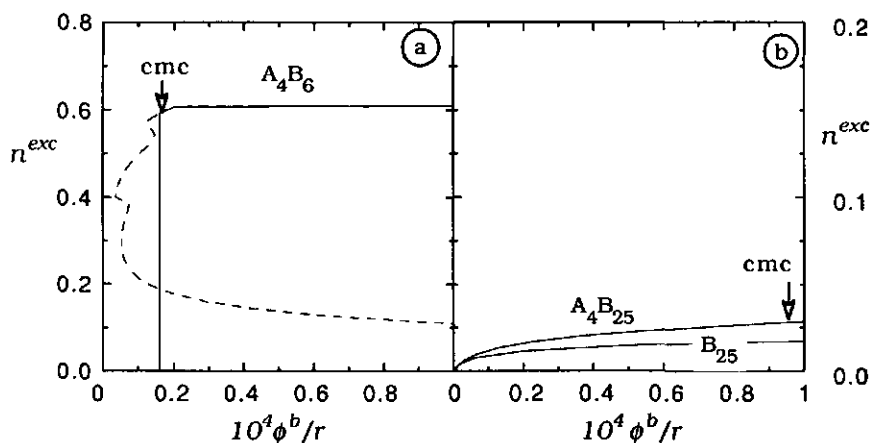


Figure 12: Calculated 1D adsorption isotherm of A_4B_6 , Figure (a). The dashed curve represents the calculated points, the full curve, which coincides with a dotted curve at high coverage, shows the phase separation. The results for A_4B_{25} and B_{25} are given in Figure (b). The cmc is indicated by an arrow. The χ -parameters are: $\chi_{AW} = \chi_{AS} = 4.3$, $\chi_{AB} = 2$, $\chi_{BW} = 0.4$, $\chi_{BS} = -3$ and $\chi_{WS} = 0$.

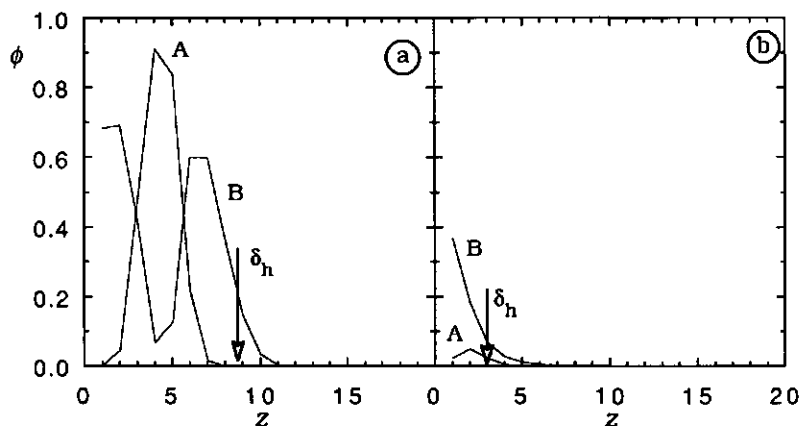


Figure 13: Volume fraction profiles in the plateau of the adsorption isotherm for A_4B_6 and A_4B_{25} . The hydrodynamic layer thickness, δ_h , is indicated. See Figure (12) for interaction parameters.

A₄B₂₅ no significant aggregation of A segments has occurred. From the volume fraction profile the hydrodynamic layer thickness, δ_h , can be calculated, assuming a friction coefficient.⁽⁴⁵⁾ For A₄B₂₅ the thickness is about twice as small as that of the A₄B₆ layer, which does not agree with the experimental results.

In spite of the different choice of parameters the volume fraction profiles are very similar to those presented in ref (14). The shapes of the isotherms have changed slightly: the A₄B₆ isotherm starts to increase sharply at a concentration close to the cmc, whereas the A₁₀B₆ isotherm from ref (14) increased well below the cmc due to the higher value of χ_{BS} . Also for the surfactant with longer head groups the high-affinity shape has disappeared which is in better agreement with experimental work. The difference in plateau values of the two isotherms is, however, about the same for the two sets of parameters used.

As the head group of A₄B₂₅ is very long compared to the tail, it is unlikely that a homogeneous A₄B₂₅ bilayer will form. Nevertheless, the experiments show pronounced interaction between the aliphatic tails. It is possible that in the adsorbed layer the A segments form hydrophobic clusters. This effect can be studied using the 2D SCFA theory.

For A₄B₆ the resulting adsorption isotherm is given in Figure (14a). Due to lattice artefacts the shape of the isotherm is not perfect, nevertheless it is clear that the instability region has become much smaller. This is due to the fact that no longer a critical concentration in a certain layer is needed to get phase separation, but this critical concentration is needed in just one ring. The adsorption isotherm increases almost vertically, close to the step in the 1D adsorption isotherm. The main drawback of the 2D theory is that we can only study 1 aggregate and its growth with bulk solution concentration. If the amount of surfactant in the system becomes high, not just one aggregate in the center of the lattice is found, but surfactant molecules also start to accumulate near the system boundaries (near

ring 10) and then the calculated volume fraction profile depends strongly on the number of rings used. Because this is unrealistic the calculated isotherm is truncated at $n^{exc} = 0.3$. As both in 1D calculations and in experiments a condensation step in the adsorption isotherm, leading to bilayer coverage close to the cmc, was found, there is no need to use 2D theory for intermediate coverages.

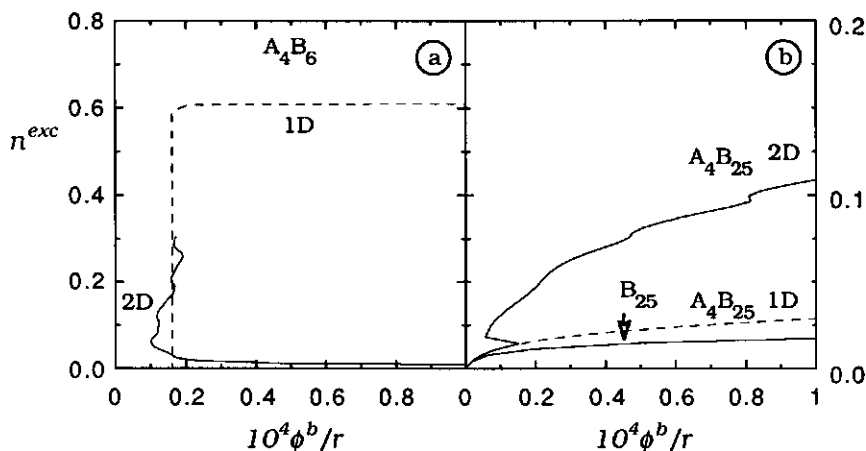


Figure 14: Calculated 1D and 2D adsorption isotherms of A_4B_6 (a), A_4B_{25} and B_{25} (b). See Figure (12) for interaction parameters.

For A_4B_{25} the difference between the 1D and 2D isotherms is quite significant, see Figure (14b). The adsorbed amount calculated with the 2D theory is much higher than that with the 1D theory. Moreover, the adsorption is much higher than that of B_{25} . These differences and the high adsorption values indicate that strong association must have taken place. This is more clearly illustrated in Figure (15) where the volume fraction profiles in the plateau of the isotherm are shown. The B segments are located at the surface and on the outside of the core formed by the A segments. The aggregate consists of about 30 molecules. Note that in layer 10 and ring 1 we

still find a significant volume fraction of B segments. For the 2D system we cannot yet calculate the hydrodynamic layer thickness, but obviously a much thicker layer has been formed compared to the 1D calculations.

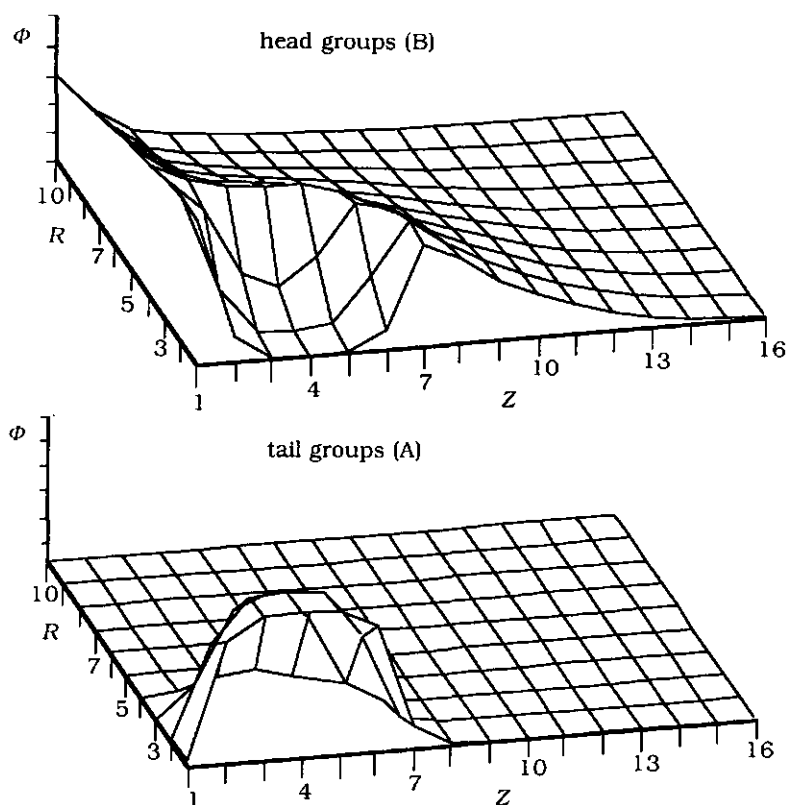


Figure 15: Volume fraction profiles of B and A segments of A_4B_{25} in the plateau of the adsorption isotherm. See Figure (12) for interaction parameters.

Discussion

Both from theory and experiment the bilayer formation of $C_{12}(EO)_6$ on a hydrophilic surface is evident and the shape of the isotherm is predicted correctly in agreement with other experimental work. Although we did not experimentally find a complete bilayer on the surface, previous neutron reflection studies have indicated that almost complete bilayer coverage with $C_{12}(EO)_6$ can occur.^(5,39) If the results are compared in more detail also some other differences appear. The thickness of the hydrophobic region in the $C_{12}(EO)_6$ layer is about one stretched aliphatic chain length while for A_4B_6 it is less, see Figure (12). A similar discrepancy exists for the head groups. From the neutron reflection results we find that the $(EO)_6$ part is rather stretched: the length of a stretched $(EO)_6$ chain is 2.1 nm.⁽⁴⁵⁾ while the SCFA theory gives a thickness of 3 lattice layers for the head group which is 6 segments long. Moreover, the calculated volume fraction of water in the head group region is too low because no specific hydration effects are incorporated. Although these differences are not very pronounced, the SCFA profile will not fit the neutron reflection curve. The calculated hydrocarbon core is too thin because the flexibility of the molecules is overestimated. This could be circumvented by choosing longer statistical chain segments but this will lead to an increase in the lattice artefacts. In a more detailed model the hydration of the EO groups should be incorporated; this change will lead to thicker head group regions.

For A_4B_{25} the 2D SCFA theory predicts the formation of aggregates on the surface. The presence of these aggregates is responsible for high adsorbed amounts and thick layers in comparison with those for the polymer B_{25} . These differences were also found experimentally between $C_{12}(EO)_{25}$ and $(EO)_{22}$. The calculated aggregation number of the aggregate (30) at the plateau of the adsorption isotherm is about the same as that for A_4B_{25} micelles, calculated at high surfactant concentrations. Experimentally, using pyrene excimer formation this was also found by Levitz et al.⁽³⁾

One typical difference from the results of Levitz is that we find that the aggregate grows as the solution concentration becomes higher, while Levitz et al. find for surfactants with long polar chains, i.e. 30 EO units, that the aggregation number stays approximately constant but that the number of aggregates increases. However, below half of the maximum coverage, they failed to solubilize pyrene in the adsorbed layer, indicating that the hydrophobic cores, if present, are too small to accommodate pyrene. Therefore some change in aggregation number may occur in reality as well. For a surfactant with a medium long polar chain, $(EO)_{13}$, Levitz et al. did find a growth in aggregate size with the concentration. The theory does not allow us to calculate the number of aggregates or their size distributions. Nevertheless, the layer thickness measurements for $C_{12}(EO)_{25}$ show that the aggregates on the surface grow gradually with solution concentration. Moreover, the shapes of the layer thickness vs. concentration curves closely follow the adsorption isotherms. If only the number and not the size of aggregates increases with concentration then little change in hydrodynamic layer thickness would be expected. The thicknesses of the layer obtained by neutron reflection of $C_{12}(EO)_{25}$ at the two coverages also indicate that the layer thickness increases gradually. Therefore, from our experimental results it appears that the growth of the aggregates forms an important aspect of the development of the adsorbed layers.

Conclusions

The adsorption of $C_{12}(EO)_6$, $C_{12}(EO)_{25}$ and $(EO)_{22}$ on silica, glass and quartz surfaces was studied using different methods. In general the results obtained by batch adsorption, reflectometry, and neutron reflection for the adsorbed amount and DLS, streaming potential and neutron reflection for the layer thickness, agree closely with each other. The 1H solvent relaxation shows that in both the $C_{12}(EO)_6$ and $C_{12}(EO)_{25}$ the mobility of (hydration) water is more reduced compared to that in adsorbed PEO layers. All these results show that

the net attraction between the aliphatic tails is of crucial importance for the structure of adsorbed layers of nonionic surfactants. The attraction between the tails leads to bilayer formation of $C_{12}(EO)_6$ just before the cmc is reached. For $C_{12}(EO)_{25}$ it leads to the formation of rather small aggregates on the surface. Due to aggregate formation both the adsorbed amount and the layer thickness for $C_{12}(EO)_{25}$ are considerably higher than for an EO-oligomer of comparable molecular weight.

These experimental features were confirmed theoretically using the 2D SCFA theory. With the 1D SCFA theory the adsorbed amount and layer thickness for nonionics with a relatively large head group are underestimated. Therefore, even though, at present, with the 2D SCFA theory only one surface aggregate and its growth with concentration can be studied, it is to be preferred over the 1D SCFA theory for nonionic surfactants with long polar head groups.

References

- 1 Levitz, P.; El Miri, A.; Keravis, D.; Van Damme, H. *J. Colloid Interface Sci.* **1984**, *99*, 484
- 2 Levitz, P.; Van Damme, H.; Keravis, D. *J. Phys. Chem.* **1984**, *88*, 2228
- 3 Levitz, P.; Van Damme, H. *J. Phys. Chem.* **1986**, *90*, 1302
- 4 Levitz, P. *Langmuir* **1991**, *7*, 1595
- 5 Lee E. M.; Thomas, R. K.; Cummins, P. G.; Staples, E. *J. Chem. Phys. Letters* **1989**, *162*, 196
- 6 Cummins, P. G.; Staples, E.; Penfold, J. *J. Phys. Chem.* **1990**, *94*, 3740
- 7 Zhu, B. Y.; Zhao, Z.; Gu, T. *J. Chem. Soc. Faraday Trans I* **1988**, *84*, 3951
- 8 Gu, T.; Zhu, B. Y. *Colloids Surf.* **1989**
- 9 Gellan, A.; Rochester, C. H. *J. Chem. Soc., Faraday Trans. 1*, **1985**, *81*, 2235
- 10 Partyka, S.; Zaini, S.; Lindheimer, M.; Brun, B. *Colloids Surf.* **1984**, *12*, 255
- 11 Thomas, F.; Bottero, J. Y.; Partyka, S.; Cot, D. *Thermochimica Acta* **1987**, *122*, 197
- 12 Denoyel, R.; Rouquerol, F.; Rouquerol, J. in "Fundamentals of Adsorption", A. J. Liapis ed. Engineering Foundation, New York 1987, p. 199
- 13 Partyka, S.; Lindheimer, M.; Zaini, S.; Keh, E.; Brun, B. *Langmuir* **1986**, *2*, 101
- 14 Böhmer, M. R.; Koopal, L. K., *Langmuir* **1990**, *6*, 1478, this thesis Ch. 2
- 15 Scheutjens, J. M. H. M.; Fleer, G. J. *J. Phys. Chem.* **1979**, *83*, 1619

- 16 Scheutjens, J. M. H. M.; Fleer, G. J. *J. Phys. Chem.*, **1980**, 84, 178
- 17 Evers, O. A.; Scheutjens, J. M. H. M.; Fleer, G. J. *Macromolecules* **1990**, 23, 5221
- 18 Leermakers, F. A. M.; Scheutjens, J. M. H. M.; Lyklema, J. *Biochimica Biophysica Acta* **1990**, 1024, 139
- 19 Dijt, J. C.; Cohen Stuart, M. A.; Hofman, J. E.; Fleer, G. J. *Colloids Surf.* **1990**, 51, 141
- 20 Koopal, L. K.; Hlady, V.; Lyklema, J. *J. Colloid Interface Sci.* **1987**, 121, 49
- 21 Cohen Stuart, M. A.; Tamai, H. *Macromolecules* **1988**, 21, 1863
- 22 Crowley, T. L.; Lee, E. M.; Simister, E. A.; Thomas, R. K.; Penfold, J.; Rennie A. R. *Colloids Surf.* **1990**, 52, 85
- 23 Van der Beek, G. P.; Cohen Stuart, M. A.; Cosgrove, T. C. *Langmuir*, **1991**, 7, 327
- 24 Nuysink, J.; Koopal, L. K. *Talanta*, **1982**, 29, 495
- 25 Hansen, W. N. *J. Optical Soc. Am.* **1968**, 58, 380
- 26 Born, M.; Wolf, E. in "Principles of Optics", 5th ed.; Pergamon Press, Oxford, 1975 p51
- 27 Chiu, Y. C.; Chen, L., *Colloids Surf.* **1989**, 239, 41
- 28 Van der Beek, G. P.; Cohen Stuart, M. A. *J. Phys. France* **1988**, 49, 1449
- 29 Dijt, J. C.; Cohen Stuart, M. A. in preparation
- 30 Tadros, Th. F.; Lyklema, J. *J. Electroanal. Chem.* **1968**, 18, 341
- 31 Abendroth, R. P. *J. Colloid Interface Sci.* **1970**, 34, 591
- 32 Hiemstra, T.; De Wit, J. C. M.; Van Riemsdijk, W. H. *J. Colloid Interface Sci.* **1989**, 133, 105
- 33 Penfold, J. "The adaptation of methods in multilayer optics for the calculation of specular neutron reflection" Rutherford Appleton Laboratory Report RAL-88-0088, Didcot, U. K.
- 34 Willis, B. T. M. (Ed); "Chemical Application of thermal neutron scattering" Oxford University Press, 1973
- 35 Van der Beek, G. P.; Cohen Stuart, M. A.; Fleer, G. J.; Hofman, A. *Macromolecules* in press
- 36 Somasundaran, P.; Turro, N. J.; Chandar, P. *Colloids Surf.* **1986**, 20, 145
- 37 Chandar, P.; Somasundaran, P.; Waterman, K. C.; Turro, N. J. *J. Phys. Chem.*, **1987**, 91, 150
- 38 Tanford, C. *J. Phys. Chem.* 1972, 76, 3020
- 39 McDermott, D. C.; Lu, J. R.; Lee, E. M.; Thomas, R. K. submitted to *Langmuir*
- 40 Flory, P. "Principles of Polymer Chemistry", Cornell University Press, Ithaca New York 1953
- 41 Leermakers, F. A. M.; Scheutjens, J. M. H. M. *J. Colloid Interface Sci.* **1990**, 136, 231
- 42 Van Lent, B.; Scheutjens, J. M. H. M. *Macromolecules*, **1989**, 22, 1931
- 43 Amu, T. C. *Polymer*, **1982**, 23, 1775
- 44 Van den Boomgaard, A. *Ph. D. Thesis*, Wageningen Agricultural University, Wageningen, The Netherlands. **1985**
- 45 Scheutjens, J. M. H. M.; Fleer, G. J.; Cohen Stuart, M. A. *Colloids Surf.* **1986**, 21,

285

- 46 Tanford, C.; Nosaki, Y.; Rohde, M. F. *J. Phys. Chem.* **1977**, *81*, 1555

CHAPTER 4

Micellization of Ionic Surfactants

Analysis based on a self-consistent field lattice model

Abstract

The equilibrium structure of micelles formed in aqueous solutions of ionic surfactants is studied using the self-consistent field lattice approach of Scheutjens, Fleer and Leermakers. Equilibrium volume fraction profiles of micelles are obtained and it appears that the surfactant head groups have a rather wide distribution. The boundary between the hydrocarbon core of the micelle and the solution is rather sharp and does not vary with salt concentration. An electrostatic potential develops, which causes accumulation of indifferent counterions in between the head groups and, consequently, leads to partial neutralization of the charges. The remaining net charge in the head group region is independent of the salt concentration. The calculated effects of chain length, salt concentration and branching on the cmc and the aggregation numbers show a good agreement with experimental data. Using lattices of different geometry transitions from small spherical micelles to large rod-like aggregates can be predicted.

Introduction

Since long it has been recognized that the formation of micelles of ionic surfactants in aqueous solution is a result of at least two opposing forces. Hydrophobic interaction promotes aggregation and the electrostatic repulsion between the charged head groups opposes it. If the length of the hydrophobic tail is increased, the hydrophobic effect becomes stronger and, consequently, the critical micelle concentration (cmc) decreases and larger micelles are formed. By adding salt the electrostatic repulsion between the head groups decreases, which also induces a decrease in cmc, and an increase in aggregation number. When the salt concentration is raised small globular micelles may, in some cases, no longer be the

preferred structures, but transitions to e.g. long cylinders may take place.

Many, sometimes very detailed, thermodynamic theories of micellization, see e.g. refs (1-5) allow a calculation of the balance between hydrophobic interaction and electrostatic repulsion. Beside the electrostatic repulsion and the number of aliphatic groups, also the structure (linear or branched) of the surfactant chain has an effect on the cmc, the aggregation number and the micelle shape. For instance, branched aliphatic tails suffer more spatial restrictions on packing into aggregates with a hydrocarbon core than linear chains, therefore the cmc's of branched surfactants are higher and the aggregation numbers lower than those of their linear isomers. The thermodynamic models in refs (1-5) can be used to calculate cmc's, aggregation numbers and in some cases counter-ion binding, but they do not elucidate the molecular structure of the micelle. On the contrary, the molecular arrangement, the distribution of head and tail groups, is presupposed.

An important aspect in the molecular structure of micelles is the flexibility of the surfactant tail.⁽⁶⁾ In theoretical treatments insight regarding the tail conformations can be gained using statistical thermodynamic theories.⁽⁷⁻⁹⁾ A theory describing chain conformations in the liquid interior of a micelle has been put forward by Gruen⁽⁷⁾ and was followed by Eriksson et al.⁽⁵⁾ who combined Gruen's chain statistics with macroscopic thermodynamics thereby introducing such parameters as the surface tension of the hydrocarbon/water interface. The main drawback of Gruen's and other models^(8,9), in which chains are generated by a statistical (step weighted walk) procedure is that the aliphatic chain parts all start their walk on a shell (or a single plane) fixing the positions of the head groups on the outside of this shell. Due to this assumption the structure of the micelle is still presupposed to some extent. Both for entropic and enthalpic reasons the alignment of head groups is a severe simplification. Gruen⁽¹⁰⁾ and Szleifer et al.⁽¹¹⁾ relaxed the constraints imposed on the positions of the head

groups and the sharpness of the interface between the hydrocarbon and the aqueous phase, which is important since Molecular Dynamics simulations on micellar systems have shown that the head groups of the surfactants are not exactly aligned.⁽¹²⁻¹⁵⁾ Neutron scattering experiments revealed that the head group region in micelles is thicker than the thickness of a single head group.^(16,17)

In the improved theories of Gruen⁽¹⁰⁾ and Szleifer et al.⁽¹¹⁾ the surface density of the head group is still an input parameter. A theory that does not a priori assume localization nor density of head groups (or any other segments), but calculates them as equilibrium properties of the formed structure is the self-consistent field lattice theory for adsorption or association of chain molecules (SCFA).⁽¹⁸⁻²⁰⁾ This theory, originally developed by Scheutjens and Fleer to model the adsorption of uncharged homopolymers^(18,19), has been adapted by Leermakers et al.⁽²¹⁻²³⁾ to describe membrane and micelle formation of non-ionic lipids and surfactants. Recently, electrostatic interactions have been incorporated in the theory.^(24,25) In the present study elements of the polyelectrolyte theory will be combined with those of the surfactant theory to study the aggregation of ionic surfactants.

The main results of a calculation with the SCFA theory include equilibrium segment distributions, such as the distribution of head and tail groups of the surfactant. Moreover, the electrostatic potential in every lattice layer is obtained. The critical micelle volume fraction and the micelle size as a function of the total surfactant concentration can be found using arguments from small system thermodynamics.^(22,26-28)

In this chapter a brief overview of the SCFA theory will be given with some emphasis on the electrostatic interactions. A more detailed treatment of the SCFA theory can be found in the literature^(20,21), modeling of the electrostatics is presented in refs^(24,25). The structure of micelles formed by ionic surfactants will be studied in some detail. Calculations with respect to the effects of salt

concentration, chain length and branching on the critical micelle concentration and the aggregation number will be presented. Transitions from spherical micelles to cylindrical or flat aggregate structures will be investigated by comparing results obtained with lattices of different geometries.

SCFA Theory

General outline

The SCFA theory involves an *ab initio* treatment. Starting from system characteristics such as the number of different molecule types and the amount of each of them, together with molecular properties such as numbers of segments, structure, charge and the interactions between the various segments, the equilibrium distribution of molecules is calculated. To account for all interactions and to weigh the relative occurrence of different chain conformations a lattice is used.

To study the shapes of the aggregates, we considered flat, cylindrical and spherical lattices. In a flat lattice the fraction of contacts of a lattice site in layer z with sites in layer $z-1$, denoted as λ_{-1} , equals the fraction of contacts with sites in layer $z+1$, denoted as λ_1 . These fractions are independent of z . In spherical and cylindrical lattices the number of lattice sites is not the same in every lattice layer, therefore λ_{-1} , λ_0 and λ_1 will be functions of z . These functions have been given elsewhere.^(22,28) For spherical and cylindrical symmetries the layers will be numbered starting from the center of the lattice.

To each segment of type x , in each layer z , we assign a volume fraction $\phi_x(z)$. This implies that we only consider inhomogeneities in the direction perpendicular to the lattice layers. The calculated aggregate is in equilibrium with the bulk solution, where the volume fractions of molecules i are denoted by ϕ_i^b . As the volume fractions in the layers z are not the same as those in the bulk solution, a free

energy difference per segment (or potential of mean force), $u_x(z)$, exists for every type of segment with respect to the bulk solution. The expression for $u_x(z)$ follows from statistical thermodynamics^(20, 24):

$$u_x(z) = u'(z) + kT \sum_y (<\phi_y(z) > - \phi_y^b) \chi_{xy} + v_x e \psi(z) \quad (1)$$

Three terms contribute to $u_x(z)$, $u'(z)$ quantifies the local hard core interaction with respect to the bulk solution and must be the same for every segment type in layer z . As no explicit expression for $u'(z)$ is available, it has to be numerically adjusted to ensure that the sum of the volume fractions equals unity.⁽²⁰⁾ Physically, $u'(z)$ equals $+\infty$ or $-\infty$ if the sum of the volume fractions in a layer is not unity. The second term on the right hand side contains the contact interactions: χ_{xy} is the familiar Flory-Huggins parameter accounting for nearest neighbor interactions between segments x and y , $<\phi_y(z) >$ is the contact volume fraction of y in layer z , which has contributions from layers $z-1$, z and $z+1$. The last term in eq (1) covers the electrostatic interactions: v_x is the valency of segment x and $\psi(z)$ is the electrostatic potential in layer z , e is the elementary charge. From $u_x(z)$, segment weighting factors, $G_x(z)$, are calculated:

$$G_x(z) = \exp[-u_x(z) / kT] \quad (2)$$

The Boltzmann factor $G_x(z)$ indicates the probability to find an unbound segment x in layer z relative to finding it in a layer in homogeneous equilibrium solution. In the case of a molecule containing just one segment in equilibrium with the bulk solution the volume fraction $\phi_x(z)$ of a segment of type x in layer z is calculated from its bulk volume fraction ϕ_i^b and the segment weighting factor $G_x(z)$:

$$\phi_x(z) = \phi_x^b G_x(z) \quad (3)$$

Chain statistics

To obtain the volume fractions of segments s belonging to chain i , consisting of r_i segments, we must take into account that the segments of the chain are connected to each other. Several types of chain statistics can be applied to arrive at the segment distribution of chain segments. The simplest form used in the SCFA theory is first order Markov statistics, where the chain segments follow a step-weighted walk and backfolding is not forbidden. For not too long surfactant chains we prefer a rotational isomeric state (RIS) scheme, a type of third order Markov statistics as developed by Leermakers and Scheutjens.^(21,23) This RIS method precludes backfolding in a series of five consecutive segments of a chain and allows for a distinction between trans and gauche conformations. The application of RIS results in a decrease of chain flexibility compared to first order Markov statistics. This is important if we want to consider every chemical group like a CH_2 unit as one segment, because these groups are too small to be regarded as statistical chain elements.

To calculate the volume fractions of segments s of chains i containing r segments, we need the chain segment weighting factor, $G_i(z, s | 1:r)$. The chain segment weighting factor combines two chain end segment distribution functions. One describes a walk starting at segment 1 located at an arbitrary position in the system. The start value is given by $G_1(z)$ (the subscript 1 refers the segment type 1, which is of type x , see eq 2) and it ends at segment s in layer z after a walk of $s-1$ steps along the chain, the index 1 in $G_i(z, s | 1:r)$ refers to this walk. The other chain end segment distribution function starts at the other chain end, i.e. segment r , where $G_r(z)$ is the start value. This walk also ends at the same segment s in layer z after a walk of $r-s-1$ steps along the chain. The index r in $G_i(z, s | 1:r)$ refers to this starting point. In each step of the walk along the chain the $u_x(z)$ value appears in a Boltzmann factor which has been described elsewhere, see e.g. ref (24).

If the RIS method is applied the chain segment weighting factor, $G_i(z, s | l; r)$, of segments s of chains i containing r segments depends not only on $u_x(z)$ and the positions of the neighboring segments of a chain but also on the orientation of the bonds between these segments, which has been demonstrated elsewhere.^(21,23) This RIS procedure has been generalized to branched chains.⁽²¹⁾

From the chain segment weighting factors the volume fractions of segments s , belonging to chain i , are calculated, using the analogue of eq (3) for chain segments^(20, 24):

$$\phi_i(z, s) = C_i G_i(z, s | l; r) \quad (4)$$

The normalization constant C_i equals ϕ_i^b / r_i or, more generally, $\theta_i / r_i G_i(r | l)$, where θ_i is the total amount of chain i and $G_i(r | l)$ is the sum of the chain end segment weighting factors for segment r , over the total number of layers, defined as M . Equating C_i to ϕ_i^b / r_i is equivalent to taking a special case of $\theta_i / r_i G_i(r | l)$ since in a homogeneous bulk solution $\theta_i = M \times \phi_i^b$ and $G_i(r | l) = M \times 1$.⁽²⁰⁾

The volume fraction, $\phi_i(z)$, that each molecule type i has in layer z can be obtained by a summation of $\phi_i(z, s)$ over all segments that this molecule type has in layer z :

$$\phi_i(z) = \sum_{s=1}^r \phi_i(z, s) \quad (5)$$

The volume fractions of segments of type x , belonging to molecules i , $\phi_{xi}(z)$ can be obtained if the sum is restricted to segment s of type x .

Because of the use of volume fractions instead of number of segments (or molecules) the definition of the total amount, θ_i , in the system is not entirely straightforward. For spherical geometry the number of lattice sites per layer, $L(z)$, can be calculated from the difference between volume $V(z)$ and volume $V(z-1)$, where $V(z)$ equals $4\pi z^3/3$ and the total amount is most conveniently expressed as:

$$\theta_i = \sum_z L(z) \phi_i(z) \quad (6a)$$

For lattices with cylindrical geometry only the relative change in the number of lattice sites with layer number is known and not the total number of lattice sites, since the cylinder has an infinite length. The volume of a disk with the thickness equal to the length of one lattice site is given by $V(z) = \pi z^2$. In eq (6a) we now use for $L(z)$ the difference in volume of disks with radius z and $z-1$. For flat geometry the amount θ_i is defined per unit cross section of a lattice site and is thus simply given by:

$$\theta_i = \sum_z \phi_i(z) \quad (6b)$$

Electrostatic interactions

The uneven distribution of charged molecules leads to the development of electrostatic potentials. These potentials are calculated using a multi-Stern layer model and depend on the net charge and the electrostatic capacitance in each layer. The charge is assumed to be exclusively located on the midplanes of the lattice layers, as shown schematically in Figure (1). The charge density in each layer, $\sigma(z)$, follows directly from:

$$\sigma(z) = \sum_x v_x e \phi_x(z) / a_s \quad (7)$$

where a_s is the cross section of a lattice site. For the dielectric constant $\epsilon(z)$ in layer z we assume a linear combination of the dielectric constants of the species, ϵ_x , present in that layer:

$$\epsilon(z) = \sum_x \epsilon_x \phi_x(z) \quad (8)$$

The field strength E as a function of the distance ζ may change discontinuously at the midplanes of the lattice layers, which are separated by a distance ℓ , located at $z = 1, 2, \dots$ ($\zeta = 1/2\ell, 3/2\ell, \dots$) due to the presence of charge and at $z = 1/2, 3/2, \dots$ ($\zeta = 0, \ell, \dots$) due to a

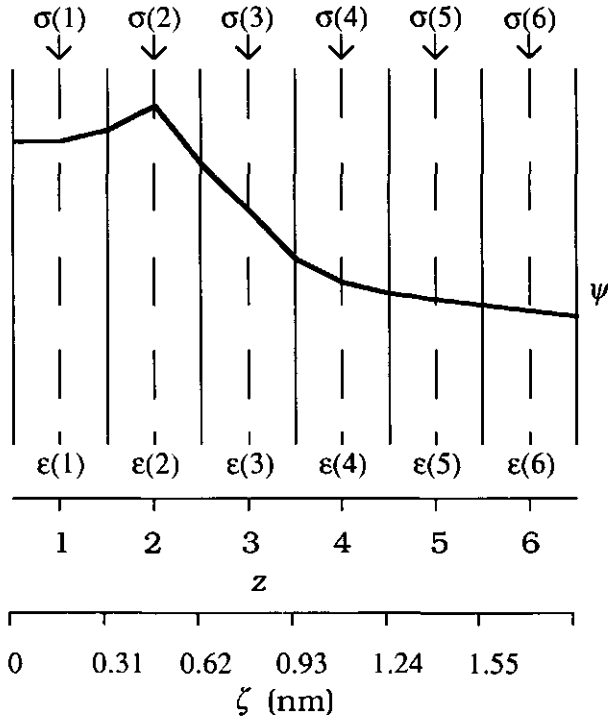


Figure 1: Schematic two-dimensional representation of a flat lattice. The lattice consists of z layers and is entirely filled with molecules. The electrostatic charges, σ , are located on the midplanes in each lattice layer. For the calculation of the electrostatic potentials, ψ , the charges, the distance, l , between the midplanes and the average dielectric constant, $\epsilon(z)$, in each layer are needed. For l a value of 0.31 nm is chosen. A discontinuous change in the field strength occurs at the midplanes where charge is present and at the boundary planes between two lattice layers where the dielectric constant changes. In a curved lattice the distance, ζ , from the center of the lattice with has unit length, determines the divergence of the electric field.

change in dielectric constant, see Figure (1). In addition in curved lattices a continuous decrease of $E(\zeta)$ exists due to the divergence of the electric field. The field strength at distance ζ from the central point (spherical), line (cylindrical) or plane (flat) geometry of the lattice follows from Gauß' law, $\oint E dA_s = q / \epsilon$, where q is the charge and A_s the area. Application to the different geometries yields:

$$\text{flat: } E(\zeta) = \frac{1}{\varepsilon(\zeta)} \sum_{z'=1}^{\text{int}(\zeta/\ell + \frac{1}{2})} \sigma(z') \quad (9a)$$

$$\text{cylinder: } E(\zeta) = \frac{1}{2\pi\zeta^2\varepsilon(\zeta)} \sum_{z'=1}^{\text{int}(\zeta/\ell + \frac{1}{2})} L(z')\sigma(z') \quad (9b)$$

$$\text{sphere: } E(\zeta) = \frac{1}{4\pi\zeta^2\varepsilon(\zeta)} \sum_{z'=1}^{\text{int}(\zeta/\ell + \frac{1}{2})} L(z')\sigma(z') \quad (9c)$$

The upper boundary of the summation is the Entier function of $\zeta/\ell + 1/2$ indicated as $\text{int}(\zeta/\ell + 1/2)$.

Since the charges are located on the midplanes of the lattice layers, only the potentials on these midplanes are relevant for the calculation. The potential difference between two neighboring midplanes at $z+1$ and z is given by:

$$\psi(z+1) - \psi(z) = - \int_{\zeta=(z-\frac{1}{2})\ell}^{\zeta=(z+\frac{1}{2})\ell} E(\zeta) d\zeta \quad (10)$$

Using this we obtain for the three geometries:

flat:

$$\psi(z+1) = \psi(z) - \frac{\ell}{2} \left[\frac{1}{\varepsilon(z)} + \frac{1}{\varepsilon(z+1)} \right] \sum_{z'=1}^z \sigma(z') \quad (11a)$$

cylinder:

$$\psi(z+1) = \psi(z) - \frac{1}{2\pi} \left[\frac{1}{\varepsilon(z)} \ln \left(\frac{z}{z-\frac{1}{2}} \right) + \frac{1}{\varepsilon(z+1)} \ln \left(\frac{z+\frac{1}{2}}{z} \right) \right] \sum_{z'=1}^z L(z')\sigma(z') \quad (11b)$$

sphere:

$$\psi(z+1) = \psi(z) - \frac{1}{8\pi\ell} \left[\frac{1}{\epsilon(z)(z-\frac{1}{2})z} + \frac{1}{\epsilon(z+1)z(z+\frac{1}{2})} \right] \sum_{z'=1}^z L(z')\sigma(z') \quad (11c)$$

In all geometries there is a contribution of layer z where the dielectric constant is $\epsilon(z)$ and a contribution of layer $z+1$ where the dielectric constant is $\epsilon(z+1)$. In the middle of layer z the distance to the center of the lattice is $(z-1/2)\zeta$, this causes the $z-1/2$ term and the absence of a $z+1$ term in equations (11b) and (11c). Except for cylindrical geometry the distance between two midplanes, ℓ , has to be quantified to obtain the potential difference. For uncharged systems this distance is arbitrary.

To calculate the potentials with respect to the bulk solution a starting point at layer M is needed; for this purpose the electroneutrality condition has to be used.⁽²⁴⁾

Excess and Aggregation numbers

An interesting quantity is n_i^{exc} , the excess number of molecules i in the system with respect to the equilibrium solution, due to the presence of a micelle. It can be calculated from the volume fraction profile using:

$$n_i^{exc} = \sum_z L(z) [\phi_i(z) - \phi_i^b] \quad (12)$$

The number of aggregated molecules in a micelle, n_i^{agg} may differ from the excess number of molecules in the system because in layers adjacent to the micelle a depletion of surfactant molecules can occur. To calculate the aggregation number of a micelle we use eq (12) for layers where $[\phi_i(z) - \phi_i^b]$ is positive:

$$n_i^{agg} = \sum_z L(z) [\phi_i(z) - \phi_i^b] \text{ for } [\phi_i(z) - \phi_i^b] > 0 \quad (13)$$

Thermodynamics of small systems

Using the SCFA theory the equilibrium structure of a single micelle can be calculated. In combination with the thermodynamics of small systems^(22, 26-28) the composition of a micellar solution, consisting of a number of identical micelles, can be found. To this end, the solution is divided into a number of subsystems with volume V_s , where every subsystem contains one micelle, with volume V_m . To distinguish between the equilibrium volume fraction of i in homogeneous bulk solution, ϕ_i^b and the average volume fraction of i in both the system and each subsystem, the latter is denoted by $\bar{\phi}_i$. The excess free energy of the subsystem, A_s^{exc} consists of two parts: the translational entropy of the micelle, $k \ln(V_m/V_s)$ (micelles may move freely in the solution) and the excess free energy for creation of a micelle with a given aggregation number and a fixed position, A_m^σ , hence:

$$A_s^{exc} = A_m^\sigma + kT \ln(V_m/V_s) \quad (14)$$

For micelles in equilibrium with a homogeneous solution A_s^{exc} is zero. Equation (14) allows calculation of V_s for a given value of V_m and A_m^σ . As $k \ln(V_m/V_s)$ is always negative, micelles can only exist if A_m^σ is sufficiently positive. The excess free energy for formation of a micelle with a fixed position, A_m^σ , can be obtained from a SCFA calculation and is given by^(20, 24):

$$A_m^\sigma = kT \sum_z L(z) \left\{ \sum_x \phi_x(z) \ln G_x(z) - \sum_i \frac{\phi_i(z) - \phi_i^b}{r_i} + \frac{1}{2} \sum_x \sum_y \chi_{xy} \left[\phi_x(z) \left(\langle \phi_y(z) \rangle - \phi_y^b \right) - \phi_x^b \left(\phi_y(z) - \phi_y^b \right) \right] + \frac{\sigma(z) \psi(z)}{2} \right\} \quad (15)$$

To obtain V_m for a charged micelle we have to choose a cut-off distance for the electrostatic interactions between the micelles. For the effective range of the electrostatic interactions we take the distance at which the electrostatic potential has dropped to $1/e$ of its maximum value, a choice quite common in colloid chemistry.

Consequently, the potential decay depends on the ionic strength and so does the chosen cut-off distance.

Once V_m is determined V_s can be calculated with eq (14) and $\bar{\phi}_i$, follows from:

$$\bar{\phi}_i = \frac{n_i^{exc} r}{V_s} + \phi_i^b \quad (16)$$

Contrary to small spheres, structures like infinitely long membranes and cylinders have a negligible kinetic energy. Therefore for these geometries we may neglect the translational entropy term and assume that for equilibrium membranes and cylinders $A_m^\sigma = 0$.

Numerical procedure

To obtain the volume fractions, the segment weighting factors must be found. They are calculated from $u_x(z)$, which, in turn, depend on the volume fractions and the electrostatic potentials. Therefore numerical methods have to be used to make the field and the corresponding volume fraction profile self-consistent. The calculations were started with a chosen, fixed amount, θ_i , of surfactant. This implies that $\theta_i/r_i G_i(r|1)$ is the normalization constant. The bulk volume fraction with which this amount is in equilibrium, is a result of the calculation. Regarding the ions the concentration was entered and converted to the bulk volume fraction, ϕ_i^b using the given size of a lattice site. In this case ϕ_i^b/r_i is the normalization constant and θ_i , the amount of ion i in the M layers which is in equilibrium with the bulk solution volume fraction results from the SCFA calculation.

Details of the numerical method, with emphasis on the calculation of the reference potential are given in ref [24].

Choice of parameters

In principle there is no limit to the number of different molecules and segment types that can be handled in a SCFA calculation. For practical reasons we choose the molecular structures and interaction parameters as simple as possible to model ionic surfactants in aqueous solutions. We will incorporate the main interactions, mentioned in the introduction, involved in micellization. These are the mutual attraction between the flexible tails caused by contact interactions, which can be modeled through the value of the χ -parameters, and the electrostatic repulsion between the head groups which will be affected by the ionic strength. For the moment we will neglect ion specificity. Incorporation of this effect is possible, but it is regarded as a second order effect.

In an aqueous system containing micelles at least three molecule types have to be present: water, modeled as monomer W, an ionic surfactant, for which we choose a chain A_nB_3 , i.e. a chain with n aliphatic segments and a head group consisting of 3 segments. The energy difference between a trans and a gauche conformation is taken to be 1 kT, just as in ref (29). The oppositely charged monomeric counterion is represented as C and the co-ion, if present, as monomer D.

Segment A mimicks a CH_2 (or CH_3) group, its Flory-Huggins interaction parameter, χ_{Ay} with all other segments y (W, B, C and, if present, D) is set equal to 2 to express the mutual repulsion between A and the other segments. This value gives the correct cmc dependence on the aliphatic tail length for nonionic surfactants. An alternative way to fit the χ_{AW} value is to calculate the partition equilibria for homologous series of alkanes between a water and an oil phase, for which experimental data were reported by Tanford⁽¹⁾, with the multicomponent Flory equations.⁽²⁸⁾ This yields an only slightly higher value, $\chi_{AW} = 2.3$. Following refs (25,29,30) we will use $\chi_{AW} = 2$.

The remaining interaction parameters are set equal to zero, that is to say W is a perfect solvent for B, C and D. In that case, B, C and D interact with each other through coulombic forces only. The valency of the head group B_3 is -1 , each B carries a charge of $-1/3$, the valency of the counterion, C is $+1$ and that of the co-ion, D, -1 . In general the head group of an ionic surfactant is larger than a CH_2 group or a water molecule, our choice to equate the size to three head group segments is arbitrary. A different choice of the number of head group segments, say 2 or 4, has an insignificant effect on the results.

The dielectric constants used are $\epsilon_W = \epsilon_B = \epsilon_C = \epsilon_D = 80\epsilon_0$, $\epsilon_A = 2\epsilon_0$. In the present study the thickness of a lattice layer is $\ell = 0.31$ nm and the cross section of a lattice site is $a_s = \ell^2$. This choice leads to 55.5 moles of lattice sites per dm^3 . Consequently, volume fractions can be converted to concentrations in mol/dm^3 by $c_i = 55.5 \cdot \phi_i / r$. This choice of ℓ is appropriate for water molecules. A consequence, however, is that the C-C distance in an aliphatic chain is overestimated considerably, although the volume of a CH_2 group, as calculated from the bulk density of alkanes, is correct. Therefore some caution is required in comparing calculated micellar radii with experimental data, we cannot expect quantitative agreement. However, the contribution of each CH_2 to the overall hydrophobicity of the chain is expected to be in agreement with experimental work since χ_{AW} has been fitted as mentioned above.

The above choice of parameters implies that segments B, C and D differ only with respect to their valency. They all have the same size. This is of course a simplification; in reality the salt ions will be hydrated and they may differ in size, water forms H-bridges and it is more likely that water is present as clusters than as monomers. These effects are not explicitly included in the choice of the system parameters because we first want to emphasize the role of purely coulombic interactions and the association of the tails. Apart from the fact that, in the present treatment, the molecules have a non-zero size, the assumptions made for the monomeric molecules,

regarding dielectric constants and interaction parameters, correspond with those made to obtain the Poisson-Boltzmann equation.

Results

Aggregate shape as a function of the surfactant chain length

In order to decide which aggregate shape should be studied in more detail, first some results obtained for different aggregate shapes will be compared. In Figure (2) the equilibrium volume fractions of aggregate formation of a homologous series of A_nB_3 for spherical aggregates, infinitely long cylinders and infinite membranes, all at a salt concentration of 0.1 M CD, are presented. For the spheres two curves are given, one at the critical micelle volume fraction, $cm\phi$, the other curve at a total volume fraction, $\bar{\phi}_t$, of 0.01 (For $A_{12}B_3$ the equilibrium bulk volume fraction at the maximum of A_m^σ vs the aggregation number is $\phi_t^b = 4.8 \cdot 10^{-4}$. For $\bar{\phi}_t = 0.01$, $\phi_t^b = 6.4 \cdot 10^{-4}$). It appears that the spherical structures are in equilibrium with lower bulk volume fractions than the cylinders and the membranes. For all chain lengths given here, the first-formed aggregates are spherical. The equilibrium volume fractions for aggregate formation decrease with increasing chain length with a slope which is hardly different between the various aggregates. This slope is mainly dependent on the choice of the χ_{Ay} parameter and the segment size. The calculated slopes correspond to that measured for a homologous series of ionic surfactants at high ionic strength⁽¹⁾, indicating an appropriate combination of parameter values.

As n increases the equilibrium volume fractions at which cylinders and spheres ($\bar{\phi}_t = 0.01$) are formed approach each other. In this situation it is to be expected that deviations from the spherical shape will occur and intermediate forms, such as ellipsoids may be present and/or the system will be polydisperse. At present we have not yet

considered other shapes than spheres, cylinders and flat membranes.

As spherical structures have the lowest equilibrium volume fractions under the conditions considered here, we will focus on results obtained with the spherical lattice.

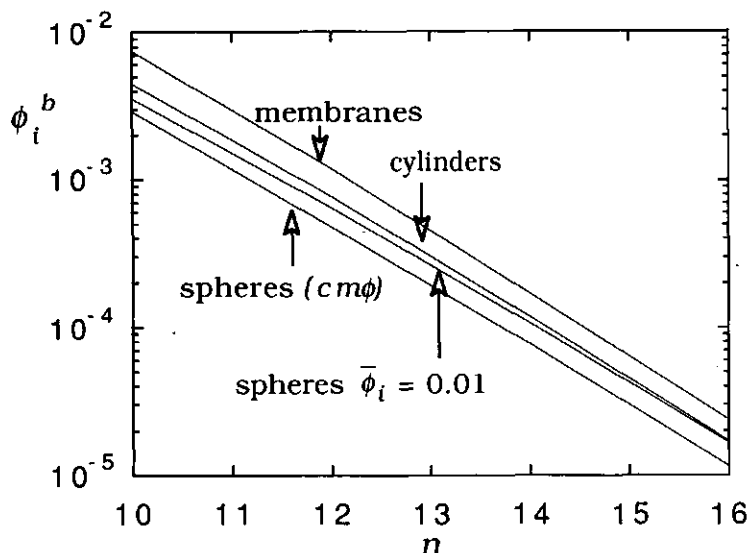


Figure 2: Equilibrium bulk volume fractions as a function of the number, n , of aliphatic segments, A , of spherical, cylindrical and flat structures formed by A_nB_3 molecules, with a valency of -1 on the B_3 head group ($-1/3$ per B) in a univalent symmetrical electrolyte (C^+ and D^-) solution with $c_s = 0.1$ M, solvent W . Interaction parameters: $\chi_{AW} = \chi_{AB} = \chi_{AC} = \chi_{AD} = 2$, the remaining χ -values are set to zero. The energy difference between a gauche and a trans conformation is taken as $1kT$, lattice dimensions: $\ell = 0.31$ nm, $a_s = \ell^2$, dielectric constants: $\epsilon_W = \epsilon_B = \epsilon_C = 80\epsilon_0$, $\epsilon_A = 2\epsilon_0$.

Volume fraction profiles

$A_{12}B_3$ in the absence of added salt: In Figure. (3a) the volume fraction profiles of A , B , C and W are given. The equilibrium bulk volume fraction of $A_{12}B_3$ is $3.06 \cdot 10^{-3}$, whereas the total volume fraction of amphiphile in the system is 0.01 , so about 70% of the surfactant is

present in the form of micelles. The average aggregation number, n_i^{agg} of this micelle is 37.1. From Figure (3a) it follows that, in agreement with the expectation, the A segments are at the inside of the aggregate. The interface between the hydrophobic segments A and the aqueous phase is rather sharp, it drops from about 0.9 to less than 0.1 over only 3 lattice layers (≈ 1 nm). This distance is in agreement with MD simulations.^(12,14-16) Inside the micelle the volume fraction of solvent is low but non-zero. This is a result of our choice for the modelling of the alkyl chains and the water. Instead we could have grouped e.g. 3 CH₂ units in one segment which might be more realistic with respect to the C-C bond length and the chain flexibility and is closer to the choice in the MD simulations by Smit et al.⁽¹¹⁾ In that case, χ_{AW} should have been increased to 4.3 in order to predict the cmc dependence on the aliphatic chain length. This higher value of χ_{AW} would have led to far less water in hydrocarbon core. However, such a choice will lead to enormous lattice artefacts (see later) and is therefore not feasible in the present treatment. Another way to arrive at a dry hydrocarbon core is to allow for cluster formation by the water molecules, a more detailed model for liquid water is currently being developed in our laboratory.

As expected, the charged head groups are located on the outside of the aggregate. The head groups are, however, not aligned in a plane but distributed over about 5 lattice layers. Calculations performed for other head group sizes (B, B₂, B₄) at fixed total head group charge indicate that the size of the head group not significantly affects this distribution of head groups. The volume fraction profile of the counterions, C, is hardly visible on this scale, a clearer picture results from a logarithmic plot of the volume fractions (Figure 3b). The counterions, C, accumulate mainly in the same layers as the charged head groups. This implies an effective partial neutralization of the charge of the micelle. Outside the micelle, at about $z = 12$, a diffuse electric layer has developed. In this layer the counterions are positively adsorbed and the surfactant anions are depleted. Due to this, the excess number of surfactant molecules is smaller than the

number of aggregated molecules. In the present case $n_i^{exc} = 33.3$, so that the difference with n_i^{agg} is about 4 molecules.

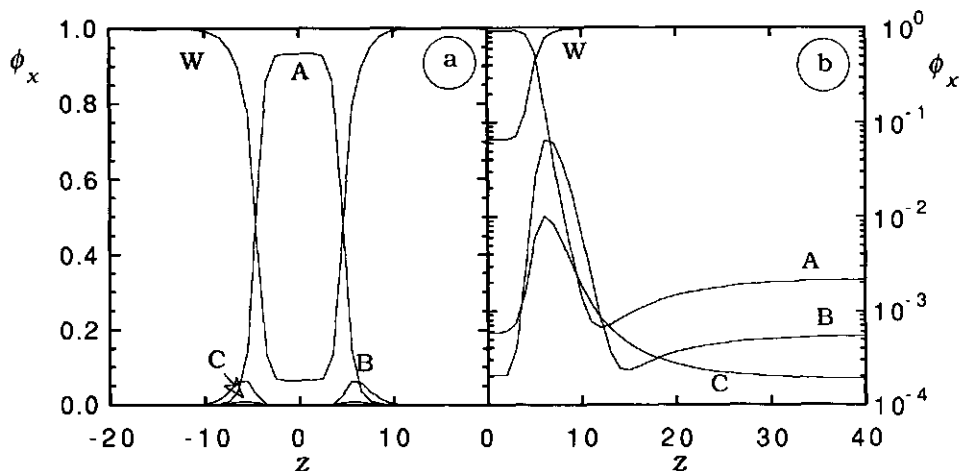


Figure 3: Equilibrium volume fraction profiles for W, A, B, and C for an $A_{12}B_3$ micelle at $\bar{\phi}_i = 0.01$ in the absence of added electrolyte. In Figure (3a) a cross section through the micelle is displayed, in Figure (3b) the volume fractions are plotted on a logarithmic scale, starting from the center of the micelle. See Figure (2) for other parameters.

$A_{12}B_3$ in a 0.1 M salt solution: The volume fraction profile of an $A_{12}B_3$ micelle in a 0.1 M CD solution is given in Figure (4a). At the lattice size chosen a 0.1 M univalent salt solution has bulk solution volume fractions of $1.8 \cdot 10^{-3}$ for both C and D. As before, $\bar{\phi}_i = 0.01$. The micelle formed at this composition consists of 85.3 ($=n_i^{agg}$) molecules and the equilibrium solution volume fraction, ϕ_i^b , equals $6.4 \cdot 10^{-4}$. In agreement with experimental findings the theory gives a lower cmc and a larger micelle when salt is added. We will discuss these effects in more detail in a next section. Just as in the absence of salt the A segments are at the inside of the aggregate, the interface between the hydrophobic segments A and the aqueous segments is rather sharp and the head groups are spread over about

5 layers. The accumulation of counterions in the head group region is more pronounced than in the absence of salt.

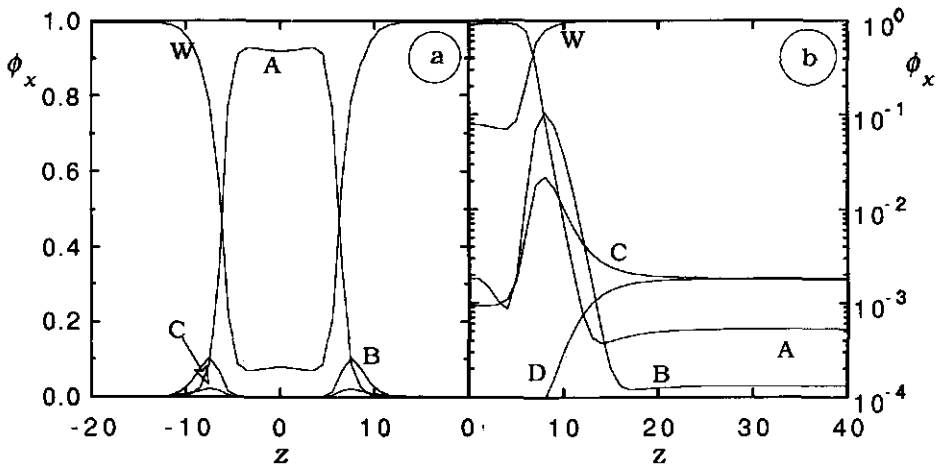


Figure 4: Equilibrium volume fraction profiles for W, A, B, C and D for an $A_{12}B_3$ micelle at a total volume fraction of 0.01 in the presence of 0.1 M added electrolyte. In Figure (4a) a cross-section through the micelle is displayed, in Figure (4b) the volume fractions are plotted on a logarithmic scale, starting from the center of the micelle, $\bar{\phi}_i = 0.01$, see Figure (2) for other parameters.

In the center of the micelle we find a shallow minimum in the volume fraction of A, corresponding to a weak maximum in W. This may be interpreted as an indication that at $\bar{\phi}_i = 0.01$ a micelle with a not exactly spherical shape might become more favorable. As, however, only a minor deviation from sphericity suffices to eliminate the minimum we conclude that a spherical structure is still close to reality. We shall mainly neglect this aspect and restrict ourselves to purely spherical structures.

When the volume fractions are plotted on a logarithmic scale (Figure 4b) the co-ion and counterion distribution are more clearly visible. Some typical differences with the structure in the absence of salt appear. Since the volume fraction of co-ions D is much higher than

that of the surfactant, the depletion zone of surfactant outside the micellar core has now almost disappeared. As a consequence, the aggregation number is virtually equal to the excess number of surfactant molecules (85.3). The co-ions are depleted near the micelle, but far from the micelle the volume fractions of C and D are almost the same, their difference is caused by the contribution of the free surfactant ions to the total charge.

Table I: Results for $A_{11}B_3$ and data for SDS (sodium dodecyl sulfate) and SDeS (sodium decyl sulfate) from ref (33). The total surfactant concentration is \bar{c} , the concentration of free surfactant is equivalent to the cmc in practical systems.

surfactant	c_{salt} (M)	\bar{c} (mol/dm ³)	c_{free} (mmol/dm ³)	n^{agg}
$A_{12}B_3$	0	0.037	11.3	37.1
$A_{12}B_3$	0	0.5	11.8	43.6
$A_{12}B_3$	0.1	0.037	2.37	81.2
$A_{12}B_3$	0.1	0.5	2.41	87.0
$A_{10}B_3$	0	0.042	32.9	28.2
$A_{10}B_3$	0.1	0.042	14.9	56.8
<hr/>				
cmc (mM)				
SDS	0		8.1	62
SDS	0.1		1.9	94
SDeS	0		33	38
SDeS	0.1		15.1	51

The calculated aggregation numbers and cmc's compare rather well with experimental data see e.g. refs (31,32), and Table I where values obtained by Huisman⁽³³⁾ are given together with some theoretical results. The concentration of free surfactant is equivalent to the practically observed cmc. The calculated n_i^{agg} values in both the absence and the presence of salt are slightly lower than those for sodium dodecyl sulfate (SDS) and it seems that the predicted effect of the salt concentration on the aggregation number is too strong. The agreement with experimental cmc's and aggregation numbers, might be improved by introduction of a more hydrophobic terminal group. However, regarding the assumptions made with respect to the equality of segment sizes, chain statistics, dielectric constants

and interaction parameters we think that the results are already in nice agreement with experiments.

Charge distribution and potential profile

The charge distribution of the micelle and its surroundings is given in Figure (5a), in the absence of salt and in Figure (5b) in a 0.1 M CD solution. The total charge of the system is zero, the negative charge of the head groups is spread over about 5 lattice layers, while the counter charge distribution is much wider. The extension of the diffuse layer, which starts at $z \approx 12$, is considerably larger in the absence of salt. Inside the micelle the charge is very low, but a small net positive charge is found just in the outer region of the hydrocarbon core.

If we plot the net charge number per lattice site (Figure 5c and 5d) instead of the charge number per layer, we find that the maximum of the net negative charge hardly depends on the salt concentration. The maximum net charge per layer is about 20 mC/m². Also for other salt concentrations, total surfactant volume fractions and chain lengths the same net negative charge is obtained. This result is important for the development of simpler models: a good approximation results if a micelle is modeled as a sphere with a fixed charge, independent of the salt concentration. The contributions of the different charge components to the net charge are given in Figure (6a) in the absence of added salt and in Figure (6b) in the presence of 0.1 M salt. From these figures it is clear that the counterions do indeed reduce the charge of head groups to a significant extent directly in the layers where the head groups are located. The volume fraction of water in the layers containing the head group segments is at least 0.5, see Figure (3). Therefore, exchange of some water molecules for salt ions in the head group region is spatially not restricted.

We find for A₁₂B₃ in the absence of salt an average neutralization degree of 50% in the layers where the net charge is positive. In the

presence of 0.1 M indifferent electrolyte we find 74%. The difference is caused by the change in the micelle size. Both neutralization values are in the range of reported experimental values.⁽³²⁾ As the calculated difference in micelle size between the two salt concentration is larger than what is found experimentally for e.g. SDS, see Table I, the difference in degree of neutralization is also

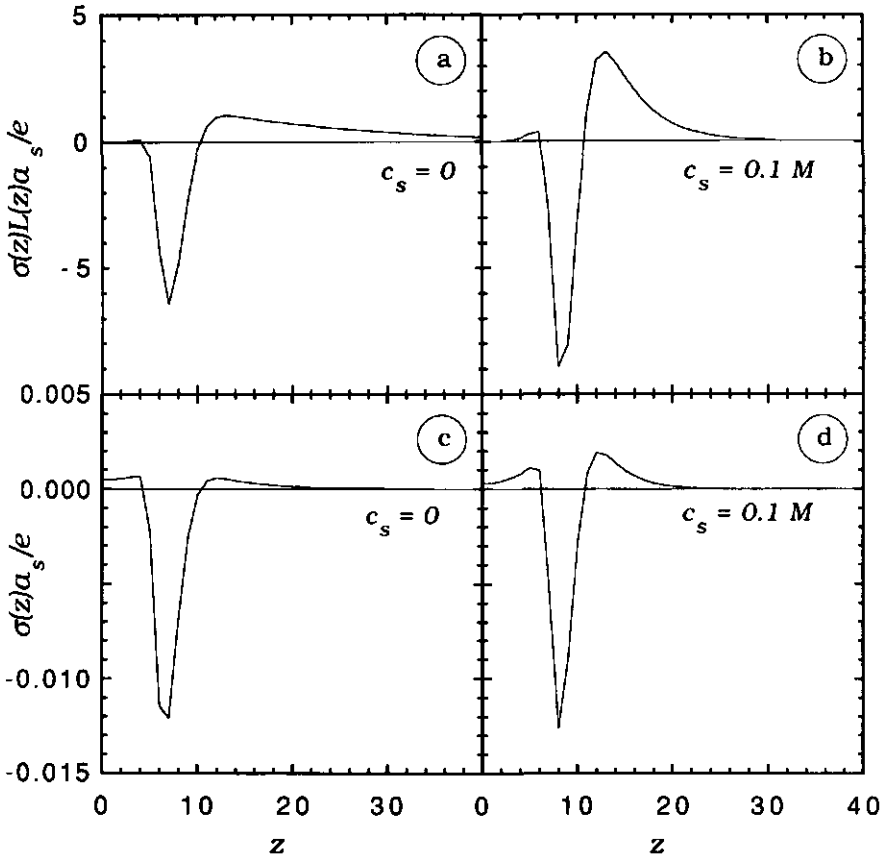


Figure 5: Charge distribution of $A_{12}B_3$ micelles. In Figure (5a) the charge distribution of an $A_{12}B_3$ micelle in the absence of added salt is given as the net number of charges per lattice layer, in Figure (5b) the charge distribution of an $A_{12}B_3$ micelle in a 0.1 M salt solution is given in number of charges per lattice layer. In Figures (5c) (no salt added) and (5d) (0.1 M salt) the charge distributions are plotted as net charges per lattice site, $\bar{\phi}_i = 0.01$, see Figure (2) for other parameters.

too pronounced. However an increase of the degree of neutralization with micelle size has been found experimentally, for instance, for homologous series of sodium alkanolates⁽³²⁾ and alkyl trimethyl ammonium bromides.^(34,35)

To find a high number of counterions in between the head groups a high negative potential is needed. The potential profiles for the two salt concentrations are given in Figure (7). For both ionic strengths the potential drops steeply for $z > z(\psi_{max}) + 1$, where $z(\psi_{max})$ is the layer where the maximum potential is reached. At $c_s = 0.1$ M the potential vanishes at about layer 20. The potential decay for the two salt concentrations is very similar in the region between $z(\psi_{max})$ and $z = 12$ (end of the head group region), which is a consequence of the invariant charge profile. Outside the head group region, the potential decay for $c_s = 0$ is much slower than in 0.1 M salt. The maximum negative value of the potential is reached in layer 5, (-110.6 mV), in the absence of salt and in layer 7, (-72.8 mV) in the 0.1 M salt solution. The maximum potentials are located at lower layer numbers than the maximum charge since the distance from the center where $E = 0$ does not coincide with the maximum charge, but it is related to the compensation of the small net positive charge in (near) the hydrocarbon core.

Some potential decay also takes place in the micelle interior. As stated before, our model overestimates the amount of water inside the micelle, and, as we model counterions as "charged water", the number of counterions inside the hydrocarbon core is also overestimated. Due to the low dielectric constant in this core, the presence of a small number of counterions will give rise to a significant potential decay. If χ_{AC} is chosen to be more repulsive, i.e. $\chi_{AC} > 2$ or χ_{CW} more attractive, i.e. $\chi_{CW} < 0$, the potential decay inside the micelle would become smaller. However we shall not consider this feature further.

For a separate series of calculations for micelles of a constant aggregation number, we found that the net charge density in the

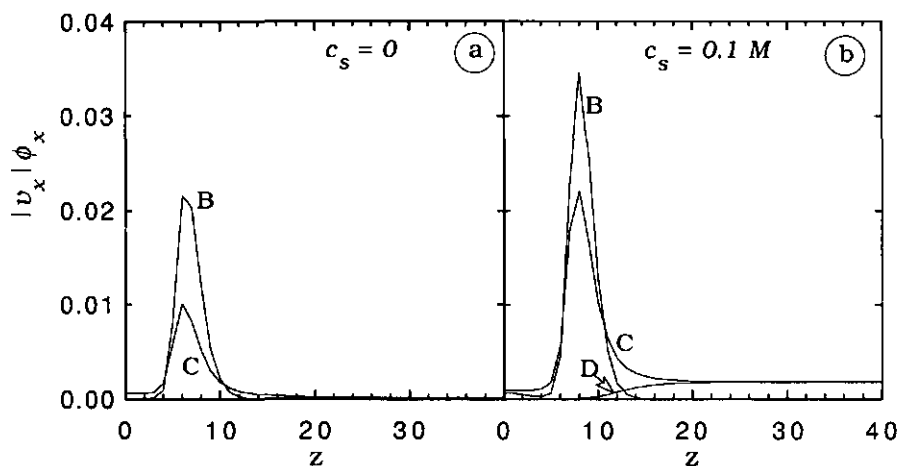


Figure 6: Contribution of head groups, counterions and co-ions to the net charge per lattice site. Figure (6a): no salt added, Figure (6b): 0.1 M salt, $\bar{\phi}_l = 0.01$. See Figure (2) for parameters values.

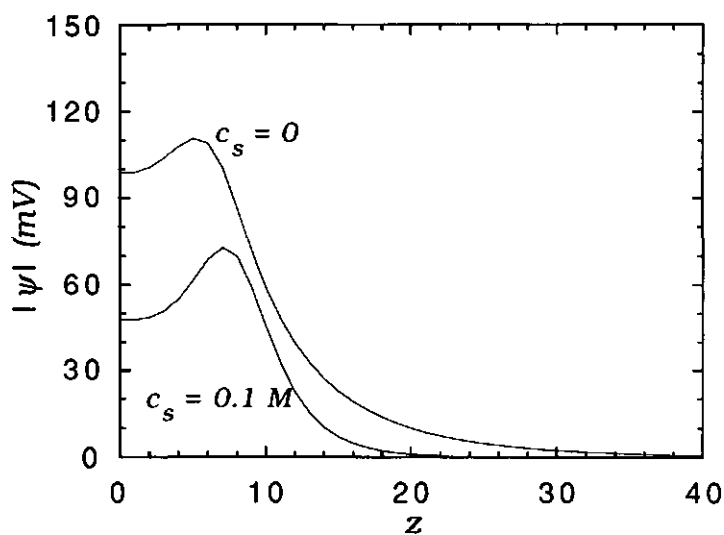


Figure 7: Profile of the potential of $A_{12}B_3$ micelles in 0 and 0.1 M salt solution. $\bar{\phi}_l = 0.01$. See Figure (2) for parameters values.

head group region is nearly independent of the salt concentration and that exclusion of co-ions is almost complete. Since at constant aggregation number the volume fraction profile of B segments in the head group region is independent of c_s , also the counterion volume fraction in layer z must be invariant with respect to the salt concentration. To obtain the same volume fraction of counterions in layer z at different values of the salt concentration, the potential in layer z has to be different; for a tenfold decrease in salt concentration an increase in potential is needed of 59 mV for a 1-1 electrolyte.

The presented calculations for micelles at a constant total volume fraction, show an increasing aggregation number as a function of the salt concentration. Consequently, the volume fractions of counterions increase slightly with salt concentration and a somewhat smaller value for the potential difference between micelles at two salt concentrations is calculated. Between micelles of $A_{12}B_3$ in the absence of salt, where the ionic strength (0.012 M) is completely determined by the surfactant, and in 0.1 M CD the calculated difference in the maximum potential is 38 mV while it would have been 50 mV when there was no difference in aggregation number.

Healy et al.⁽³⁶⁾ measured the potential in the head group region of surfactant micelles as a function of the cmc, using suitable acid-base indicators as probes. For a particular surfactant the cmc was varied by changing the salt concentration. A linear relation between $\ln(\text{cmc})$ and $\ln(c_s)$ appeared to exist in agreement with data reported by Lindman and Wennerström.⁽³²⁾ We have replotted the results of Healy et al.⁽³⁶⁾ for SDS and for dodecyl trimethyl ammonium bromide (DTAB) in Figure (8) together with our calculated results for ψ_{max} . The slope of the experimental and theoretical curves is about the same, moreover the agreement between the calculated potentials and the experimental data for DTAB is very good. The potentials calculated with models such as the 'dressed micelle' model⁽³⁷⁾ are much higher, because here the head groups are placed on a single shell. Note that, since the potential decay in the head group region is

virtually independent of the salt concentration, see Figure (7), the choice of the layer number from which ψ is taken is not so relevant; if we had used the potential, $z(\psi_{\max}) + \Delta z$, i.e. a few layers away from $z(\psi_{\max})$ the slope of the curve would have been the same.

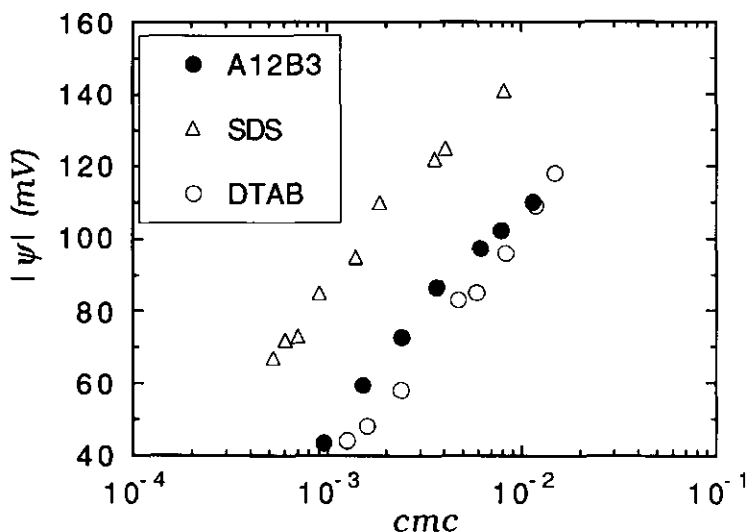


Figure 8: The surface potential of SDS and DTAB from ref⁽³⁵⁾, and ψ_{\max} of A12B3 as calculated with our model as a function of the cmc. Calculations at $\bar{\phi}_i = 0.01$ were used. The univalent salts used are NaCl for SDS and NaBr for DTAB.

Based on the relation shown in Figure (8) Healy et al. have proposed a model in which the surfactant ions are regarded as potential determining ions; the change in the cmc relative to the cmc at the highest salt concentration determines the potential shift. Our calculated results support this way of modelling as the slope of the plots in Figure (8) is about +59 mV. We can analyse these findings in more detail using the Esin-Markov coefficient.⁽³⁸⁾ If the surfactant ion is considered as the potential determining ion, the Esin-Markov coefficient β , for a micellar system can be defined as:

$$\beta = \left(\frac{\partial \ln cmc}{\partial \ln a_s} \right)_{n^{agg}}$$

where a_s is the salt activity. Thermodynamic analysis shows that the Esin-Markov coefficient is unity if the screening of a small charge increase is entirely compensated by an increased accumulation of counterions. This is the case where the co-ion exclusion is at its maximum value. Using the SCFA theory for micelles we have found that co-ion exclusion is high in the head group region. For micelles at different salt concentration but at constant aggregation number, this means that β is close to unity and that $\delta \ln c_{mc} = \delta \ln c_s$. We found a slope of 0.9 which is indeed close to unity. Further small deviations in the slope of a plot of $\ln c_{mc}$ vs $\ln c_s$ are caused by changes in aggregation number as a function of salt concentration, in that case n^{agg} is no longer constant. The Esin-Markov coefficient provides a coupling between the cmc and salt concentration. Therefore the dependence of the micelle potential on the cmc is very similar to the dependence of the micelle potential on the salt concentration.

The net charge of layer z in the head group region of a micelle is low, nevertheless co-ion exclusion is almost complete. The reason for the very low net charge density is that the head groups are distributed over a number of layers. The negative charge of the head groups in a layer z cannot be neutralized in lattice layers $z + 1$ or $z - 1$ if, due to the presence of other B segments, a net negative charge exists in these layers. Because layers $z + 1$ or $z - 1$ have the same net charge sign as layer z and they are excluded for the screening of the charge in layer z . Also co-ions are expelled because the incorporation would make the situation worse. Consequently, the screening of the charge is difficult and low net charges result. This effect is stronger if the head groups are spread over more layers. With micelles where the head groups are distributed over about 5 layers, quite a thick region is excluded for the screening of the charge and this situation can only exist if the net charge per layer is low.

Free energy of micelle formation

The excess free energy of micelle formation, A_m^σ , for the calculated spherical micelles with a fixed position is positive both at $c_s = 0$ and

$c_s = 0.1$ M. The contributions to A_m^σ per site in each lattice layer are shown in Figure (9a) and (9b) for the $c_s = 0$ and $c_s = 0.1$ M respectively. In Figure (9a) it is shown that far from the micelle there is no contribution to A_m^σ even though the potentials are non-zero. This is a consequence of compensation of the electric and entropical contributions in the diffuse double layer.⁽³⁹⁾ The deviation from zero at about $z < 12$, indicates that other contributions become significant. First a negative contribution to the excess free energy appears. The leading term in this region is due to the head groups: $\phi_B(z)\ln G_B(z)$, the volume fraction of the head groups is fairly high but the segment weighting factor is very low. As the contribution per lattice site, which is plotted here, has to be multiplied with the number of sites in layer z , $L(z)$, to obtain the contribution of layer z to A_m^σ , this is an important contribution to the micellar free energy. The electrostatic repulsion between the head groups as well as the A/W contacts lead to a positive contributions to A_m^σ in layers 5, 6, and 7. The maximum value of $A_m^\sigma(z)/L(z)$ is found in the interface between the hydrophobic A segments and the other segments, and not by the head group repulsion, as it is found in layer 5, where the head group density is below its maximum. In the interior of the micelle negative values $A_m^\sigma(z)/L(z)$ are again found as a consequence of the favorable association of A segments, which outweighs the entropy loss of the molecules upon packing in an aggregated structure.

In a 0.1 M salt solution the contributions to the excess free energy of micelle formation per site in each lattice layer are remarkably similar to those in the absence of salt, except in the heart of the micelle, where in 0.1 M salt $A_m^\sigma(z)$ is slightly positive. This indicates that an exactly spherical shape may not be the one with the lowest free energy, in agreement with the conclusion from Figure (4). The shape of the volume fraction profiles in the interfacial region between the A segments and the other segments do not change with the salt concentration, which explains why in this region the profile of $A_m^\sigma(z)/L(z)$ does not depend significantly on the salt concentration. Therefore the simplification made in some theories for micellization

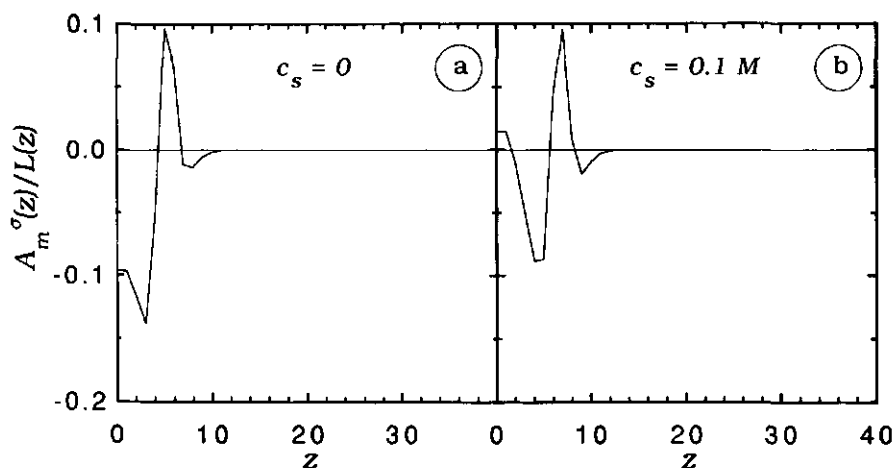


Figure 9: Contributions to the excess free energy, A_m^σ , of $A_{12}B_3$ micelles in the absence (Figure 9a) and presence (Figure 9b) of 0.1 M salt. Total surfactant volume fraction 0.01. See Figure (2) for other parameter values.

to introduce a salt-independent surface tension between the hydrophobic and the hydrophilic phase⁽²⁻⁵⁾ seems to be legitimate.

Micelle size and total surfactant concentration

The micelles discussed above were claimed to be structures representing existent micelles because they had a positive A_m^σ . This is not the only criterion in the determination of the stability of a calculated micellar structure. Also the slope of A_m^σ vs. n_i^{agg} must be negative, because insertion of another molecule in the micelle must lead to a decrease in the free energy. In general the excess free energy of a micelle with a fixed center of mass as a function of the micelle size, exhibits a maximum, as shown in Figure (10a), where the cmc is located.^(22,28) The calculated curve for the excess free energy of micelle formation vs. the aggregation number for the system studied here, $A_{12}B_3$ in a 0.1 M salt solution, is given in Figure (10b) (drawn line). This curve should have been smooth as the curve

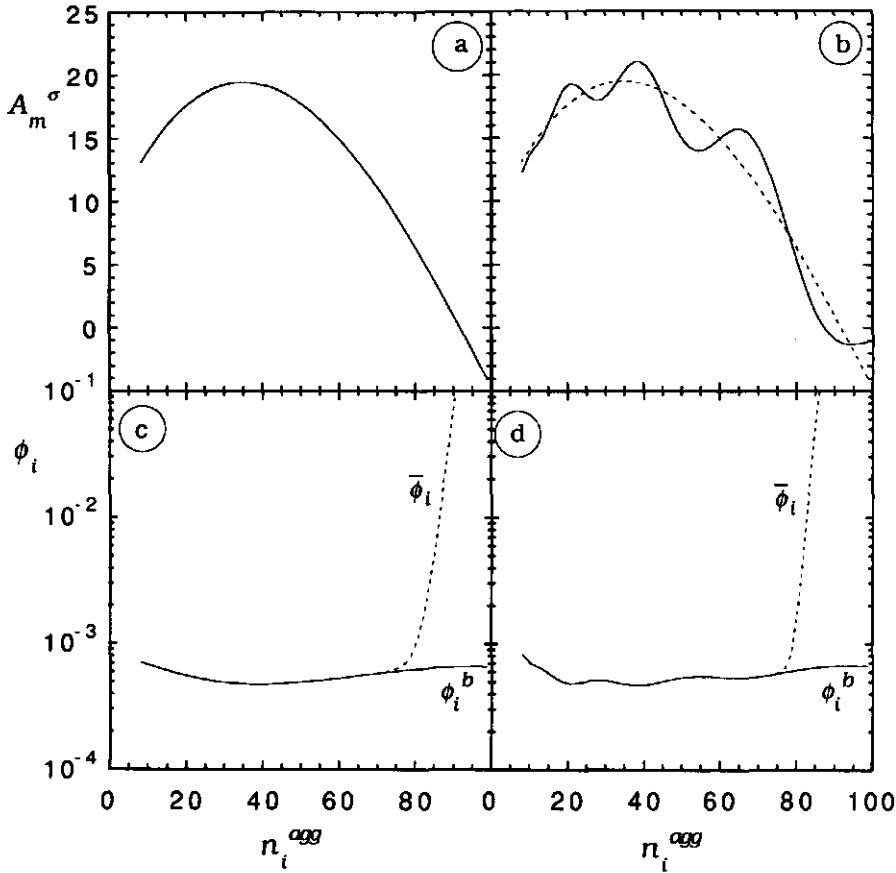


Figure 10: Micelle Formation

Figure 10a: General representation of the excess free energy of the formation of a micelle with a fixed position as a function of the aggregation number.

Figure 10b: Excess free energy of micellization as a function of the aggregation number. The drawn line is the calculated curve for A_m^σ as a function of n_i^{agg} for $A_{12}B_3$ in 0.1 M electrolyte, the dotted curve represents a fit with a third order polynomial.

Figure 10c: The bulk volume fraction, ϕ_i^b , and total volume fraction, $\bar{\phi}_i$, as a function of n_i^{agg} for $A_{12}B_3$ in a 0.1 M salt solution as obtained from smoothed curves with a polynomial for ϕ_i^b . The total volume fraction, $\bar{\phi}_i$ is recalculated from the smoothed curves for A_m^σ and ϕ_i^b .

Figure 10d: Calculated curves for ϕ_i^b and $\bar{\phi}_i$ without smoothing as a function of n_i^{agg} . See Figure (2) for parameters values.

in Figure (10a). The fact that it shows a series of local maxima and minima is caused by lattice artefacts: because of the discretization introduced by the lattice, a small shift of the A/W interface over the lattice leads to an unrealistic change in the excess free energy of micelle formation.

To be able to handle our data we have chosen to approximate the "artefact-free" curve for A_m^σ vs n_i^{agg} by fitting a third order polynomial through the calculated points. The result is shown by the dotted curve in Figure (10b). Besides A_m^σ also ϕ_i^b is affected by lattice artefacts, see the drawn curve in Figure (10d). To ϕ_i^b as a function of n_i^{agg} we also applied a third order polynomial fit. The result is shown by the drawn curve in Figure (10c).

From the excess free energy, A_m^σ , the bulk volume fraction, ϕ_i^b , and the micelle size, n_i^{agg} , the average concentration, $\bar{\phi}_i$, has been determined using eq (9). Both the bulk solution volume fraction and the excess free energy are subject to lattice artefacts and so does $\bar{\phi}_i$. The results for the "artefact-free" system (i.e. using a third order

polynomial fit for both A_m^σ and ϕ_i^b) are shown in Figure (10c). The crude results for the $A_{12}B_3$ system are shown in Figure (10d). It should be noted here that all results presented in this chapter for aggregation numbers and equilibrium volume fractions are obtained after smoothing the calculated curves with third order polynomials.

The cmc for $A_{12}B_3$ in a 0.1 M salt solution is located at an aggregation number of 38, where the maximum in A_m^σ and the minimum in ϕ_i^b are located. The overall concentration starts to deviate from the bulk volume fraction at an aggregation number of about 75, where $\bar{\phi}_i$ starts to increase steeply with n_i^{agg} , see also Table I. In this region the number of micelles increases strongly but not their size, which is in agreement with experiments, see e.g. ref (34,40). As the difference in A_m^σ and ϕ_i^b values between aggregation numbers around the cmc is rather small, the system is probably polydisperse near the cmc. Based on the present calculations less polydispersity is expected at higher overall concentrations, but we

note that at higher overall concentrations deviations from the spherical shape may contribute to the polydispersity of the aggregates.

Effect of salt concentration and chain length on the cmc

The cmc and aggregation number are influenced by the length of the aliphatic tail and the salt concentration. In Figure (11a) we give the cmc as a function of the aliphatic tail length in the absence and in the presence of 0.1 M indifferent salt. For both situations the cmc decreases with increasing chain length, but the decrease is stronger in the presence of salt. The slopes of the curves agree very well with experimental data for e.g. alkylsulfates as compiled by Tanford.⁽¹⁾

As pointed out by Tanford⁽¹⁾ the difference in slope of $\ln(\text{cmc})$ as a function of the tail length for the two salt concentrations has an electrostatic origin. In the absence of added electrolyte, the ionic strength is determined by the surfactant. A surfactant with a longer aliphatic tail has a stronger tendency to associate than one with a short tail due to the stronger hydrophobic interactions. This leads to a lower cmc. At this low cmc however, the repulsion between the head groups is strong because the ionic strength, determined by the cmc, is low. This repulsion counteracts the hydrophobic attraction and an increase of the chain length with one CH_2 segment has a relatively small effect on the cmc. In the presence of 0.1 M electrolyte the ionic strength is not significantly affected by the surfactant, the head group repulsion is relatively small and independent of the surfactant chain length. An increase in chain length manifests itself exclusively in the increase of the hydrophobic attraction. Hence a considerably larger slope results than in the absence of salt. As mentioned before this slope is the same as that obtained for homologous series of non-ionic surfactants.

In Figure (11b) the dependence of the aggregation numbers on the chain length is shown. In the absence of salt the aggregation numbers, at a constant total volume fraction of 0.01, remain

relatively low and are only weakly dependent on n as discussed above. In the presence of salt much larger micelles are formed and their size more strongly increases with n . These trends in aggregation numbers are in reasonable agreement with experimental data.^(32,34,40)

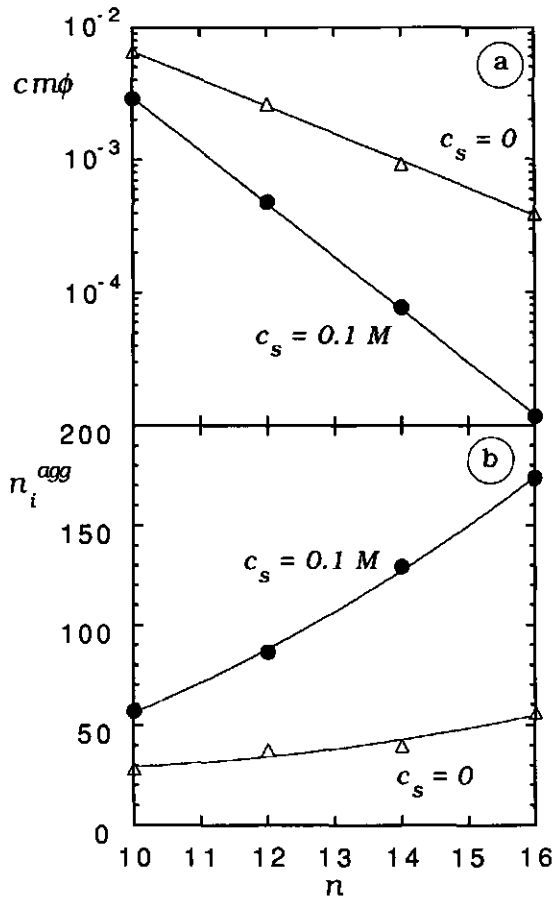


Figure (11): Effect of the chain length on the $cm\phi$ (Figure 11a) and the aggregation number (Figure 11b) at $\bar{\phi}_i = 0.01$ at $c_s = 0$ and $c_s = 0.1\text{ M}$ for A_nB_3 molecules. The calculated values are indicated with markers, the drawn lines are fits through the calculated points. See Figure (2) for other parameters.

Branching

Besides the chain length, also branching of surfactants is known to affect the cmc and the aggregation number. In Figure (12) we present results for an isomeric series of $A_{12}B_3$ surfactants. The segment of attachment of the chain of 12 aliphatic segments to the head group is varied. The tail is always connected to the third of the three head group segments. For the linear $A_{12}B_3$, studied before in this chapter, the first segment of the aliphatic chain is connected to the head group. In this case the branch length is 0 and the segment of attachment, which we define as the segment ranking number in the aliphatic tail, S_B , which is connected to the head group, is 1. The branch length is defined as the length of the shortest branch of the molecule. In this way we can make 6 different isomers of $A_{12}B_3$. The longest branch length is 5 because we chose to count the segment connected to the head group as a segment of the main chain.

The results are shown in Figure (12). The cmc increases with increasing branch length. For the most strongly branched molecule, with branch length 5 and S_B is 6 the cmc is about twice as high as for linear $A_{12}B_3$. The reason for this behavior is that for molecules with a thick but short hydrophobic part the packing into a spherical micelle is more difficult than for long and thin molecules. The increase in cmc as a function of branching is in agreement with experimental findings for isomers of sodium alkylbenzene sulfonates⁽⁴¹⁾, but for sodium alkyl sulfates the effect of branching is more pronounced.⁽⁴²⁾ The difference in aggregation behavior between these two classes of surfactants as a function of branching originates from the distance between the head group and the branch point, some test calculations where the surfactant was modeled as $A_{12}B$ with a charge of -1 on the B head group, showed a more pronounced effect of branching. The aggregation number of the micelles, which is plotted in Figure (12b) decreases from 37 for the unbranched isomer (at $\bar{\phi}_i = 0.01$) to 26 for the most strongly branched form. This decrease is, just as the change in cmc, in reasonable agreement with experimental data.

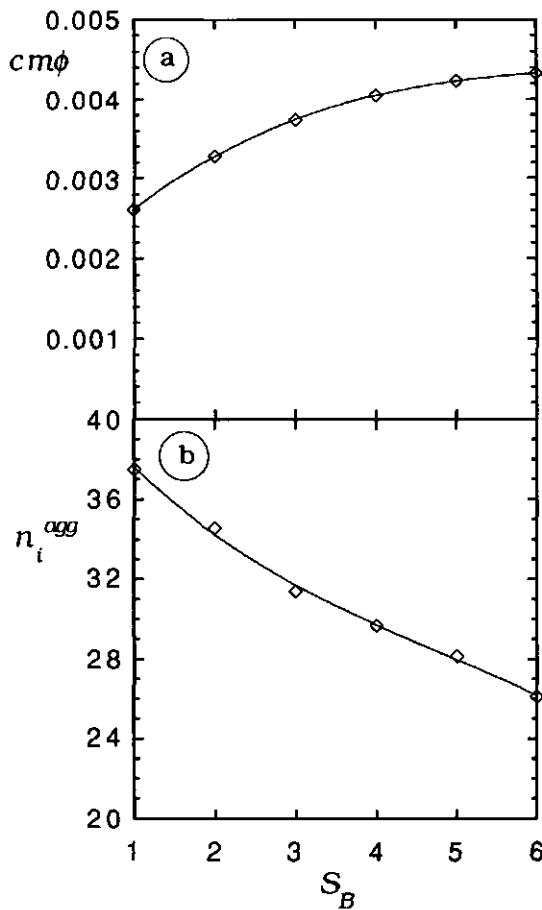


Figure (12): Effect of branching on the $cm\phi$ (Figure 12a) and aggregation numbers at $\bar{\phi}_i = 0.01$ (Figure 12b) of molecules with 12 A segments, no salt added. The segment number to which the head group is attached, S_B , is given on the horizontal axis, parameters as in Figure (2). The calculated values are indicated with markers, the drawn lines are fits through the calculated points.

Aggregate shape and salt concentration

A serious drawback of the lattice approach is that an a priori assumption has to be made regarding the shape of the aggregate. To get some impression on the preferred aggregate shape we have

compared results for spherical, cylindrical and flat lattices. For the infinitely long structures A_m^σ must be zero, as mentioned before. The equilibrium volume fractions for spherical micelles (near the cmc, and at $\bar{\phi}_i = 0.01$), cylindrical micelles and flat membranes are given in Figure (13a) for $A_{12}B_3$ ($S_B = 1$). At low salt concentration, where the repulsion between the head groups is strong, spherical micelles are favored over cylindrical aggregates and membranes. At higher salt concentrations, the equilibrium bulk volume fractions for spheres at $\bar{\phi}_i = 0.01$, cylinders and membranes are rather close to each other. Spherical micelles are still preferred at low concentration but at higher overall concentrations the system may be very polydisperse because the equilibrium volume fractions of the different shapes are hardly different.

For the branched isomer of $A_{12}B_3$, $S_B = 6$, the equilibrium volume fractions for spheres (at the cmc and at $\bar{\phi}_i = 0.01$), cylinders and membranes are given as a function of salt concentration in Figure (13b). At low salt and surfactant concentration spherical aggregates are always preferred, i.e. the micelles first formed are spherical. If more surfactant is added globular micelles remain preferred at low salt concentration. However, at higher salt concentration, about 0.2 M in this case, membranes and cylinders are preferred over spherical micelles: a transition from a spherical to a cylindrical shape occurs as function of salt or surfactant concentration. If the number of experimentally viable shapes correspond with those studied by us, this transition is fairly sharp. However, it is possible that still other geometries occur in practice, e.g. ellipsoids, which can make the transition smooth.

The effect of branching and salt concentration on aggregate shape is in agreement with experimental data obtained by Binana Limbèle et al.⁽⁴³⁾ They observed a growth of alkylbenzene sulfonate micelles with increasing salt concentration. Compared to linear molecules, branched isomers had lower aggregation numbers in the absence of salt. At higher salt concentrations the aggregation number of the branched surfactants increased to a very high value (too high to

determine) while the aggregation number of the linear alkylbenzene sulfonate did show an increase but not as dramatic as for the branched isomer.

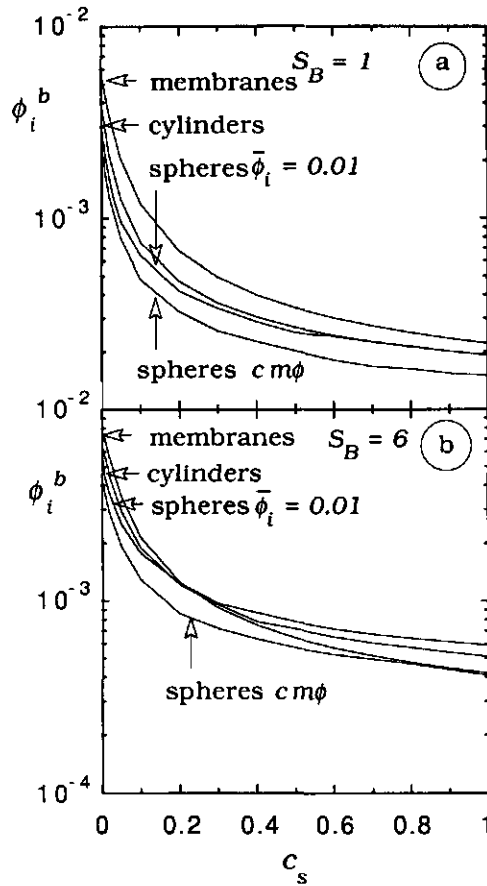


Figure (13): Comparison between aggregated of different shapes. Effect of the salt concentration on the equilibrium volume fraction of (Figure 13a) linear A₁₂B₃ and isomer with branch length 5 ($S_B = 6$), (Figure 13b). Equilibrium volume fractions at the cmc and $\bar{\phi}_i = 0.01$ for spheres are shown together with those for cylinders and membranes, parameters as in Figure (2)

Conclusions

With the SCFA theory micellization of ionic surfactants can be described and predicted trends in aggregation number and cmc as a function of chain length, salt concentration and branching are in good agreement with experimental findings. Transitions between aggregates of different shapes will occur as a function of salt concentration.

According to our model the micelles formed by ionic surfactants have a hydrocarbon core surrounded by a rather wide head group region in which the volume fractions of the head groups are fairly low. Counterions accumulate in between the head groups and cause an effective reduction of the charge density in this region. The net charge density of a micelle is low and does not depend on the salt concentration. The electrostatic potential has a maximum in the head group region, of which the magnitude and the dependence on ionic strength are about the same as measured experimentally. As the charge distribution in the head group region is independent of the salt concentration also the decay of the potential in the head group region does not depend on the salt concentration, contrary to the potential decay outside the micelle. The profile of contributions to the free energy of a micelle with a fixed center of mass shows that an important positive contribution exists in the A/W (W and other hydrophilic segments) interface. This contribution does not change with salt concentration. The main negative contributions to A_m^σ arise from the core of the micelle and the outer side of the head group region.

These observations indicate why a simple model for micelle formation, assuming a low, fixed surface charge and a constant surface tension between hydrocarbon and hydrophilic segments may work well in practice.

References

- 1 Tanford, C., "The Hydrophobic Effect", Wiley Interscience NY, 1980
- 2 Israelachvili, J. N.; Mitchell, D. J.; Ninham, B. W. *J. Chem. Soc. Faraday Trans. 2* **1976**, *72*, 1525.
- 3 Jönsson, B.; Wennerström H. *J. Colloid Interface. Sci.* **1981**, *80*, 482
- 4 Ruckenstein, E.; Beunen, J.A. *Langmuir* **1988**, *4*, 77
- 5 Eriksson, J. C.; Ljunggren, S.; Henriksson, U. *J. Chem. Soc. Faraday Trans. 2*, **1985**, *81*, 833
- 6 Wennerström, H.; Lindman, B. *Physics Reports*, **1979**, *52*, 1
- 7 Gruen, D. W. R. *J. Colloid Interface Sci.* **1985**, *89*, 153
- 8 Dill, K. A.; Flory, P. J. *Proc. Natl. Acad. Sci. USA* **1981**, *78*, 676
- 9 Ben-Shaul, A.; Szleifer, I.; Gelbart, W. M. *Proc. Natl. Acad. Sci. USA* **1984**, *81*, 4601
- 10 Gruen, D. W. R. *J. Phys. Chem.* **1985**, *89*, 146
- 11 Szleifer, I.; Ben Shaul, A.; Gelbart, W. M. *J. Chem. Phys.* **1986**, *85*, 5345
- 12 Egberts, E.; Berendsen H. J. C. *J. Chem. Phys.* **1988**, *89*, 3718
- 13 Smit, B.; Hilbers, P. A. J.; Esselink, K.; Rupert, L. A. M.; Van Os, N. M. *Nature* **1990**, *348*, 264
- 14 Jönsson, B.; Eldholm, O.; Teleman, O. *J. Chem. Phys.* **1986**, *85*, 2259
- 15 Watanabe, K.; Ferrario, M.; Klein, M. *J. Phys. Chem.* **1988**, *92*, 819
- 16 Hayter, J. B.; Penfold, J. *Colloid Polymer Sci.* **1983**, *261*, 1022
- 17 Berr, S. S.; Coleman, M. J.; Jones, R. R.; Johnson, J. S. *J. Phys. Chem.* **1986**, *90*, 6492
- 18 Scheutjens, J. M. H. M.; Fleer, G. J. *J. Phys. Chem.* **1979**, *83*, 1619
- 19 Scheutjens, J. M. H. M.; Fleer, G. J. *J. Phys. Chem.* **1980**, *84*, 178
- 20 Evers, O. A.; Scheutjens, J. M. H. M.; Fleer, G. J. *Macromolecules* **1990**, *23*, 5221
- 21 Leermakers, F. A. M.; Scheutjens, J. M. H. M. *J. Chem. Phys.* **1988**, *5*, 3264
- 22 Leermakers, F. A. M.; Scheutjens, J. M. H. M. *J. Colloid Interface Sci.* **1990**, *136*, 231
- 23 Leermakers, F. A. M.; Scheutjens, J. M. H. M. *J. Phys. Chem.* **1989**, *93*, 7417
- 24 Böhmer, M. R.; Evers, O. A.; Scheutjens, J. M. H. M. *Macromolecules* **1990**, *23*, 2288
- 25 Barneveld, P. A.; Scheutjens, J. M. H. M.; Lyklema, J. *Colloids Surf.* **1991**, *52*, 107
- 26 Hill, T. L. "Thermodynamics of Small Systems", Vols I and II, Benjamin, N.Y. 1963, 1964
- 27 Hall, D. and Pethica, B. A., in "Nonionic Surfactants", Schick, M. J. ed. Marcel Dekker: New York, 1976, Ch. 16.
- 28 Van Lent, B.; Scheutjens, J. M. H. M. *Macromolecules* **1989**, *22*, 1931
- 29 Böhmer, M. R.; Tjissen, R.; Koopal, L. K. *J. Phys. Chem.* **1991**, *95*, 6285
- 30 Böhmer, M. R.; Koopal, L. K. *Langmuir* **1990**, *6*, 1478

- 31 Hayashi, S. and Ikeda, S. *J. Phys. Chem.* **1980**, *84*, 744
- 32 Lindman, B.; Wennerström, H., *Top. Curr. Chem.* **1980**, *87*, 1
- 33 Huisman, H. F. *Proc. Kon. Ned. Akad. v. Wetensch.* **1964**, *67*, 388
- 34 Zana, R. *J. Colloid Interface Sci.* **1980**, *78*, 330
- 35 Lianos, P.; Zana, R. *J. Colloid Interface Sci.* **1981**, *84*, 100
- 36 Healy, T. W.; Drummond, C. J.; Grieser, F.; Murray, B. S. *Langmuir* **1990**, *6*, 506
- 37 Evans, D. F.; Mitchell, D. J.; Ninham, B. W. *J. Phys. Chem.* **1984**, *88*, 6344
- 38 Lyklema, J., *J. Electroanal. Chem.* **1972**, *37*, 53
- 39 Verwey, E. J. W. and Overbeek, Th. O. "Theory on the Stability of Lyophobic Colloids"; Elsevier: Amsterdam, The Netherlands, 1948
- 40 Roelants, E.; De Schryver, F. C. *Langmuir* **1987**, *3*, 209
- 41 Van Os, N. M.; Daane, G. J.; Bolsman, T. A. B. M. *J. Colloid Interface Sci.* **1987**, *115*, 402
- 42 Evans, H. C. *J. Chem. Soc.* **1956**, *117*, 579
- 43 Binana-Limbelé, W.; Van Os, N. M.; Rupert, L. A. M.; Zana, R. *J. Colloid Interface Sci.* **1991**, *141*, 157

CHAPTER 5

Adsorption of Ionic Surfactants on Constant Charge Surfaces

Analysis based on a self-consistent field lattice model

Abstract

Adsorption isotherms of ionic surfactants onto surfaces with a constant charge density have been calculated using the self-consistent field lattice theory for adsorption and/or association, initiated by Scheutjens, Fleer and Leermakers. At low salt concentrations the adsorption isotherms show a two step behavior, after the first step the surface charge is compensated and a surfactant monolayer is formed on the surface. At about 0.1 of the cmc a second step occurs and bilayer formation takes place. At higher salt concentrations the initial adsorption is reduced, the distinction between the two steps tends to disappear and the final plateau values are slightly higher than those at low salt concentrations. The isotherms at different salt concentrations have a common intersection point at the iso-electric point, which is in agreement with thermodynamic analysis and experiments. The predicted effects of salt concentration, surface charge and surfactant chain length are also in agreement with experimental findings.

Introduction

Many energetic and entropic effects contribute to the free energy in the adsorption of surfactants at solid/liquid interfaces. Therefore simple models often fail to give an accurate prediction of adsorbed amounts and the structure of the adsorbed layer over a large concentration domain. The interactions involved include both interactions between surfactant and surface and mutual interactions between the surfactant molecules. Especially the latter is a complicated interplay of attraction and repulsion. For ionic surfactants the main factors involved are (1) electrostatic interaction between the surfactant head group and the surface, which depends on the surface charge, (2) attraction between the tails, which can be

studied by varying the aliphatic chain length and (3) electrostatic repulsion between the head groups, which is a function of the salt concentration.⁽¹⁻⁶⁾

A promising starting point for the theoretical description of surfactant adsorption may be formed by a theory describing micelle formation. In such a theory attraction between the aliphatic tails and repulsion between the head groups is necessary in order to form micelles. Also in models for adsorption of amphiphiles it is expedient to distinguish between interactions originating from the lyophilic and the lyophobic parts.

Regarding the interactions between the surfactant and the surface it is mandatory to establish the part of the surfactant molecule which interacts with the surface. If the tails adsorb, the head groups will most likely be at the solution side of the layer. If the head groups adsorb the tails may be on the solution side or a bilayer is expected. Most models are based upon a presupposed structure of the adsorbed layer, hence the resulting equations are applicable only to a limited adsorption region. In models which allow for a change in the adsorbed layer structure⁽⁶⁾ with adsorbed amount or which consider different structures⁽⁷⁾, the free energy of assumed structures may be compared to find the preferred one.

A theory that meets the two requirements: (1) distinction of the modeled molecules in a lyophilic and a lyophobic part and (2) calculation instead of assuming the structure of the adsorbed layer, is the self-consistent field lattice theory for adsorption and/or association (SCFA) originally developed by Scheutjens and Fleer to study polymer adsorption⁽⁸⁻¹¹⁾ and extended to association structures of lipids and surfactants in solution by Leermakers et al.⁽¹²⁻¹⁴⁾ In the latter case use is made of the thermodynamics of small systems to calculate the critical micelle concentration of the amphiphiles.^(11,14) The theory has recently been extended with electrostatic interactions.⁽¹⁵⁻¹⁷⁾

The original SCFA theory is an extension of the Flory theory⁽¹⁸⁾ to systems which have inhomogeneities in one direction, e.g. perpendicular to a surface. Using the SCFA theory the equilibrium volume fraction profiles of surfactant head and tail groups, solvent molecules and salt ions in the vicinity of a surface or in a micelle can be calculated starting from molecular properties, such as e.g. chain length and interactions with other (parts of) molecules. From the volume fraction profiles near the surface the adsorbed amounts can be obtained.

In this chapter we will present, after a summary of the theory, calculated adsorption isotherms of anionic surfactants on a surface with a fixed positive surface charge. Special attention will be given to the adsorption at different salt concentrations and to the charge distributions and electrostatic potential profiles. The effects of surface charge and surfactant chain length will be discussed.

SCFA Theory

We will summarize the main principles and notations of the SCFA theory, closely following Cohen Stuart et al.⁽¹⁷⁾ For a more detailed description of the theory and the incorporation of electrostatics in it we refer to the literature.^(10,15)

Lattice model and electrostatics

In the model each molecule consists of one or more segments which may be of different types. The molecules are placed on lattice layers with thickness l which are parallel to the surface. Each segment is located on a lattice site. Compositional inhomogeneities in the lattice layers are neglected by adopting a mean field approach in every layer. The layers are numbered, starting from $z = 0$ at the surface, to $z = M$ in the bulk solution as indicated in Figure (1). The electrical potentials can be calculated from basic electrostatics if the charges

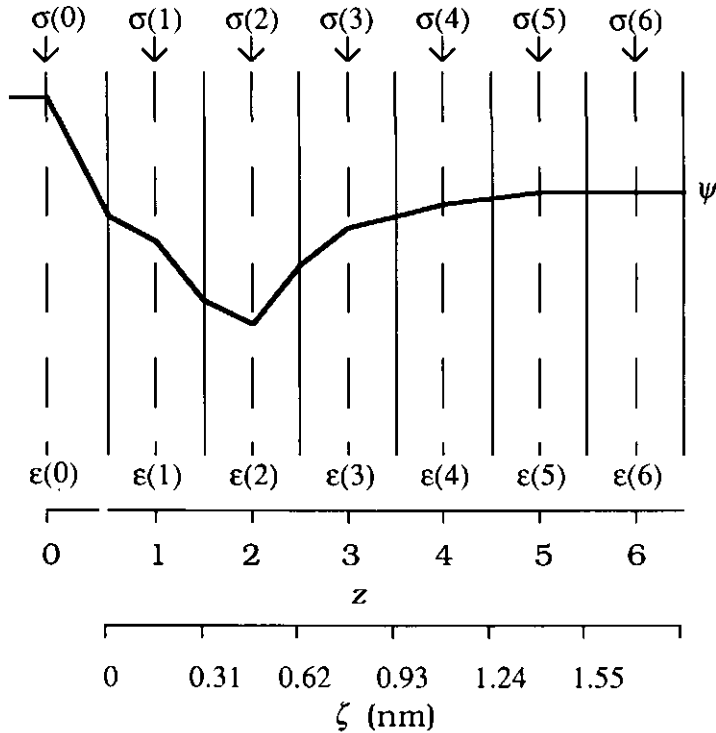


Figure 1: Schematic two-dimensional representation of a flat lattice. The lattice consists of z layers and is entirely filled with molecules. The electrostatic charges, σ , are located on the midplanes in each lattice layer. For the calculation of the electrostatic potentials, ψ , the charges, the distance, ℓ , between the midplanes and the average permittivity, $\epsilon(z)$, in each layer are needed. For ℓ a value of 0.31 nm is chosen. A discontinuous change in the field strength occurs at the midplanes where charge is present and at the boundary planes between two lattice layers where the dielectric constant changes.

are known. It is assumed that the charges are located at the midplanes of the lattice layers, see Figure (1). In that case the space in between two midplanes is free of charge and, consequently, the dielectric displacement, $D(\zeta)$, between two midplanes is constant. This quantity can be calculated from:

$$D(\zeta) = \epsilon(\zeta)E(\zeta) \quad (1)$$

where $\epsilon(\zeta)$ is the dielectric permittivity at distance ζ from the surface and $E(\zeta)$ is the field strength. To calculate $\epsilon(\zeta)$ we assume a linear combination of the dielectric constants of the components, ϵ_x , present in the layer. Since we used a mean field approximation we only consider averaged volume fractions, $\phi_x(z)$, of segment type x in layer z so that the average permittivity is given by:

$$\epsilon(z) = \sum_x \epsilon_x \phi_x(z) \quad (2)$$

The field strength $E(\zeta)$ changes at the midplanes due to the presence of charge and may change at the boundaries between two lattice layers due to a change in dielectric permittivity, $\epsilon(\zeta)$. The dielectric displacement at position ζ is calculated as:

$$D(\zeta) = \sum_{z=0}^{\text{int}\{\zeta/\ell + 1/2\}} \sigma(z) \quad (3)$$

The Entier function of $\zeta/\ell + 1/2$ is indicated as $\text{int}\{\zeta/\ell + 1/2\}$.

The charge density of a midplane must be calculated from the volume fractions, summing the contributions of all charged components we obtain:

$$\sigma(z) = \sum_x v_x e \phi_x(z) / a_s \quad (4)$$

The valency of x is denoted by v_x , e is the elementary charge and a_s is the cross sectional area of a lattice site. Using eqs (1-4) the field strength can be calculated from the volume fractions. From the field strengths the potentials, $\psi(z)$, on the midplanes can be calculated using a recurrence relation:

$$\psi(z+1) = \psi(z) - \frac{\ell}{2} \left\{ E(z) + E\left(z + \frac{1}{2}\right) \right\} \quad (5)$$

In practice, the calculations are carried out for a symmetrical system between two surfaces.⁽¹⁵⁾ The electroneutrality condition yields a reference potential with the bulk which has to be used to start the

stepwise calculation of all potentials.⁽¹⁵⁾ For adsorption calculations on one surface we chose a large separation between the two surfaces, so that the potential difference between layer M and the bulk solution is very small. An example of a potential profile is shown in Figure (1). The electrostatic potentials are related to the electrical energy u_x^{el} according to:

$$\exp[-u_x^{el}(z)/kT] = \exp[-v_x e \psi(z)/kT] \quad (6)$$

Together with non-electrostatic contact interactions, volume filling constraints, and chain statistics the electrical potentials determine the equilibrium volume fraction profiles. Expressions for these interactions and for the chain statistics will be given in the next sections.

Volume filling

In the theory it is assumed that there are no empty lattice sites. This volume filling constraint can be materialized by imposing that the sum of the volume fractions in every layer z must be unity:

$$\sum_x \phi_x(z) = 1 \quad (7)$$

Unlike the electrical potentials, which affect different types of segments in different ways, because they may differ in valency, the volume filling constraint is the same for all segment types in the layer. The volume filling constraint may also be denoted as a Boltzmann factor: $\exp[-u'(z)/kT]$ as has been shown by Evers et al.⁽¹⁰⁾ The introduction of $u'(z)$ simplifies the further notation. The effect of this Boltzmann factor is that all volume fractions are multiplied by a factor that normalizes their sum in layer z . The value of $u'(z)$ is adjusted numerically to achieve this.⁽¹⁰⁾

Contact interactions

The Flory-Huggins χ -parameter is used to quantify the non-electrostatic contact free energies between different segments. We consider the surface as an additional component in the system with a volume fraction equal to unity in layers ≤ 0 and zero for layers ≥ 1 . The contact free energy of a segment of type x in layer z with segments of type y , χ_{xy} has contributions from layers $z-1$, z and $z+1$. The contact energy per segment relative to that in the bulk solution, where the volume fractions are denoted by ϕ_x^b , is expressed as:

$$u_x^{ct}(z) = kT \sum_y \chi_{xy} \{ \langle \phi_y(z) \rangle - \phi_y^b \} \quad (8)$$

The term $\langle \phi_y(z) \rangle$ is made up of the relative contributions of the layers $z-1$, z and $z+1$ to the contact fraction of segment type y in layer z :

$$\langle \phi_y(z) \rangle = \lambda_1 \phi_y(z-1) + \lambda_0 \phi_y(z) + \lambda_1 \phi_y(z+1) \quad (9)$$

The type of lattice is characterized by the λ' values which indicate the fraction of neighboring sites in the same (λ_0) layer and in the adjacent layers (λ_1). In a hexagonal lattice λ_1 equals $1/4$ and λ_0 is $1/2$.

Self consistency

So far we have identified three contributions to the free energy per segment, $u_x^{el}(z)$, $u'(z)$ and $u_x^{ct}(z)$ which can all be represented with Boltzmann factors. For monomers these Boltzmann factors can be used to obtain the relative abundance of monomers x in layer z with respect to the bulk solution. In other words they serve to calculate the volume fractions using the following equation for each segment in each layer:

$$\phi_x(z) = \phi_x^b \exp \left[\left(-u'(z) - u_x^{ct}(z) - u_x^{el}(z) \right) / kT \right] \quad (10)$$

It is evident however that all three contributions to the free energy per segment depend on the volume fraction profile itself: (1) the electrostatic potentials depend on the charges, see eqs (1, 3 and 5), which are according to eq (4) a result of the volume fraction profiles. (2) The magnitude of the contact interactions depend on the number of interactions as shown by eq (8), and (3) the volume filling constraint depends on the sum of the volume fractions. The next task is to find a solution to the set of equations which is self consistent, i. e. the volume fraction profile must match the profile of the free energies per segment, $u_x(z) = u'(z) + u_x^{ct}(z) + u_x^{el}(z)$: the volume fractions that are used to calculate $u_x(z)$ in equations (1-5) and (8) must be the same as those which result after application of eq (10). Such a solution can be found numerically, see ref (10).

Chain statistics

A major stimulus to develop the SCFA theory and to apply it to polymer adsorption was formed by the possibility to evaluate the chain statistics of polymer molecules on a lattice. For chain molecules composed of several segments eq (10) must be modified to calculate the volume fractions from the segmental free energies. The relative occurrence of segment 2 of a dimer to be in layer z depends on its own Boltzmann factor but also on the Boltzmann factor of segment number 1 to which it is connected, which will either be in layer $z-1$, z or $z+1$. The same reasoning applies to segment 1, its probability to be in a certain layer depends on the position of segment 2. For the calculation of these probabilities two types of chain statistics can be used. For polymers first order Markov statistics are usually applied. The chain conformations are calculated as step weighted walks, each step from segment s in a chain to segment $s+1$ does not depend on the position of segment $s-1$ and, consequently segment $s+1$ also may find itself in the same lattice site as segment $s-1$. For short chain molecules, such as lipids and surfactants, where we prefer to treat every CH_2 group as a single segment, this leads to an overestimation of the chain flexibility, therefore Leermakers and Scheutjens developed a rotational

isomeric state scheme, (RIS), which forbids backfolding of five subsequent segments and allows for a distinction between trans and gauche conformations.⁽¹³⁾

In first order Markov statistics an end segment distribution function of a chain of s segments, $G_x(z, s | 1)$, is defined, which expresses the average weight of walks along the chain starting from segment 1, which may be located anywhere in the system. The end segment distribution function of a chain i of s segments can be expressed in that of a chain of $s-1$ segments and a recurrence relation can be used starting at the first segment where $G_i(z, 1 | 1) = G_x(z) G_i(z, 1)$, which is just the abbreviation of $\exp\left[\left(-u'(z) - u_x^{ct}(z) - u_x^{el}(z)\right)/kT\right]$, called the free segment weighting factor. This recurrence relation reads:

$$G_i(z, s | 1) = G_i(z, s) [\lambda_1 G_i(z-1, s-1 | 1) + \lambda_0 G_i(z, s-1 | 1) + \lambda_1 G_i(z+1, s-1 | 1)] \quad (11)$$

End segment distributions must also be calculated starting from the other chain end i.e. at r : $G_i(z, s | r)$. By combination of the two end segment distributions the volume fraction of segment s in layer z can now be calculated using:

$$\phi_i(z, s) = C_i G_i(z, s | 1) G_i(z, s | r) / G_i(z, s) \quad (12)$$

The volume fractions of chains or parts of chains, e.g. the head groups of the surfactants, can then be obtained by summing the appropriate volume fractions. The normalization constant, C_i , has been shown to be equal to ϕ_i^b / r , where ϕ_i^b is the volume fraction of i in bulk solution. Equation (12) is the analogue of eq (10) for chain molecules, only the segmental free energies are written in the form of weighting factors for the sake of simplicity.

With RIS the weighting factors will also depend on the orientation of the segments. End segment distribution functions have to be calculated for every orientation using an equation very similar to eq (11). We refer to the literature for details regarding this method.⁽¹³⁾

Choice of Parameters

The surface (S) has a fixed positive charge, $\sigma(0)$, located in the middle of layer 0. Surfactants are treated as chains consisting of a number of aliphatic segments, A, and three sequential head group segments B. The energy difference between a trans and a gauche conformation in the chain is taken to be 1 kT. The valency of the head group, B_3 , equals -1; $-1/3$ charge per B segment. The relative dielectric constant of the segments of type A is 2 and that of the head group segments is 80, just as that of the water, W. Water is modeled as an uncharged monomer. Cations and anions (C, D) are modeled as monomers with a valency of +1 and -1 respectively. As segments B, C and D are defined as charged segments, we chose not to indicate their charge in a superscript. The relative dielectric constants of the salt ions are also assumed to be 80.

The non-electrostatic interaction parameters between the A segments and the other segments in solution are set to 2: $\chi_{AW} = \chi_{AB} = \chi_{AC} = \chi_{AD} = 2$. The interaction parameter between B and the surface, χ_{BS} is chosen to be -10. The remaining χ -values are 0. This set of parameters, in combination with our choice to treat one CH_2 group as a segment, is the same as used previously and enables us to correctly predict the change in cmc with aliphatic chain length.⁽¹⁶⁾ The choice of parameters implies that salt ions only differ from the solvent by their charge. Apart from the fact that salt ions and solvent have a volume this situation is comparable to that in diffuse double layer theories such as the Gouy Chapman theory.

Some adsorption of B on the surface through non-electrostatic interactions is necessary to obtain a sufficiently thick adsorbed layer before the cmc is reached, see the results section. A negative χ_{BS} is physically not unreasonable as the interaction of many ions with the surface has besides an electrostatic component also a specific component. As adsorption is a displacement process in which a segment replaces a fraction λ_1 of its contacts with the solvent for contacts with the surface it should be realized that χ_{BS} is not the

"adsorption energy". The free energy of displacement, $\chi_{d(x)}$ of a solvent molecule by a segment of type x is defined as⁽¹⁹⁾:

$$\chi_{d(x)} = \lambda_1(\chi_{xs} - \chi_{xw} - \chi_{ws} + \chi_{ww}) \quad (13)$$

With the present choice of parameters this amounts to -2.5 kT for a B segment and -0.5 kT for an A segment.

The distance ℓ between two midplanes of lattice layers, which only has to be quantified in the computation of electrostatic interactions, is 0.31 nm and the cross section of a lattice site is assumed to be ℓ^2 . Using ℓ^3 as the volume of a lattice site this choice leads to 55.5 moles of lattice sites per dm^3 , i.e. every monomer is assumed to have the size of a water molecule. This size of a lattice site corresponds approximately with the volume of a CH_2 group as calculated from the bulk density of alkanes. However, the length of a C-C bond is overestimated, which was commented upon in ref (16). Some care should be taken in quantitative comparison between the SCFA theory and experiments. This reservation especially applies for layer thicknesses.

Results

Critical micelle concentrations

The cmc is a crucial concentration for the surfactant adsorption isotherm. Since beyond the cmc the concentration of free surfactant is almost constant, the adsorption holds at a pseudo plateau. The cmc values of the model surfactants used below have been calculated using the SCFA theory with a lattice of spherical geometry. A more detailed account of these calculations can be found in ref (16). Results for the surfactants and salt concentrations used in this study are summarized in table I.

Table I: Calculated critical micelle volume fractions

surfactant	A ₁₀ B ₃	A ₁₂ B ₃	A ₁₄ B ₃	A ₁₆ B ₃
<i>c_s</i>				
0.001 M	6.6E-03	2.5E-03	8.8E-04	2.6E-04
0.01 M		1.7E-03		
0.1 M	2.9E-03	4.7E-04	7.9E-05	1.2E-05

Adsorption isotherms

Adsorption isotherms of A₁₂B₃ at 3 salt concentrations (*c_s* = 10⁻³, 10⁻², and 10⁻¹ mol/dm³) are calculated for a surface with a fixed charge of 0.1 charges per lattice site. The results are given in Figure (2), where the adsorbed amount is expressed as *n^{exc}*, the excess number of molecules per cross section of a lattice site with respect to the bulk solution, which is defined as:

$$n^{exc} = \sum_z (\phi_i(z) - \phi_i^b) / r \quad (14)$$

The isotherms are plotted as a function of $\bar{\phi}$, the total volume fraction of surfactant. Below the cmc this is equal to ϕ_i^b , above the cmc, $\bar{\phi}$ also has a contribution from the surfactant present in the form of micelles as calculated as in ref (16). The cmc is indicated with an asterisk. At low salt concentrations the adsorption isotherms show two steps, but at *c_s* = 0.1 mol/dm³ the stepwise nature of the isotherm has almost disappeared. Another important result is that at low salt concentration the initial adsorption is higher than at high salt concentration. The difference is due to the competition between salt ions and surfactant ions for screening the surface charge. As a consequence, the position of the first step in the isotherm is shifted with about a factor of ten for each decade in the salt concentration. The strong increase in adsorption just before the first plateau is due to tail-tail attraction and it indicates that the attraction between tails is already substantial at very low adsorbed amounts. A similar conclusion was reached for nonionic surfactants.⁽¹⁹⁾

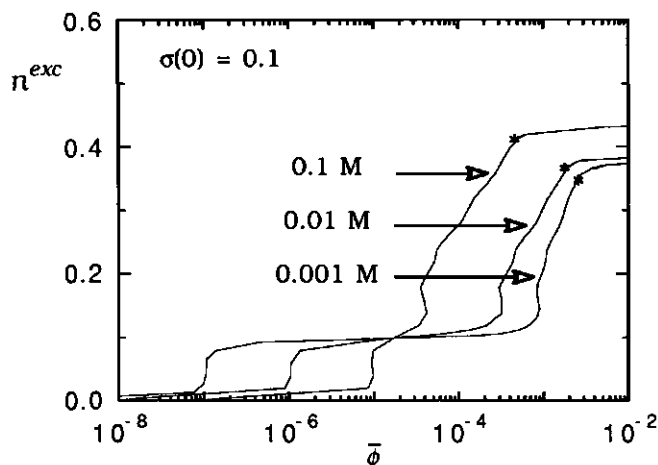


Figure 2: Adsorption isotherms of $A_{12}B_3$ on a surface with a fixed charge of 0.1 charge per lattice site at three salt concentrations. The interaction parameters are: $\chi_{AW} = \chi_{AB} = \chi_{AC} = \chi_{AD} = 2$, $\chi_{BS} = -10$, the remaining χ -parameters are zero. The relative dielectric constants are: $\epsilon_w = \epsilon_B = \epsilon_C = \epsilon_D = 80\epsilon_0$, $\epsilon_A = 2\epsilon_0$, the lattice layers have a thickness, ℓ , of 0.31 nm and the cross section, as is ℓ^2 . The cmc's are indicated with an asterisk.

Once the surface charge has been compensated there is no electrostatic driving force for surfactant adsorption anymore, the adsorption will only increase because the tail segments dislike the aqueous environment and can reduce the number of contacts with water by association and, consequently, adsorption. At low salt concentration and values of n^{exc} equal to or slightly larger than $\sigma(0)/F$ a strong electrostatic repulsion between the head groups occurs. This repulsion is so strong that the adsorption hardly increases with increasing equilibrium surfactant volume fraction. At about a factor of 10 before the cmc a second step occurs in the isotherm and a bilayer is formed. At high salt concentrations (0.1 M) the repulsion between head groups is much smaller; in fact the first and the second step in the isotherm are so close that the two steps can hardly be distinguished. Also in this case the second step is found at about 0.1 of the cmc.

At high salt concentration the adsorbed amount beyond the cmc is somewhat higher than at low salt concentrations. The decreasing repulsion between the head groups with increasing ionic strength causes more adsorption as well as a lower cmc. The decrease of the cmc with increasing salt concentration largely cancels the effect of the salt concentration on the adsorbed amount so that the differences in the plateau of the isotherm are relatively small.

The first plateau in the adsorption isotherm exists at a coverage of 0.1 molecule per surface site. This corresponds with the neutralization of the surface charge or iso-electric conditions. Moreover, the adsorption isotherms as a function of salt concentration show a common intersection point (cip) at these iso-electric conditions. As the potential in the plane (or region) where the surfactant ions adsorb is zero, the surfactant concentration at which $n^{exc} = \sigma(0)/F$ does not depend on the salt concentration. The cip has also been observed in experimental surfactant adsorption studies⁽²⁷⁾ and the coincidence of the cip with charge neutralization has been proven on a thermodynamic basis in ref (27).

Experimentally a "two step" isotherm has been found for a number of surfaces e.g.: silica^(1,21-23), mica⁽²⁴⁾, polystyrene⁽²⁵⁾, biotite⁽²⁶⁾, and graphitized carbon (Spheron).⁽²⁵⁾ According to the classification in ref (20) it is a L4 or H4 isotherm. In the cases where the adsorption was studied as a function of salt concentration^(1,25) the two step shape disappeared at high c_s . Bijsterbosch⁽¹⁾ also showed that at low salt concentrations the iep is located in the first plateau. We will compare our calculations with his results in more detail later in this chapter. On rutile⁽²⁷⁾, kaolinite^(27,28) and alumina^(2,29-32) a first plateau at an intermediate coverage has not been found at low salt concentration. The difference may be connected with the adjustment of the surface charge for the latter group of surfaces. Such an adjustment upon surfactant adsorption has been measured for alumina^(31,32) and rutile.⁽³³⁾ We will focus on variable charge surfaces in the next chapter.⁽³³⁾

Structure of the adsorbed layer

The structure of the adsorbed layer changes with the equilibrium surfactant concentration. Volume fraction profiles of A, B, C and D ($c_s = 0.001$ M) at three adsorbed amounts of surfactant: (i) "sub monolayer coverage", (ii) charge neutralization or "monolayer coverage" and, (iii) "bilayer coverage" are given in Figure (3) on a linear and a logarithmic ϕ scale. When the surface excess of surfactant is low ($n^{exc} = 0.006$) Figures (3a) and (3b), adsorption will make the surface somewhat hydrophobic. The surface charge is mainly compensated by positive adsorption of D and negative adsorption of C. At $n^{exc} = 0.1$ the surface charge is almost exclusively compensated by surfactant, Figures (3c) and (3d). As the A segments accumulate at the solution side of the adsorbed layer the surface will become considerably hydrophobic around the charge neutralization point. A small local maximum in the volume fraction profile of B segments appears in layer 5, indicating the start of the formation of a bilayer. This maximum is better visible on a logarithmic scale.

At coverages above the cip in the isotherms ($n^{exc} = 0.3$), Figures (3e) and (3f), a surfactant bilayer is present on the surface. In general the bilayer is asymmetric; the head groups near the surface are distributed over three lattice layers, whereas at the solution side the head group distribution is much wider. Moreover, the second step is much larger than the first one but not all additionally adsorbing surfactants orient with their hydrophilic heads to the solution side. At both sides of the layer counterions (C) accumulate between the head groups whereas coions (D) are excluded from the adsorbed layer. Head groups are located on both sides of the hydrophobic core, the system is hydrophilic again at these high coverages.

Experimentally the existence of surfactant bilayer structures at or above the cmc has been shown to be line with neutron reflection results.⁽³⁴⁾ Moreover, the volume fraction profiles at the different adsorbed amounts clearly relate to the experimentally observed force profiles for mica plates covered with surfactant.^(24,35) Also the

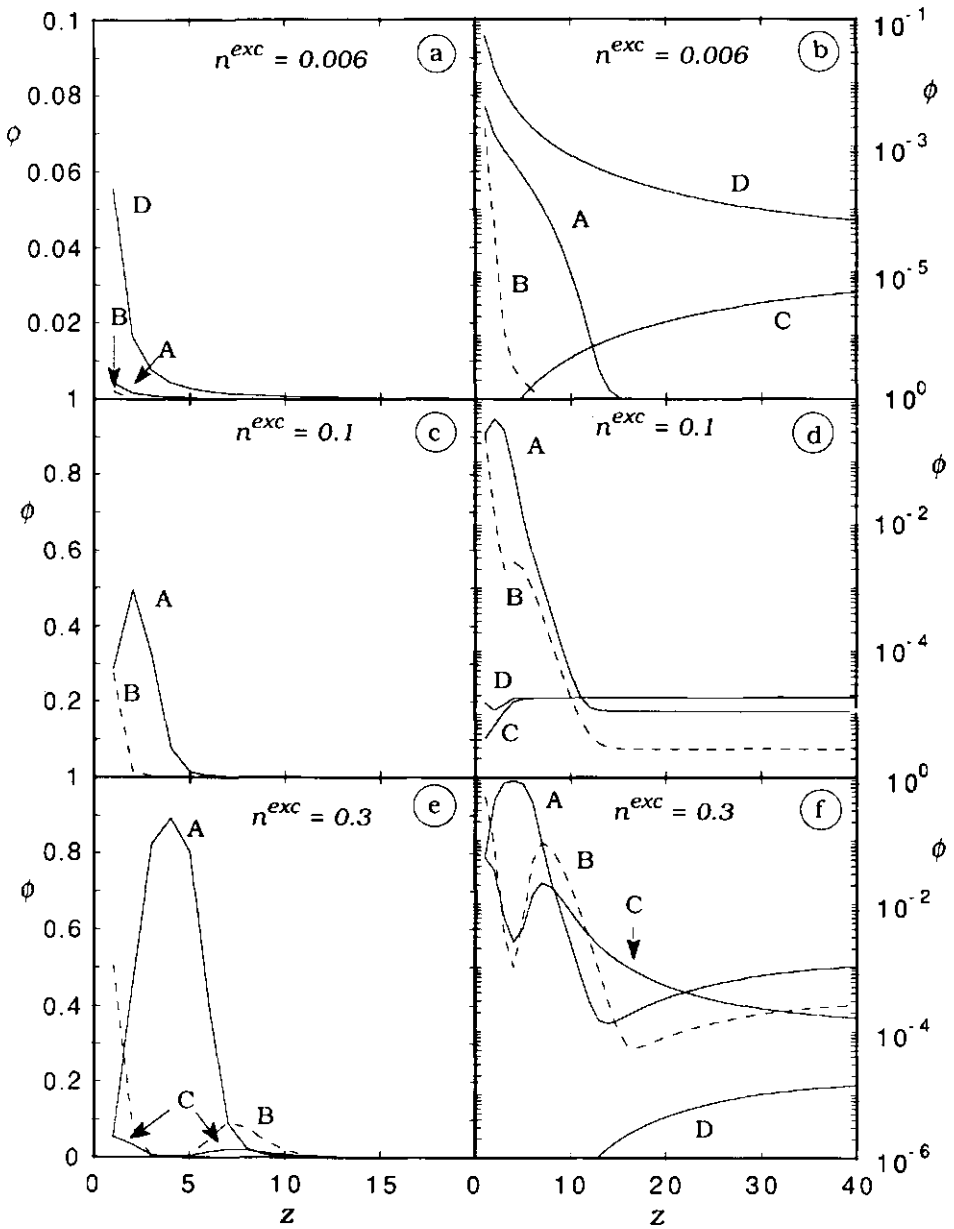


Figure 3: Volume fraction profiles of A, B, C and D at three surface coverages in the adsorption isotherm of $A_{12}B_3$ in 0.001 M CD solution. Figures (3a and 3b) $n^{exc} = 0.006$, Figure (3c and 3d) $n^{exc} = 0.1$ and Figure (3e and 3f) $n^{exc} = 0.3$. See Figure (2) for parameters.

maximum in the hydrophobicity of the surface plus adsorbed layer as a function of surfactant concentration as found by contact angle^(24,36,35), and flotation⁽³⁷⁾ experiments on silica points towards bilayer formation.

Charge and potential profiles

The charge distribution and potential profile in the adsorbed layer at $c_s = 0.001$ M are shown in Figure (4a) and (4b), respectively, for the same three values of n^{exc} as above. At the lowest coverage the charge and the potential decrease slowly and monotonically with distance from the surface. A typical diffuse layer picture results. At a coverage corresponding to the cip the surface charge is neutralized effectively by the surfactant and the potential decay is fast, both σ and ψ vanish after just a few lattice layers. At $n^{exc} = 0.3$ superequivalent surfactant adsorption leads to charge reversal. The charge reversal already takes place in the layer adjacent to the surface, $|\sigma(1)| > 0.1$, consequently the potential in this layer is now strongly negative. In layers 2 and 3 small net positive charge densities exist due to a surplus of positive counterions (C) which screen the charge due to the excess adsorbed surfactant in layer 1. The sum of the charges of layers 0 until 3 is almost zero. In the hydrocarbon core region ($2 \leq z \leq 7$) the net charge is very low and the electrical potential stays approximately constant. At the solution side of the hydrocarbon core the net charge density becomes negative again due to the presence of surfactant head groups. The hydrocarbon core separates two net uncharged parts of the system: (1) the surface charge plus the charge of the adjacent head groups and interpenetrated counterions on the surface side, and (2) the exterior layer of head groups and its counter charge, the latter including counterions between the head groups and in the diffuse electrical double layer on the solution side. In the region at the surface side it is very unfavorable to have a net charge left since it cannot be screened in the rather thick hydrocarbon core where it is difficult for the salt ions to accumulate because of the poor solubility of C and D in A.

In simpler theories for the adsorption of ionic surfactants, the abstraction has been made that only one electrostatic potential in the hypothetical plane of adsorption is needed to describe the adsorption of the entire molecules.^(2,4) As in the adsorbed bilayer the potential does not vary strongly with distance from the surface, the approximation now is a posteriori justified. However, it should be realized that the hypothetical plane of adsorption shifts outward with increasing adsorption.

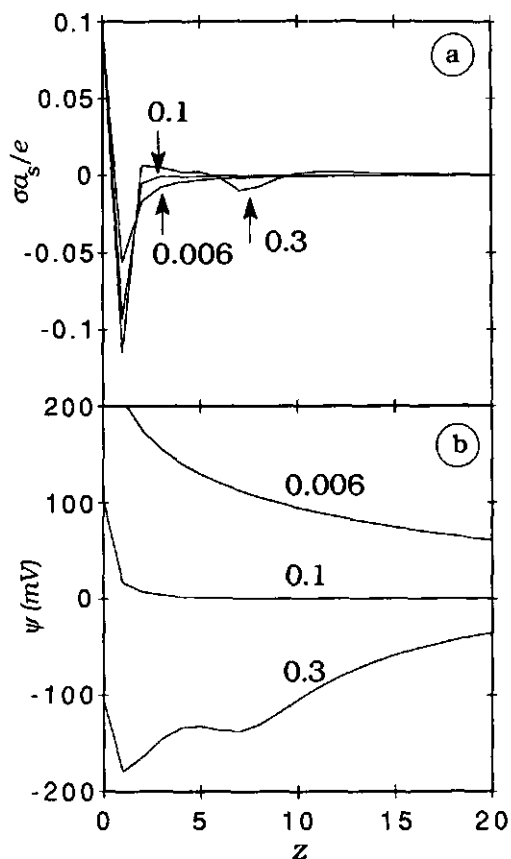


Figure (4): Charge (Figure 4a) and potential, (Figure 4b) profiles for $A_{12}B_3$ adsorbed from a 0.001 M CD solution near a charged surface for the three surface coverages presented in Figure (3). See Figure (2) for parameters.

An interesting phenomena is that the net charge distribution at $n^{exc} = 0.3$ is almost the same for all salt concentrations, see Figure (5a), only the diffuse part of the double layer, $z > 9$, differs. To a good approximation the surface plus adsorbed layer can be seen as a "constant net charge surface" independent of c_s . Consequently, the potentials differ significantly for the three salt concentrations, Figure (5b).

The maximum charge density in the head group region at the solution side occurs in layer 7. This charge density is small and about -0.01 charge per lattice site or -17 mC/m^2 for all salt concentrations. This is slightly lower than the net charge in the head group region of micelles⁽¹⁶⁾, which have a very similar distribution of head groups. The difference is due to the difference in geometry. Around a sphere the potential decays more rapidly than for a flat surface. This causes a somewhat higher charge on a sphere at given bulk composition.

For micelles we have reasoned⁽¹⁶⁾ that the net charge remains low because the head groups are distributed over several layers. The same applies here. The B segments at the solution side are spread over about five layers. Screening of the charge from B segments in a layer z by counterions cannot occur in layer $z + 1$ if B segments cause layer $z + 1$ to be negative. The charge in each of these layers can only be screened directly by incorporation of counterions in the layer itself or in the diffuse layer.

The number of counterions between the head groups at the surface side is possibly overestimated. This is a consequence of our choice of parameters, the size of a hydrated ion is bigger than one lattice site, which is 0.31^3 nm^3 in the present case. Neither is hydration of surfactant head groups accounted for, which would leave less space between the head groups to accommodate counterions. As the net charge of the layer on the surface side, including the surface charge, will always be approximately zero, less counterions near the surface would also lead to less surfactant at the surface side.

Effect of the surface charge

The effect of the surface charge on the adsorption of $A_{12}B_3$ from a 0.001 M salt solution is given in Figure (6). As expected the adsorption increases with surface charge. A pseudo plateau is again found at the coverage where the surface charge is neutralized. The second step in the adsorption isotherm takes place close to the cmc. The lower the surface charge density, the closer the second step

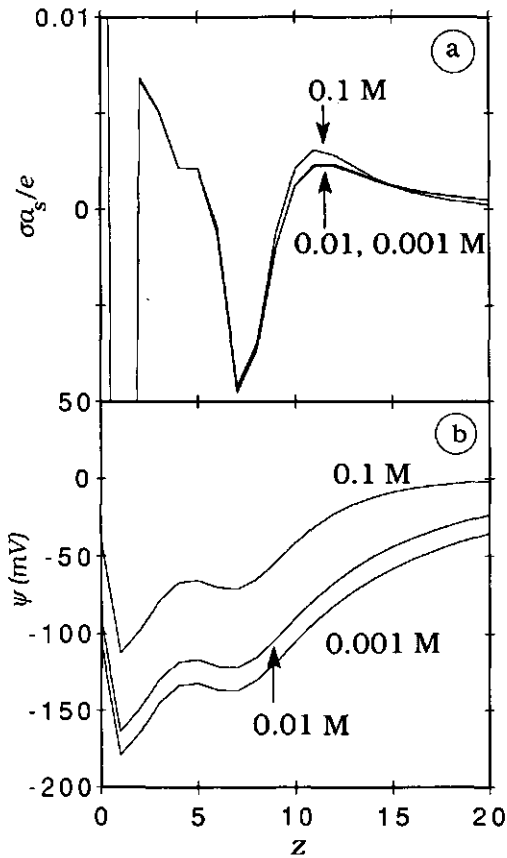


Figure (5): Charge (Figure 5a) and potential (Figure 5b) profiles near a surface covered with $A_{12}B_3$, $n^{exc} = 0.3$, at three salt concentrations. See Figure (2) for parameters.

approaches the cmc. For $\sigma(0) = 0$ a large step, at which a bilayer is formed, occurs just before the cmc. However, when χ_{BS} would have been taken slightly lower the adsorption would remain negligible over the same concentration region. The isotherm shape at low surface charge is typical for surfactants adsorbing with their head groups on a surface for which the heads have only a small adsorption energy. This situation is comparable with that of nonionic surfactants with a weakly adsorbing, rather short head group.⁽³⁸⁾ An experimental example of this behavior for charged surfactants is the adsorption of dodecyltrimethyl ammonium bromide on Cab-O-Sil silica at pH 8 as measured by Bijsterbosch.⁽¹⁾

At all surface charges values considered bilayers are formed at sufficiently high concentration. At the highest surface charge, $\sigma(0) = 0.2$ charges per lattice site, the first step is a condensation step, the tails associate strongly. In Figure (7) the segment density profiles at charge neutralization are shown for the case $\sigma(0) = 0.2$.

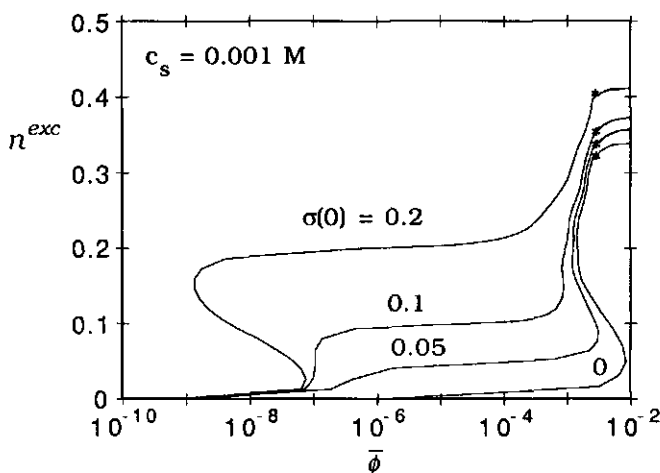


Figure (6): Effect of the surface charge on the adsorption isotherms of $A_{12}B_3$, at a salt concentration of 0.001 M. See Figure (2) for parameters.

Although the adsorption is considerable a bilayer has not yet formed and the surface has become strongly hydrophobic. Comparison with Figure (3c) shows that the hydrophobicity of the surface plus adsorbed surfactant layer at the first plateau is governed by the surface charge. This is of direct importance for flotation behavior and colloid stability of the system. The hydrophobic particles form strong flocs around the isoelectric point.⁽³⁹⁾

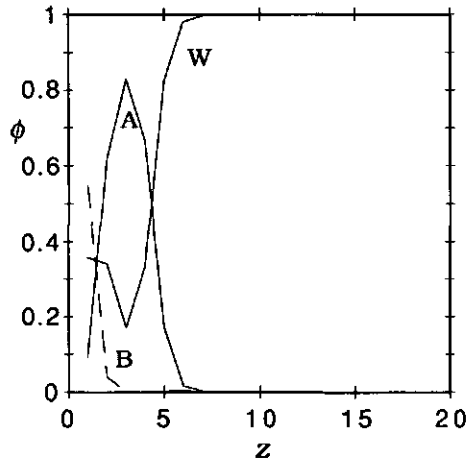


Figure (7): Volume fraction profiles of W, A, B at $n^{exc} = 0.2$ for $\sigma(0) = 0.2$ in a 0.001 M CD solution. See Figure (2) for parameters.

Independent of the surface charge density it is hard to form a second layer on the first one at low salt concentrations, only if $\bar{\phi}$ increases to about 0.1 of the cmc a second layer is formed. For surface charges up to 0.1 charge per lattice site the second step starts with a weak condensation. The condensation in the second step becomes more apparent the lower the adsorption in the first layer is. For $\sigma = 0$ a bilayer may form in one step.

Effect of chain length

The effect of chain length on the adsorption of A_nB_3 molecules at two salt concentrations is shown in Figure (8). Beyond the cmc longer chains give slightly higher adsorbed amounts. The tendency to aggregate increases with chain length, not only at the surface but also in solution: the steps in the isotherm occur at lower concentrations and the cmc decreases.

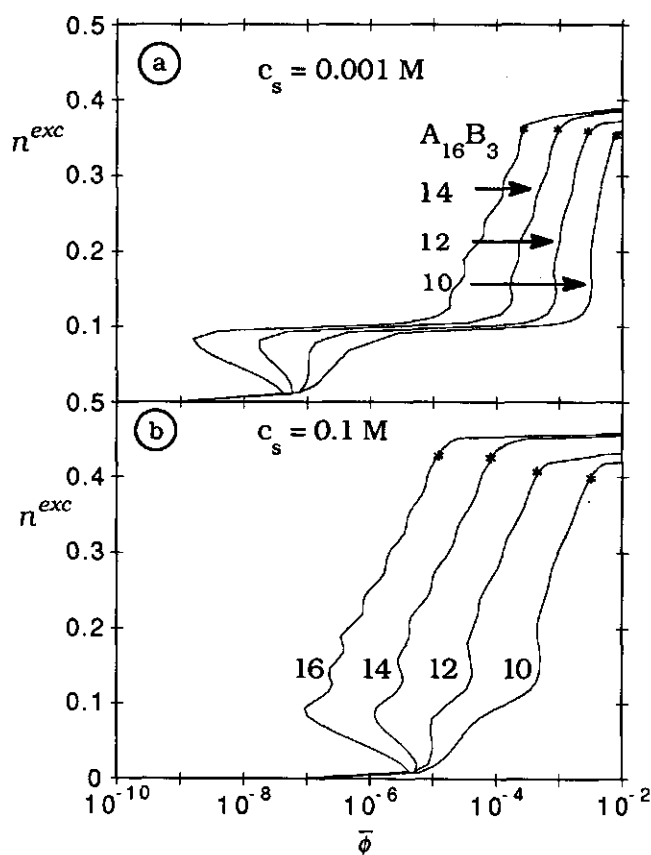


Figure (8): Effect of the chain length of A_nB_3 molecules on the adsorption on a surface with a fixed charge of 0.1 charge per lattice site from a salt solution of 0.001 M (Figure 8a) and 0.1 M (Figure 8b). See Figure (2) for parameters.

Consequently, the increase in plateau adsorption is only small. At low salt concentration the two step behavior of the isotherm is retained for all chain lengths studied. At longer chain lengths we observe a large condensation step in the first part of the isotherm, indicating a very strong association between the tails. The second step in the adsorption isotherms becomes slightly more gradual with increasing chain length at low salt concentration.

At high salt concentration only the $A_{10}B_3$ and the $A_{12}B_3$ isotherms show a slight hesitation to form a bilayer. The isotherms for $A_{16}B_3$ to $A_{12}B_3$ run about parallel with a small kink in the isotherm at the charge neutralization point.

Effect of adsorption energy

Besides the electrostatic, the specific or contact interactions between B segments and A segments with surface determine the shape of the adsorption isotherm. In Figure (9) we show some typical examples to illustrate this. The isotherm for $\chi_{BS} = -10$ and $\chi_{AS} = 0$ (isotherm II) is the same as discussed before. If the value of χ_{BS} is reduced to zero and χ_{AS} is set to -2 (isotherm III) a more gradual increase in the first part of the isotherm takes place. The molecules are adsorbed in a flat orientation on the surface. The surface charge is neutralized but a large second step cannot take place because the cmc is reached before this would occur: the molecules prefer to associate in solution rather than form a bilayer on the surface. These type of isotherms may reflect the situation for graphitized carbon surfaces.⁽²⁵⁾ If we set χ_{BS} again to -10 but maintain the value of -2 for χ_{AS} , isotherm I, a bilayer is again formed. In this case the head groups have the ability to displace the A segments from the surface. If both χ_{AS} and χ_{BS} are zero, isotherm IV, the characteristic two step nature of the adsorption isotherm is maintained, however, the second step becomes very steep, but also very close to the cmc.

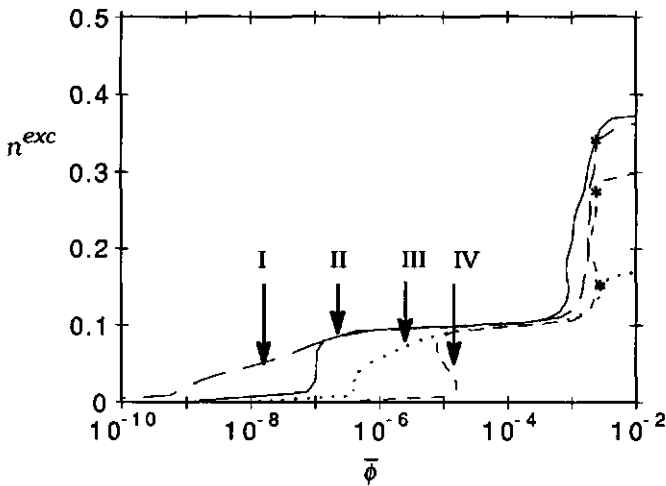


Figure (9): Adsorption isotherms of $A_{12}B_3$ at different values of χ_{AS} and χ_{BS} . I: $\chi_{AS} = -2$ and $\chi_{BS} = -10$, II: $\chi_{AS} = 0$ and $\chi_{BS} = -10$, III: $\chi_{AS} = -2$ and $\chi_{BS} = 0$ and IV: $\chi_{AS} = 0$ and $\chi_{BS} = 0$. See Figure (2) for other parameters.

Discussion

Comparison with experimental results by Bijsterbosch

L4 (two-step) isotherms have been found for cationics on silica by Bijsterbosch⁽¹⁾ and we will analyze the present results in more detail by making a comparison with his data. We have replotted his results for the adsorption of dodecyltrimethyl ammonium bromide on BDH silica at pH 8 in the absence of extra salt in Figure (10a). At the first plateau of DTA^+ adsorption, Br^- ions are not yet incorporated, the adsorbed amount is just high enough to compensate the surface charge, which is shown explicitly by electrophoresis measurements. At higher adsorbed amounts an approximately 1-1 relation between additional adsorbed DTA^+ and Br^- exists. Since both the sediment and the supernatant obey the electroneutrality condition this implies

that the surface charge of the BDH silica hardly changes in this region of the isotherm. Hence we may indeed consider BDH at this pH as having a constant charge surface. At pH 9 and 10 the behavior is similar but here the surface charge may adjust somewhat as a result of surfactant adsorption. For Cab-O-Sil at pH 8 or 9 Bijsterbosch also finds a clear two step isotherm and the Br^- adsorption starts when the first plateau is reached. For pH 10 the isotherm does not show a clear two step behavior but the Br^- adsorption starts when the surface charge is neutralized. Moreover the Br^- adsorption plus the surface charge almost match the total adsorbed surfactant charge. Applying the electro-neutrality argument mentioned above we may conclude that in practice also Cab-O-Sil behaves as a constant charge surface at all three pH values.

For the Cab-O-Sil-DTA⁺ system at pH 8 and 10 Bijsterbosch finds at 0.1 M salt concentration lower initial adsorption as compared to the situation in the absence of salt. Moreover the two step nature of the isotherm at pH 8 has disappeared. Experimentally, the effect of the salt concentration on the plateau adsorption is small, just as the effect of chain length. These features are in good agreement with our calculations.

Bijsterbosch also investigated the effect of butanol on the adsorption. It appeared that the cmc reduced markedly and the plateau adsorption roughly coincided with the first step in the isotherm where the surface charge is compensated. In our model we can introduce butanol as an additional component with structure A_4W . The introduction of this molecule leads to a marked decrease of the cmc and the adsorption holds indeed at the compensation of the surface charge as indicated in Figure (10b). The volume fraction profiles (Figure 11) show that the A_4 tails are strongly penetrated in the surfactant monolayer and that the butanol molecules are located on the solution side of the layer. With A_4W a rather thick hydrocarbon region can be formed without a concomitant large repulsion between surfactant head groups.

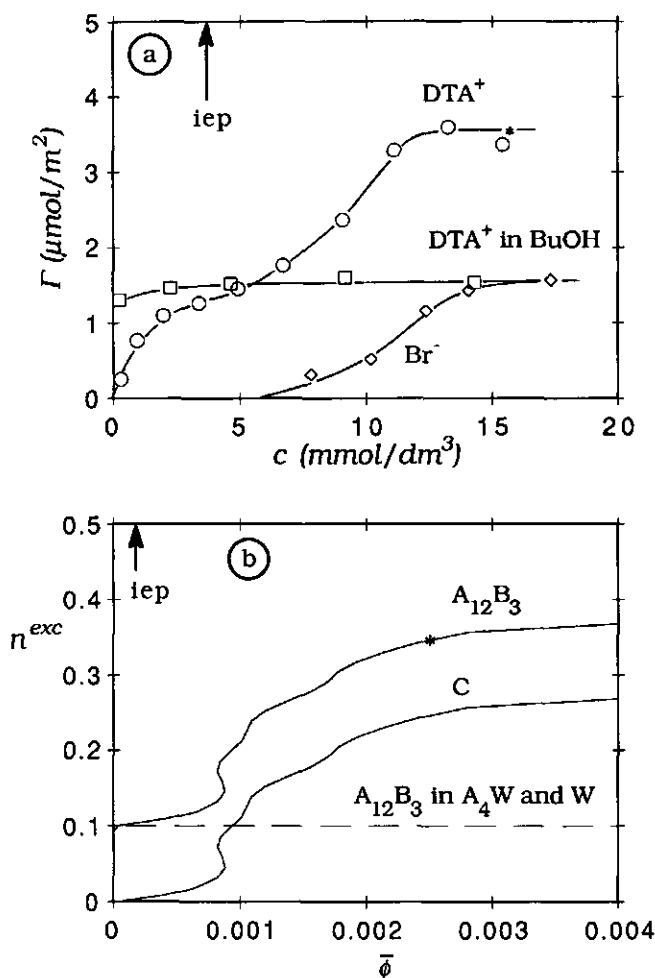


Figure (10a): Adsorption isotherms of DTA^+ , Br^- from water at pH 8 on BDH silica and from an aqueous DTAB solution containing $1 \text{ mol} \cdot \text{dm}^{-3}$ butanol, results of Bijsterbosch.⁽¹⁾

Figure (10b): Calculated adsorption isotherms for A_{12}B_3 and C from a 0.001 M salt solution and A_{12}B_3 from a 0.001 M salt solution containing a 0.03 bulk volume fraction of A_4W . See Figure (2) for parameters.

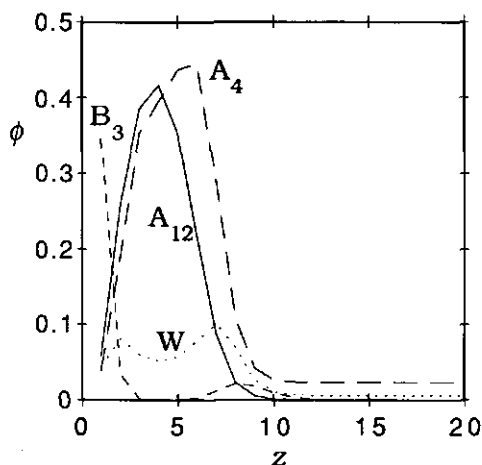


Figure (11): Volume fraction profiles of $A_{12}B_3$ and A_4W in the plateau of the isotherm, see Figure (10b) for parameters.

Aggregation in the adsorbed layer

Island formation of adsorbed surfactants in so-called hemimicelles^(2,22,23,29), admicelles^(7,30,31) or solloids⁽⁴⁰⁾ has received much attention in literature. As we use a mean field approximation in each lattice layer, we cannot calculate inhomogeneities parallel to the surface which are necessary to describe such structures. Nevertheless the calculated adsorption isotherms closely resemble the measured ones. We must note however, that the theoretically found condensation loops do not appear so strongly in reality. Here cooperative effects usually show up as a more gradual increase of the adsorption isotherm. With local aggregation, the "hesitation" of aggregation resulting in large condensation loops is much smaller, see ref (38) and the adsorption increases more gradually. However, in general the trends in the adsorption of ionic surfactants on surfaces with a fixed charge can be well reproduced with the present model. This observation does not hold for all surfactant adsorption systems, for instance we showed that the formation of aggregates on

the surface is necessary to interpret the adsorption of nonionic surfactants on silica.⁽³⁸⁾

The important difference between the adsorption of nonionics and cationics on silica is in that the head group segments of nonionics have a weaker interaction with the surface. In the case of fixed surface charges, the tendency to neutralize this charge close to the surface is strong. This will first lead to a structure of the adsorbed layer where the surface charge dominates the adsorption: the head groups are oriented towards the surface, each of them screening a surface charge. If charge effects dominate, mean field models can do a reasonable job, which can e.g. be concluded from Monte Carlo simulations of electrical double layers and comparison of these results with solutions of the Poisson-Boltzmann equation.⁽⁴¹⁾ Therefore, the structure of the adsorbed layer in the first plateau can be described successfully with a mean field model such as the present SCFA theory.

If we neglect for the moment the additional head on adsorption beyond the iso-electric point we may say that on the first a layer a second layer adsorbs with the head groups located at the solution side. In the bilayer the aliphatic tails have formed a phase well separated from the other segments, consequently the mean field approximation may well be justified again. Inhomogeneities perpendicular to the surface are clearly present, which also appeared from experiments⁽³⁴⁾ and at this high coverage they are more important than lateral inhomogeneities.

Gu and co-workers^(23,42,43) claim that the ratio of the two plateau values is the aggregation number of hemi-micelles. They assume that in the first part of the curve the surfactant ions to adsorb at the charged sites without lateral attraction and that in the second part of the isotherm an aggregate or hemi-micelle will be formed around every molecule. We have shown that it is not always correct to assume that in the first step no lateral attraction takes place, on the contrary the strong increase in adsorption forming the first step

is largely due to lateral attraction. If the charge density is moderate or high, the initial adsorption is high and interaction between aliphatic chains will be very strong in this first layer. A further argument against the presence of hemimicelles in the plateau of the isotherm is that the coverage in the plateau is fairly high, therefore it is hard to imagine that the hemimicelles do not interact or fuse with each other.

Conclusions

The adsorption isotherms, the effects of salt concentration and chain length on the adsorption of ionic surfactants on surfaces with a constant surface charge can be predicted successfully with the SCFA theory, even though this theory uses a mean field approximation.

The calculated volume fraction profiles provide information on the structure of the adsorbed layer. At the coverage where the surface charge is compensated, the surface is hydrophobized. At low salt concentrations the solution concentration regime where the surface is apparently hydrophobic is large, which is important for flotation and colloidal stability. However, unless the affinity of the tail groups for the surface is strong, bilayers are formed at high surfactant concentrations making the surface hydrophilic again.

The structure of the solution side of the bilayer formed close to the cmc has many aspects in common with the structure of micelles: the head groups at the solution side are distributed over several layers, the boundary region between the aliphatic segments and the other segments is fairly sharp and the charge profile does not change with salt concentration. The maximum charge density remains fairly low and is almost the same as in micelles. The electrical potentials are fairly high and different for different salt concentrations. At each salt concentration the potential is adjusted to obtain the maximum charge density in the head group.

References

- 1 Bijsterbosch, B. H. *J. Colloid Interface Sci.* **1974**, *47*, 186
- 2 Chander, S.; Fuerstenau, D. W.; Stigter, D. in "Adsorption from Solution", Ottewill, R. H.; Rochester, C. H.; Smith, A. L. Eds. Academic Press London 1983 p197
- 3 Osseo-Assare, K.; Fuerstenau, D. W.; Ottewill, R. H. "ACS Symposium Series" 1975, p63
- 4 Koopal, L. K.; Keltjens, L. *Colloids Surf.* **1986**, *17*, 371
- 5 Koopal, L. K.; Ralston, J. J. *Colloid Interface Sci.* **1986**, *112*, 362
- 6 Koopal, L. K.; Wilkinson, G. T.; Ralston, J. J. *Colloid Interface Sci.* **1988**, *126*, 493
- 7 Yeskie, M. A.; Harwell, J. H. *J. Phys. Chem.* **1988**, *92*, 2346
- 8 Scheutjens, J. M. H. M.; Fleer, G. J. *J. Phys. Chem.* **1979**, *83*, 1619
- 9 Scheutjens, J. M. H. M.; Fleer, G. J. *J. Phys. Chem.* **1980**, *84*, 178
- 10 Evers, O. A.; Scheutjens, J. M. H. M.; Fleer, G. J. *Macromolecules* **1990**, *23*, 5221
- 11 Van Lent, B.; Scheutjens, J. M. H. M. *Macromolecules* **1989**, *22*, 1931
- 12 Leermakers, F. A. M.; Scheutjens, J. M. H. M.; Lyklema, J. *Biophys. Chem.* **1983**, *18*, 353
- 13 Leermakers, F. A. M.; Scheutjens, J. M. H. M. *J. Chem. Phys.* **1988**, *89*, 3264
- 14 Leermakers, F. A. M.; Scheutjens, J. M. H. M. *J. Colloid Interface Sci.* **1990**, *136*, 231
- 15 Böhmer, M. R.; Evers, O. A.; Scheutjens, J. M. H. M. *Macromolecules* **1990**, *23*, 2288
- 16 Böhmer, M. R.; Koopal, L. K.; Lyklema, J. *J. Phys. Chem.* (acc), this thesis Ch. 4
- 17 Cohen Stuart, M. A.; Fleer, G. J.; Lyklema, J.; Norde, W.; Scheutjens, J. M. H. M. *Adv. Colloid Interface Sci.* **1991**, *31*, 477
- 18 Flory, P. "Principles of Polymer Chemistry", Cornell Univ. Press, Ithaca, NY, 1953
- 19 Böhmer, M. R.; Koopal, L. K. *Langmuir* **1990**, *6*, 1478, this thesis Ch. 2
- 20 Parfitt, G. D.; Rochester, C. H. in "Adsorption from Solution at the Solid/Liquid Interface", Parfitt, G. D.; Rochester, C. H. eds. Academic Press, London 1983 p. 3
- 21 Rupprecht, H. *Acta Pharmaceutica Technologica* **1976**, *22*, 37
- 22 Huang, Z.; Gu, T. *Colloids Surf.* **1987**, *28*, 159
- 23 Gao, Y.; Du, J.; Gu, T. *J. Chem. Soc. Faraday Trans 1* **1987**, *83*, 2671
- 24 Pashley, R. M.; Israelachvili, J. N. *Colloids Surf.* **1981**, *2*, 169
- 25 Hough, D. B.; Rendall, H. M. in "Adsorption from Solution at the Solid/Liquid Interface", Parfitt, G. D.; Rochester, C. H. eds. Academic Press, London 1983 p. 247
- 26 Cases, J. M. *Bull. Minéral.* **1979**, *102*, 684
- 27 De Keizer, A.; Böhmer, M. R.; Mehrian, T.; Koopal, L. K. *Colloids Surf.* **1990**, *51*, 339

- 28 Siracusa P. A. and Somasundaran, P. J. *Colloid Interface Sci.* **1986**, 114, 184
- 29 Scamehorn, J.; Schechter, R. S.; Wade, W. H. J. *Colloid Interface Sci.* **1982**, 85, 463
- 30 Harwell, J. H.; Hoskins, J. C.; Schechter, R. S.; Wade, W. H. *Langmuir* **1985**, 1, 251
- 31 Bitting, D.; Harwell, J. H. *Langmuir* **1987**, 3, 500
- 32 Partyka, S.; Rudzinski, W.; Brun, B.; Clint, J. H. *Langmuir* **1989**, 5, 297
- 33 Böhmer, M. R.; *Ph. D. Thesis*, Wageningen Agricultural University 1991, Ch. 6
- 34 Rennie, A. R.; Lee, E. M.; Simister, E. A.; Thomas, R. K. *Langmuir* **1990**, 6, 1031
- 35 Herder, P. J. *Colloid Interface Sci.* **1990**, 135, 346
- 36 Menezes, J. L.; Yan, J.; Sharma, M. M. *Colloids Surf.* **1989**, 38, 365
- 37 Novich, B. E. *Colloids Surf.* **1990**, 46, 255
- 38 Böhmer, M. R.; Koopal, L. K.; Janssen, R.; Lee, E. M.; Thomas, R. K.; Rennie, A. R. submitted to *Langmuir*, this thesis Ch. 3
- 39 Zhou, Z.; Wu, P.; Ma, C; *Colloids Surf.* **1990**, 50, 177
- 40 Somasundaran, P.; Kunjappu, J. T. *Colloids Surf.* **1989**, 37, 245
- 41 Carney, S. L.; Torrie, G. M. *Adv. Chem. Phys.* **1984**, 56, 141
- 42 Zhu, B.; Gu, T.; Zhao, X. *J. Chem. Soc. Faraday Trans. 1*, **1989**, 85, 3819
- 43 Gu, T.; Rupprecht, H. *Colloid Polym. Sci.* **1990**, 268, 1148

CHAPTER 6

Adsorption of Ionic Surfactants on Variable Charge Surfaces I

Charge effects and structure of the adsorbed layer

Abstract

The adsorption of an anionic surfactant on a variable charge surface has been studied by comparing results obtained for sodium para 3-nonylbenzene sulfonate (SNBS) on rutile with theoretical predictions based on the self-consistent field lattice theory (SCFA) by Scheutjens Fleer and Leermakers. Both the measured and the calculated isotherms show strong cooperative effects at low coverages and have shapes which are characteristic for the adsorption of anionic surfactants on metal oxides. The experimental and calculated adsorption isotherms at different salt concentrations have a common intersection point (cip) corresponding to surface charge neutralization. Before the cip the surfactants are adsorbed with their head groups in contact with the surface. After the cip bilayer formation starts. Surfactant ions screen effectively the surface charge, so that this charge increases upon surfactant adsorption. From the surface charge the amount of surfactant adsorbed "head-on" can be calculated. This amount depends on the surface potential, which is fixed by the pH, but not on the concentration of indifferent electrolyte. On the other hand, the amount of surfactant at the solution side of the bilayer depends mainly on the salt concentration but hardly on the surface potential. Due to the different charge screening mechanisms at the inner and the outer side of the adsorbed layer, the layers are asymmetrical.

Introduction

Adsorption isotherms of anionic surfactants from aqueous solution on oxide surfaces have been the subject of much research. The experimental work of the groups of Fuerstenau⁽¹⁻³⁾ and Somasundaran^(4,5) on alkane sulfonates adsorbed on alumina is often cited and general agreement exists about the shape of the isotherm of an anionic surfactant on a metal oxide such as alumina, see e.g.

refs (1-9). Electrokinetic measurements have been frequently used to provide additional information.(1-6,9)

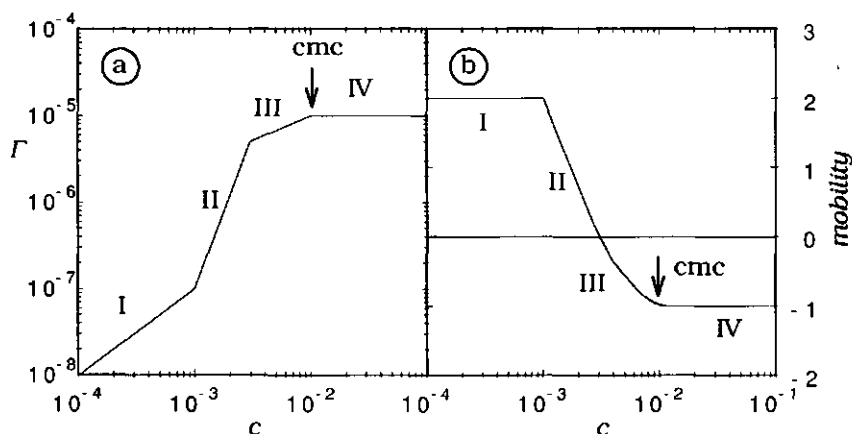


Figure (1): Characteristic four region isotherm for an anionic surfactant on a metal oxide surface on a log-log scale (a) and the electrophoretic mobility of the metal oxide particles as a function of the concentration of anionic surfactant (b).

Typically, when plotted on a log-log scale, four regions can be distinguished in the adsorption isotherms, as shown in Figure (1a). The isotherm extends over about three decades in concentration and adsorbed amount. In region I isolated surfactant molecules adsorb. In region II, which starts at very low coverages, the isotherm is steeper due to association of adsorbed molecules. The slope of the log-log isotherm decreases at the transition between region II and III. To interpret this change, the adsorption isotherm can be described with the relation $\Gamma = ac^b$, where Γ is the adsorbed amount, c is the concentration and a is constant in each region and takes care for the correct dimensionality. It follows that in each region b is constant and that at each transition b changes. The II/III transition is marked by a decrease of b , which is probably caused by a drastic increase of the head group repulsion, due to a change in the structure of the

adsorbed layer. In region III net lateral attraction may still exist if b is larger than unity. In ref (1-6) it is claimed that the II/III transition corresponds with the isoelectric point (iep), as indicated in Figure (1b). Beyond the iep the net coulombic interaction between surface plus adsorbed layer and an additionally adsorbing surfactant molecule is repulsive. Bitting and Harwell⁽⁹⁾, however, showed that the iep does not always coincide with the II/III transition. Region IV begins at the critical micelle concentration (cmc), beyond which the chemical potential of the surfactant hardly increases.

Although the four-region type isotherm is well established its interpretation has led to differences in opinion. An issue, already mentioned, is whether or not the transition between region II and region III coincides with the iep. A second, rather controversial issue is the structure of the adsorbed layer in region II. It is beyond doubt that strong attraction between the adsorbed molecules occurs and spectroscopic techniques indicate that local aggregates may be present.^(5,10,11) However, no agreement exists on their structure. Fuerstenau and co-workers call the solution concentration at the I/II transition the hemi-micelle concentration or hmc. Hemi-micelles, envisaged as small aggregates of surfactants with the head groups in contact with the surface and tails at the solution side. Harwell and co-workers^(8,9) call the I/II transition the critical admicelle concentration, (cac), and picture admicelles as local bilayer structures with head groups at both sides of the layer. The main difference between these two structures is that hemi-micelles can make the system surface (plus adsorbed layer) hydrophobic, whereas admicelles will hardly change the hydrophilicity of the surface.

To shed more light on these issues we will focus our attention on the effects of surface charge and salt concentration on surfactant adsorption. For alumina^(9,12) and kaolinite⁽¹³⁾ a change in pH upon adsorption of surfactants has been observed, indicating a change in surface charge. To our knowledge, however, this change in surface charge has not been quantified. Neither has it been used to obtain information regarding the structure of the adsorbed layer. The

magnitude of the surface charge reflects, among others, the extent to which the surface charge is screened. Due to the addition of specifically adsorbing counterions the surface charge increases at otherwise fixed conditions. More specifically, if a surfactant molecule adsorbs with its head group adhered to the surface, a pronounced effect on surface charge can be expected, whereas for adsorption of surfactant in a second layer, with its head group directed to the solution, the effect on the surface charge will be small.

To assess the charge effects experimentally we will investigate the well studied metal oxide rutile, TiO_2 . Rutile is known to have a pH and salt concentration dependent surface charge with a pristine point of zero charge (pzc) at about $\text{pH} = 5.8^{(14-16)}$, so the surface charge can be controlled in a convenient pH range. As the surfactant sodium para 3-nonylbenzene sulfonate (SNBS) was selected because it was available to us in isomerically pure form and its concentration can be easily determined using UV spectroscopy. The results for adsorption isotherms are complemented by electrophoresis data and surface charge-pH curves both in the presence and the absence of surfactant.

We will compare the trends that emerge from the experimental results with calculations obtained with the self-consistent field lattice theory for adsorption and/or association (SCFA) by Scheutjens, Fleer and Leermakers.⁽¹⁷⁻²³⁾ We have used this theory before to study the micellization⁽²⁴⁾ and adsorption⁽²⁵⁻²⁷⁾ of surfactants. With the SCFA theory volume fraction profiles perpendicular to an homogeneous surface can be calculated of, for instance, surfactant head groups, tails, and salt ions. These volume fraction profiles determine the structure of the layer. Other theories that have been developed for surfactant adsorption presuppose the structure of the adsorbed layer and use surface heterogeneity to explain the isotherm shape.^(7-9,12,28) The SCFA theory allows for gradual changes of the structure of the adsorbed layer with the equilibrium concentration without recourse to surface heterogeneity.

The basic or 1D SCFA theory uses a lattice in which layers parallel to the surface are distinguished. Within every lattice layer a mean field approximation is made, hence inhomogeneities in only one direction (1D) are considered. With this theory, for nonionic surfactants⁽²⁶⁾ with relatively short head groups good agreement between theory and experiment was obtained. For nonionics with very long head groups, the agreement was less satisfactory. Only with the 2D SCFA theory^(22,27), which allows for inhomogeneities in two directions: perpendicular and parallel to the surface, good agreement between theory and experiment could be obtained. For the adsorption of ionic surfactants a 2D extension of the theory is not yet available. For ionic surfactants good agreement between the 1D SCFA theory and experimental results for adsorption on surfaces with a constant charge was obtained. This led us to the conclusion that inhomogeneities parallel to the surface are not of major importance for these systems. Application of the theory to variable charge surfaces can be used to test whether this is a general feature for adsorption on charged surfaces. The variable charge surfaces will be modeled as surfaces with a fixed potential, such a surface serves as an adequate model for many crystalline metal-oxides at constant pH.^(15,29) We will not try to fit the measured adsorption isotherms but pay attention to the existence of the characteristic four region isotherm and the relation between surface charge (adjustment) and structure of the layer.

It should be noted here that an analysis of the experimental results on the basis of the SCFA theory is not the only one of its kind. One could also use classical macroscopic thermodynamics to analyse the relations between proton, salt and surfactant adsorption. This remains a task for the future.

Experimental

Chemicals

Sodium para 3-nonylbenzene sulfonate (SNBS) was a gift from Dr. N. M. van Os, Koninklijke Shell Laboratories Amsterdam (KSLA), The Netherlands. At KSLA the cmc values at 20°C were determined by Dr Van Os. The results are given in Table I.

Table I: cmc values of SNBS at 20°C

electrolyte	c_s (M)	cmc (mM)
NaCl	0.001	10.5
NaCl	0.01	10.0
NaCl	0.1	2.8
Na ₂ SO ₄	0.005	8
Na ₂ SO ₄	0.05	3

Rutile (TiO₂) with a BET surface area of 50 m²/g was synthesized by Fokkink⁽¹⁴⁾ using the method of Bérubé and de Bruyn.⁽³⁰⁾

All other chemicals were of pro-analyse quality and water was deionized using a Millipore Super Q system.

Adsorption isotherms

Adsorption isotherms were measured at 21°C using the depletion method. To prepare the rutile suspension, 0.5 grams TiO₂ were weighted into a 10 ml polycarbonate tube, 2 ml of NaCl solution was added, followed by sonication for 3 minutes. The pH was adjusted to the desired value using 0.03 M HCl. After one night the pH was checked and, if necessary, adjusted and the desired amounts of NaCl solution and surfactant solution of the same pH value were added up to a total volume of 8.5 ml. After end-over-end rotation for at least 8 hours the pH was measured again and re-adjusted to its original value where necessary. More than 4 hours later the pH was checked and, if necessary, again readjusted. When no changes in pH were observed the rutile was separated from the solution using Acrodisk filters (0.2

μm). The UV absorption of SNBS in the filtrate was measured at 225 and/or 262 nm.

Electrophoretic mobilities

Electrophoretic mobilities were measured at 20°C in a Malvern Zeta-sizer II with 0.1 g rutile in 50 ml. The measurements were repeated at least twice.

Surface charge determination

Charge-pH curves of rutile in NaCl and Na₂SO₄ and in the presence of SNBS and salt were determined at 20°C using an automated titration set up described elsewhere.⁽¹⁵⁾ 50 ml of solution and 0.5 g of rutile were mixed and purged with nitrogen during several hours before the titration was started. The rutile suspension was titrated between pH = 4 and pH = 8 with 0.1 M KOH and 0.1 M HCl. A "Van Laar bridge"^(14,15) was used if the rutile sample was titrated at different salt concentrations. In other cases a salt bridge with ceramic plug and filled with the same electrolyte (NaCl or Na₂SO₄) and concentration as present in the titration vessel was used. Small amounts of concentrated NaCl or surfactant solution were added through a septum. Blank titrations, i.e. titrations in the absence of rutile, were performed and subtracted from the titration curves in the presence of rutile to calculate of the charge-pH curves.

Experimental Results

Adsorption as a function of salt concentration

Different ways are used in the literature to plot surfactant adsorption isotherms: log-log, lin-log and lin-lin. The log-log plot has the advantage that it explicit information over a wide range of both surface coverage and solution concentration. Cooperative effects, which are often present in the low concentration range in surfactant

adsorption isotherms show up most clearly in log-log plots and, if they occur at relatively high concentrations, in lin-lin plots. The adsorption plateau becomes more clear if the adsorbed amount is plotted on a linear scale. With the use of log-log plots it should be kept in mind that: 1) the experimental reliability of the very low adsorptions, region I, is often poor and 2) changes in slope often seem abrupt on a log-log axis, while they may be gradual on a lin-log scale. The use of a lin-log plot favors thermodynamic analyses of the isotherm⁽³¹⁾, as the log of the equilibrium concentration equals the concentration dependent part of the chemical potential. We will plot our results in various ways.

In Figures (2a-2c) adsorption isotherms of SNBS on rutile at pH 4.1 ± 0.1 at three salt concentrations are given as log-log, lin-log and lin-lin plots. Indeed, in the double logarithmic plot four regions in the adsorption isotherms can be distinguished. The initial adsorption decreases with increasing salt concentration because the surfactant head groups, which contribute significantly to the screening of the surface charge, have to compete with small salt ions. In region I the coverage is too low for the adsorbed molecules to interact with each other, the slope is unity. Mutual interaction starts in region II, where the coverage is still very low: roughly between 10^{-9} and 10^{-7} mol/m², i.e. between 0.03 and 3% of the maximum coverage. A straight line with a slope of about four fits the data points in region II for all salt concentrations, but a curve with a gradual increase in slope, and, therefore, a more smooth transition between regions I and II also fits the data. The slope is again lower in region III, which starts at about the same surface coverage for all salt concentrations. The slope in region III may well be less than unity, depending on the salt concentration. The transition between regions II and III is more pronounced for low salt concentrations, which indicates that the repulsion between head groups becomes more important in region III. The isotherms show a common intersection point (cip) in region III. For surfactant concentrations above the cip the salt effect is reversed: adsorption at high salt concentration is

promoted due to improved screening of the head group charges. The cmc marks the transition to region IV, where the plateau is reached.

In the lin-log plot we can neither observe the strong cooperativity present at the low coverages nor the decrease in slope at the II/III transitions, but the top parts of the isotherm, regions III and IV, and the existence of a common intersection point become more clear. The cip is located at $\Gamma \approx 0.6 \mu\text{mol}/\text{m}^2$ where the equilibrium

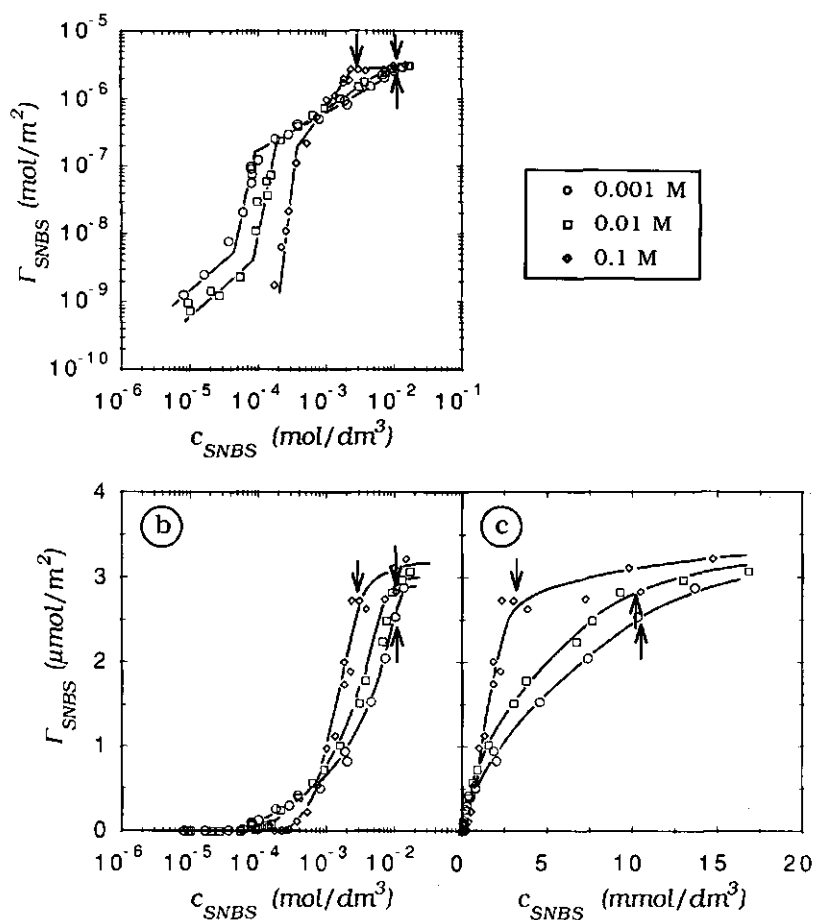


Figure (2): Adsorption isotherms of SNBS on rutile at pH = 4.1 ± 0.1 at three NaCl concentrations on log-log (a), lin-log (b) and lin-lin (c) scales. The arrows indicate the cmc values, see table 1.

concentration is about 0.8 mmol/dm^3 . In the cip the two salt effects compensate each other. A thermodynamic analysis of the occurrence of a cip in adsorption isotherms of organic ions has been given in ref (31). The plateau values reached are about the same for the different salt concentrations; an increase in the salt concentration causes a steeper rise of the isotherm but also a decrease in the cmc, leading to a shorter concentration range over which the isotherm can rise.

In the lin-lin plot all isotherms seem to be Langmuir-like which is misleading as shown in the previous figures. The advantage of linear plots is that the concentration where region IV is reached, is now shown more clearly. It is attained shortly after the cmc and it may well be a pseudo plateau; the coverage seems to increase slightly with surfactant concentration after the cmc. In connection to the fact that the pseudo plateau is reached after and not at the cmc it can be noted that the concentration of free surfactant is not entirely constant above the cmc: the γ -ln c curves showed a negative slope beyond the cmc.

Adsorption as a function of pH

Adsorption isotherms (log-log) of SNBS on rutile at pH 4.1, 5.1 and 6 are shown in Figure (3a) for $c_{\text{NaCl}} = 0.01 \text{ M}$. Results for $c_{\text{NaCl}} = 0.1 \text{ M}$ are presented in Figure (3b). Changing the pH from 4 to 6, i.e. passing the pristine pzc at pH 5.85, the initial affinity decreases, causing a shift of region I to higher surfactant concentrations. Moreover, region III starts at a lower surface coverage, indicating that the repulsion between the head groups becomes significant at lower coverages. In $c_{\text{NaCl}} = 0.1 \text{ M}$ (Figure 3b) it is hard to distinguish the different regions in the adsorption isotherm, region I could not be reached due to the low adsorptions (at a relatively high concentration) and the transition from region II to region III is not very clear.

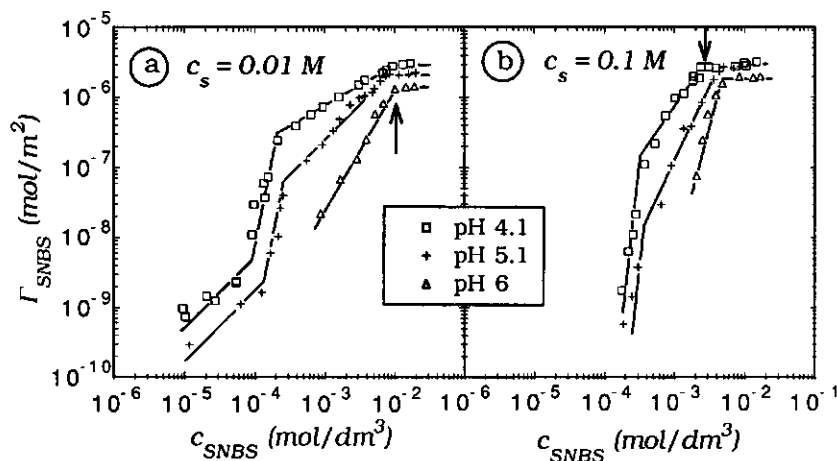


Figure (3): Adsorption of SNBS on rutile as a function of pH. The arrows indicate the cmc values.

Similarly to the situation at pH 4.1 the isotherms at pH 5.1 at two salt concentrations have an intersection point in region III. It is located at a lower surface coverage than at pH = 4.1, i.e. $0.35 \mu\text{mol}/\text{m}^2$ (not shown). At pH 6 no intersection point was found. The surface charge in the absence of SNBS is slightly negative at pH 6. Nevertheless SNBS still adsorbs which is indicative of specific adsorption. This has also been found for other systems, e.g. for sodium dodecyl sulfonate on alumina⁽⁹⁾ and for sodium dodecyl sulfate on rutile.⁽³²⁾

Surface charge and surfactant adsorption

The surface charge of rutile in the absence of surfactant as a function of pH was measured with potentiometric titrations at the three salt concentrations used. The results are shown in Figure (4), the cip of the charge-pH curves, which reflects the pristine point of zero charge (pzc)⁽³¹⁾, was 5.85. It agrees well with the isoelectric point of

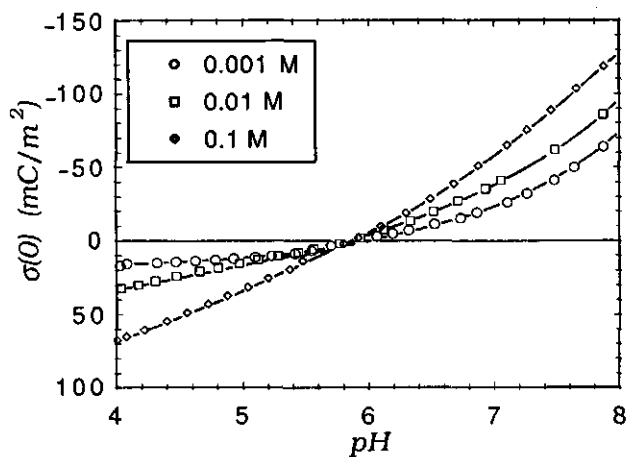


Figure (4): Charge-pH curves for rutile at three salt concentrations.

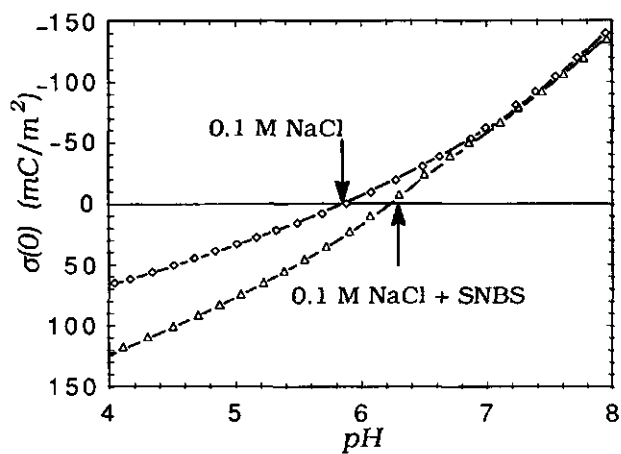


Figure (5): Charge-pH curves of rutile in 0.1 M NaCl in the absence and presence of $0.28 \cdot 10^{-3}$ mol SNBS. The equilibrium concentration exceeded the cmc, ensuring maximum adsorption.

rutile measured by electrophoresis in 0.001 M KNO_3 .⁽¹⁵⁾ The pzc serves as a reference point for the calculation of the absolute surface charges. The charge on the positive branch stays slightly lower than in KNO_3 ⁽¹⁵⁾, indicating some specific adsorption of Na^+ . However, since we do observe a fairly sharp cip, at the same pH as the iep, we may assume that around the pzc the specific adsorption of Na^+ is small.

To find the pH at which SNBS starts to adsorb, a rutile titration was carried out in the absence and presence of SNBS at $c_s = 0.1$ M. The residual SNBS concentration was always above the cmc, so the maximum adsorption could be reached. The result is given in Figure (5). The deviation between the two curves starts at about pH 7 indicating that from there onwards SNBS is adsorbed specifically. Upon adsorption of SNBS the pzc of rutile shifts and already at pH 6.3 the surface charge becomes positive.

In the experiments the charge of rutile changes by the uptake of protons when SNBS adsorbs. The amount of HCl added to re-establish the initial pH is a measure of this change. Association between surfactant and protons can be neglected: the cmc for alkylbenzenesulfonates is almost independent of pH.⁽⁷⁾

In Figure (6) the effect of adsorbed surfactant on the surface charge at pH = 4.1 is plotted. To facilitate the comparison the surface charge and the adsorbed amount are both expressed in $\mu\text{mol}/\text{m}^2$. That is, the surface "charge" is expressed as $\Gamma(0) = \sigma(0)/F$. The proton uptake by the surface is a maximum at low surfactant and low salt concentrations: with almost every adsorbing surfactant molecule a proton is adsorbed, indicating that all surfactant molecules will have their head groups close to the surface. At higher salt concentrations the initial slope is less, since besides the presence of more charges on the surface, also a displacement of Cl^- ions at the surface by NBS $^-$ ions has to take place. At high adsorbed amounts the surface charge becomes almost independent of the salt concentration: now only the surfactant is responsible for the screening of the surface charge.

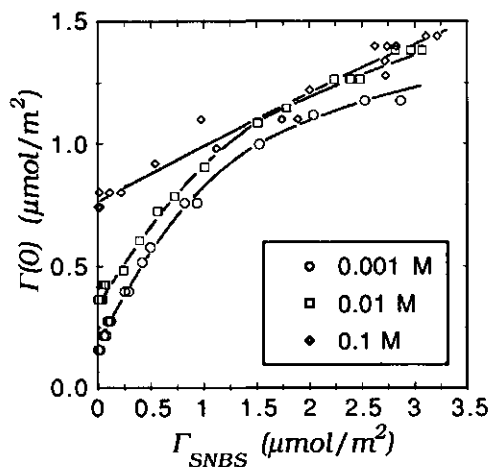


Figure (6): Effect of SNBS adsorption on the surface charge of rutile. The surface charge is expressed as $\Gamma(0) = \sigma(0)/F$, $\text{pH} = 4.1 \pm 0.1$.

In 0.001 M and 0.01 M NaCl, the slopes of the curves in Figure (6) decrease after passing the cip in the isotherms, which is located at a coverage of $0.6 \mu\text{mol}/\text{m}^2$. This suggests that beyond the cip some of the additionally adsorbing molecules will be oriented with their head groups towards the solution. In other words, the cip indicates the onset of bilayer formation. Changes in surface charge still occur beyond the cip. This demonstrates that the "head-on" adsorption is not completed at the cip.

The sum of the rutile charge, expressed as $\Gamma(0)$, and charge of the adsorbed surfactant, expressed as Γ_{SNBS} , is plotted versus the equilibrium surfactant concentration for the three salt concentrations at pH 4.1 in Figure (7a). These curves also show a cip, which is located at a net charge density equal to 0 and a surfactant concentration of about $1 \text{ mmol}/\text{dm}^3$ which is slightly higher than the cip concentration found in the adsorption isotherms. After the cip overcompensation of the surface charge has taken place.

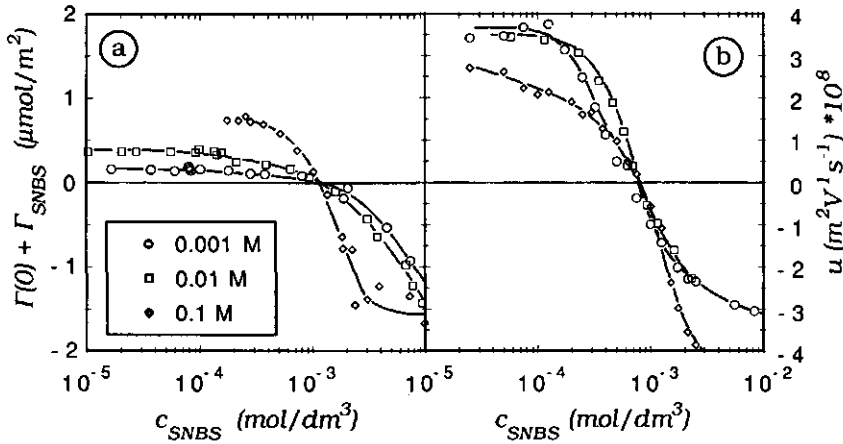


Figure (7): Charge adjustment due to surfactant adsorption at $\text{pH} = 4.1 \pm 0.1$ and at three NaCl concentrations.

(a) Effect of SNBS on the net particle charge, $\Gamma(0) + \Gamma_{\text{SNBS}}$.

(b) Electrophoretic mobilities, u , of rutile particles as a function of the SNBS concentration.

Electrophoretic mobilities, u , of rutile at pH 4.1 in the presence of surfactant confirm this view, see Figure (7b). The iep is at almost the same surfactant concentration as the common intersection point in the adsorption isotherms and at a slightly lower surfactant concentration than the point where $\Gamma(0) + \Gamma_{\text{NBS}} = 0$. This shows that a few small salt ions are present within the plane of shear. As the difference between the cip in Figure (7a) and the iep is small, association of counterions with adsorbed surfactant ions or specific adsorption of salt ions on the surface are not of major importance around the iep.

At high surfactant concentrations and in 0.1 M NaCl, the mobility becomes more negative than at low salt concentration. The same effect was observed for SNBS adsorbed on hematite (not shown). At still higher salt concentrations the mobility starts to decrease again,

but measurements at and above $c_s = 0.5$ M are rather inaccurate. In the literature maxima in electrophoretic mobility as a function of salt concentration have been reported⁽³³⁾ and the effect has been attributed to conductance within the plane of shear.

To study the surface charge effects in more detail additional experiments were done at pH 5 and 6. In Figure (8) the results are summarized. The adsorptions of SNBS and $\Gamma(0)$ are shown as functions of the surfactant concentration. At pH 4.1 the difference in SNBS plateau values between the two salt concentrations is within experimental error the same but at pH 5 and 6 the maximum surfactant adsorption increases somewhat with salt concentration. In the plateau of the SNBS isotherm the proton adsorption (surface charge) does not depend on the salt concentration. Clearly the surfactant screens the surface charge far more effectively than NaCl. In general the proton adsorption tends to levels off after charge compensation. The change in surface charge corresponds well with the change shown in the titration experiments, see Figure (5). Moreover, titrations confirmed that in the presence of adsorbed surfactant the surface charge is entirely screened by surfactant, starting from pH 7 upward, the $\sigma(0)$ -pH curves for 0.01 and 0.1 M NaCl merge.

Counterion effect

When we used 0.1 M KCl instead of NaCl in an adsorption experiment higher plateau adsorptions were obtained: at pH 4.1, $3.8 \mu\text{mol}/\text{m}^2$ is adsorbed, at pH 5.1, $3.5 \mu\text{mol}/\text{m}^2$ and at pH 6, $3.3 \mu\text{mol}/\text{m}^2$. This points to a stronger attraction between K^+ and the surfactant head group than between Na^+ and the head group. This has also been noted comparing SDS and KDS adsorption on alumina.⁽⁹⁾ The surface charges, however, are the same as in NaCl at all three pH values. This last observation again demonstrates that at a certain pH the surface charge determined by the surfactant anion exclusively.

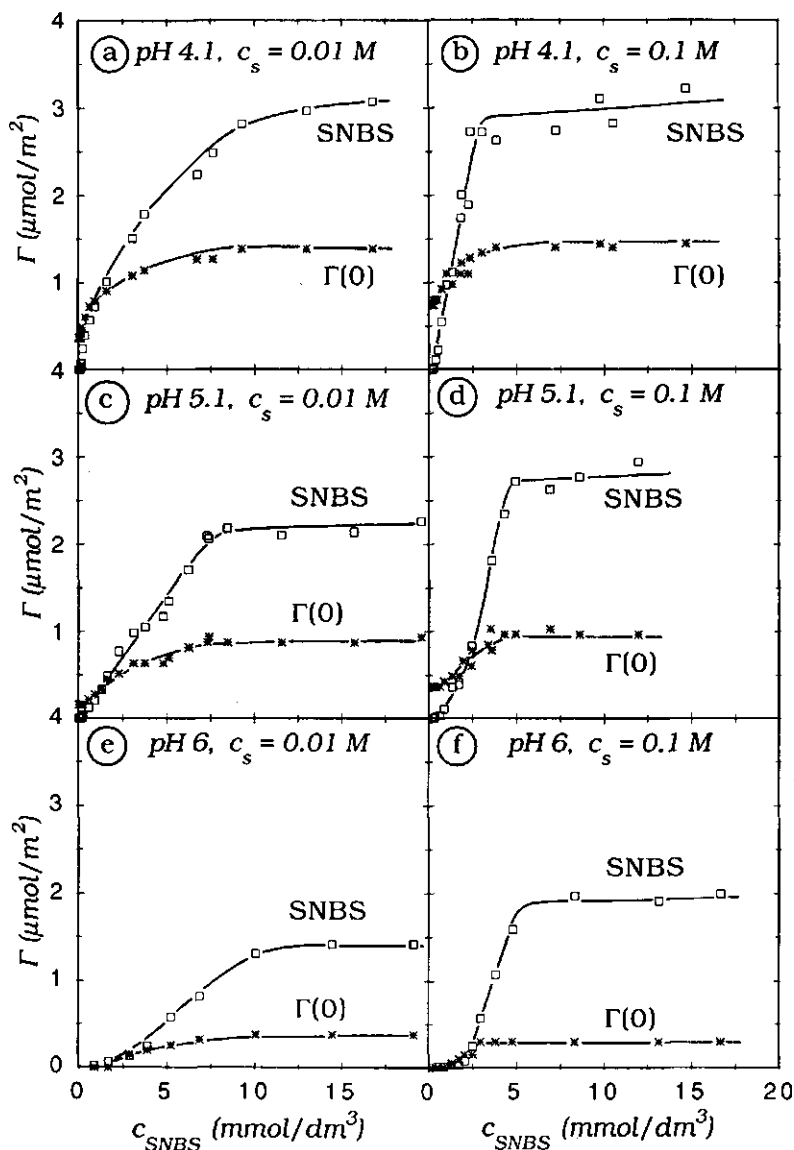


Figure (8): Adsorption of SNBS and proton adsorption on rutile as a function of the SNBS concentration. the pH values and salt concentrations are indicated in each figure.

Structure of the adsorbed layer

As mentioned in the introduction, in the presence of specifically adsorbing ions the absolute value of the surface charge increases at otherwise fixed conditions. If a surfactant molecule adsorbs with its head group adhered to the surface an effective screening of the surface charge can be expected, whereas for adsorption of surfactant with its head group directed to the solution the effect on the surface charge will be small. Moreover, the net charge at the surface side of the bilayer will stay very low, since the screening of any remaining net charge in the hydrophobic core is very limited. Hence, to a first order approximation it is safe to assume that in the upper part of the isotherm the charge of the "head-on" adsorbed surfactants just cancels surface charge. In other words the amount of head-on adsorbed surfactants can be estimated from the surface charge. As the total adsorbed amount is also known, the amount adsorbed with head groups at the solution side can be estimated in this way. In the calculation we neglect the intercalation of salt ions between the head groups at the surface side and this seems to be justified, as no effect of the salt concentration or salt type on the surface charge was found. A further justification of these assumptions will be given in the theory section.

The calculated amounts of head groups in contact with the surface for the plateau region of the isotherm are presented in Table (2). At all pH values the bilayers formed are asymmetrical. The amount adsorbed head-on, Γ_s , decreases by about $0.5 \mu\text{mol}/\text{m}^2$ upon an increase in the pH of 1 unit. The amount at the solution side does not depend on pH in 0.1 M NaCl, but in 0.01 M NaCl a small decrease with increasing pH is found. The amount at the solution side is merely affected by the salt concentration. In KCl the second layer is more dense than in NaCl and it becomes slightly more dense with increasing pH. This is due to a stronger interaction between K^+ and the surfactant head group.

Table 2: Division of the total amount adsorbed at the plateau of the isotherm, Γ_t , into its contribution adsorbed with the head group towards the surface, Γ_s , and that with the head groups towards the solution, Γ_b . Adsorbed amounts are in $\mu\text{mol}/\text{m}^2$.

pH	c_s (M)	Γ_t	Γ_s	Γ_b
4.1	0.001	3.0	1.4	1.6
4.1	0.01	3.0	1.4	1.6
4.1	0.1	3.1	1.4	1.7
4.1	0.1 (KCl)	3.8	1.4	2.4
5.1	0.01	2.3	1.0	1.3
5.1	0.1	2.8	1.0	1.8
5.1	0.1 (KCl)	3.5	0.9	2.6
6.0	0.01	1.4	0.4	1.0
6.0	0.1	2.0	0.3	1.7
6.0	0.1 (KCl)	3.3	0.4	2.9

Since beyond the cip, practically speaking, the head-on adsorbed surfactant cancels the surface charge, the formation of the second surfactant layer can be seen as adsorption of surfactant on an uncharged surface modified with grafted aliphatic chains. Using the SCFA theory it has been shown that the adsorption of amphiphilic molecules on such surfaces does not depend strongly on the grafting density⁽³⁴⁾, which supports the present experimental results.

Adsorption of SNBS from Na_2SO_4 solutions

To further investigate the effect of the non-electrostatic interactions on the adsorption of SNBS on rutile, SNBS adsorption experiments were performed in Na_2SO_4 solutions at pH 4. Titration and electrophoretic mobility experiments showed that SO_4^{2-} adsorbs strongly on rutile. At 0.05 M Na_2SO_4 and pH 4, the electrokinetic charge of rutile is negative due to superequivalent adsorption of SO_4^{2-} .

In Na_2SO_4 we still find SNBS adsorption, see Figure (9). Clearly the NBS^- ions can replace the SO_4^{2-} ions from the surface although the adsorption of SNBS in a Na_2SO_4 solution is lower than in NaCl. The adsorption isotherms at 0.05 and 0.005 M Na_2SO_4 show two

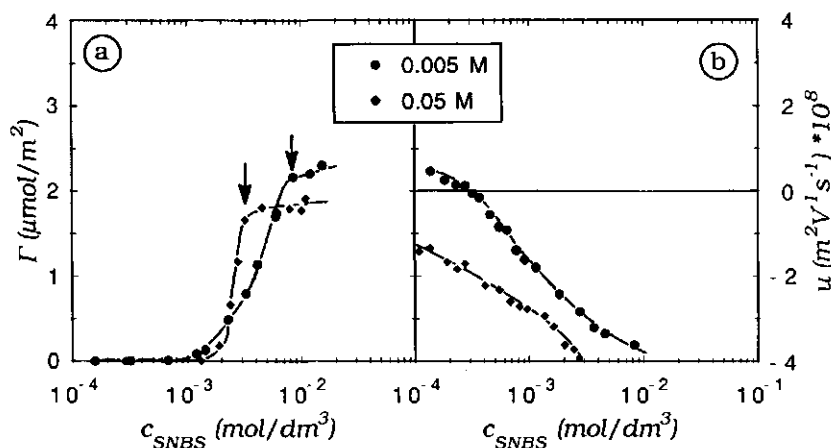


Figure (9): SNBS adsorption from Na_2SO_4 solutions at pH 4.

(a) adsorption of SNBS on rutile in 0.005 M and 0.05 M Na_2SO_4 at pH = 4. The arrows indicate the cmc's.

(b) Electrophoretic mobilities of rutile as a function of the SNBS concentration.

intersection points, which do not relate to the iep as can be inferred from the electrophoretic mobilities, see Figure (9b). The decrease in mobility as a function of surfactant concentration indicates that NBS^- adsorbs at all concentrations measured. In 0.005 M Na_2SO_4 the iep occurs at very low amounts NBS^- adsorbed. Just as in the case of adsorption at different NaCl concentrations the initial SNBS adsorption is higher for the low Na_2SO_4 concentration, whereas at higher surfactant concentrations the situation has reversed. Up to the first intersection point competition between NBS^- and SO_4^{2-} for the surface sites dominates the behavior. Beyond the first intersection point screening of the NBS^- charge by Na^+ becomes important. Although the first intersection point does not correspond to the iep, it roughly marks the onset of bilayer formation. The second intersection point results from the difference in cmc between the two salt concentrations. At 0.05 M the isotherm is

steeper, but the cmc is lower. The plateau adsorption is reached at a SNBS concentration of 3 mmol/dm^3 , which is the cmc of SNBS in $0.05 \text{ M Na}_2\text{SO}_4$. In $0.005 \text{ M Na}_2\text{SO}_4$ the cmc is 8 mmol/dm^3 which allows the adsorption to become higher than at 0.05 M .

Contrary to the adsorption from NaCl solutions, we did not observe a change in pH upon the adsorption of SNBS, which was confirmed by titration experiments of rutile in a $0.05 \text{ M Na}_2\text{SO}_4$ solution in the presence and absence of SNBS. This behavior is typical for an exchange between specifically adsorbed SO_4^{2-} and NBS^- . Finally we note that the error in the experimental points in the adsorption isotherm is smaller than for the isotherms in NaCl, because their main source results from the adjustment of the pH, which was not necessary in sodium sulfate.

SCFA Theory

Introduction

A detailed account of the SCFA theory and its extension with electrostatics can be found in refs (17-23). Basically the theory calculates the equilibrium distribution of segments perpendicular to the surface or in an association structure in solution by minimizing the free energy of the system. We modeled surfactants as chains of r segments and considered salt ions and solvent molecules as monomers (1 segment). The conformational statistics of the chains are evaluated using a rotational isomeric state (RIS) scheme developed by Leermakers et al.^(19,20) The RIS scheme prevents backfolding and allows for a distinction between trans and gauche bonds in the chain.

The contact interactions between the various segments are accounted for using Flory-Huggins interaction parameters. For the electrostatic interactions it is assumed that all charges are located on planes in the middle of the lattice layers. The space in between

these planes is free of charge. Consequently, two neighboring planes can be treated as a charged condenser and their potential difference can be calculated using basic electrostatics. The potential on the solid surface serves as the reference point for the calculation of the electrostatic potentials.⁽²³⁾

Choice of Parameters

Model calculations were performed for a linear surfactant ion adsorbing on a surface with a given surface potential, intended to mimick a metal oxide surface at constant pH. We model the surfactant as a linear chain molecule, instead of a branched structure containing a benzene ring, since the latter would complicate the modeling considerably. The choice of the molecular structure of the surfactant is close to that of SDS, which also has a four region isotherm and adsorbs specifically on metal oxides.^(9,32) As it is the first time that the SCFA theory is applied to surfactant adsorption on variable charge surfaces, we want to focus on general features in surfactant adsorption, such as the existence of a four region isotherm and the structure of the adsorbed layer rather than on details related to the architecture of the surfactant. The latter effect will be studied in the next chapter.

As the surfactant we modeled a molecule containing 3 head group segments and 12 aliphatic segments, called $A_{12}B_3$. To each of the head group segments a charge of $-1/3$ was assigned, making the total charge of the head group, B_3 , -1 . Furthermore a monomeric salt is present with ions C and D which have a charge of $+1$ and -1 , respectively. Since we define B, C and D as charged species, we choose not to indicate their charge in a superscript. The Flory-Huggins interaction parameter between the aliphatic segments A and all other segments in solution, i.e. the monomeric solvent W, the surfactant head group segments B, and the salt ions C and D, are set to 2. The remaining χ -parameters for components in solution are 0. Consequently, the charged components, B, C, D only differ from water with respect to their charge.

In order to calculate the electrostatic potentials the thickness of a lattice layer, l , has to be specified. We have chosen 0.31 nm. The area of a lattice site, a_s is ℓ^2 . The dielectric constants are $2\epsilon_0$ for segment type A and $80\epsilon_0$ for the other segment types. The choice of the surfactant and the parameters are the same as in previous chapters.^(24,25)

We also use χ -parameters to express the contact interactions with the surface. The chemical affinity of the sulfonate group for the surface was estimated from the SNBS adsorption on rutile in Na_2SO_4 . Test calculations were performed for B_3 , with a valency of $-2/3$ for each B segment which served as a (very primitive) model for sulfate, adsorbing on a surface with a fixed potential of 100 mV. If for χ_{BS} the value -10 is given, overcompensation of the surface charge was found at a concentration of 0.05 M and not for 0.005 M in agreement with the electrophoresis data. As the chemical structures of sulfate and the sulfonate head groups are not too different we adopted the value $\chi_{\text{BS}} = -10$ for the contact interaction between head group and surface. In terms of displacement free energy this amounts to -2.5 kT per segment. The exact value of χ_{BS} is not very important as long as the specific adsorption is strong. The remaining interaction parameters with the surface are set to zero. For the A segments this leads to a small displacement free energy (-0.5 kT per segment), because it is squeezed out of the water by the high χ_{AW} value.⁽²⁶⁾

Theoretical results

Adsorption isotherms at different salt concentrations

The calculated adsorption isotherms for a surface potential of 100 mV are given on log-log, lin-log and lin-lin scales in Figure (10). The adsorbed amount is expressed as n^{exc} , the excess number of surfactant molecules per surface site. On the horizontal axis the overall or total volume fraction, $\bar{\phi}$ is shown. Below the cmc $\bar{\phi}$ is equal to the bulk volume fraction and above the cmc it is the average

volume fraction of free surfactant and surfactant in micelles.⁽²⁴⁾ The calculated critical micelle volume fractions, $cm\phi$, at different salt concentrations, c_s , are tabulated in Table 3.

Table 3: critical micelle volume fractions of $A_{12}B_3$ at different of the salt concentrations.

c_s (M)	$cm\phi$
0.001	2.5E-03
0.01	1.7E-03
0.1	4.7E-04

The log-log isotherms are presented in Figure (10a). They are at least in qualitative agreement with the experimental results and do show the four regimes and the salt effects. In region I the slope is unity and the adsorption decreases with increasing salt concentration. Instead of a region II with constant slope theory predicts a phase transition or condensation step. The phase transition indicates that two coexisting phases are present on the surface at a given bulk solution volume fraction. Region II starts at a coverage of a few percent of the amount adsorbed at the cmc and ends at a coverage of $n^{exc} = 0.2$. Region III has a slope much smaller than region II and the adsorption increases with salt concentration. A plateau is reached slightly above the cmc where region IV starts.

Because of the large condensation step in region II the four regions can also be seen in the theoretical lin-log isotherm, Figure (10b). The cip and the inversion of the salt effect are also visible. The lin-lin plots, Figure (10c), are rather featureless but the behavior around the cmc is shown more clearly. The plateau adsorption increases only slightly with increasing salt concentration. Before discussing these results in more detail some volume fraction profiles along the isotherm will be given.

Volume fraction profiles

Volume fraction profiles, ϕ , as a function of the layer number, z , starting at $z = 1$ next to the surface, give information on the structure

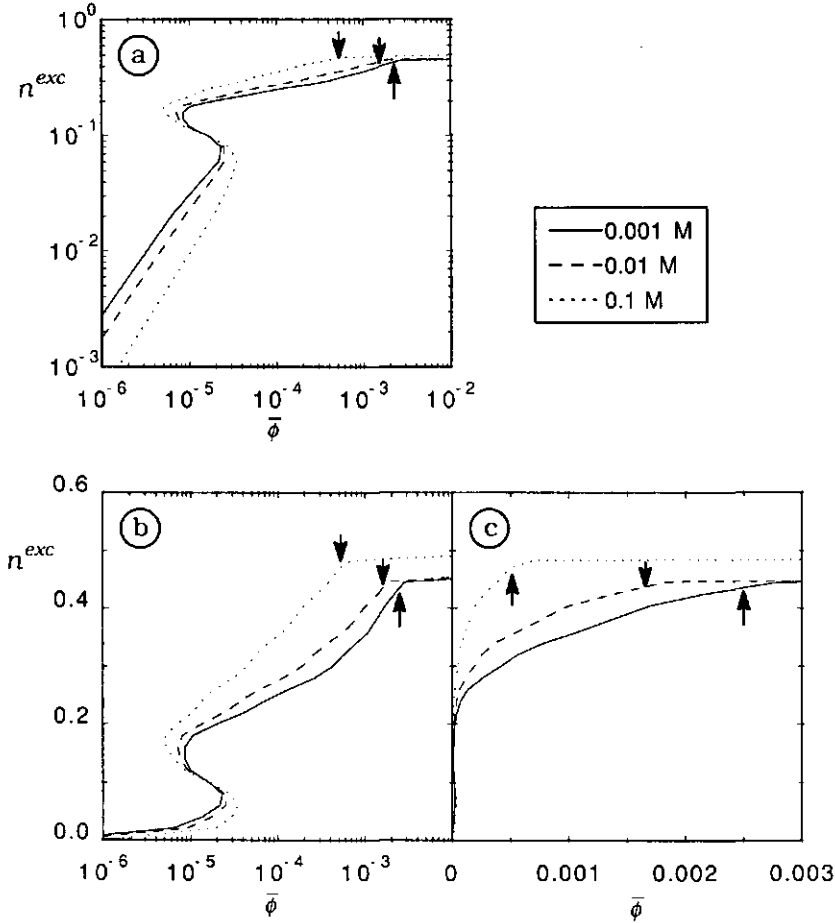


Figure (10): Adsorption isotherms of $A_{12}B_3$ on a surface with a fixed potential of 100 mV at three salt (CD) concentrations. The interaction parameters are: $\chi_{AW} = \chi_{AB} = \chi_{AC} = \chi_{AD} = 2$, $\chi_{BS} = -10$, the remaining χ -parameters are zero. The relative dielectric constants are: $\epsilon_W = \epsilon_B = \epsilon_C = \epsilon_D = 80$, $\epsilon_A = 2$, the lattice layers have a thickness, ℓ , of 0.31 nm and the cross section is ℓ^2 . The cmc's are indicated with arrows, see table 3. The isotherms are plotted in three ways: (a) log-log, (b) lin-log and (c) lin-lin.

of the adsorbed layer. The results for four surface coverages, corresponding with the four regions in the isotherm are shown in Figure (11) for a salt concentration of 0.01 M and a surface potential of 100 mV.

In region I the adsorbed molecules are fairly flat on the surface, see Figure (11a). Besides the coulombic and specific interaction between

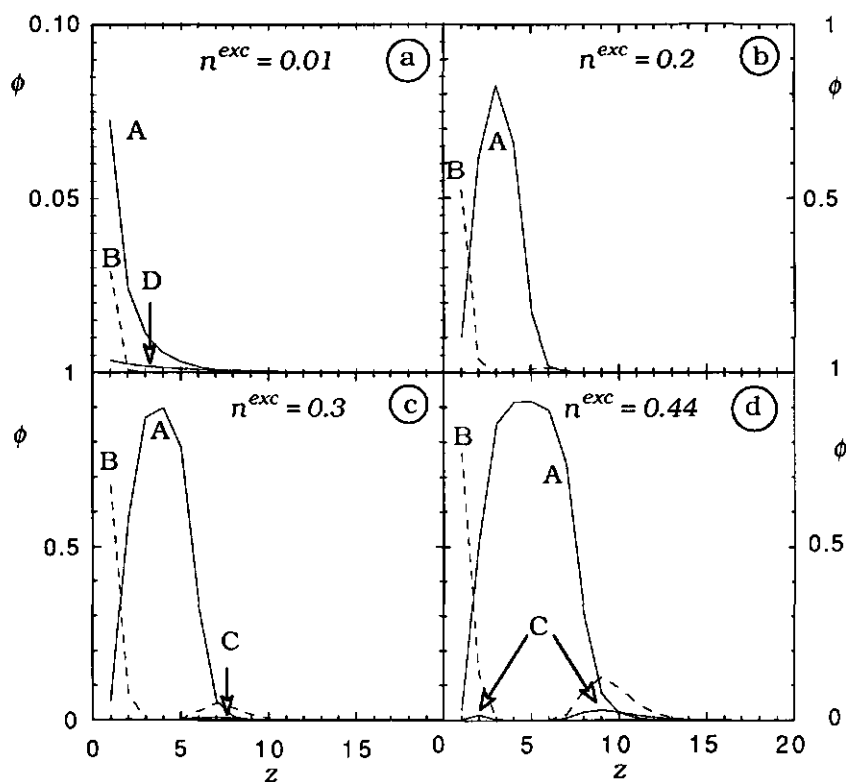


Figure (11): Adsorbed layer structure for $A_{12}B_3$. Volume fraction profiles of the A and the B segments and the counterions C near a surface with a constant potential of 100 mV in a 0.01 M CD solution are shown. The volume fractions of D are too small to be seen except in (a). See Figure (10) for parameters.

the head groups and surface the tails are squeezed out of the water because of the high value for χ_{AW} (for the effects of χ_{AS} and χ_{BS} on the adsorption see ref (25)). The surface charge is screened by both surfactant and salt ions. For the given value of the surface potential the cip is in region II. At the end of region II half a membrane is on the surface, see Figure (11b), and the surface is hydrophobized by the A segments. Although the formation of the second layer starts at the cip, the volume fractions of head groups at the solution side of the layer are still very low. In region III, Figure (11c), the second layer grows significantly and the solution side of the layer becomes gradually more hydrophilic until the plateau is reached, Figure (11d). The head group charges at the solution side are partly compensated by the accumulation of C ions in between the head groups, partly by the diffuse double layer. Some counterions enrich the surface side of the bilayer.

We may conclude that the hydrocarbon core of the adsorbed surfactant bilayer separates two net uncharged parts of the system. On the surface side the sum of the surface charge and the charge of the surfactant head groups plus some intercalated salt ions equals zero and on the solution side the head groups, salt ions in between them and salt ions in the diffuse double layer have a total charge of zero, see also ref (25).

Quality of the predictions

The ability of the 1D SCFA theory to predict the four region isotherm is gratifying. So far no other theory could do this unless ad hoc assumptions were made about surface heterogeneity and the structure of the adsorbed layer. Nevertheless some typical differences with the experimental isotherms appear. Notably, region II is not predicted correctly, because in the model association has to take place in at least one entire lattice layer instead of locally. Therefore, it starts at a relatively high coverage and it does not stop before a dense layer of surfactant has been formed on the entire surface. In other words region II is overestimated. In reality due to

the high local volume fractions small aggregates are formed so that the I/II transition can occur at lower surfactant concentrations than predicted theoretically. In the mean field approximation the phase separation is "postponed", it shows up in an exaggerated manner at a higher concentration.

The SCFA theory can also be used to analyse membranes⁽¹⁹⁾ and it appears that the area per molecule on each side of an equilibrium membrane is to a good approximation identical to that at the end of region II. In the calculations half a membrane is the favorable aggregation structure marking the end of region II. In practice the II/III transition occurs at a lower surface coverage and the structure of the surfactant molecules and the salt concentration determine the size and geometry of the local aggregates.

As the calculated region II was too long the absolute value of the slope in region III is too low. Nevertheless the 1D SCFA theory predicts a significant increase in adsorption in region III (see Figure 10b) and shows that the salt effect is mainly caused by the screening of the head group charges at the solution side of the layer.

The volume fraction profiles also relate very well to experimentally observed maxima in hydrophobicity⁽⁴⁾ and flotation recovery⁽³⁵⁾ of particles as a function of surfactant concentration: at low adsorbed amounts the particles are hydrophobized, whereas at high adsorbed amounts the presence of head groups at the solution side make the particles more hydrophilic again. The theory also predicts that around the iep the colloidal stability will be at its minimum, not only because isoelectric conditions are met, but also because the particles are hydrophobized. In general we may conclude that although the theory is not perfect it nevertheless gives a lot of insight into the adsorption behavior.

Adsorption as a function of the surface potential

According to refs (1-5) the II/III transition coincides with the iep. However, Bitting and Harwell⁽⁹⁾ found the iep to be in region II and in our experiments the iep is located in region III. The calculated isotherms have a cip, corresponding to the iep, in region II. To study the location of the iep in more detail the surface potential was varied from +200 mV to -100 mV at a salt concentration of 0.001 M. Results are given in Figure (12), the iep is indicated with an asterisk. At a surface potential of 200 mV the iep is located in region III, at 100 and 50 mV it is in region II. These results show that the iep can indeed be anywhere in the adsorption isotherm. The II/III transition does not correspond to surface charge neutralization but with an optimal primary aggregate form.

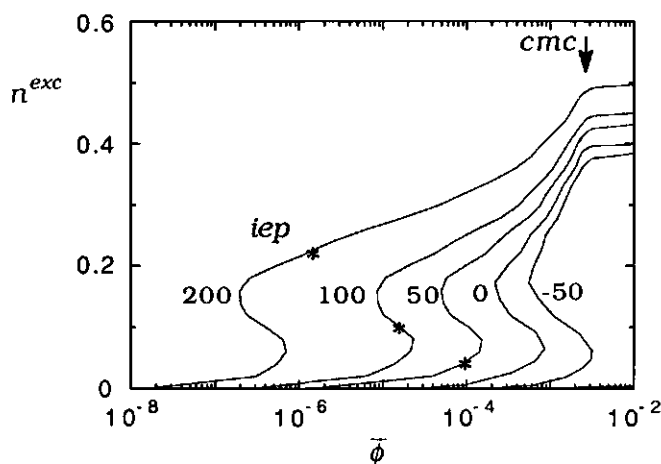


Figure (12): Effect of the surface potential on the adsorption isotherms of $A_{12}B_3$ in a 0.001 M CD solution. The iep's are indicated with an asterisk. See Figure (10) for parameters.

A general aspect emerging from Figure (12) is that at higher potentials the adsorption starts at lower concentration and slightly

higher adsorbed amounts are reached. These trends correspond well with the experimental results shown in Figure (3), although the theoretical differences in plateau adsorption tend to be somewhat small. Because of the non-electrostatic interaction between head group and surface, adsorption still occurs if the surface potential is fixed to -50 mV, but not if we decrease the potential to -100 mV (not shown).

Surface charge and surfactant adsorption

In the experimental section attention was paid to the adjustment of the surface charge upon adsorption. This has also been investigated theoretically. In Figure (13) the surface charge, expressed in number of charges per lattice site: $\sigma(0)a_s/e$, is given vs. the adsorbed amount of surfactant for the three salt concentrations and $\psi(0) = 100$ mV. The curves have a cip, corresponding with the cip in the adsorption isotherms. Charge neutralization occurs at a surface charge considerably higher than that in the absence of surfactant. This is in agreement with the experimental findings. The initial slopes agree almost quantitatively with the experimental results and after the cip still a significant increase in surface charge occurs, see Figure (6). Beyond the cip the theory predicts that the surface charge decreases with increasing salt concentration; at higher salt concentrations more positive salt ions are incorporated in between the negative head groups located at the surface side and therefore the surface charge can stay slightly lower. Apparently this effect is not significant in the experiments where the curves merge after the cip. In relation to this we must note that in the presence of surfactant the calculated absolute values of the surface charges are much higher than the experimental ones for SNBS: 0.25 charges per site corresponds to 416 mC/m^2 , whereas in the experiments a maximum charge of about 130 mC/m^2 was reached. If we convert the calculated n^{exc} to an adsorbed amount in mol/m^2 using the lattice dimensions, we also arrive at higher adsorbed amounts ($\approx 10 \mu\text{mol/m}^2$) than observed experimentally. Obviously, this is due to our choice of parameters. For other systems like e.g. SDS on alumina⁽⁹⁾ higher plateau

adsorptions have been reported than for SNBS on rutile and then the surface charge may be higher.

An alternative way to present the results is to plot the surface charge $\sigma(0)$ and the $A_{12}B_3$ adsorption as a function of $\bar{\phi}$, see Figure (14). Both $\sigma(0)$ and $\Gamma(A_{12}B_3)$ are expressed as (excess) numbers per surface site. The calculated results can be compared with the experimental results, shown in Figure (8). Initially the surface charge adjusts strongly to neutralize the adsorbed surfactant charge. At higher coverages, but well before the cmc, the adjustment of the surface charge levels off and reaches a plateau. The plateau value of $\sigma(0)$ decreases with decreasing surface potential, similarly as found experimentally. Theoretically there is a small dependence on the salt concentration due to the incorporation of positive salt ions between the surfactant head groups at the surface side, which was not found experimentally.

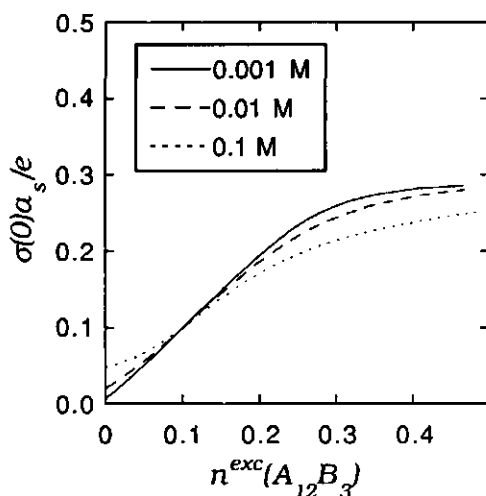


Figure (13): Effect of the adsorbed amount of surfactant on the surface charge at three salt concentrations and a fixed surface potential of 100 mV. The surface charge is expressed in the same units as the adsorbed amount. See Figure (10) for parameters.

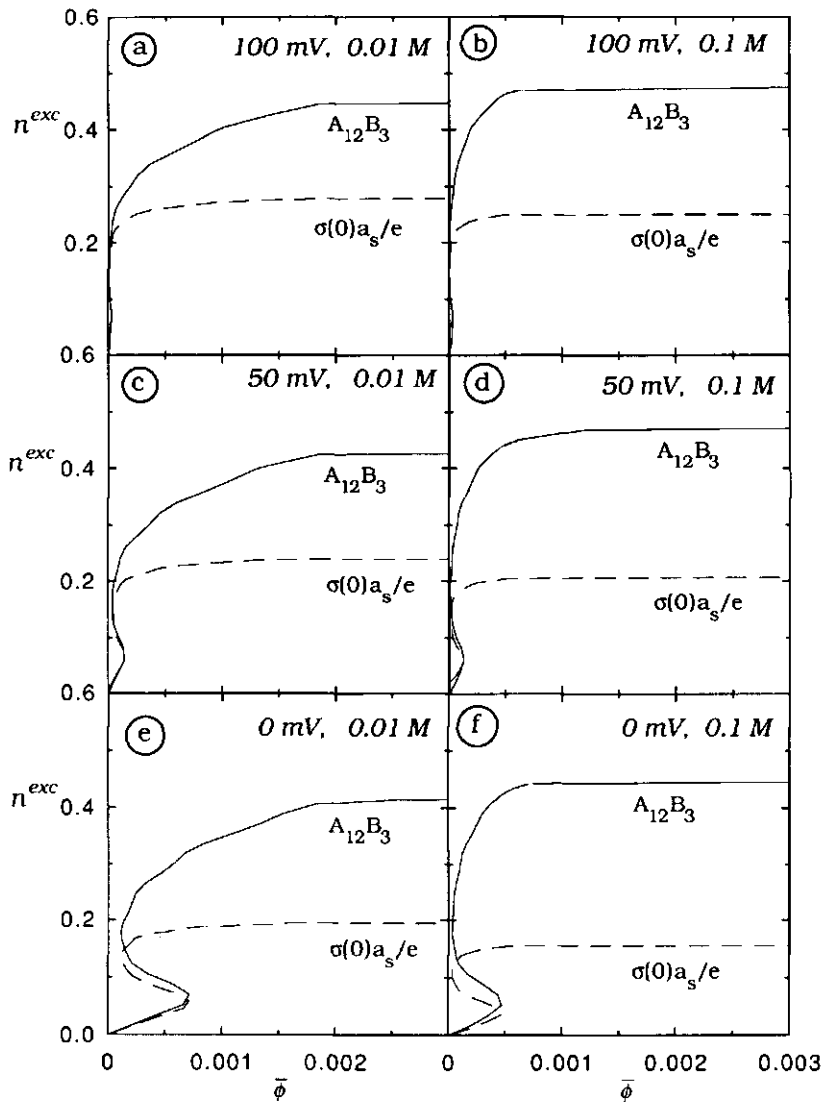


Figure (14): Adsorption of $A_{12}B_3$ and surface charges as functions of the $A_{12}B_3$ volume fraction, both expressed in the same units. The surface potential and the salt concentration are indicated. See Figure (10) for parameters.

Surface charge and head-on adsorption

In the experimental section the surface charge has been used as a measure of the number of surfactant molecules oriented with their head groups towards the surface. To test whether such a simple relation between surface charge and surfactant head groups at the surface is predicted theoretically, we summed the charge contributions of the B segments in the first two lattice layers and plotted this charge against the surface charge. Results are given in Figure (15a) for three different salt concentrations at $\psi(0) = 100$ mV and in Figure (15b) for three different surface potentials at $c_s = 0.01$ M. An approximately 1-1 relationship exists in all cases, supporting our working hypothesis. Deviations at low coverages are caused by the exchange of surfactant ions for small, equally charged salt ions. Deviations at high coverages are due to inclusion of positive salt ions in between the head groups at the surface side. As we did not observe an effect of the salt concentration or the type of salt on the surface charge in the plateau of the isotherm experimentally, it is likely that the inclusion of salt ions between the head groups at the surface side is overestimated in the model.

Discussion

Constant charge and constant potential

The shapes of adsorption isotherms and the location of the cip in the adsorption isotherm show remarkable differences for adsorption of surfactants on constant charge and variable charge surfaces. For *constant* charge surfaces we found that charge-charge interaction controls the adsorption until the surface charge is neutralized.⁽²⁵⁾ At low salt concentrations this leads to a pseudo plateau at an adsorption value corresponding with the iep and the cip in the isotherms at different c_s . On *variable* charge surfaces the neutralization of the surface charge does not lead to a plateau in the adsorption isotherm. Due to the fact that the surface charge adjusts

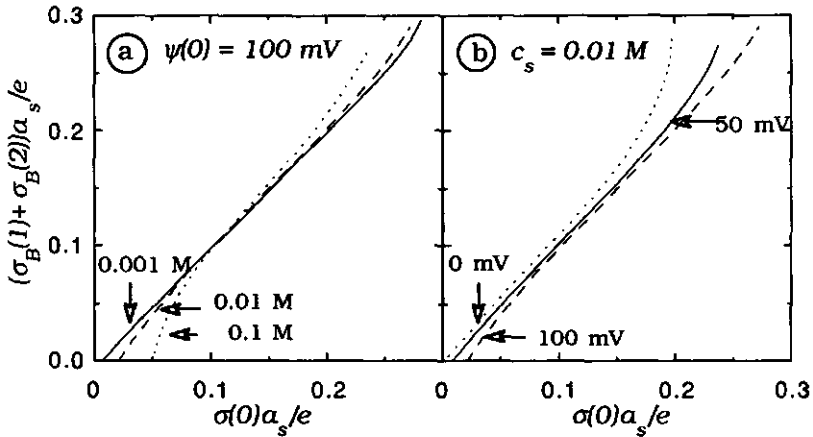


Figure (15): Relation between the surface charge and the head group charge in layers 1 and 2 for (a) a surface with a fixed potential of 100 mV at three salt concentrations and (b) at three surface potentials and for $c_s = 0.01 \text{ M}$. See Figure (10) for parameters.

itself effectively upon adsorption it minimizes the electrostatic repulsion and charge neutralization does not cause a sudden change in the isotherm. The slope of the isotherm changes at the II/III transition where a favorable aggregation structure is reached. Experimentally this change is subtle, it only appears in a log-log plot. In the model calculations which do not allow local aggregation the primary aggregation is overestimated and a strong II/III transition occurs in the isotherms. In agreement with the experimental results for different systems the theory shows that the II/III transition does not necessarily coincide with the iep.

Hemi-micelles or admicelles?

As argued above, the primary aggregates present in region II all have their head groups on the surface, each of them compensating a surface charge. Defining hemi-micelles as head-on adsorbed aggregates and admicelles as local bilayer structures it will be clear that we support the hemi-micelle concept.

We have an additional argument from the SCFA calculations to support the idea that in region II hemi-micelles rather than admicelles are present: For constant charge surfaces the formation of a second layer does not start until the solution concentration has reached a value of about $0.1 \cdot \text{cmc}$.⁽²⁵⁾ This concentration is much higher than the concentrations at the II/III transition in the adsorption isotherms on variable charge surfaces.

Although we see no arguments for the presence of admicelles in region II, the idea of the presence of local bilayer structures is not unrealistic. Local bilayers will only form in region III beyond the iep. In this region primary aggregates will grow into larger structures with a bilayer character. However, as long as the surface charge adjusts upon surfactant adsorption head-on adsorption does occur and the aggregates will not only grow in a direction perpendicular to the surface but also parallel to the surface. The latter will make the adsorbed layer more homogeneous, especially when the adsorbed amount is large.

Conclusions

The adsorption of SNBS on rutile follows the characteristic isotherm for anionic surfactants on oxides and the trends with varying pH and salt concentration are in good agreement with other experiments. The distribution of the molecules adsorbed head-on and with their head group towards the solution can be calculated from the adsorbed amount and the surface charge. The amount of head-on surfactant

depends on the pH, while the amount at the solution side depends on the indifferent electrolyte concentration.

Using 1D-SCFA theory it is possible to obtain the characteristic four region isotherm and to predict the formation of a bilayer in the plateau of the isotherm. Up to or even somewhat beyond the iep the surfactant molecules adsorb head-on. Consequently, around the iep (or cip) the surface (plus adsorbed layer) is made hydrophobic. After the iep bilayer formation starts and the hydrophobicity decreases. In the calculated adsorption isotherm region II starts and ends at too high coverages as compared to the experimental results; this indicates that the mean field approximation is an oversimplification. Nevertheless, the calculated trends with respect to the effect of surface potential and salt concentration agree well with experiments. Theoretical calculations provide further arguments for the calculation of the adsorbed layer structure from the surface charge and show that the iep can be either in region II or region III.

References

- 1 Chander, S.; Fuerstenau, D. W.; Stigter, D. in "Adsorption from Solution", Ottewill, R. H.; Rochester, C. H.; Smith, A. L. Eds. Academic Press London (1983), p197
- 2 Somasundaran, P.; Fuerstenau, D. W. *J. Phys. Chem.* **1966**, 70, 90
- 3 Fuerstenau, D. W.; Wakamatsu, T; *Faraday Discussions of the Chemical Society* **1975**, 59, 157
- 4 Moudgil, B. M.; Somasundaran, P; Soto, H. in "Reagents in Mineral Technology", Somasundaran, P; Moudgil, B. M. eds. *Surfactant Sci. Series*, **1988**, 27, 79
- 5 Chandar, P.; Somasundaran, P.; Turro, N. J. *J. Colloid Interface Sci.* **1987**, 117, 31
- 6 Hough, D. B.; Rendall, H. M. in "Adsorption from Solution at the Solid/Liquid Interface", Parfitt, G. D.; Rochester, C. H. eds. Academic Press, London (1983) p. 247
- 7 Scamehorn, J. F.; Schechter, R. S.; Wade, W. H.; *J. Colloid Interface Sci.* **1982**, 85, 463
- 8 Harwell, J. H.; Hoskins, J. C.; Schechter, R. S.; Wade, W. H. *Langmuir* **1985**, 1,251

- 9 Bitting, D.; Harwell, J. H. *Langmuir* **1987**, 3, 500
- 10 Chandar, P.; Somasundaran, P.; Waterman, K. C.; Turro, N. J., *J. Phys. Chem.* **1987**, 91, 150
- 11 Somasundaran, P.; Kunjappu, J. T. *Colloids Surf.* **1989**, 37, 245
- 12 Partyka, S.; Rudzinski, W.; Brun, B.; Clint, J. H. *Langmuir* **1989**, 5, 297
- 13 Siracusa, P. A.; Somasundaran, P. *J. Colloid Interface Sci.* **1986**, 114, 184
- 14 Fokkink, L. G. J.; De Keizer, A.; Lyklema, J. *J. Colloid Interface Sci.* **1989**, 127, 116
- 15 Gibb, A. W.; Koopal, L. K. *J. Colloid Interface Sci.* **1990**, 134, 122
- 16 Yates, D. E.; Healy, T. W. *J. Chem. Soc. Faraday Trans. 1*, **1980**, 76, 9
- 17 Scheutjens, J. M. H. M.; Fleer, G. J. *J. Phys. Chem.* **1979**, 83, 1619
- 18 Evers, O. A.; Scheutjens, J. M. H. M.; Fleer, G. J. *Macromolecules* **1990**, 23, 5221
- 19 Leermakers, F. A. M.; Scheutjens, J. M. H. M. *J. Chem. Phys.* **1988**, 89, 3264
- 20 Leermakers, F. A. M.; Scheutjens, J. M. H. M. *J. Phys. Chem.* **1989**, 93, 7417
- 21 Leermakers, F. A. M.; Scheutjens, J. M. H. M. *J. Colloid Interface Sci.* **1990**, 136, 231
- 22 Leermakers, F. A. M.; Scheutjens, J. M. H. M.; Lyklema, J. *Biochimica Biophysica Acta* **1990**, 1024, 139
- 23 Böhmer, M. R.; Evers, O. A.; Scheutjens, J. M. H. M. *Macromolecules* **1990**, 23, 2288
- 24 Böhmer, M. R.; Koopal, L. K.; Lyklema, J. *J. Phys. Chem.* in press, this thesis Ch. 4
- 25 Böhmer, M. R.; Koopal, L. K. submitted to *Langmuir*, this thesis Ch. 5
- 26 Böhmer, M. R.; Koopal, L. K. *Langmuir* **1990**, 6, 1478, this thesis Ch. 2
- 27 Böhmer, M. R.; Koopal, L. K.; Janssen, R.; Lee, E. M.; Thomas, R. K. and Rennie, A. R. submitted to *Langmuir*, this thesis Ch. 3
- 28 Cases, J. M. *Bull. Minéral.* **1979**, 102, 684
- 29 Lyklema, J.; Fokkink, L. G. J.; De Keizer, A. *Progr. Colloid Polym. Sci.* **1990**, 83, 46
- 30 Bérubé, Y. G.; De Bruyn, P. L. *J. Colloid Interface Sci.* **1968**, 27, 305
- 31 De Keizer, A.; Böhmer, M. R.; Mehrian, T.; Koopal, L. K. *Colloids Surf.* **1990**, 51, 339
- 32 Imae, T.; Muto, K.; Ikeda, S. *Colloid Polym. Sci.* **1991**, 269, 43
- 33 Galisteo Gonzáles, F.; Cabrerizo Vilchez, M. A.; Hidalgo- Alvarez, R. *Colloid Polym. Sci.* **1991**, 269, 406
- 34 Böhmer, M. R.; Koopal, L. K.; Tijssen, R. *J. Phys. Chem.* **1991**, 95, 6285
- 35 Mishra, S. K. in "Reagents in Mineral Technology", Somasundaran, P.; Moudgil, B. M. eds. *Surfactant Sci. Series* **1988**, 27, 195

CHAPTER 7

Adsorption of Ionic Surfactants on Variable Charge Surfaces II*Molecular architecture and structure of the adsorbed layer***Abstract**

The adsorption of alkylbenzene sulfonates on rutile is studied as a function of chain length and branching. The results are compared with theoretical predictions using a self-consistent field lattice theory for adsorption and or association. Both experiment and theory predict that the adsorption increases with chain length and decreases if the point of attachment of the aliphatic chain to the hydrophilic part of the molecule is shifted from a terminal to a medial position. The measured and calculated results agree well with each other in the initial part and the upper part of the isotherm. Around the cmc the adsorbed layer resembles a bilayer membrane. In the intermediate part of the isotherm the predicted association is too strong, which is due to the neglect of inhomogeneities parallel to the surface. A simple model is proposed to estimate the average size of the adsorbed surfactant aggregates in this region. Branching decreases the aggregation number whereas an increase in chain length increases this number.

Introduction

In this thesis⁽¹⁻⁴⁾ the adsorption of surfactants from aqueous solutions at the solid/liquid interface has been analyzed by comparing experimental results with theoretical predictions based on a self-consistent field lattice theory for adsorption and association (SCFA).⁽⁵⁻⁹⁾ The theory takes into account the amphipolar nature and the flexibility of surfactant molecules and incorporates both electrostatic and contact interactions. The basic result from a calculation with the SCFA theory are the equilibrium volume fraction profiles of the different components of the system perpendicular to

the surface. The volume fraction profiles give information on the structure of the layer.

For nonionic surfactants the effect of the size of the head group was studied with adsorption on both hydrophilic and hydrophobic surfaces.^(1,2) On hydrophilic surfaces local aggregation is rather important especially for adsorption of nonionics with head groups which are large as compared to the hydrophobic tail. Theoretically the aggregates could be modeled with an extension of the SCFA theory.⁽⁸⁾

With adsorption^(3,4) and micellization⁽¹⁰⁾ of ionic surfactants electrostatic interactions play a crucial role. For adsorption on a surface with a constant charge good agreement between theoretical and experimental results has been obtained, both for the shape of the adsorption isotherm and the changes in structure of the adsorbed layer with surfactant concentration.⁽³⁾ At low salt concentrations "two-step" isotherms are found. In the first plateau the surface charge is compensated, the surfactant is adsorbed "head-on" and the particles become hydrophobic. In the concentration range of about 0.1 cmc up to the cmc (critical micelle concentration) an asymmetrical bilayer forms which makes the particles hydrophilic again. At high salt concentrations the two-step shape of the isotherms is less clear. Isotherms, measured at different salt concentrations, exhibit a common intersection point (cip), corresponding to the iso-electric point (iep).

Experimental adsorption isotherms of ionic surfactants on variable charge surfaces^(4,11-17) do not have a distinct two-step shape. However, the isotherms at different salt concentrations still have a cip corresponding with the iep. On a log-log plot the isotherms show four regions. In region I the surfactant molecules adsorb without interaction with other surfactants. In region II strong attraction between the surfactant tails occurs. Primary aggregates are formed of surfactants with their head groups in contact with the surface and their tails clustering together. In region III the primary aggregates

grow and gradually a asymmetric bilayer is formed. In region IV the adsorbed amount remains constant because the cmc has been reached. Strong indications for the presence of local aggregates have been obtained from spectroscopic methods.⁽¹⁸⁻²⁰⁾

Qualitatively, the characteristic shape of the isotherm has been reproduced with the SCFA theory⁽⁴⁾ and the electrostatic effects are well predicted. The main deviations between theory and experiment occur in region II. This deviation occurs because in theory only inhomogeneities perpendicular and not parallel to the surface are considered. In reality inhomogeneities in the form of local aggregates are present. Nevertheless the fact that a good qualitative picture of the complicated four region isotherm is observed, is promising.

An interesting aspect of surfactant adsorption on variable charge surfaces is how the size of the primary aggregates depends on the architecture of the surfactant molecules. To investigate this we will study the effects of chain length and branching on the surfactant adsorption in general and on the size of the primary aggregates in particular.

Experiments will be carried out for the adsorption of sodium para-3-nonylbenzene sulfonate (3SNBS) and sodium para-3-dodecylbenzene sulfonate (3SDBS) on rutile (TiO_2). The effect of branching is studied using isomers of SDBS where the point of attachment of the dodecyl chain to the benzene ring is varied between the third and the sixth carbon atom: 3SDBS until 6SDBS.

The experimental results will be compared with results obtained with SCFA theory. Although the theory cannot predict the local aggregates it is well equipped to describe the effects of chain length and branching, especially for region I, and the upper part of the isotherm.

Experimental

Chemicals

Sodium para 3-nonylbenzene sulfonate, SNBS and the sodium para dodecylbenzene sulfonate isomers, SDBS were gifts from KSLA, Koninklijke Shell Laboratories Amsterdam, The Netherlands. At KSLA the critical micelle concentrations were determined by Dr. Van Os. They are listed in Table 1

Table 1: cmc values of SNBS and SDBS at 20°C and 0.01 M NaCl

<i>surfactant</i>	<i>cmc (mmol/dm³)</i>
3SNBS	10.0
3SDBS	0.37
4SDBS	0.49
6SDBS	0.72

Rutile (TiO₂) with a BET surface area of 50 m²/g was synthesized by Fokkink⁽²¹⁾ using the method of Bérubé and de Bruyn.⁽²²⁾

All other chemicals were of pro-analyse quality and water was deionized using a Millipore Super Q system.

Methods

Adsorption isotherms: Adsorption isotherms were measured at pH 5.1 and 21°C using the depletion method. To prepare the suspension 0.5 grams of TiO₂ were weighted into a 10 ml polycarbonate tube, 2 ml of NaCl solution was added, followed by sonication for 3 minutes. The pH was adjusted to 5.1 using 0.03 M HCl. After one night the pH was checked and the desired amounts of NaCl solution and surfactant solution, both of pH 5.1, were added up to a total volume of 8.5 ml. After end-over-end rotation for at least 8 hours the pH was measured again and adjusted. More than 4 hours later the pH was checked and adjusted again. When no changes in pH were observed the rutile was separated from the solution using

Acrodisk filters (0.2 μm) or centrifugation. The UV absorption of SNBS in the filtrate was measured at 225 and/or 262 nm.

Results

Chain length

The adsorption isotherms of 3SNBS and 3SDBS are given in Figure (1) and shown as log-log (a) and log-lin (b) plot. In the log-log plot the four characteristic regions can be distinguished. In region I the slope of the isotherm is unity, whereas in region II the slope is much higher than unity due to the strong attraction between the adsorbed molecules. In region III the slope of the isotherm is lower again because the repulsion between the head groups becomes important and in region IV plateau adsorption is reached at the cmc.

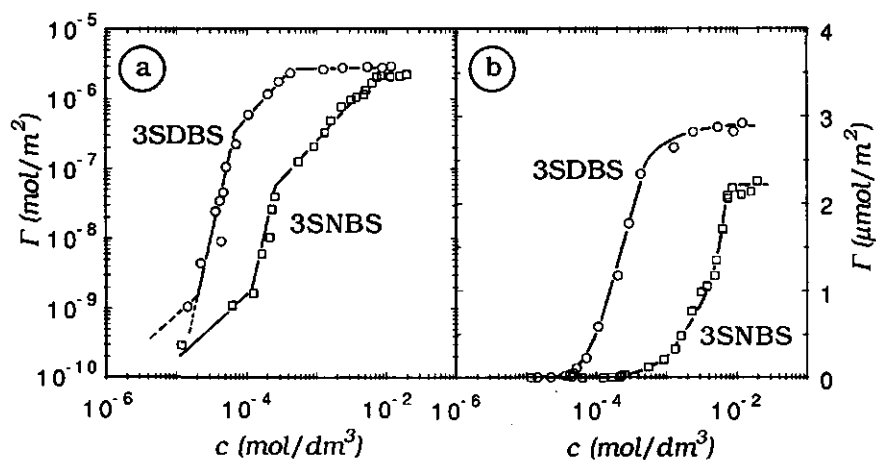


Figure 1: Adsorption as a function of chain length. Adsorption isotherms of 3SNBS and 3SDBS on rutile at $\text{pH} = 5.1 \pm 0.1$ and $c_{\text{NaCl}} = 0.01 \text{ M}$ on a log-log (a) and a log-lin (b) scale.

The isotherm of 3SDBS starts to increase sharply at an equilibrium concentration which is about 7 times lower than that where the 3SNBS isotherm increases sharply. This is in agreement with the chain length effect found for the adsorption of alkylsulfonates on alumina.⁽¹¹⁾ For alkylsulfonates on alumina the initial adsorption was independent of the chain length. It is not entirely clear whether this is the case for alkylbenzene sulfonates on rutile; we have not reached region I for 3SDBS. Different adsorption levels in region I may result if the interaction between surfactant and surface is not purely determined by the head group but also by the tail. The two extreme possibilities are shown as dotted lines in Figure (1a).

The plateau adsorption is better shown in Figure (1b) where the adsorbed amount is plotted on a linear axis. The maximum adsorbed amount is higher for 3SDBS than for 3SNBS; 3.0 and 2.3 $\mu\text{mol}/\text{m}^2$ respectively. For SDBS the adsorption still seems to increase above the cmc (0.4 mmol/dm^3). This is probably an artifact, because in the $\gamma\text{-Inc}$ curve a slightly negative slope was obtained beyond the cmc making the precise value of the cmc somewhat uncertain. Judging from the adsorption results we would predict that the cmc is at about 0.8 mmol/dm^3 SDBS.

The equilibrium concentrations at the start of region II differ by about a factor of 7, whereas the cmc values differ by about a factor of 27. In regions I and II the attraction between the surfactant and surface is strong and, apart from a perhaps small contribution from the tail, the same for both chain lengths. The repulsion between the head groups is not of major importance in these regions, because the head group charges are screened effectively by the surface charge. In region III the head group repulsion becomes more and more important. Consequently, the differences between the equilibrium concentrations at the same adsorbed amount become larger and resemble the differences in cmc values.

Branching

The results for the adsorption of the isomers 3SDBS, 4SDBS, 5SDBS and 6SDBS are given in Figure (2). In Figure (2a) the results for 3SDBS and 5SDBS are given in a log-log plot. The adsorption of 5SDBS is lower than that of 3SDBS except in the plateau where their adsorption is about the same. Isomers for which the point of attachment of the aliphatic chain to the hydrophilic part of the molecule is shifted from a terminal to a medial position have increasingly more problems in packing into dense aggregates and, consequently, their adsorption starts to increase at a higher concentration. This can well be related to differences in aggregation behavior in solution. The longer the length of the side chain of the isomer, the higher the cmc and the lower the aggregation number.⁽²³⁻²⁶⁾

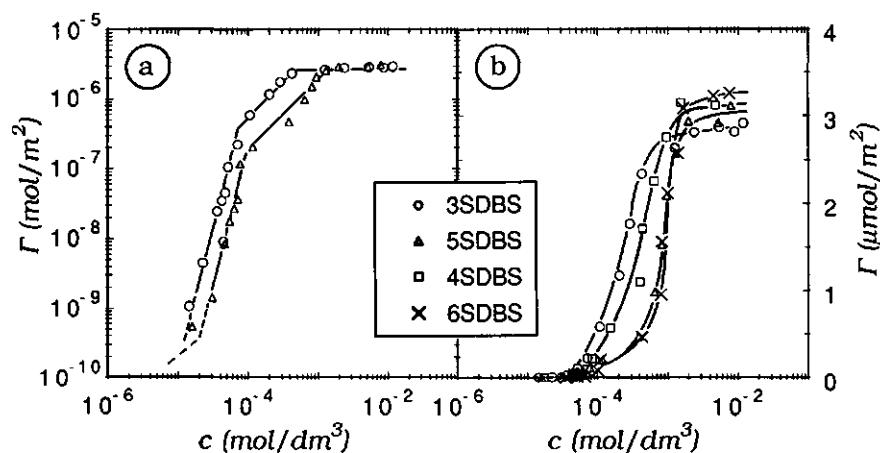


Figure 2: Adsorption as a function of branching. Adsorption isotherms of 3SDBS and 5SDBS on a log-log scale (a) and isotherms of 3SDBS, 4SDBS, 5SDBS and 6SDBS on a lin-log scale (b), $\text{pH} = 5.1 \pm 0.1$, $c_{\text{NaCl}} = 0.01 \text{ M}$.

In the log-lin plot (Figure 2b) adsorption isotherms for 4 isomers are given. The difference between 5SDBS and 6SDBS is negligible. The adsorption isotherm of 4SDBS is in between that of 3SDBS and 5SDBS. All four isotherms reach the same plateau value, within experimental error. As the stronger branched molecules have a higher cmc their adsorption can still increase at a concentration where linear chains have already reached their cmc. As a consequence 5SNBS can reach the same adsorbed amount as 3SDBS.

Chander et al.⁽¹¹⁾ reported the initial part of the adsorption isotherms of these molecules on alumina. They found the same trend and, in addition, they also found differences between the isomers in region I, this indicates that for SDBS not only the interactions between the sulfonate group and alumina determine the initial adsorption but that also other parts of the molecule may be in contact with the surface, most likely the phenyl ring.

Aggregation in region II

In the previous chapter we have shown that in region II primary aggregates or hemi-micelles are formed. From the surface charge and its adjustment upon surfactant adsorption it was deduced that in these aggregates the head groups are located at the surface side. The present results allow us to estimate the size of the primary aggregates at the II/III transition. For the calculation we follow an approach somewhat similar to that of Gao et al.⁽²⁷⁾ At the start of region II the surface coverage is very low, we consider all molecules adsorbed as nuclei for the formation of a hemi-micelle. Around every adsorbed molecule a primary aggregate forms in region II and at the transition to region III these primary aggregates have reached their optimal size. As the surfactant concentration increases the number of unassociated surfactant molecules on the surface also increases. To compute the number of nuclei for aggregate formation on the surface at the II/III transition we extrapolate region I as shown in Figure (3). Up to the II/III transition we now assume that: (1) all monomers are starting points for the formation of a primary aggregate, (2) all

primary aggregates are equal in size at the II/III transition and (3) primary aggregates do not fuse to form big aggregates or a monolayer. The last assumption is justified only if the adsorbed amount at the II/III transition is still low, which is the case for SNBS and SDS (sodium dodecyl sulfonate) at relatively high pH values⁽¹¹⁾, where region II ends below $0.3 \mu\text{mol}/\text{m}^2$. For lower pH values and longer chain lengths the II/III transition occurs at a higher coverage, so in those cases the calculation is more tentative. Considering the fact that our main objective is to obtain first order estimates of the size of the primary aggregates and the variations in size as a function of chain length and branching these assumptions seem fair. Applying the suggested procedure to the available data^(4,11) we arrive at the aggregation numbers shown in Table 2.

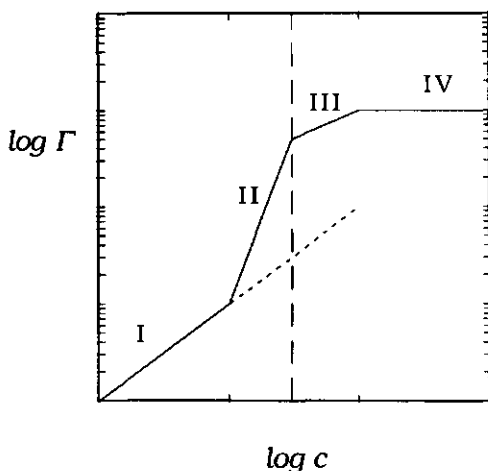


Figure 3: Schematized adsorption isotherm illustrating the calculation of $n^{\text{II/III}}$. The quotient of the intersection point of the full curve and the dashed line is taken to be the minimum aggregation number of a primary aggregate at the II/III transition.

Note that the absolute numbers are not very accurate because they were obtained from a log-log plot using straight lines for the four regions of the adsorption isotherm. Nevertheless some clear trends emerge. First of all the order of magnitude of $n^{\text{II/III}}$ for SNBS and

Table 2: Aggregation numbers of primary aggregates at the II/III transition, $n^{II/III}$,

<i>surfactant</i>	<i>pH</i>	<i>c_{NaCl} (M)</i>	<i>n^{II/III}</i>
<i>Sodium alkylbenzene sulfonates on rutile</i>			
3SDBS	5.1	0.01	100-300*
5SDBS	5.1	0.01	40-100*
3SNBS	4.1	0.001	16
3SNBS	4.1	0.01	30
3SNBS	4.1	0.1	>70
3SNBS	5.1	0.01	13
3SNBS	5.1	0.1	>30
<i>Sodium alkyl sulfonates on alumina</i>			
SC ₁₀ S	7.2	0.002	5
SC ₁₂ S (SDS)	7.2	0.002	14
SC ₁₄ S	7.2	0.002	45
SC ₁₆ S	7.2	0.002	300
SDS	7.2	0.0002	8
SDS	7.2	0.002	14
SDS	7.2	0.02	25
SDS	8.2	0.002	5
SDS	7.2	0.002	14
SDS	6.2	0.002	8
SDS	5.2	0.002	10
SDS	4.2	0.002	13
SDS	3.2	0.002	20

SDS is 10-50. Secondly the aggregation number increases with increasing chain length and salt concentration, both for the systems we studied as for the alkyl sulfonates. Thirdly branching reduces the aggregation number and finally the effect of the pH or surface potential is not very pronounced. Whether also the type of surface is

* The lower number is calculated assuming that region II for SDBS starts at the same adsorbed amount as in the case of SNBS, the high number from extrapolation of region II of SDBS until region I of SNBS is reached.

of influence cannot be concluded because different surfactants were used for different surfaces.

In general the effects of chain length, salt concentration and branching on $n^{II/III}$ are in line with the effects of these factors on the aggregation number of micelles^(25,26), although the effect of chain length on $n^{II/III}$ is stronger than the effect of chain length on the micelle size. However by judging the results it should be realized that the long chain surfactants, for which we calculate rather large aggregation numbers, may form monolayer structures on the surface at the II/III transition and the assumption that the primary aggregates do not fuse may be violated.

SCFA Theory

System and parameters

For a detailed description of the theory we refer to previous publications^(3, 5-9). In the present study we use the 1D SCFA lattice theory, i.e. lattice layers are considered to be homogeneous parallel to the surface but perpendicular to the surface the equilibrium volume fraction profiles are a function of distance. The electrostatic interactions are calculated using a multi-Stern layer approach with a distance between the lattice layers of 0.31 nm. As a model for a variable charge surface we use a surface with a fixed potential, such a surface corresponds with a metal oxide surface at constant pH.^(28,29) For the calculations the surface potential is fixed to 50 mV. In practice this corresponds to a pH less than one unit different from the point of zero charge.

We model the surfactants as A_nB_3 chain molecules, A being a hydrophobic segment and B a charged hydrophilic segment. For the branched molecules the branch point is defined as the segment number of the aliphatic chain to which the head group is connected. The head group segments have a charge of $-1/3$ making the total

charge of B_3 -1. Each A_nB_3 fills $n + 3$ lattice sites. The conformational statistics are calculated using the rotational isomeric state scheme developed by Leermakers and Scheutjens.⁽⁷⁾ The remaining molecules: salt ions and solvent are modeled as monomers and occupy one lattice site only.

The χ -parameters between the aliphatic segments A and the monomeric solvent, W, a surfactant head group segment, B and the small salt ions C and D, which have a charge of +1 and -1 respectively, are all set to 2. To express the contact interactions with the surface, S, we use the value $\chi_{BS} = -10$. The exact value is not very important as long as the specific adsorption is strong.⁽⁴⁾ Remaining χ -parameters are set to zero. The relative dielectric constant of the A segments is 2, those of all other components are 80. These choices imply that charged components only differ from water with respect to their charge. This allows us to study electrostatic effects disregarding specific interactions.

Results

Critical micelle concentrations

Critical micelle volume fractions of the surfactants at a salt concentration, $c_s = 0.01$ M were calculated as described elsewhere⁽¹⁰⁾. They were divided by the chain length, r , to obtain a quantity proportional to the concentration. The results are listed in Table 3. The branch point number, S_B , indicates which segment of the A_{12} chain is connected to the head group.

Chain length

Results for the adsorption of a series of linear A_nB_3 molecules on a surface with a fixed potential of 50 mV and a salt concentration of 0.01 M are given in Figure (4). The adsorbed amount is expressed as the excess number of molecules per surface site, n^{exc} , and on the

horizontal axis the total surfactant volume fraction, $\bar{\phi}$, is given, which is comprised of surfactant free in solution and, above the cmc, surfactant present in micelles.⁽¹⁰⁾

Table 3: $cm\phi/r$ of A_nB_3 at $c_s = 0.01$ M. $S_B = 6$ indicates that segment 6 of the A_{12} chain is connected to the head group.

surfactant	$cm\phi/r$
A_6B_3	8.0E-03
A_8B_3	2.0E-03
$A_{10}B_3$	4.7E-04
$A_{12}B_3$	1.1E-04
$A_{14}B_3$	2.4E-05
$A_{16}B_3$	4.2E-06
$A_{12}B_3$ ($S_B = 6$)	2.3E-04
$A_{12}B_3$ ($S_B = 3$)	1.9E-04

In the log-log plot (4a) the four regions are shown for all chain lengths. In region I the isotherms do not coincide. This because the tail has some adsorption energy. The tails are squeezed out of the water onto the surface because $\chi_{AW} = 2$ and $\chi_{AS} = 0$. Upon replacing a contact between A and W by a contact between A and S 0.5 kT per segment is gained. However it will also cost entropy for a chain to lie flat on the surface and therefore the differences are small.^(1,30)

In region II the isotherms increase steeply. Region II starts at lower coverages for longer chain lengths. For chain lengths smaller than 10 segments no condensation is found but for longer chains we find an instability in region II. As a result of the assumed homogeneity in each the lattice layer the predicted association is too strong.⁽⁴⁾ At the end of region II a monolayer with the composition of approximately half an equilibrium membrane, calculated with the SCFA theory, is present on the surface.

Regions III and IV of the isotherms are shown more clearly in Figure (4b) where the adsorbed amount is plotted on a linear scale. If the tail is longer higher adsorbed amounts are reached. In region III the

monolayer on the surface at the end of region II gradually transforms into an asymmetric bilayer.

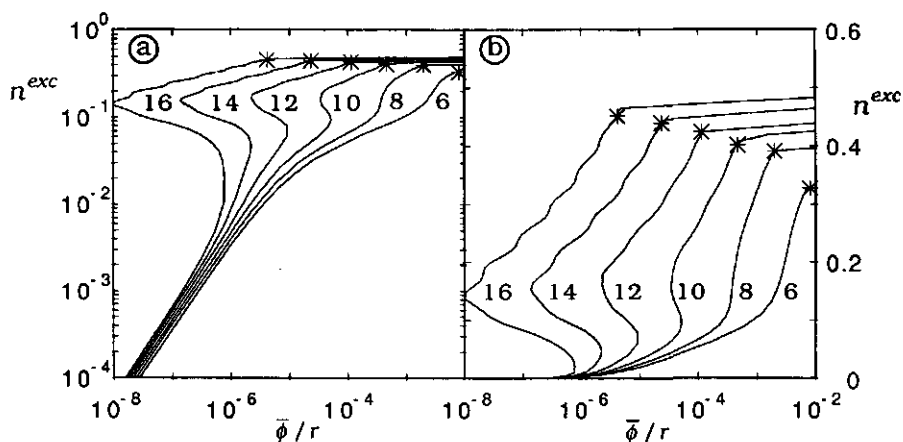


Figure 4: Effect of aliphatic chain length, n , on the adsorption of A_nB_3 molecules on a surface with a fixed potential of 50 mV. See text for parameters. The results are given on a log-log (a) and a log-lin (b) scale. The cmc values are indicated with an asterisk.

The effect of chain length on the adsorption is in qualitative agreement with experiment. Region II starts at lower coverages for longer chain lengths, which is in agreement with the adsorption of alkyl sulfonates on alumina.⁽¹¹⁾ Our experimental results are not accurate enough to judge this aspect. The trends shown in Figure (1b) and (4b) correspond: long chains increase somewhat more gradual in region III but reach higher plateau levels. Comparison of the start of region II or region III relative to the cmc is difficult because the prediction of region II is not correct.

Branching

The calculated effects of branching on the adsorption isotherm of three $A_{12}B_3$ isomers are given in Figures (5a) and (5b). In the log-log

plot. Figure (5a) a difference between the adsorption isotherms shows up in region I. Through the choice of χ_{AW} the tail segments have some affinity for the surface. The isomers with longer side chains will have less initial adsorption, because the entropy loss for a branched molecule to lie flat on the surface will be larger than for a linear one. As expected region II of the calculated adsorption isotherms is not in agreement with the experimental results. Due to the mean field approximation a too strong condensation step occurs.

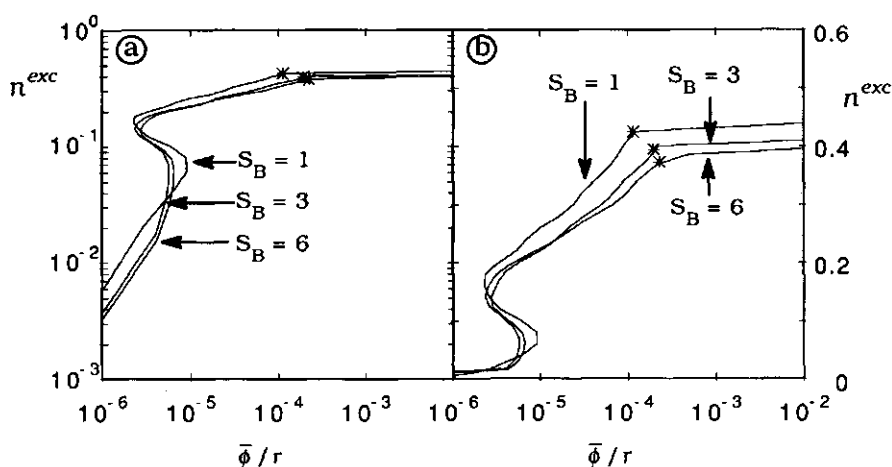


Figure 5: Effect of branching on the adsorption of $A_{12}B_3$ molecules on a surface with potential of 50 mV. See text for parameters. The results are given on a log-log (a) and a log-lin (b) scale. The cmc values are indicated with an asterisk.

The trends shown in the upper part of region III of the isotherms, see Figure (5b) corresponds with the experimental results. The differences in the adsorbed amounts at the cmc are small, but the results show that packing of the molecules becomes more difficult when the chain are strongly branched. The error in the experimental isotherms is too large to check this trend.

Volume fraction profiles

Isomers of $A_{12}B_3$ show the same adsorbed amounts at different solution concentrations. This can only be the case if differences in the structure of the adsorbed layer are present. Therefore, we will study the volume fraction profiles at $n^{exc} = 0.35$ which is close to the adsorption at the cmc for the isomers with $S_B = 1$ and $S_B = 6$. In Figure (6) the volume fraction profiles are given. The A segments form a hydrophobic core and the B segments are present on both sides of this core. The differences in the adsorbed layer for the isomers are small. The head group segments of the branched molecules have a somewhat sharper distribution and the distribution of A segments is slightly more compact.

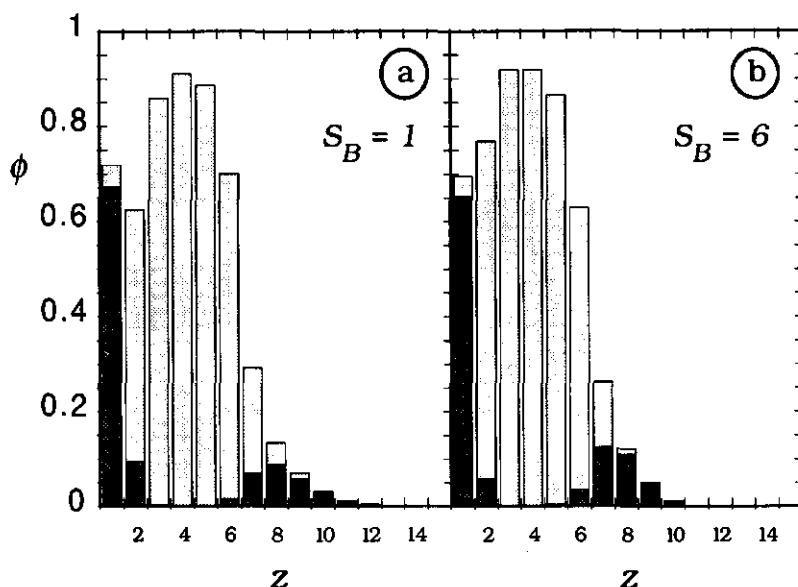


Figure 6: Volume fraction profiles for head and tail segments at $n^{exc} = 0.35$ for linear $A_{12}B_3$, ($S_B = 1$), Figure (a) and branched $A_{12}B_3$ with $S_B = 6$, Figure (b). The head groups are represented in the bottom bars (dark) and the tails in the upper bars (light).

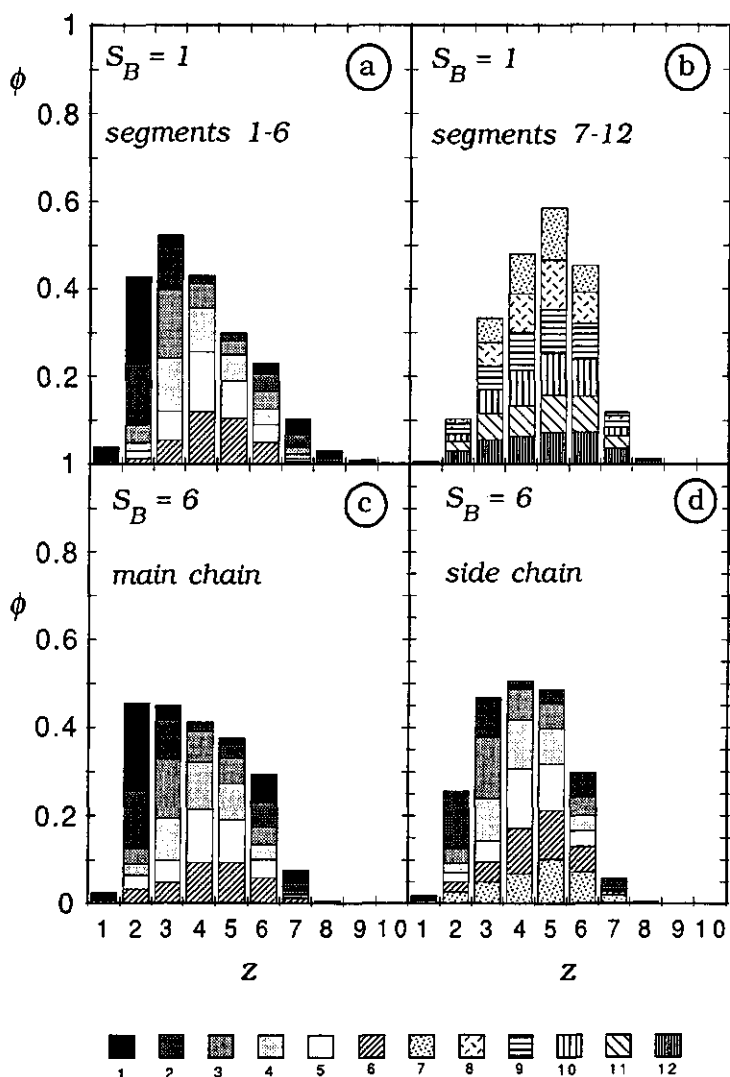


Figure 7: Volume fraction profiles for tail segments at $n^{exc} = 0.35$ for linear $A_{12}B_3$, ($S_B = 1$), Figures (a, b) and branched $A_{12}B_3$ with $S_B = 6$, Figures (c, d). In Figure (a) the first six segments (next to the head group) of the linear chain are given. In Figure (b) the 6 segments and the chain end are given. In Figure (c) the distribution of the 6 segments of the main chain of the branched molecule is shown and in Figure (d) the distributions of the 6 segments of the side chain, which is connected to the first segment of the aliphatic chain are given. The first segment of the side chain is given in grey just as the second segment of the main chain, since these segments are at the same position relative to the head group.

The differences between the structures of the hydrophobic regions can be illustrated more clearly if we plot the volume fractions of all individual segments of the aliphatic chain. In Figures (7a) and (7b) the segment distributions of the A segments of the linear chain ($S_B = 1$) are given. In Figure (7a) the volume fraction profiles of segment connected to the head group (black) and the five adjacent segments are given. The profiles of the remaining six segments at the end of the chain are given in Figure (7b). The segment that is connected to the head group has a maximum in layer 2, it is hardly present in layers 4 and 5 and in the outer layers it is present again. This segment has to accumulate near the boundaries of the core since they are connected to the head groups which are located on the both sides of the hydrocarbon layer. The distribution of the tail segment at the end of the chain is shown in the bottom block of Figure (7b) and it is considerably more homogeneous than the first segment. Also the other segments close to the chain end have a fairly homogeneous distribution, see the blocks on top of the bottom block. In Figures (7c) and (7d) the segment distributions of the branched isomer are shown. For the branched surfactant none of the segments is distributed in a more or less homogeneous way as was the case for the end segments for the linear chain. The results for the two end segments for this molecule, shown in the bottom blocks, resemble the distribution of the segment at position 6 of the linear molecule, see Figure (7a) much closer than that of the end segments of the linear chain. These results confirm that the packing of branched molecules in a planar bilayer is more difficult than that of linear molecules.

Discussion

Both theoretically and experimentally the differences in the adsorption at the cmc as a function of chain length, branching and salt concentration⁽⁴⁾ are small. Yet, micelle aggregation numbers vary strongly for the different surfactants and conditions.^(10,26) The reason for this difference is that the surface imposes restrictions on

the geometry of the adsorbed layer. In flat association colloids, such as membranes in solution, the relative variation of the aggregation number, calculated with SCFA theory for A_nB_3 molecules as a function of salt concentration, chain length or branching, is much smaller than the variation of the calculated differences in aggregation number for spherical structures. This must have a geometrical reason: if the number of molecules in a micelle doubles, the volume doubles but the micelle radius increases only slightly. Consequently, the effects on the chain conformations are small. However, for flat structures a doubling of the aggregation number leads to a doubling of the thickness and this will have considerable consequences for the chain conformations. Inspecting the experimental data with respect to differences in the adsorbed amount at the plateau of the isotherm as a function of salt concentration, chain length and branching, we may conclude that a "membrane-like" structure present in region IV.

In region II of the experimental adsorption isotherms pronounced differences in aggregation numbers are present between the various chain lengths, isomers and salt concentrations and these differences are in line with the differences in micelle aggregation numbers. This corresponds well with the view that in region II the adsorbed layer is inhomogeneous both parallel and perpendicular to the surface. Therefore, several degrees of freedom are present for the creation of aggregated structures and pronounced variations in aggregation numbers can exist. In region III a layer consisting of aggregates is gradually transformed into layer which is more homogeneous parallel to the surface and the inhomogeneities present are mainly perpendicular to the surface. The 1D SCFA theory takes the latter inhomogeneities into account and therefore it can predict the structure of the layer in the upper half of the isotherm rather well.

Conclusions

The measured effects of chain length and branching of alkylbenzene sulfonates on rutile are in agreement with other experimental work. An increase in chain length leads to higher maximum adsorbed amounts and a lower start of region II. Branched molecules have more problems with packing into dense aggregates, which leads to less adsorption at a given concentration, but by virtue of their higher cmc, about the same adsorbed amount is reached in region IV.

Most trends for adsorption as a function of chain length and branching could be reproduced by calculations with the 1D SCFA theory. Especially for region I and the upper part of region III of the isotherms the results agree with experiments. The SCFA theory exaggerates region II, the mean field approximation is a too drastic simplification in this region. An improved version of the theory, which allows for inhomogeneities in two directions should be able to make better predictions on region II.

The adsorption of a homologous or isomeric series of surfactants, such as alkyl (benzene) sulfonates, increases with decreasing cmc and increasing micelle aggregation number. Because the surface imposes restrictions on the geometry of the adsorbed layer the differences in the plateau adsorption are however smaller than the differences between micelle aggregation numbers. In the plateau region the adsorbed layer rather resembles a bilayer membrane. At low coverages local aggregates are formed on the surface. Their variation in size as a function of chain length and branching resembles that of micelles more closely.

References

- 1 Böhmer, M. R.; Koopal, L. K. *Langmuir* **1990**, 6, 1478, this thesis Ch. 2
- 2 Böhmer, M. R.; Koopal, L. K.; Janssen, R.; Lee, E. M.; Thomas, R. K.; Rennie, A. R. submitted to *Langmuir*, this thesis Ch. 3
- 3 Böhmer, M. R.; Koopal, L. K., submitted to *Langmuir*, this thesis Ch. 5

- 4 this thesis, Ch. 6
- 5 Scheutjens, J. M. H. M.; Fleer, G. J. *J. Phys. Chem.* **1979**, *83*, 1619
- 6 Evers, O. A.; Scheutjens, J. M. H. M.; Fleer, G. J. *Macromolecules* **1990**, *23*, 5221
- 7 Leermakers, F. A. M.; Scheutjens, J. M. H. M. *J. Chem. Phys.* **1988**, *89*, 3264
- 8 Leermakers, F. A. M.; Scheutjens, J. M. H. M.; Lyklema, J. *Biochimica Biophysica Acta* **1990**, *1024*, 139
- 9 Böhmer, M. R.; Evers, O. A.; Scheutjens, J. M. H. M. *Macromolecules* **1990**, *23*, 2288
- 10 Böhmer, M. R.; Koopal, L. K.; Lyklema, J. *J. Phys. Chem.* in press, Ch. 4
- 11 Chander, S.; Fuerstenau, D. W.; Stigter, D. in "Adsorption from Solution", Ottewill, R. H.; Rochester, C. H.; Smith, A. L. Eds. Academic Press London (1983), p197
- 12 Somasundaran, P.; Fuerstenau, D. W. *J. Phys. Chem.* **1966**, *70*, 90
- 13 Moudgil, B. M.; Somasundaran, P.; Soto, H. in "Reagents in Mineral Technology", Somasundaran, P.; Moudgil, B. M. eds. *Surfactant Sci. Series*, **1988**, *27*, 79
- 14 Fuerstenau, D. W.; Wakamatsu, T. *Faraday Discussions of the Chemical Society* **1975**, *59*, 157
- 15 Scamehorn, J. F.; Schechter, R. S.; Wade, W. H.; *J. Colloid Interface Sci.* **1982**, *85*, 463
- 16 Harwell, J. H.; Hoskins, J. C.; Schechter, R. S.; Wade, W. H. *Langmuir* **1985**, *1*, 251
- 17 Bitting, D.; Harwell, J. H. *Langmuir* **1987**, *3*, 500
- 18 Chandar, P.; Somasundaran, P.; Turro, N. J. *J. Colloid Interface Sci.* **1987**, *117*, 31
- 19 Chandar, P.; Somasundaran, P.; Waterman, K. C.; Turro, N. J., *J. Phys. Chem.* **1987**, *91*, 150
- 20 Somasundaran, P.; Kunjappu, J. T. *Colloids Surf.* **1989**, *37*, 245
- 21 Fokkink, L. G. J.; De Keizer, A.; Lyklema, J. *J. Colloid Interface Sci.* **1989**, *127*, 116
- 22 Bérubé, Y. G.; De Bruyn, P. L. *J. Colloid Interface Sci.* **1968**, *27*,
- 23 Evans, H. C. *J. Chem. Soc.* **1956**, *117*, 579
- 24 Van Os, N. M.; Daane, G. J.; Bolsman, T. A. B. M. *J. Colloid Interface Sci.* **1987**, *115*, 402
- 25 Tanford, C. "The Hydrophobic Effect" Wiley Interscience, NY, 1980
- 26 Binana-Limbelé, W.; Van Os, N. M.; Rupert, L. A. M.; Zana, R., *J. Colloid Interface Sci.* **1991**, *141*, 157
- 27 Gao, Y.; Du, J.; Gu, T. *J. Chem. Soc., Faraday Trans I* **1987**, *83*, 2671
- 28 Gibb, A. W.; Koopal, L. K. *J. Colloid Interface Sci.* **1990**, *134*, 122
- 29 Lyklema, J.; Fokkink, L. G. J.; De Keizer, A. *Progr. Colloid Polym Sci.* **1990**, *83*, 46
- 30 Koopal, L. K.; Wilkinson, G. T.; Ralston, J. *J. Colloid Interface Sci.* **1988**, *126*, 493

Summary

The purpose of this thesis is to extend the knowledge of micellization and adsorption of surfactants in aqueous solutions or the solid/electrolyte interface. To this end experimental results for well defined systems have been compared with theoretical calculations.

The theoretical calculations have been performed with the self-consistent field lattice theory for adsorption and association developed in this laboratory by Scheutjens, Fleer, and Leermakers. The theory uses a lattice and a mean field approximation is applied to each lattice layer. The calculations start from molecular properties of all molecules present in the system. For surfactants these include the sizes of the head and tail groups, the fact that the chains are flexible, the charge and the intra- and intermolecular interactions. Using these properties together with the amounts of the different molecules present, equilibrium volume fraction profiles are calculated, for instance, perpendicular to an adsorbing surface. From the volume fraction profiles, experimentally easily accessible quantities such as the adsorbed amount and layer thickness can be derived.

In chapter 2 the micellization and adsorption of nonionic surfactants is calculated. Due to steric repulsion between the head groups the cmc increases and the aggregation number decreases as the polar chain becomes longer. Similarly the steric repulsion also causes a decrease in the maximum adsorbed amount as a function of the length of the head groups both on hydrophilic and hydrophobic surfaces, which agrees with experimental work. On hydrophobic surfaces surfactant monolayers are formed, on hydrophilic surfaces bilayers are formed if the head group is not too long relative to the tail. For nonionic surfactants with long head groups only weak association of the tails was found.

In chapter 3 the effect of polar chain length on the adsorption of nonionic surfactants is investigated in more detail. Experimental data are obtained for adsorbed amounts and hydrodynamic layer thicknesses. Moreover, with neutron reflection, the structure of the adsorbed layer is measured more directly. The experiments show that even for surfactants with very long head groups strong association between the tails occurs. The theory used in chapter 2 did not predict this behavior. However, with an extension of the theory allowing for inhomogeneities not only perpendicular but also parallel to the surface, a much better agreement between experiment and theory is reached. On hydrophilic surfaces nonionic surfactants with long polar head groups are found to form aggregates with a hydrophobic core. Nonionic surfactants with short polar head groups form bilayers on these surfaces.

Chapter 4 deals with micelle formation of ionic surfactants. The critical micelle concentration decreases and the micelle aggregation number increases with rising salt concentration and tail length. Transitions to other than spherical shapes at high salt concentrations and for branched chains were predicted. The calculated profiles show that the head groups are not located on a single shell but have a rather wide distribution. Micelles behave as spheres with a low but constant net charge density. The potential in the head group region is adjusted by attracting as many counterions to maintain this charge density. The agreement with experimental results on aggregation numbers, cmc-values and electrical potentials in the head group region is good.

In chapter 5 calculations on the adsorption of ionic surfactants on surfaces with a constant charge are performed. The most typical effect is that "two-step" adsorption isotherms are obtained, especially at low c_{salt} . After the first step the surface charge is compensated and at a solution concentration of about 10% of the cmc the adsorbed amount starts to increase again to form a bilayer. At high salt concentrations, the two steps cannot be distinguished so clearly. The adsorption isotherms have a common intersection point which

coincides with the isoelectric point. The head group distribution of the bilayer at the solution side is rather wide and the charge profile at the solution side of the bilayer does not depend on the salt concentration. Just as was the case with micelles, the potentials at the solution side of the bilayer depend strongly on the salt concentration. Experimental results from literature indeed show the calculated isotherm shapes and changes in structure of the adsorbed layer from a "single layer" to a bilayer.

In chapter 6 the adsorption of ionics on variable charge surfaces is studied. If the experimental data for sodium nonylbenzene sulfonate on rutile are plotted on a double logarithmic scale the characteristic shape of the adsorption isotherm of anionic surfactants on metal-oxides appears. The adsorption increases steeply at very low adsorbed amounts (region II), due to the interaction between adsorbed molecules. At a few percent of the maximum coverage the slope in the log-log plot decreases again (region III) and at the cmc a plateau is reached (region IV). A common intersection point in the adsorption isotherms at different salt concentrations is found in region III. The common intersection point coincides with the isoelectric point.

The measured isotherms do not have a "two-step" shape as found for constant charge surfaces. This due to the adjustment of the surface charge upon surfactant adsorption. From the measured surface charge, the amount of surfactant adsorbed with their head group on the surface can be estimated. These data show that after the common intersection point bilayer formation starts. The bilayer structures that have been formed can be asymmetrical: the amount at the surface is dictated by the surface charge while the amount at the solution side depends mainly on the repulsion between the head groups and the attraction between the tails.

The calculated results show the characteristic regimes in the adsorption isotherm. For the initial part and the upper part of the isotherm the results agree qualitatively with the experimental ones

and corroborate that first head-on adsorption and later bilayer formation takes place. The part of the isotherm where lateral interaction dominates the behavior agrees less satisfactorily with experimental data. At the calculated II/III transition a monolayer of surfactants, with an area per head group equal to that in bilayer membranes, is on the surface. In reality the II/III transition occurs at a lower coverage and local aggregates are present on the surface. The mean field approximation turns out to be an oversimplification for the description of region II.

In chapter 7 the effects of chain length and branching are investigated. Experimentally it is shown that the adsorption increases with chain length and decreases with degree of branching. These trends are also calculated. Just as the aggregation number of micelles increases with chain length and decreases with the degree of branching, the size of primary aggregates (hemi-micelles) at the II/III transition increases with chain length and decreases with degree of branching. This indicates that similar packing constraints apply to micellization and adsorption in region II. At the cmc the adsorbed layer is more like a bilayer membrane.

Most of the observations do not need a complex theory to be understood qualitatively. If the repulsion between the head groups increases, either by reducing the ionic strength or by making the head group longer, one can expect the cmc to increase, the aggregation number to decrease and the adsorption to decrease as well, all of this because the molecules have less tendency to get together. The benefit of the theory is however twofold. Firstly, it allows for an approximate quantification of these effects. A nice example is the variation of the plateau adsorption with salt concentration. The salt concentration affects the repulsion between charged head groups. In general this will lead to an increase in adsorption and a decrease of the cmc. Because of the lowering of the cmc the concentration range in which the adsorption can increase decreases. The net result is that a priori the effect of salt on the plateau adsorption is not clear. However, using the theory it

appeared that both effects almost cancel, which was also shown to be the case experimentally.

The other advantage of using the theory is that information on the structure of the adsorbed layer or the micelle can be deduced. A typical example of a new feature emerging from the calculations is the charge regulation mechanism in micelles and adsorbed layers. Other examples are the wide distribution of the head groups, and the change of the structure of the layer with equilibrium concentration.

Qualitatively, the many different isotherm shapes observed in surfactant adsorption studies can all be described with one single theory. The theoretical calculations predict the structure of micelles and adsorbed layers and therefore this theory can be used to obtain insight in the behavior of surfactants at interfaces and in solution. It can be concluded that surfactant adsorption on hydrophilic surfaces and micellization have many aspects in common, because aggregation in adsorbed layers is very important.

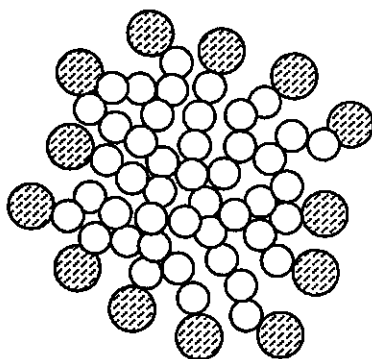
Samenvatting

Oppervlakte-actieve stoffen adsorberen, d.w.z. hopen zich op, aan vele oppervlakken, bijvoorbeeld dat tussen water en lucht. Ook aan het grensvlak tussen een waterige en een olie-achtige fase of aan het vast-vloeistof grensvlak adsorberen ze vaak in grote hoeveelheden. Oppervlakte-actieve stoffen bestaan uit een hydrofobe of "watervrezende" staart en een hydrofiele of "waterminnende" kop. Zeep is een voorbeeld van oppervlakte actieve stof. De kopgroep van een zeepmolekuul is een negatief geladen carbonaatgroep, de staart een alkaanketen. Een positief geladen zoution maakt het zeepmolekuul compleet. In het grensvlak tussen water en een olie of lucht zullen ze zich zodanig proberen te oriënteren dat de kop in de waterige oplossing steekt en de staart in de lucht of in de olie zwaait.

Zeepmolekulen, en in bredere zin oppervlakte-actieve stoffen worden ook in het Nederlands vaak aangeduid met de engelse term *surfactants*. Surfactants worden veel gebruikt in huishoudelijke en industriële processen. Bij wassen leidt de toevoeging van surfactant tot een beter resultaat. Stoffen die normaal gesproken niet in water oplossen, kunnen, als er surfactant aan de oplossing toegevoegd wordt, vaak wel verwijderd worden. Als de surfactantconcentratie hoog genoeg is, vindt micelvorming plaats. Micellen zijn aggregaatjes van surfactantmolekulen met een hydrofobe kern die omringd is door de kopgroepen. Zo'n micel is schematisch weergegeven in Figuur (1). Hydrofobe of gedeeltelijk hydrofobe molekulen kunnen in het micel "oplossen" en zo verwijderd worden ondanks hun slechte oplosbaarheid in water.

Een ander voorbeeld van het gebruik van surfactants is flotatie. Deze techniek wordt gebruikt om kleine deeltjes te scheiden. Luchtbelletjes worden door een mengsel van verschillende soorten deeltjes in water geleid en plakken bij voorkeur aan de meer hydrofobe deeltjes. Door de aangehechte luchtbellen worden de deeltjes naar het oppervlak getransporteerd. Op deze manier wordt

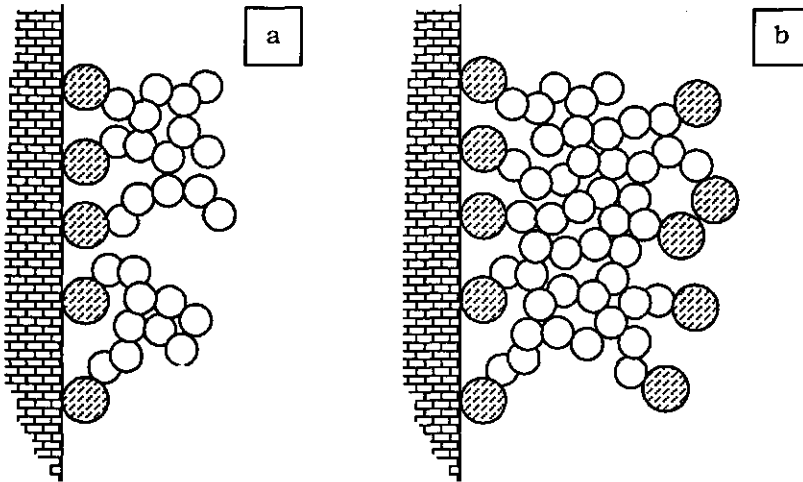
een scheiding op grond van hydrofobiciteit bewerkstelligd. De adsorptie van surfactants aan het vast-vloeistof grensvlak beïnvloedt de hydrofobiciteit van de deeltjes. Voor flotatie is de structuur van de geadsorbeerde laag van groot belang. Als de adsorptie plaatsvindt met de kop aan het oppervlak en de staart steekt in de oplossing, zie Figuur (2a), dan zorgt de surfactant voor een hydrofobisering van het oppervlak en luchtballen hechten zich makkelijk. Als er echter meer surfactant adsorbeert, kan er een dubbele laag of bilaag ontstaan, zoals in Figuur (2b) aangegeven is. Nu bevinden zich ook koppen aan de oplossingskant. Hierdoor wordt het hydrofobe deel van de geadsorbeerde laag afgeschermd en kunnen luchtbelletjes moeilijker aanhechten. De flotatie-opbrengst zal lager uitvallen.



Figuur 1: Schematische voorstelling van een micel. De kopgroepen van de surfactant, aangegeven als gestreepte bolletjes bevinden zich aan de buitentkant en zijn in contact met de waterige oplossing. De staarten, aangegeven als kleine egaal witte bolletjes vormen het hydrofobe hart van het micel.

Nog een voorbeeld van de toepassingen van surfactants is te vinden in de zogenoemde tertiaire oliewinning. In principe kunnen hoge opbrengsten verkregen worden door een olieveld met een surfactant oplossing te spoelen. De surfactant wast dan als het ware de olie uit de gesteenten. Een probleem hierbij is dat er veel surfactant

verloren gaat door adsorptie op gesteenten. De molekulen zouden selektief moeten zijn: ze moeten zich sterk aan het olie/water grensvlak ophopen maar juist niet aan het grensvlak met de gesteenten.



Figuur 2: Schematische voorstelling van geadsorbeerde lagen surfactants. In de linker figuur zijn de kopgroepen (gestreept) op het oppervlak en de staarten (wit) aan de oplossingskant. In de rechter figuur is een bilaag aanwezig. Koppen bevinden zich zowel tegen het oppervlak aan als aan de kant van de oplossing, gescheiden door een hydrofobe laag gevormd door de staarten.

Inzicht in het gedrag van surfactants in oplossing en aan grensvlakken is nodig om de toepassingen te optimaliseren. Het wat, hoe en waarom van de vorming van micellen en vooral van geadsorbeerde lagen is veel bestudeerd maar nog niet geheel begrepen. Dit maakt een onderzoek aan micelvorming en adsorptie van surfactants ook vanuit een zuiver wetenschappelijk oogpunt interessant. In dit proefschrift is een aantal fundamentele aspecten van micelvorming en adsorptie aan vast/vloeistof grensvlakken verder uitgediept. Hierbij zijn theoretische resultaten vergeleken met experimentele.

Voor de modellering van surfactantgedrag is het noodzakelijk binnen het molekuul onderscheid te maken tussen kop en staart. Verschillende surfactants vertonen verschillend gedrag in oplossing en aan grensvlakken. Zo hangt bijvoorbeeld de concentratie waarbij micelvorming begint af van de lengte van de staart en de grootte en/of lading van de kopgroep. Daarom moeten de aard en grootte van beide delen van het molekuul in het gekozen model kunnen variëren, evenals de intra- en intermoleculaire interacties. Behalve de eigenschappen van de molekulen is het nodig om te weten hoeveel er van iedere molekuulsoort aanwezig is.

Een model dat deze mogelijkheden biedt is de zg. zelf-consistente veldtheorie voor adsorptie en associatie van Scheutjens, Fler en Leermakers. In deze theorie wordt een rooster gebruikt. Voor surfactantadsorptie-berekeningen is de ruimte verdeeld in een aantal lagen parallel aan een wand. Voor de berekening van de structuur van micellen is een bolsymmetrisch rooster gekozen. In beide gevallen wordt aangenomen dat elke roosterlaag homogeen is. Het doel van een berekening is het vinden van het volumefractieprofiel. Het volumefractieprofiel geeft de verdeling van koppen, staarten, oplosmiddel en indien aanwezig, zoutionen over de roosterlagen en aldus informatie over de structuur van het micel of de geadsorbeerde laag. Als voorbeeld zijn in Figuur (3) de volumefracties van een surfactant in de roosterlagen grenzend aan een oppervlak gegeven. In Figuur (3a) zijn de koppen vlak bij het oppervlak en de staarten bevinden zich aan de kant van de oplossing, deze situatie komt overeen met de in Figuur (2a) geschetste. In Figuur (3b) is een bilaag op het oppervlak aanwezig. Zowel direct bij het oppervlak als aan de oplossingskant zijn koppen die gescheiden worden door een aantal roosterlagen die bijna volledig gevuld zijn met staarten, deze situatie correspondeert met Figuur (2b). Een opvallend aspect is dat de kopgroepen aan de oplossingskant niet precies op een rijtje liggen, zoals in veel bestaande theoriën is aangenomen, maar een zekere spreiding vertonen.

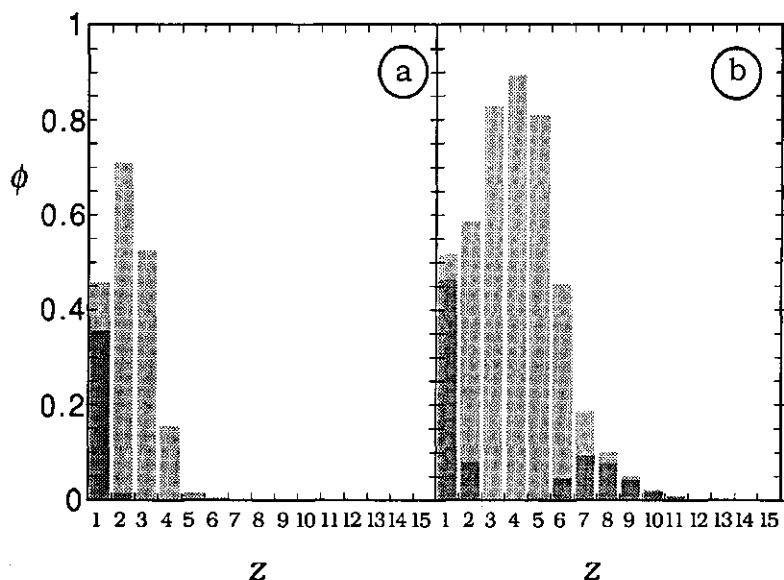


Figure 3: Voorbeelden van volumefrakteprofielen, ϕ als functie van z , in de geadsorbeerde laag van surfactants. De kopgroepen zijn in donkergrijs weergegeven en bevinden zich in Figuur (a) voornamelijk in de roosterlaag die grenst aan het oppervlak, laag nummer 1. De staarten (lichtgrijs) hopen zich met name op in lagen 2, 3, en 4. In Figuur (b) zijn er zowel vlak bij het oppervlak als aan de kant van de oplossing (lagen 6-10) koppen aanwezig. De staarten vullen bijna het gehele volume van lagen 3 tot 5. De volumefrakties van de overige molekulen zijn hier weggelaten.

Uit het volumefrakteprofiel kunnen o.a. de geadsorbeerde hoeveelheid en de laagdikte afgeleid worden. Deze gegevens zijn ook experimenteel toegankelijk en zo kunnen de berekeningen met experimenten vergeleken worden. Als de overeenstemming goed is, leren we via het volumefrakteprofiel iets over de structuur van de laag.

In hoofdstuk 2 zijn resultaten gegeven over de micelvorming en adsorptie van niet-ionogene surfactants, dat zijn surfactants met een vrij lange, niet elektrisch geladen kop. Door de sterische repulsie

tussen de koppen stijgt de kritische micelvormingsconcentratie (kmc) en daalt het aggregatiegetal van de gevormde micellen als functie van de lengte van de kopgroep. De repulsie tussen de koppen zorgt ook voor een daling van de maximale adsorptie voor langere kopgroepen, ongeacht of de surfactants met hun staart of met hun kop aan het oppervlak hechten. Op hydrofobe oppervlakken zijn de staarten bij het oppervlak en bevinden de koppen zich aan de oplosmiddelkant. Op hydrofiele oppervlakken bevinden de koppen zich tegen het oppervlak aan. Als de koppen niet al te groot zijn kunnen bilagen gevormd worden, er bevinden zich dan koppen aan beide zijden van het hydrofobe deel van de laag. Als de koppen erg lang zijn, associëren de staarten niet sterk.

In hoofdstuk 3 is de invloed van de lengte van de hydrofiele kop op de adsorptie van niet-ionogene surfactants aan hydrofiele oppervlakken in meer detail bestudeerd. Experimentele gegevens betreffende de adsorptie en de hydrodynamische laagdikte zijn gepresenteerd, en met behulp van neutronenreflektie is meer directe informatie over de structuur van de geadsorbeerde laag verkregen. De experimenten geven aan dat ook voor niet-ionogene surfactants met een kopgroep zes maal zo lang als de staart sterke associatie van de staarten plaatsvindt in de geadsorbeerde laag. De theorie, gebruikt in hoofdstuk 2 gaf dit niet aan. Met een uitbreiding van de theorie die inhomogeniteiten niet alleen loodrecht, maar ook parallel aan het oppervlak toestaat, kan wel een goede overeenstemming tussen theorie en experiment verkregen worden. Op hydrofiele oppervlakken vormen surfactants met een lange kopgroep aggregaatjes met een hydrofoob hart.

Hoofdstuk 4 gaat over de theorie van micelvorming van ionogene surfactants, surfactants met een geladen kopgroep. De kmc daalt en het aggregatiegetal stijgt als functie van de lengte van de staart en de zoutconcentratie. De eerst gevormde micellen zijn bolvormig maar als de staart lang is en/of de zoutconcentratie hoog, kunnen overgangen naar andere vormen plaatsvinden. Aan de volumefractie profielen is te zien dat de kopgroepen zich niet in een enkele

roosterlaag bevinden, wat in veel theoriën aangenomen wordt, maar gespreid zijn over een aantal roosterlagen. Micellen van ionogene surfactants gedragen zich in goede benadering als bolletjes met een konstante netto ladingsdichtheid. De potentiaal in het koppengebied wordt aangepast door tegengesteld geladen ionen aan te trekken en wel juist zoveel als nodig zijn om deze ladingsdichtheid te handhaven. Berekende en experimentele gegevens voor wat betreft de kmc's, aggregatiegetallen en de potentiaal in het koppengebied komen goed overeen.

In hoofdstuk 5 worden berekeningen van ionogene surfactants op oppervlakken met een konstante wandlading gepresenteerd. Het meest opvallende aspect is dat de adsorptieisothermen (de adsorptie als functie van de surfactantconcentratie), bij lage zoutconcentraties twee stappen vertonen. Na de eerste stap is de wandlading gecompenseerd en pas als de surfactantconcentratie tot ongeveer 10% van de kmc is gestegen begint de geadsorbeerde hoeveelheid weer te stijgen en wordt een bilaag gevormd. Adsorptie-isothermen, berekend bij verschillende zoutconcentraties, hebben een gemeenschappelijk snijpunt dat overeenkomt met het isoëlectrisch punt. In het isoëlectrisch punt zijn de omstandigheden zodanig dat het deeltje niet meer beweegt in een elektrisch veld. De kopgroepverdeling en de ladingsdichtheid aan de oplossingszijde van de bilaag lijken erg veel op die in micellen. Uit een vergelijking met literatuurgegevens blijkt dat de berekende isothermvormen en veranderingen in de structuur van de laag reëel zijn.

Hoofdstuk 6 gaat over de adsorptie op oppervlakken met een variabele lading. De experimentele gegevens laten zien dat adsorptieisothermen van nonylbenzeensulfonaat op rutiel, uitgezet in een dubbel logaritmische grafiek, vier regimes vertonen en dat is karakteristiek voor anionogene surfactants geadsorbeerd op metaaloxiden. De isotherm gaat al bij zeer lage bedekkingsgraad steil omhoog door attractie tussen de geadsorbeerde molekulen. Bij enkele procenten van de maximale geadsorbeerde hoeveelheid neemt de helling van de log-log grafiek echter al weer af. Het adsorptie-plateau wordt bij de

kmc bereikt. Wederom hebben adsorptie-isothermen, gemeten bij verschillende zoutconcentraties, een gemeenschappelijk snijpunt, dat overeenkomt met het isoëlektrisch punt.

Op oppervlakken van variabele lading hebben de gemeten isothermen niet de twee-staps vorm, die op konstante ladingsoppervlakken gevonden is. Dit komt omdat de wandlading zich aanpast tengevolge van surfactantadsorptie. Voorbij het isoëlektrisch punt begint bilaagvorming. Indien het isoëlektrisch punt gepasseerd is, kan uit de grootte van de wandlading de hoeveelheid die geadsorbeerd is met de kop tegen het oppervlak geschat worden. De hoeveelheid surfactant met zijn kop aan de oppervlaktekant hangt voornamelijk van de oppervlaktepotentiaal af. De oppervlaktepotentiaal kan worden gevarieerd door het aanpassen van de pH. De hoeveelheid aan de oplossingskant is nauwelijks afhankelijk van de pH maar is een functie van de attractie tussen de staarten en de repulsie tussen de koppen. Het laatste is te regelen via de zoutconcentratie.

De berekende resultaten laten ook zien dat de adsorptieisothermen van geladen surfactants op variabele ladingsoppervlakken vier gebieden hebben. Bij lage geadsorbeerde hoeveelheden is de overeenkomst tussen theorie en experiment niet erg goed. Het steile gebied in het begin van de isotherm wordt overschat, omdat aangenomen is dat elke roosterlaag parallel aan het oppervlak homogeen is. De bovenste helft van de adsorptieisotherm komt wel overeen met het experiment en ook de ladingseffekten worden goed beschreven.

In hoofdstuk 7 wordt het effect van de staartlengte en de vertakking van de surfactantstaart op de adsorptie op variabele ladingsoppervlakken bestudeerd. Experimenteel blijkt dat de adsorptie stijgt met de ketenlengte, maar daalt als de staart, van gegeven totale lengte, sterker vertakt is. Deze trends komen ook in de berekeningen naar voren. Ook nu wordt met de theorie de associatie in de onderste helft van de isotherm overschat. Theoretisch gezien is

er na het steile stuk in de isotherm een halve membraan op het oppervlak, in werkelijkheid zijn er na het steile deel (op log-log schaal), lokale aggregaatjes. Net zoals het aggregatiegetal van micellen stijgt als functie van ketenlengte en zoutconcentratie neemt de adsorptie toe als functie van deze variabelen. Dit geeft aan dat vergelijkbare pakkingseffekten van belang zijn voor micelvorming en adsorptie.

De berekeningen geven aan dat de structuur van micellen en geadsorbeerde lagen veel overeenkomst vertonen. Met behulp van de in dit proefschrift gebruikte theorie kunnen de onderling sterk verschillende vormen van adsorptieisothermen van surfactants aan het vast-vloeistof grensvlak beschreven worden. Met andere woorden met behulp van de theorie wordt aan de micelvorming en adsorptie van surfactants een gemeenschappelijke basis gegeven.

Curriculum Vitae

Marcel René Böhmer werd op 28 november 1962 om 23.15 in Arnhem geboren. In 1981 behaalde hij het VWO diploma aan het Thomas a Kempis College te Arnhem. In september van dat jaar begon hij aan de studie Moleculaire Wetenschappen aan de toenmalige Landbouw-hogeschool in Wageningen. Hij volgde de fysisch-chemische oriëntatie en studeerde in november 1987 af. Het doktoraalpakket bestond uit een hoofdvak fysische chemie en de bijvakken wiskunde en moleculaire fysica. Zijn stageperiode bracht hij door aan het "Department of Mechanical Engineering, University of Toronto" in Canada. Van november 1987 tot november 1991 werkte hij als toe-gevoegd onderzoeker bij de vakgroep Fysische en Kolloïdchemie van de Landbouwuniversiteit te Wageningen. Vanaf 1 januari 1991 zal hij in tijdelijke dienst zijn bij "Laboratoire d'Electrochimie des Solides, Université de Franche Comté" in Besançon, Frankrijk.

Dankwoord

Bij een goede vakgroep is het niet zo moeilijk om een proefschrift te schrijven. Er is altijd wel een expert in de buurt. Enkelen wil ik met name noemen.

Van Luuk Koopal heb ik veel geleerd. Waar vind je nog een begeleider die tot 3 uur 's nachts opblijft om de volgende versie van een manuscript met gulle hand van kommentaar te voorzien zodat meneer de promovendus 's ochtends om 9 uur weer verder kan. Zijn openhartige, direkte manier van communiceren heeft zowel het proefschrift als mijzelf veel goed gedaan. Hans Lyklema heeft zich meesttijds bewust op afstand gehouden en dat is een kenmerk van goed leiderschap. Desalniettemin heeft hij in de afrondingsfase zeer waardevol kommentaar gegeven. Zijn daden benne groot. Hans, ik wens je "good luck" met FICS II en III.

De meeste berekeningen zijn uitgevoerd met het programma "Goliad" van Peter Barneveld. Dat werkt goed zeg. Goliad maakt op zijn beurt weer gebruik van "Newton" van Jan Scheutjens en dat is ook geen slecht programma. Het is een genoegen te konstateren dat de Scheutjens-Fleer theorie nu ver ontwikkeld is, dat geldt zowel voor theorievorming als gebruikersgemak. Dit heeft een vergelijking van de theorie met experimenten mogelijk gemaakt, waarbij aan theoretische kant van alles uitgeprobeerd is. Aan allen die meegewerkt hebben aan uitbreidingen van de Scheutjens-Fleer theorie mijn hartelijke dank.

Het project is gesponsord door KSEPL (Koninklijke Shell Exploitatie en Produktie Laboratorium) waarvoor mijn dank. De kontakten met Shell verliepen veelal via Nico van Os en Rob Tijssen van KSLA (Koninklijke Shell Laboratorium Amsterdam). Een telefoontje naar Nico was voldoende om weer een voorraadje isomeerzuivere surfactant in de wacht te slepen. Aldus bepaalde Nico in grote mate de kwaliteit van de experimenten. Rob Tijssen heeft mij de ogen

geopend voor andere werelddelen. Het deel tussen half zeven en half acht 's ochtends op de snelweg naar Amsterdam en de chromatografie. Helaas konden we geen adsorptie-isothermen met kolomexperimenten meten, de ervaring en introductie in de analytische chemie zijn niettemin waardevol.

Rob Janssen heeft, in het kader van zijn afstudeervak, een groot aandeel gehad in de resultaten van hoofdstuk 3. Daarbij is gebruik gemaakt van de opstellingen van Jaap Dijt. Angelien Snaar van de vakgroep moleculaire fysica heeft geholpen met de NMR metingen. Ellen Lee, Dawn Kanelleas, Adrian Rennie and Bob Thomas carried out the neutron reflection experiments in Grenoble. I invite you all for "des éclairs au chocolat" in Besançon.

Rest mij nog mijn illustere kamergenoten te bedanken, niet voor niets deed ik tijdens de aanwezigheid van Frans Leermakers en Boudewijn van Lent het meest theoretisch werk en bij Gerrit van der Beek het meeste experimentele werk. Doe mij nog een stel van zulke kollega's.

Marcel